Quantum dynamics and isotope effects of hydrogen in physico-chemical systems studied with Neutron Compton Scattering

vorgelegt von
Diplom-Chemiker
Tyno Abdul-Redah
aus Dresden

Von der Fakultät II - Mathematik und Naturwissenschaften -
der Technischen Universität Berlin
zur Erlangung des Grades

Doktor der Naturwissenschaften
- Dr. rer. nat. -

genehmigte Dissertation

Promotionsausschuss:

Vorsitzender: Prof. Dr. M. Lerch
Berichter: Prof. Dr. C.A. Dreismann
Berichter: Prof. Dr. G. Renger

Tag der wissenschaftlichen Aussprache: 04. Juli 2005

Berlin 2005
D83

To my family, my friends and to everybody who suffered from the lack of time I had during the becoming of this Thesis.

To whom it may concern

"In science, new ideas are at first completely neglected, later fiercely attacked, and finally regarded as well known."

Konrad Lorenz
(after: H. D. Zeh,
"The Physical Basis of The
Direction of Time",
Springer, 3. edn., 1999, p. 99).

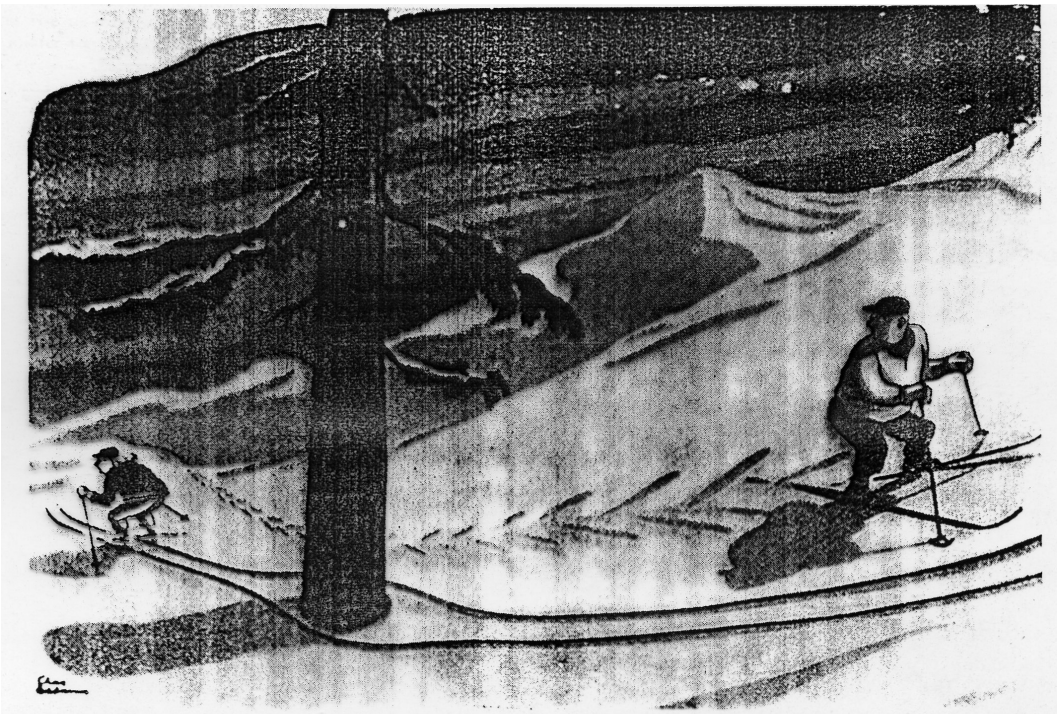

Bild 1: Interferenzvorgang. (Mit freundlicher Genehmigung durch „The New Yorker". Zeichnung Charles Addams; © 1940, 1968 The New Yorker Magazine, Inc.)

-Verlag GmbH, D-6940 Weinheim, 1985

Zusammenfassung

In dieser Arbeit wurde auf experimentellem Wege das Gesamtstreuvermögen von Wasserstoffkernen in verschiedenen chemischen Umgebungen in flüssigen und festen Verbindungen mit der inelastische Neutronen-Compton-Streuung (NCS) untersucht. Die Experimente wurden am VESUVIO Spektrometer an der Neutronenspallationsquelle ISIS am Rutherford Appleton Laboratory in Großbritannien durchgeführt. Die vorliegende Arbeit wurde durch theoretische Arbeiten über die mögliche Existenz von dynamischen Quantenverschränkungen in der kondensierten Materie motiviert. Diese Theorie hat zur Voraussage geführt, dass wenn das Zeitfenster, während dessen das System beobachtet wird, kurz genug ist, die quantenverschränkten Teilchen das elektromagnetische oder Materiefeld nicht so streuen, wie wenn sie sich als individuelle Teilchen verhalten würden. Dabei gilt das Wasserstoffatom wegen seiner geringen Masse und der daraus resultierenden relativ großen thermischen de Broglie-Wellenlänge als besonders geeignet, solche quantenverschränkten Zustände aufzuweisen. Die den Untersuchungen zugrunde liegenden chemischen Verbindungen enthielten Wasserstoff in unterschiedlichen Bindungsverhältnissen: (1) Wasserstoffbrückenbindungen, in denen der Wasserstoff einem raschen Austausch unterliegt, (2) C-H Bindungen, bei denen der Wasserstoff keinen Austausch erfährt, und (3) Metall-Wasserstoff-Verbindungen, in denen der Wasserstoff interstitiell oder ionisch gebunden vorkommt. Die unterschiedlichen Bindungsverhältnisse implizieren, dass der Wasserstoff verschiedene chemische und elektronische Umgebungen hat und somit in jeder Umgebung einer speziellen Quantendynamik (Dekohärenz) unterliegt. Es hat sich zum einen gezeigt, dass der Wasserstoffkern eine Anomalie, die sich als starke Abnahme seines Streuvermögens äußert, aufweist. Zum anderen verursachen die verschiedenen chemischen Umgebungen unterschiedliche Anomalien. Mit diesen Erkenntnissen findet die oben genannte theoretische Voraussage eine eindeutige Bestätigung. In den meisten eingesetzten Verbindungen wurde durch Ersatz der Protonen durch Deuteronen der Isotopeneffekt auf das Streuverhalten untersucht. Es zeigte sich, (1) dass in flüssigem H_2O/D_2O das Streuquerschnittsverhältnis σ_H/σ_D des Protons und des Deuterons kleiner ist als nach der konventionellen Streutheorie zu erwarten wäre und (2) dass σ_H/σ_D sehr stark von der H/D-Zusammensetzung der Probe abhängt. Dieses Experiment hat erstmalig den direkten Beweis für die Existenz quantenverschränkter Kernzustände erbracht. Während die Anomalien der H_2O/D_2O-Mischungen auf einen intermolekularen Effekt hindeuten, scheint der Effekt bei einigen organischen Molekülen von intramolekularen Wechselwirkungen herzurühren. Darüber

hinaus zeigte sich bei einigen der Metallhydride eine starke Abhängigkeit des σ_H von der Streuzeit, was stark auf die dynamische Natur des Effektes hindeutet. Weiterhin konnten starke Hinweise dafür gefunden werden, dass die elektronische Umgebung des Wasserstoffs in der jeweiligen chemischen Verbindung eine wesentliche Rolle für den Effekt spielt. Diese experimentellen Resultate verletzen eine fundamentale Annahme der Streutheorie, nämlich die der strengen Proportionalität zwischen Teilchenzahldichte und Streuintensität. Insbesondere spricht man bei der Neutronenstreutheorie von der Verletzung der Summenregel des nullten Moments des dynamischen Strukturfaktors. Deshalb wurden die experimentellen Daten einer eingehenden theoretischen und experimentellen Prüfung unterzogen. Es gilt als gesichert, dass der vorliegende neue Effekt weder auf experimentelle Artefakte zurückzuführen ist, noch eine auf einer konventionellen Theorie der kondensierten Materie basierde Erklärung hat. Es hat sich gezeigt, dass die experimentellen Resultate nur im Rahmen einer wesentlichen Erweiterung der Neutronenstreutheorie eine Intrepretation finden. Es wird vermutet, dass der vorliegende neuartige Quanteneffekt für die Chemie in der kondensierten Materie eine fundamentale Rolle spielt. Diese Vermutung wird dadurch unterstützt, dass die Zeitskala des Experiments im Femtosekunden- und Subfemtosekunden-Bereich liegt und dass bei der NCS Methode aufgrund der hohen Energieüberträge auf das Proton beim Streuprozess die chemischen Bindungen gebrochen werden. Diese Zeitskala ist nämlich vergleichbar mit der für die Umverteilung der Elektronendichten bei chemischen Prozessen. D.h., dass das in der Quantenchemie oft verwendete Born-Oppenheimer-Schema für die Berechnung von Energiehyperflächen in dieser Zeitskala seinen Sinn verliert, da sich nun die Dynamik der Elektronen nicht mehr von der der Kerne trennen lässt. Demnach ist die Verwendung dieser Hyperflächen für die Beschreibung des Ablaufs chemischer Reaktionen nicht so generell anwendbar wie allgemein angenommen wird.

Abstract

This work deals with the experimental investigation of the scattering behavior of hydrogen nuclei in different chemical environments in liquid as well as solid compounds. The experimental method used is the inelastic technique of neutron Compton scattering (NCS) as applied on the VESUVIO spectrometer at the neutron spallation source ISIS of the Rutherford Appleton Laboratory in UK. The present work has been motivated by previous theoretical work on the possible existence of dynamical quantum entanglement in condensed matter which lead to the prediction that, if the time window of an experimental method is short enough, then the quantum entangled particles would not scatter electromagnetic or matter field in the way they would do if they would behave individually. The proton is considered to be particularly suitable to exhibit such quantum entangled states because of its relatively low mass and the resulting long thermal de Broglie wavelength. The compounds investigated in the present work comprise a wide range of different bonding conditions the proton is involved in: (1) H-bonds in which the protons experience rapid exchange, (2) C-H bonds, in which the protons do not experience such an exchange, and (3) metal hydrogen systems, in which the protons occupy interstitial sites or are involved in ionic bonds. These different bonding conditions imply that the proton is involved in different chemical and electronic environments and is consequently subject to different quantum dynamics (decoherence). The experimental results showed that the proton exhibits an anomaly which manifests itself in a strong decrease of its ability to scatter neutrons. In addition, the different chemical environments cause different anomalies. These experimental findings confirm the above mentioned theoretical prediction. In most cases, the protons have been partly exchanged by deuterons in order to investigate the effect of isotope exchange on the scattering behavior. It has been found that (1) the ratio σ_H/σ_D of the scattering cross sections of H and D in liquid H_2O/D_2O is significantly smaller than expected according to conventional scattering theory and (2) that σ_H/σ_D is strongly dependent on the H/D composition of the mixture. This experiment provided for the first time a direct evidence for the existence of nuclear quantum entanglement in condensed matter. While the anomalies in the H_2O/D_2O mixtures indicate an intermolecular origin of the effect, it seems to be of intramolecular origin in some of the organic systems. Furthermore, some metal hydrogen systems exhibited a strong dependence of σ_H on the scattering time, which indicates the dynamical nature of the effect. It has also been found that the electronic environment of the proton in the compound does play a significant role for the anomalous effect.

These experimental results violate a fundamental assumption of any scattering theory, i.e., the strict proportionality of the particle number density and the scattering intensity. Expressed in the terms of neutron scattering theory, it is the zeroth moment sum rule of the dynamic structure factor which is violated. Therefore, the experimental data have been subject to a thorough experimental and theoretical scrutiny. It can be safely said that the underlying novel effect is neither caused by experimental artifacts nor can it be explained in terms of a conventional theory of condensed matter. Rather, it has been shown that the experimental results can be interpreted only by a considerable extension of the neutron scattering theory. It is anticipated that the underlying novel quantum effect plays a fundamental role for chemistry in condensed matter. This anticipation is supported by the facts that the time scale of the experiment which is in the range of femtoseconds and less and that the chemical bonds are broken in the NCS method due to the high energy transfer to the proton. This time scale is comparable with that one of the rearrangement of electronic densities during chemical reactions. This means that the widely applied Born-Oppenheimer scheme for the calculation of energy surfaces loses its validity within this time range, since the dynamics of the electrons can no longer be separated from that of the nuclei. Hence, the applicability of the energy surfaces for the description of chemical reaction paths is not as general as commonly believed.

Contents

Chapter 1

Introduction and summary of main results

In this work the existence of short lived protonic Quantum Entanglement (QE) in hydrogen containing condensed matter systems was explored. If one deals with condensed quantum systems, the questions about the appropriate description of the state and the dynamics of the relevant system arise. Usually, physical systems are treated as they were *closed systems*, i.e., one neglects or oversimplifies their interaction with their environment. In this framework and if these systems are treated quantum mechanically, then the operators corresponding to physical observables are self adjoint (or hermitian) and have real eigenvalues. Due to the closeness of the system, there is no energy exchange with the environment so that the corresponding Hamiltonian is time independent. The system is then called *conservative*. The solutions of the time independent closed Schrödinger equation using this time independent Hamiltonian are *stationary states* with the phase oscillating as a function of time. The dynamics of such a system is described as follows: One introduces a formal evolution operator which acts on a wave function at time $t = 0$ to yield another wave function at a later time $t > 0$. Then the time dependent Schrödinger equation is applied on this wave function which gives then a time evolution operator governed by the Hamiltonian. This means that the time evolution is intimately related to the Hamiltonian describing the system. The dynamics of a conservative system is described by a time evolution which is unitary due to the hermiticity and time independence of the corresponding Hamilton operator. This implies that the *dynamics of the closed system is invariant under time reversal* [1]. Therefore, the Schrödinger equation already ceases to be useful when it comes to the description of time asymmetric processes like, e.g., spontaneous emission, in which energy is irreversibly exchanged between the system and the environment.

Such an approach (i.e. stationarity and the use of equations of motion which are invariant under time reversal) might be strictly valid for a diluted gas in which the energy level separations are significantly larger than any interaction energy. However, in condensed or macroscopic systems, the density of states is very high. If the particles are completely non-interacting, the energy levels of this system are built by the sums of the energies of individual particles, each of which ranging over an infinite series of discrete levels. One should bear in mind that the level spacing for a macroscopic body decreases exponentially with the number of particles of the system [2]. Now, due to the interaction of the particles, the energy levels are in addition smeared out. And because the interaction energy, however its smallness is, is much higher than the level spacing, *the constituents of a condensed system can never be in strictly stationary states*.

Another reason for the impossibility of a macroscopic body to be in a stationary state lies in the "energy-time" uncertainty. The state of a quantum mechanical system is prepared by an interaction of this system with a classical measurement device. In the case of a macroscopic body the energy levels are so closely lying that the energy time uncertainty principle would require an interaction time that is exceptionally long in order to get this small energy indeterminacy required for the state to be stationary [2].

However, there is another difficulty that is connected to the fact the constituents of a macroscopic body are subject to interaction with each other. For example, an isolated particle can in principle be generally described by a superposition of eigenstates if no measurement has been taken on this particle. If, however, this particle is immersed in a macroscopic body of a large number of degrees of freedom then there is accordingly a large number of possible interactions of this particle with its surrounding. Therefore, it is not even possible to describe this particle by a state vector. Since every realistic system is never really isolated from its surrounding, the conventional framework of QM in terms of state vectors is always an idealization [1].

Since a macroscopic body cannot be described by a single wavefunction, it is necessary to find another formalism which takes into account that the state of the system is not completely determined [3]. A quantum mechanical description based on the incomplete information about a system is possible utilizing the *density matrix formalism* [1, 2]. The knowledge of the density matrix permits the calculation of the mean values of any variable relevant to the system and the corresponding dynamics is treated using equations of motion for density matrices, the so called *master equations* [1, 4].

Since *any realistic system is subject to coupling to an uncontrollable environment* which influences it in a non-negligible way, a condensed system must be regarded as an *open system* in which the relevant system S is regarded as

embedded in a larger system *Env* (usually called environment). As stated above, if two systems do interact or interacted in the past, it is in general not possible to assign a single wave vector to either of the two subsystems [1]. Therefore, it is not possible to describe the "relevant" system S on its own but one must account for the existence of the environment. Now, the wavefunction of the composite system S+*Env* cannot in general be decomposed in a product of wavefunctions depending only on coordinates of S or *Env*, respectively, so that the *subsystem S does not possess a wavefunction* [5]. *The relevant system S and its environment Env are then said to be inseparable, quantum entangled, or Einstein-Podolsky-Rosen (EPR) correlated.*

In the case of a *closed macroscopic quantum system*, the appropriate equation of motion of the density matrix is represented by the *Liouville-von Neumann equation* which can be derived from the time dependent Schrödinger equation [4]. Apart from some time symmetry breaking processes known from elementary particle physics, all known (classical as well as quantum) physical laws of microscopic systems are *invariant under time reversal* [4, 5], i.e. *the time evolution is unitary.* An essential feature of unitarity is that it strictly *preserves the norm of the state vector.* Despite their success for our understanding of nature, these laws do not account for the irreversible features of macroscopic systems (which consists of microscopic bodies), for example, the increase of entropy with time. The dynamics of an *open quantum system S cannot, in general, be represented in terms of a unitary time evolution* [4]. I.e., the dynamics of an open quantum system is *highly irreversible and therefore no longer invariant under time reversal.* This is due to the interaction of S with the infinite degrees of freedom of *Env.*

If one deals with an unstable state, then the aspect of a *life time* of this state enters the scene. Phenomenologically, the life time of an unstable state is related to a *complex energy eigenvalue.* This means that the corresponding Hamiltonian is not self-adjoint and the corresponding time evolution is not unitary anymore [3].

This is equivalent to the extension of the usual treatment of quantum mechanics using self adjoint Hamiltonians into the context of *complex valued operators.* In fact, the theoretical treatment of the dynamics of a system being part of a larger system necessitates a partial abandonment of the Hamiltonian formalism which includes real valued energies [6]. One method which deals with this kind of mathematical treatment is the so called *Complex Scaling Method (CSM).* For further details, see [7].

The continuation of the CSM into the superoperator level (a superoperator is an operator acting on an operator to yield another operator), its application to the density matrix theory for fermions and the extension of the CSM into the context of the canonical ensemble formalism of quantum statis-

tics leads to the following result: The reduced second order density matrix may contain submatrices γ, called *Jordan blocks*, that cannot be diagonalized under any similarity transformation [7]. These submatrices describe the *quantum entanglement (QE)* between the fermions. The process of the destruction of QE due to "disturbances" of the entangled particle states by the environment is called *decoherence*. As one realizes, the environment plays a double role here. One part of it, Env_1, is responsible for the creation of QE, by allowing a particle S to interact with it (see p. 84 of [8]). A different part of the environment, Env_2 say, interacts at a later time with the composite system S+Env_1 and is responsible for the destruction of QE between S and Env_1 but by establishing a new QE between S+Env_1 and Env_2 (see Chapter 7 of [8]). For a discussion of decoherence, see [4, 8–10].

The Jordan blocks γ mentioned above exhibit finite life times and dimensions and are therefore called *coherent dissipative structures (CDS)*. The emergence of these correlations can not result from the fundamental equations of motion being employed within the framework of the usual microscopic level of description of natural phenomena. This is due to the fact that these equations (classical or quantal) are time reversible in nature. The order of the Jordan block gives the number s of intrinsically connected (paired) states. It is very interesting to note that the theory [7] predicts that the relaxation (decoherence) time for a Jordan block of order 2 (the smallest order possible to establish QE between particles in condensed systems) lies in the range of 10^{-15}s, i.e., in the femtosecond time regime. During this time, every individual constituent of the CDS loses its individuality. It is the spirit of the present work that the condensed systems do possess this property within this time scale. Therefore, the effects which are searched for in the present work should also be in the same or similar time range. Consequently, the experimental method required should also operate at this time scale (see below for further details).

The non-unitary time evolution approach has been put forward by Prigogine in the 70s and 80s of the 20^{th} century aiming at the explanation of macroscopic irreversibility [11]. The search for a time or entropy operator as was proposed by Prigogine [11] has been almost given up. Instead, it is generally accepted that the asymmetry in time might be attributed to coherence loss of quantum states [9, 10, 12–18]. It should be noted that the treatment of decoherence touches upon fundamental questions of quantum theory, like the definition of the borderline between system and environment, or the collapse of the wave function, and measurement theory or crossing the borderline between the quantum and classical worlds and is therefore of fundamental and general interest.

The phenomenon of QE between two or more quantum systems represents

a particularly striking feature of quantum theory [19–23]. Until now, a large number of fundamental experiments have confirmed the existence of QE in an impressive way. These experiments, however, usually deal with quantum systems (e.g. pairs of photons, atoms or ions) which are carefully isolated from their environment in order to maintain QE for a time sufficiently long to become measurable. This condition is necessary due to decoherence; cf. Refs. [9, 10, 13–18]. Besides their fundamental importance, multiparticle QE and decoherence are also in the focus of several fast developing experimental and theoretical fields, e.g. *quantum optics, quantum computation, quantum cryptography, quantum teleportation*, etc. [8, 24]. QE is not restricted to photons or small particles like neutrons or atoms but is also possible in quite complicated systems like large molecules [25]. Also worth mentioning is the fact that QE can also occur between two different objects like an atom and a photon, a phonon and an ion, or even an atom (which is a microscopic object) and the electromagnetic field in a cavity (being macroscopic) [8].

In condensed systems at ambient experimental conditions QE was widely believed to be unimportant and/or not accessible to experiments, due to its extremely fast decoherence [8, 24]. Under such conditions, the *life time of the entanglement, i.e. the decoherence time* τ_{dec}, is believed to be much shorter than the present-day time resolution techniques can achieve. Therefore, it is commonly expected to have no experimental significance. In contrast, based on the theoretical investigations briefly described in the previous paragraphs, it was proposed to make QE experimentally accessible by means of sufficiently "fast" scattering techniques [7]. Intuitively, one may appreciate the *possible existence of this new effect, provided that the decoherence time* τ_{dec} *is of the same order as the characteristic "scattering time"* τ_s*, i.e., the time interval during which an incident particle may interact with the scattering center*. In the framework of theoretical investigations [7], it was qualitatively predicted that particles participating in quantum correlated domains do not interact with external fields in an appropriate way, thus giving rise to a scattering behavior which is "anomalous" compared to the *conventional scattering theory* [26, 27] *based on stationary states and time symmetric equations of motion and on the famous Fermi Golden Rule*. To be specific, in the framework of the standard treatment of scattering theory, the scattering intensity is strictly proportional to the product of the scattering cross section σ and the number of particles in the sample. The crucial theoretical prediction being under experimental scrutiny in the present work is:
"The intensity of the (electromagnetic or matter) field being scattered from quantum correlated particles subject to decoherence is NOT proportional to the number of particles present in the sample."
Already here it should be noted that the present work fully confirms this

prediction, i.e., it has been indeed observed that the scattering intensity of, e.g., protons is not proportional to the number density of the protons in the sample (for a summary of the experimental results, see below).

Although the work presented here was motivated by the theoretical work on CDS [7], the experimental results found here may find their final or full explanation mainly in the framework of modern theory of decoherence in combination with the general theory of scattering. The cross disciplinary nature of the field of open quantum systems necessarily requires the treatment of various different aspects of quantum theory and of diverse applications in many fields of physics [4]. The work presented here is in this spirit since it combines at least two completely different fields of physics and chemistry, namely short lived QE and decoherence on the one hand and neutron scattering theory on the other.

A brief description of the creation of QE as well as its decay through the process of decoherence will be presented in the next chapter. Being experimental in nature, it is out of the scope of the present work to give a complete and rigorous theoretical treatment of QE and decoherence in all its details. In this context it should be pointed out that, despite considerable theoretical efforts during the last decades, a well established or quantitative theory of decoherence in *condensed matter* does not exist yet. E.g., as Omnès puts it: "The most general model allowing a study of decoherence is restricted by several conditions..... The case of fluids, with their formally infinite number of degrees of freedom, has not even been touched upon" (Ref. [18], pp. 291-292). Of course, the same holds for all condensed systems, too.

In this work condensed systems of physico-chemical importance have been investigated with respect to the scattering behavior of hydrogen (proton/deuteron) contained in them.

The reason why hydrogen has been chosen to test the theoretical predictions [7] stated above lies in the fact, that hydrogen represents the most simple nucleus and it is the lightest stable one having a thermal de Broglie wavelength of the order of ca. 1 Å [4, 10] which is large compared to that of other nuclei and which falls in the range of internuclear distances in condensed matter and in chemical bonds. Therefore, it is a particularly suitable candidate to exhibit quantum effects at least due to its spatial delocalization. Another reason for choosing hydrogen is that it exhibits a half integer spin, i.e., it is a fermion. Therefore, the results obtained by the measurements can be directly compared with the theoretical predictions which has arisen from the application of density matrix theory for fermions (see above).

In addition, the proton can be involved in so many different ways in chemistry. For example, the hydrogen isotope next to the proton, i.e., the deuteron, has a mass approximately twice as large as that of the proton.

This important property is widely utilized in chemistry and physics, because the replacement of (all or only a part of) the protons by deuterons without changing the electronic and/or structural properties of the system too much, provides a useful tool for many spectroscopic methods. Furthermore, while the proton is a fermion, the deuteron, having an integer spin eigenvalue, represents a boson. The importance and uniqueness of hydrogen is reflected very impressively by the fact that hydrogen is involved in many different chemical bonds, e.g. being (owing to its low electronegativity) mostly positively charged in a covalent bond, for example in water, where it exhibits dynamical exchange between different water molecules. It is also involved in C-H bonds, the main building block of organic molecules thus being also of biological importance. On the other hand, it can also be negatively charged in, for example, an ionic metal hydride like LiH. In addition, it can occupy interstitial sites in a lattice host, as is the case in niobium hydride, and can lead to a tremendous number of different structural phases depending on its concentration in the host lattice [28, 29]. Another interesting feature of the hydrogen atom in condensed systems is its ability to exhibit tunnelling due to its low mass. Last but not least, because of its occurrence in all these many different chemical circumstances, it is consequently embedded in different electronic environments. Therefore, the influence of the electronic structure on the effect searched for in this work could also be investigated.

Motivated by the theoretical work [7] described above, a Raman light scattering experiment on H_2O, D_2O and H_2O/D_2O mixtures was done and published in 1995 [30]. In this experiment the relative Raman scattering cross sections of the intramolecular stretching vibrational modes of the OH- and OD-bonds, σ_{OH} and σ_{OD}, respectively, were determined [30]. σ_{OD} of the H_2O/D_2O mixtures were found to be larger than σ_{OD} of pure D_2O, whereas the σ_{OH} of the H_2O/D_2O mixtures were found to be smaller than σ_{OH} of pure H_2O [30]. Therefore, this experiment succeeded to measure the predicted "anomalous" component in the scattered light field (see above), thus providing experimental evidence for the existence of short lived QE in water. However, since the electromagnetic field couples to the nuclei via the electronic cloud, this experiment provides an indirect evidence for the existence of nuclear QE in liquid water.

Therefore, it has been searched for a more direct method with a short interaction time of the probe with the scattering system. Neutrons couple directly to the nuclei mainly via strong interaction and are therefore particularly suitable for the investigation of nuclear QE.

The method used here is *neutron Compton scattering (NCS)* as applied on the VESUVIO (formerly eVS) spectrometer at the ISIS spallation neutron source in UK (for instrument description, see chapter 4). It is a highly

inelastic scattering technique and is therefore sometimes called *deep inelastic neutron scattering (DINS)*. Very interesting to note here is the fact that the time scale of the process of Compton scattering of a neutron off a proton is of the order of 10^{-15}-10^{-17}s depending on the transferred momentum. I.e., this experimental method accesses the dynamics in the femto- and sub-femtosecond time scale. A brief description of parts of the neutron scattering theory of relevance for the present work will be given in chapter 3 and of the NCS method in chapter 4. Already here it should be mentioned that the derivations involved in the standard neutron scattering theory use operators which (in the Heisenberg representation) evolve unitarily and therefore do not account for the intrinsically non-unitary character of the time evolution of condensed matter systems (see above). Therefore, any deviation of the measured scattered intensity from conventional theory expectations might be caused by the non-unitary evolution of the particles dynamics.

It is interesting to note, that the well known conservation of the norm of a state vector arises from the hermitian nature of the Hamiltonian and the corresponding unitarity of the evolution operator. Since the theoretical derivations explained above presume the existence of short lived states making use of complex energy eigenvalues, the corresponding Hamiltonian is no longer Hermitian and thus the state vector norm is not necessarily conserved [3].

The focus of the first experiments was on the investigation of protons involved in *hydrogen bonds*. The very first NCS experiments were done on liquid mixtures of H_2O/D_2O [31, 32]. There, it has been found that the ratio of the neutron scattering cross sections of H and D, i.e. σ_H/σ_D, was "anomalously" decreased with respect to the tabulated value $(\sigma_H/\sigma_D)_{tab}$ =10.7. This decrease was observed to be strongly dependent on the D mole fraction x_D of the mixture, to amount to ca. 40% of $(\sigma_H/\sigma_D)_{tab}$ at the lowest measured x_D and to be rather independent of temperature [33]. These surprising observations strongly contradict standard theoretical treatments of neutron scattering [31]. Interestingly, these experiments showed similar D mole dependent anomalous scattering of the proton as was found in the Raman light scattering experiments [30]. Later experiments done on pure H_2O, pure D_2O and mixtures of them showed that the decrease of σ_H/σ_D is due to a decrease of σ_H rather than an increase of σ_D and that this decrease is maximum for pure H_2O [paper in preparation]. Some of the results of the H_2O/D_2O mixtures [31] were confirmed by a new experimental technique using a considerably improved instrument resolution [34]. Measurements on solutions of urea ($CO(NH_3)_2$) dissolved in D_2O showed similar results but higher anomalies for the lowest x_D than in the H_2O/D_2O system [35].

Metal hydrides represent a very important class of materials being highly

relevant for technological applications, e.g., as hydrogen storage materials for fuel cells or as switchable mirrors. Therefore, experiments on niobium hydrides at room temperature and at lower temperatures have been performed and followed by measurements on hydrides with palladium and yttrium serving as host lattices, respectively. The work on those metal hydrides has been done in collaboration with Prof. E. B. Karlsson from the Uppsala University in Sweden and with Dr. T. Udovic from the National Institute of Standards (NIST) in the US. The niobium hydrides used in this work have been prepared in Uppsala and the yttrium hydrides at NIST whereas the palladium hydrides have been prepared in situ prior to the measurements. These experiments showed a protonic cross section anomaly which is dependent on the scattering time [32, 36–39]. A summary of the results on water and of some of the metallic hydrides can be found in the Science Highlight of the ISIS Annual Report 2000 [32] or in a very recent review [40]. Like in water, no temperature dependence has been found for these hydrides [36–38, 40].

Furthermore, protons involved in *covalent bonds* has been investigated as well. Experiments on fully protonated polystyrene involving C-H bonds, showed that the measured σ_H/σ_C is ca. 20% smaller than $(\sigma_H/\sigma_C)_{tab}$ and that this decrease is independent of the scattering time [41]. Later experiments on partially deuterated polystyrene and benzene [42] as well as on an amphiphilic molecule (2-iso-C_4E_1) dissolved in D_2O [43] showed also protonic scattering cross section density decrease and suggested that the effect is of intramolecular rather than of intermolecular origin because here the effect was rather independent of the D mole fractions of the samples. On the other hand, similar experiments on liquid mixtures of H_6-acetone and D_6-acetone showed the same D mole dependence as was found in the H_2O/D_2O system but with a significantly larger anomaly [44].

Although not being part of this thesis, it is rather worth mentioning that experiments on Formvar ($C_8H_{14}O_2$) [45] and later on polyethene [46] showed an anomaly of ca. 40% . These experiments were repeated using a completely different method, namely, electron Compton scattering (ECS) [47], and confirmed in a very impressive way that the effect found in this work is general and independent of the experimental method used or of the involved system-probe interaction. It should be noted that it is the strong interaction that mainly couples the neutron to the nuclei, whereas the electron is coupled to the nuclei via Coulombic interactions. The importance of these experiments has been recognized by the scientific community and has attracted a strong attention [48, 49].

The fact that the cross section anomaly in some of the systems described above appeared to be of intramolecular rather than of intermolecular origin led to the conclusion that the employed experimental technique might

be sensitive to the *influence of the electronic environment on the protons*. Therefore, the NCS of different H containing materials with completely different electronic structures was investigated. Experimental data taken from scattering on LiH showed for the first time (in contrast to the results of water and the metallic hydrides mentioned earlier) a dependence of the scattering cross section density decrease of H on temperature. Specifically, the anomalous decrease was larger at 20 K than at 300 K [33]. Experiments on LaH_2 – exhibiting metallic properties – and LaH_3 – being an isolator – showed significant differences of the cross section anomaly [50]. These experiments strongly indicate the relevance of the electronic environment for the decoherence process [33]. All experimental results summarized here are fully described in chapter 7.

Of course, the question arises, why these effects were not found using the usual spectroscopic methods although the systems under consideration here have been subject to thorough investigations in the last decades. As was pointed out in the beginning, the time scale of the investigated phenomena is in the range of 10^{-15}s which is considerably shorter than the time window of conventional spectroscopic methods (like vibrational spectroscopy or nuclear magnetic resonance). This short time scale is related to the high transfers of energy and momentum during the NCS process. For a discussion of the scattering time, or the time window within which the scattering particle interacts with the probe, especially in the light of recent measurements claiming the falsification of our results, see section 3.2.5 and Ref. [51]. It is interesting to note that recently, a series of publication have appeared which suggest the existence of *long lived QE of protons* in condensed systems, e.g., in $KHCO_3$ [52–54].

Of course, our results summarized above are extremely striking because they contradict conventional scattering theory. Therefore, their genuineness was doubted. The doubts range from conceptual objections concerning QE and the impossibility of its experimental accessibility by VESUVIO to instrumental faults and data analysis errors. Therefore, the results obtained in this work have been checked several times changing many experimental parameters. These tests, which are described in full detail in chapter 8, confirm the obtained results and give strong evidence that the cross section anomaly is indeed genuine and has its physical origin in a thus far unknown short time dynamical feature of the chemical bond. Of course the experiments using electron Compton scattering (see above) [45, 46, 48, 49] serve as a further very strong indication for the reliability of the effect.

Despite the doubts and criticisms the experimental effect was subject to, considerable effort has been spent by different authors aiming at providing a theoretical interpretation of the experimental results found in this work.

The published theoretical models will be described and discussed in section 9. One model which has been suggested by Karlsson and Lovesey (KL) [55, 56] makes exchange correlations fully responsible for the shortfall of the scattering cross section. It provides a quantitative assessment about the shortfall of the protonic scattering cross section and has been applied by Karlsson [57] to explain the original results on H_2O/D_2O mixtures at room temperature [31]. This model is static in nature, relies on the relevance of the neutron coherence length and imposes decoherence afterwards. Another theoretical model, put forward by Chatzidimitriou-Dreismann (CD) [41, 58], starts from the basic equations of van Hove's treatment [59] of neutron scattering theory in terms of the dynamic structure factor. This model takes explicitly into account the existence of QE and decoherence, the latter being caused by quantum dynamics effects related to the breakdown of the Born-Oppenheimer approximation. It also introduces a time averaged matrix element for the transition from the initial to the final state of the scatterer and makes use of the density matrix theory and time asymmetric master equation. The time evolution equation of the density matrix contains a factor which decays in the course of time. This decay is responsible for the shortfall of scattering intensity of the protons.

One interesting consequence of this model might be worth mentioning already here: If the QE is infinitely long lived, then this theory predicts that there should be no shortfall in scattered intensity, i.e., no anomaly is expected. In contrast the KL theory rather predicts the existence of an anomaly also for infinitely long lived QE. It is also interesting to note here, that whereas the theoretical model of Karlsson and Lovesey explains the shortfall of the scattering intensity of the protons by means of the scattering cross section, the decoherence model due to Chatzidimitriou-Dreismann makes the dynamic structure factor (containing the sample properties) responsible for the shortfall of the scattering intensity of the protons. The dynamic structure factor is of fundamental importance because it is responsible for all transport properties of the system. Thus, if the latter model is true then the effects found in this work will have far reaching consequences for many properties of condensed systems if considered in the short time scale, whereas the former theory would be restricted to neutron scattering only.

Very recently, Gidopoulos [60] on the one side and Reiter and Platzman [61] on the other provided two different theoretical models which have in common the breakdown of the Born-Oppenheimer-Approximation (BOA) due to the short time scale of the neutron proton collision being in the subfemtosecond range (see section 3.2.5). The model of Gidopoulos explains the cross section shortfall quantitatively on the basis of the distortion of the

dynamics structure factor whereas Reiter and Platzman suggest a model that relies on the breakdown of the BO approximation in the final state.

It is true that the present work has been motivated by theoretical work on the so called coherent dissipative structures [7] and their improper interaction with external fields thus leading to the predicted anomaly. However, as stated above this theoretical work is rather qualitative. A full understanding of the found cross section density anomalies is still lacking. The ultimate success of one or a combination of the theories suggested thus far will depend on further experimental work on testing their implications and consequences.

According to the conventional viewpoint, an elementary chemical reaction can be theoretically represented by the "motion" of nuclei (treated either as classical mass points, or as quantum wave packets [62, 63]) along the minimum energy path (also called *reaction coordinate*) of Born-Oppenheimer (B-O) potential energy surfaces [64]. The latter are determined by solving the electronic time-independent Schrödinger equation, by considering the nuclei as classical mass points and keeping their positions fixed at various spatial configurations. However, also nuclei are quantum objects, and thus they can occupy non-classical states, which are caused by interactions between the particles themselves, as well as interactions of the particles with electronic charges in their vicinity.

The experimental results of the present work have shown that the quantum dynamics of protons in chemical bonds are affected because the energy transfers using NCS are so high that chemical bonds are broken. Therefore, the anomalous effects found in this work *unveils a new aspect of the chemical bond during this short time scale*. Furthermore, this time scale is of the order of the rearrangement of the electronic densities during chemical processes. This means, that the BO scheme which is often used in quantum chemistry for calculating energy hypersurfaces loses its validity in this time range, because in this case it is obviously impossible to separate the nuclear dynamics from that of the electrons. Therefore, these hypersurfaces are not as generally valid as commonly believed.

Another reason for the importance of these effects for chemistry can be derived from the application of the kinetic gas theory for the description of chemical reaction kinetics. For example, in any chemical reaction the particles also undergo collisions in which bonds are broken if some energetic and geometrical requirements are fulfilled. The rate constant is then usually described by the well known empirical Arrhenius equation $k = Ae^{-E_a/RT}$. From the quantum theoretical point of view, chemical reaction processes are described by *transition matrices*. They necessarily contain the initial states (educt) and the final states (products) of the involved particles. Now, the particles in condensed systems are in continual interaction and the existence

of QE and decoherence is a trivial consequence of quantum theory. Therefore, one may appreciate that quantum interferences may lead to different transition matrix elements (or equivalently to rate constants) if QE and decoherence would be taken into account properly instead of regarding them just as individual, independent particles. For example, recently, the existence of short lived QE has been also investigated in a chemical reaction. Specifically, the electrolysis of acidic H_2O/D_2O mixtures has been performed using a mercury drop electrode. The electrochemical kinetics results show a volcano type of deviation of the rate constants from the behavior expected from nominal D and H concentrations. Various strategies have failed to explain the experimental results on a classical basis [65].

The effects found in this work give strong evidence that the nuclei possess quantum nature in chemical bonds when looked at during a time scale which is short enough. Therefore, it is believed that the effects found here are important for a better understanding of chemical kinetics and transport phenomena in condensed matter systems at room temperature.

The work on short lived protonic QE and decoherence has opened up a new window for the investigation of short time dynamics of protons in condensed matter. It made a major advance in the last few years and attracted much interest amongst the scientific community. This progress was not only governed by the large number of different experiments done on hydrogen containing materials but also by the advance of the different theoretical models suggested thus far.

It is also important to note that the NCS results do not constitute the only experimental evidence for the existence of short lived protonic QE in condensed systems. Worth mentioning is also the neutron reflectivity work on H_2O/D_2O mixtures at the hydrophobic Si surface [66]. There, it has been found that the neutron coherent scattering length density of the mixture is anomalously larger than expected. Due to the values of the tabulated coherent scattering length densities of H, D, and O, this result corresponds to a "depletion" of light water at the Si surface which is in line with the reduced ratio of, e.g., σ_H/σ_D of the H_2O/D_2O mixtures as measured with NCS [31].

It is anticipated that the future development of this research field will be directed by the following issues: (1) how does the electronic structure the proton is embedded in influence the creation and destruction of QE; (2) the different theoretical models put forward by several scientists should be subjected to experimental tests; (3) the nature of the short lived QE in condensed matter should be examined using different experimental techniques operating at time scales short enough to access the fast and effective process of decoherence; (4) visualizing the relevance of QE and decoherence for

chemistry, the theoretical as well as experimental investigation of the short time dynamics of chemical reactions is desirable.

Chapter 2

Quantum Entanglement (QE) and Decoherence

Certain features of quantum physics are undeniably strange, because they contradict the intuitive, and seemingly reasonable, assumptions about how the world should behave that can be deduced from classical physics. The most emblematic feature of quantum mechanics is the appearance of non-separability or Quantum Entanglement (QE). One can define entangled quantum states of two (or more) particles in such a way that their global state is perfectly defined, whereas the states of the separate particles remain totally undefined. Some thinking was necessary to realize how weird this is. In 1935 it led Einstein, Podolsky and Rosen (EPR) [19] to suggest that quantum mechanics is incomplete, on the basis that any theory of nature must be both "local" and "realistic" [19, 20, 67]. Local realism which is indispensable for classical mechanics is the idea that, because the properties of one particle cannot be affected by a particle that is sufficiently far away, all properties of each particle must exist before they are measured. But non-separability or QE contradicts this sort of local realism [9, 16, 19, 20, 67].

Thirty years after the seminal EPR paper [19] it became possible to test experimentally this fundamental contradiction between classical and quantum mechanics. The overall agreement with quantum mechanics observed in all experiments of quantum optics as well as experiments involving the interference of matter waves like neutron diffraction and interferometry is outstanding (compare e.g. ref. [68]) and one can safely conclude that quantum mechanics is a complete theory and cannot be reconciled with classical physics.

To begin with, let us note that QE relies on the *superposition principle* of quantum mechanics. This principle states that if ψ_1 and ψ_2 are the wavefunctions of two possible states of a system, then a superposition of them,

i.e.

$$\Psi = c_1\psi_1 + c_2\psi_2 \tag{2.1}$$

is also a legitimate state of this system. This leads to the Schrödinger's cat paradox and to interference phenomena which are well known to chemists from the first lectures of quantum mechanics. Interference patterns have been found for photons, electrons and neutrons. In the case of a double slit experiment this means that the particle passing the double slit has to be described by this kind of superposition because there is no way of knowing, not even in principle, through which slit the particle passes. As soon as a measurement is performed on this system to reveal the which way information, the interaction with the particle leads to decoherence and the interference pattern disappears.

What is harder to accept is the fact that more massive particles like atoms and small as well as large molecules also exhibit this quantum feature, i.e., they also show interference patterns on a screen placed behind a slit system. For example, in 1991 two atom interferometers have been introduced; one by Carnal and Mlynek using a supersonic beam of metastable He atoms [69] and another one by Keith et al. using Na atoms [70]. In 1995 interference patterns of Na_2 molecules have been achieved by Chapman et al. [71]. The upper limit record for the size of a system showing quantum behavior was set by Hackermüller et al. when achieving interference patterns of $C_{60}F_{48}$ molecules [72]. For more experiments see [4, 8]. These experiments suggest that an atom or a molecule as a whole must be regarded as subject to delocalization with Schrödinger's cat behavior.

So far, the experiments mentioned here dealt with *single* particles (atoms, molecules, etc.) passing an interferometer thus leading to the interference of the particle with itself. Therefore, the next question which arises is whether these quantum features are also apparent in *condensed matter* systems where more than one particle is involved in the superposition.

Consider a source emitting a pair of particles with opposite spins. If particle 1 travels to the left and carries spin up then particle 2 travelling to the right necessarily carries a spin down. Because of the lack of knowledge about which particle is carrying which spin, the system's state vector is described by

$$\Psi(1,2) = 1/\sqrt{2}(|\uparrow\rangle_1|\downarrow\rangle_2 + e^{i\Phi}|\downarrow\rangle_1|\uparrow\rangle_2). \tag{2.2}$$

This equation describes what is called *Quantum Entanglement* of particles 1 and 2. In terms of the superposition principle, quantum entanglement is the superposition of product states. These considerations can be easily extended to more than two particles and one ends up with multiparticle QE [8].

In order to point out the relevance of these considerations in the context of chemistry, let us give a simple example. Let A and B be two protons in, e.g., neighboring C-H bonds of one molecule. Furthermore, let the one-particle wave functions ψ_i (and ϕ_j) represent possible quantum states of proton A (and proton B) in the "first" (and "second") C-H bond. Since the protons A and B do not exchange their positions, all ψ_i (all ϕ_j) are located around the classical position of proton A (of proton B). Quantum mechanics predicts that a possible state $\Psi(A, B)$ of these two protons is given by

$$\Psi(A, B) = c_1\psi_1(A) \cdot \phi_1(B) + c_2\psi_2(A) \cdot \phi_2(B) + ... \tag{2.3}$$

If the sum in the right-hand side of this equation contains at least two terms, then $\Psi(A, B)$ represents an entangled state. Obviously, this $\Psi(A, B)$ does *not* factorize into an unentangled (product) state $\Psi'(A) \cdot \Phi'(B)$, in which the wave function $\Psi'(A)$ depends only on coordinates (or, more general, degrees of freedom) of proton A, and $\Phi'(B)$ only on those of B. The number of coefficients c_i (see eq.(2.3)) is invariant with respect to unitary transformations $U^{(A)}$ or $U^{(B)}$. If the absolute value of all non-vanishing Schmidt coefficients for a given state Ψ are all equal, the state is called *maximally entangled* [4].

From the viewpoint of classical mechanics, entangled states have counter-intuitive properties. E.g., if one actually performs a local measurement on proton A and finds it in a specific state, say $\psi_2(A)$, then it follows immediately and instantaneously that the "distant" proton B is in the specific state $\phi_2(B)$, without to perform any measurement on B. (This follows from the basic reduction postulate of quantum mechanics, cf. e.g. [64, 73]) How weird this is becomes obvious by noting that the above reasoning is independent of the actual distance between A and B. Indeed, in a successful experiment demonstrating quantum cryptography using entanglement between photon pairs, this distance was about 23 kilometers [74].

A well known quantum mechanical effect leading to QE are the *exchange correlations* arising from the identity of particles [73]. For example, such correlations lead to formation of ortho- and para-hydrogen, the wave functions of which exhibit spatial and spin entanglement. The spatial part of the total wave function of a H_2 molecule is given by

$$\Psi(A, B) = \frac{1}{\sqrt{2}}[\psi(A) \cdot \phi(B) \pm \psi(B) \cdot \phi(A)] \tag{2.4}$$

where the "+" and "−" cases are combined with a singlet and a triplet spin-state, respectively. Here, ψ and ϕ are single-particle states. Note that, as also eq. (2.3) above, this wave function does not factorize into an unentangled state, say $\psi'(A) \cdot \phi'(B)$. The probability for finding particle A in a space

element d^3x around its position x and particle B in a space element d^3y around its position y is:

$$\frac{1}{2}(\mid \psi_A(x) \mid^2 \mid \psi_B(y) \mid^2 + \mid \psi_A(y) \mid^2 \mid \psi_B(x) \mid^2 \pm 2Re[\psi_A(x)\psi_B(y)\psi_A^*(y)\psi_B^*(x)])d^3xd^3y. \tag{2.5}$$

If the two particles A and B are spatially separated – which is the case in the molecular systems under consideration in this work – the overlap between ψ_A and ψ_B will be negligible. Being so, the last term in eq.(2.5), which is known as the exchange density, will be negligibly small and therefore, only one of the two first terms will contribute to eq. (2.5) [73]. As a consequence, exchange correlations are important only when there is a substantial overlap between $\psi_A(x)$ and $\psi_B(y)$. Because in the molecular systems under consideration here the hydrogen nuclei are spatially well separated, exchange correlations are considered to be of less importance.

In addition to the above argument, the protons under consideration do not occupy equivalent (and thus indistinguishable) sites, because the electronic bondings and/or (intra- and intermolecular) environments of different protons are not identical. This implies that the protons may become "distinguishable" by virtue of their interactions with their environments. This process is well known in many-body physics, where one often speaks about "dressing" of particles with "environmental degrees of freedom".

It is very interesting to note that QE is not restricted to "identical" or "indistinguishable" objects but QE is also possible between two completely different objects and even between a *microscopic* and *macroscopic* system. For example an atom travelling across a cavity gets entangled with the field mode where the lifetimes of the cavity fields and the atomic two level system are much longer than the interaction time. Thus, the field and the atom remain quantum entangled via:

$$|\Psi\rangle = \frac{1}{\sqrt{2}}(|e, \alpha e^{i\Phi}\rangle + |g, \alpha e^{-i\Phi}\rangle) \tag{2.6}$$

even after the atom has left the cavity [8]. Here $|g\rangle$ and $|e\rangle$ ar the ground and excited states of the atom, respectively, and the second part represents the cavity field. This is a quantum entangled state, the energy of the atom being correlated to the phase of the cavity field. This example is instructive since it also shows how the interaction between two objects can create QE.

Since this universal mechanism for QE creation is less known in the field of chemistry, it is explained in more detail in the following.

For the following it is *not* necessarily assumed that A and B are indistinguishable particles in the sense of quantum mechanics. The two particles,

characterized by the Hamiltonians H_A and H_B, may interact either directly (e.g. through Coulombic forces) or indirectly (via a third subsystem, e.g. environmental electronic charges), the interaction Hamiltonian being

$$V_{AB} \equiv V(q_A, q_B, q_{env}). \tag{2.7}$$

(q_x: dynamical variables of system x). q_{env} refers to the additional degrees of freedom of the environment being involved in the interaction. As usually assumed, let the state of the composite system "A and B", in short AB, at time $t = 0$ be not entangled, i.e.

$$\Psi_{AB}(0) = \Psi_A \cdot \Psi_B \ . \tag{2.8}$$

In all non-trivial cases, V_{AB} does *not* commute with H_A or H_B, respectively,

$$[V_{AB}, H_A] \neq 0, \tag{2.9}$$

$$[V_{AB}, H_B] \neq 0. \tag{2.10}$$

According to basic quantum mechanics it then follows that, for $t > 0$, the complete evolution operator of the composite system AB,

$$U_{AB}(t) = \exp\{-i(H_A + H_B + V_{AB})t/\hbar\}, \tag{2.11}$$

does *not* factorize into a product of two "individual" evolution operators, say U_A and U_B, representing the dynamics of the individual systems A and B, respectively [73]. Consequently, the wave function at time t, $\Psi_{AB}(t) = U_{AB}(t)\Psi_{AB}(0)$, does not separate into a product of two wave functions, each of them representing the state of one of the two systems A and B [73]; i.e.

$$\Psi_{AB}(t) = U_{AB}(t)\Psi_{AB}(0) \neq \Psi'_A(t) \cdot \Psi'_B(t) \ . \tag{2.12}$$

As mentioned above, this is tantamount to saying that $\Psi_{AB}(t)$ represents an entangled state, and thus (a part of) the degrees of freedom of A and B are inextricably intertwined. This wave function is then of the type given by eq.(2.3).

Thus, QE is expected to appear quite naturally in interacting systems, like the condensed molecular systems studied in this work. In particular, it is noted that QE creation arises from the openness of a quantum system and is represented by a non-unitary time evolution of the system. Note also that the above mentioned dynamical process leading to QE is independent of the "exchange correlations mechanism" discussed above. Moreover, it should be emphasized that the QE considered here does not concern all

degrees of freedom of the systems A and B, but only those appearing in the interaction Hamiltonian V_{AB}. This shows that *spatial* QE is of fundamental importance, because the strongest interactions of the nuclei in the molecular systems studied here are given by the Coulombic interactions (concerning nuclei and electrons), which depend on the spatial degrees of freedom of the participating particles.

It should be also mentioned that this type of QE-creation due to the openness of the quantum system is dominant in all investigations concerning the modern (scientific and technological) fields of quantum computation, information, communication and cryptography. Controlling the interaction Hamiltonian(s) V_{AB} makes possible to engineer various degrees (and types) of entanglement; compare [8, 24, 75].

In the same sense as the interaction of particle A with B mentioned in the previous section lead to the creation of QE, the openness of the combined system S=A+B is required to address the question of decoherence. Generally speaking, an open quantum system is a system which is coupled to another quantum system *Env* called the environment. In most cases it is assumed that the combined system is closed following Hamiltonian dynamics. The state of the subsystem S, however, will change as a consequence of its internal dynamics and of the interaction with the surrounding. If initially the open quantum system S exhibits QE, then its interaction with *Env* leads to certain system-environment correlations and to the irreversible delocalization of the phase relations within S, i.e., between A and B. This environment-induced, dynamical destruction of quantum coherence is called *decoherence*. The resulting state changes of S can no longer, in general, be described in terms of unitary Hamiltonian dynamics.

The irreversibility of this process – which is extremely fast in condensed systems – is due to the existence of an infinite number of degrees of freedom of the environment [4]. Therefore, and due to the large number of present particles, it can be described only within the framework of the *density matrix formalism*. Accordingly, instead of using a wave vector equation of motion, the dynamics of an open quantum system has to be described by means of an appropriate equation of motion for its density matrix, which is called *quantum master equation* [4]. The necessity of using density matrices is due to the fact that it must be accounted for the lack of complete knowledge about the system. Consider for example a system whose state is represented by a superposition

$$|\Psi\rangle = \sum_n c_n |u_n\rangle \tag{2.13}$$

of basis states with weights $|c_i|^2$. It is appropriate to define the system's

density matrix as:

$$\rho = |\Psi\rangle\langle\Psi|. \tag{2.14}$$

The simplest density matrix is the one in which there is only one possible superposition. In this case the state of the system can be described as well by a state vector as by a density matrix. However, in the context of the present work the system consists usually of a large number of particles as well as numbers of degrees of freedom. Accordingly, there is a large number of possible superpositions the system might be involved in. Therefore, the state and dynamics of the systems relevant for this work has to be described in the framework of density matrix formalism.

Given any density matrix, its *diagonal elements* represent the *populations* of the corresponding states and the *non-diagonal elements* give the *correlations* or *coherences* between these states. It should be noted that there is no unitary transformation which makes the non-diagonal elements vanish and lets the diagonal ones unaffected. This means that there is no unitary transformation which transform a mixed state into a pure one or vice versa [1].

In thermodynamics, the density matrix (or density operator) of a system having the Hamiltonian H and being in thermal equilibrium is given by

$$\rho = Z^{-1} e^{-H/kT} \tag{2.15}$$

with Z being the corresponding partition function. Assuming the system to be in a *stationary state* $|u_n\rangle$

$$\rho_{nn} = Z^{-1}\langle u_n|e^{-H/kT}|u_n\rangle = Z^{-1}e^{-E_n/kT}\langle u_n|u_n\rangle = Z^{-1}e^{-E_n/kT}. \tag{2.16}$$

Accordingly,

$$\rho_{np} = Z^{-1}\langle u_n|e^{-H/kT}|u_p\rangle = Z^{-1}e^{-E_p/kT}\langle u_n|u_p\rangle = 0. \tag{2.17}$$

It means that at thermodynamic equilibrium, the populations are exponentially decreasing functions of energy and that there are no coherences between the stationary energy eigenstates (because of their orthogonality). However, as stated in the introduction the states of interacting particles in condensed matter system are not strictly stationary.

The rigorous theoretical description of the dynamics of an open quantum system requires the solution of a large number of coupled equations of motion due to the large (sometimes infinite) number of degrees of freedom of the total system (consisting of the system under consideration and its surrounding) [4]. This is of course far too complicated and even if a solution is known, it is sufficient if one isolates and determines the interesting physical quantities

through an average over the remaining irrelevant degrees of freedom. If the state of the total system is described by some density matrix ρ, then the expectation values of all observables acting on the Hilbert space of the open system are determined by

$$\langle A \rangle = tr_S\{A\rho_S\}, \tag{2.18}$$

where $\rho_S = tr_{env}\rho$ is the so called *reduced density matrix* of the open system S after tracing over the degrees of freedom of the environment. The dynamics of the subsystem S induced by the Hamiltonian evolution of the total system is often referred to as "reduced system dynamics", and S is also called *reduced* or *relevant* system. Therefore, instead of using the density matrix ρ of the total system, it is the *reduced density matrix* ρ_S which is of interest in the discussion of decoherence.

Since the total system is assumed to be closed, its wave vectors obey the time dependent Schrödinger equation, and consequently the time evolution of the density matrix of the closed system is given by

$$\begin{aligned} \frac{d}{dt}\rho(t) &= \left(\frac{d}{dt}|\Psi(t)\rangle\right)\langle\Psi(t)| + |\Psi(t)\rangle\left(\frac{d}{dt}\langle\Psi(t)|\right) \\ &= \frac{1}{i\hbar}\hat{H}(t)|\Psi(t)\rangle\langle\Psi(t)| + \frac{1}{-i\hbar}|\Psi(t)\rangle\langle\Psi(t)|\hat{H}(t) \\ &= \frac{1}{i\hbar}[H(t),\rho(t)] \end{aligned} \tag{2.19}$$

which is called the *Liouville-von Neumann equation*. Due to the hermiticity of the involved Hamilatonian, the time evolution of the total system's density matrix is necessarily unitary.

Due to the unitary evolution of the total system's density matrix, one obtains the reduced density matrix at time t by taking the partial trace over the degrees of freedom of the environment

$$\rho_S(t) = tr_{env}\{U(t,t_0)\rho(t_0)U^\dagger(t,t_0)\}, \tag{2.20}$$

where $U(t,t_0)$ is the time-evolution operator of the total system or, using the Liouville-von Neumann equation (eq. (2.19)),

$$\frac{d}{dt}\rho_S(t) = \frac{1}{i\hbar}tr_{env}[H(t),\rho(t)]. \tag{2.21}$$

This equation is exactly valid but cannot be solved for condensed matter systems and has therefore to be approximated.

In order to simplify the theoretical treatment, one develops a dynamical theory in the short time range, so that memory effects can be neglected and

formulates the reduced system's dynamics in terms of a so called *quantum dynamical semigroup*. It is out of the scope of the present work to go into the mathematical details of maps and semigroups. Therefore, they will be mentioned but not explained in detail. The following derivations are excerpted from [4].

Let us consider an open system S immersed in a larger environment *Env* and assume that there are no correlations between them. The total system's density matrix at time t_0=0 is then given by

$$\rho(0) = \rho_S(0) \otimes \rho_{env}(0). \tag{2.22}$$

At a later time the reduced system's density matrix will have the form

$$\rho_S(t) = V(t)\rho_S(0) \equiv tr_{env}\{U(t,0)[\rho_S(0) \otimes \rho_{env}(0)]U^\dagger(t,0)\}. \tag{2.23}$$

Expressing the *dynamical map* $V(t)$ acting on the subsystem's Hilbert space in terms of a complete set of orthonormal operators F_i, i.e.,

$$V(t)\rho_S = \sum_{i,j=1}^{N^2} c_{ij}(t) F_i \rho_S F_j^\dagger \tag{2.24}$$

such that

$$(F_i, F_j) \equiv tr_S\{F_i^\dagger F_j\} = \delta_{ij}, \tag{2.25}$$

the dynamics of the reduced system can be written as

$$\frac{d}{dt}\rho_S = \hat{L}\rho_S = -i[H, \rho_S] + \sum_{i,j=1}^{N^2-1} a_{ij}\left(F_i \rho_S F_j^\dagger - \frac{1}{2}\{F_j^\dagger F_i, \rho_S\}\right), \tag{2.26}$$

where the coefficients a_{ij} are defined by

$$a_{ij} = \lim_{t\to 0} \frac{c_{ij}(t)}{t} \tag{2.27}$$

with $i, j = 1, ..., N^2 - 1$ [4]. Equation (2.26) is the so called *Lindblad master equation*. It is used in many fields like in quantum optics, for the decay of a two level system, or in resonance fluorescence. It can be transformed in a diagonal form

$$\hat{L}\rho_S = -i[H, \rho_S] + \sum_{k=1}^{N^2-1} \gamma_k \left(A_k \rho_S A_k^\dagger - \frac{1}{2} A_k A_k^\dagger \rho_S - \frac{1}{2}\rho_S A_k A_k^\dagger\right) \tag{2.28}$$

by introducing a new set of operators

$$F_i = \sum_{k=1}^{N^2-1} u_{ki} A_k \tag{2.29}$$

and by taking advantage of the fact that the matrix a_{ij} of eq.(2.26) is positive and can be diagonalized using an appropriate unitary transformation u

$$uau^{\dagger} = \begin{pmatrix} \gamma_1 & 0 & 0 & 0 \\ 0 & \gamma_2 & 0 & 0 \\ 0 & 0 & \ddots & 0 \\ 0 & 0 & 0 & \gamma_{N^2-1} \end{pmatrix}. \tag{2.30}$$

The first term of eq.(2.28) is the usual unitary part of the dynamics generated by the system's relevant Hamiltonian whereas the second part, also called *dissipator*, describes the irreversible dynamics. In the case of initially entangled states the non-unitary part describes the decoherence process by establishing quantum entanglement between the system and the environment. The non-negative quantities γ_k's which have the dimension of an inverse time (if the A's are taken dimensionless) represent the *decoherence* or *relaxation rate*.

This equation provides the most general form for a bound generator in a separable Hilbert space. It should be noted that although this equation is valid only if the generator $\hat{L}$ is bounded and that in realistic physical applications the system's Hamiltonian as well as the Lindblad operators F are in general unbounded, all known examples for generators of quantum dynamical semigroups are either of Lindblad form or can be cast into it after slight modifications [4].

One interesting application of the Lindblad equation is the scattering of particles by a system consisting of spatially quantum correlated objects. Writing down the corresponding Lindblad equation in the position representation (see eq. 2.28)

$$\hat{L}\rho_S = -i[H, \rho_S] - \Lambda[\mathbf{x}, [\mathbf{x}, \rho_S(t)]] \tag{2.31}$$

and taking into account that the dynamics of the unitary part is orders of magnitude slower than the non-unitary one (i.e. due to decoherence), one gets the result [76]

$$\rho_S(t, \mathbf{x}, \mathbf{x}') \approx \exp^{-\Lambda(\mathbf{x}-\mathbf{x}')^2 t} \rho_S(0, \mathbf{x}, \mathbf{x}'). \tag{2.32}$$

This illustrates how the non-diagonal elements of the reduced density matrix in the position representation decay in the course of time with the decay rate Λ. $\Delta x = |\mathbf{x} - \mathbf{x}'|$ is the distance between two positions of the scattering center and is also a measure of the distance to the diagonal of the density matrix. It is used to estimate the decoherence rate [4, 10]. This particular form is shown here because it has been successfully used in a model which qualitatively interprets the anomalous scattering results found in this work (see chapter 9).

It should be noted again that the derivations briefly described here presume Markovian behavior, i.e., they neglect memory effects. However, there exist also theoretical treatments, for example the *projection operator technique* introduced by Nakajima [77] and Zwanzig [78], or the *time-convolutionless technique* [79–81], with which non-Morkovian features of the dynamics of open quantum systems can be treated [4]. However, these methods will not be considered further.

Chapter 3

Elements of neutron scattering theory

3.1 General

The basic quantity that is measured in a neutron scattering experiment is the partial differential cross section ($\frac{d^2\sigma}{d\Omega dE_1}$). This quantity gives the fraction of neutrons of incident energy E_0 scattered with an energy between E_1 and $E_1 + dE_1$ into a small solid angle $d\Omega$ (see Fig. 3.1). After applying *Fermi's Golden Rule* for the transition of the combined system consisting of the scattering target and the neutron from their initial into their final states, the partial differential cross section can be written as [26]:

$$\left(\frac{d^2\sigma}{d\Omega dE_1}\right)_{\lambda_0\to\lambda_1} = \frac{k_1}{k_0}\frac{m}{2\pi\hbar^2}|\langle\mathbf{k}_1\lambda_1|V|\mathbf{k}_0\lambda_0\rangle|^2\delta(E_{\lambda_0} - E_{\lambda_1} + \hbar\omega) \tag{3.1}$$

in which $|\lambda\rangle$ represents a many body eigenstate of the Hamiltonian of the system generally being constituted of interacting particles. $\mathbf{k}$ is the wave vector of the neutron, m is the neutron mass, $\hbar$ is Planck's constant divided by 2π and the δ-function expresses the energy conservation during the scattering process. The indices "1" and "0" refer to quantities after and before collision, respectively. $\hbar\omega$ is the energy transfer with

$$\hbar\omega = E_0 - E_1 = \frac{\hbar^2}{2m}(k_0^2 - k_1)^2 \tag{3.2}$$

being associated with the momentum transfer $\mathbf{q}$

$$\mathbf{q} = \hbar\mathbf{k}_0 - \hbar\mathbf{k}_1 \tag{3.3}$$

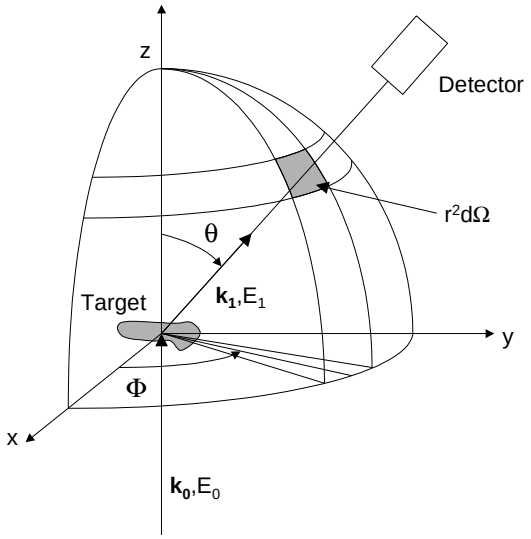

Figure 3.1: Geometry of the scattering problem. An incident neutron with wave vector $\mathbf{k}_0$ and energy E_0 is scattered by the target into a final state with wave vector $\mathbf{k}_1$ and final energy E_1.

the modulus of which varies with scattering angle θ according to the relation [82]

$$q = (k_0^2 + k_1^2 - 2k_0k_1\cos\theta)^{1/2}. \tag{3.4}$$

The ratio $\frac{k_1}{k_0}$ in eq.(3.1) arises from the normalization of the scattered intensity by the flux of the incident neutrons and from the number of momentum states appearing in Fermi's Golden Rule [26]. This ratio is very important, since it implies the momentum transfer dependence of the scattering cross section which will become relevant in view of the angle dependent cross section density of the protons in some of the metal hydrides investigated in this work (see section 7.3). V in eq.(3.1) is the scattering potential of the whole system and is dependent on the distance $\mathbf{x}_j = \mathbf{r} - \mathbf{R}_j$ between the coordinate of the neutron ($\mathbf{r}$) and the position of the scattering nucleus ($\mathbf{R}_j$) and is given by:

$$V = \sum_j V_j(\mathbf{x}_j). \tag{3.5}$$

Assuming a plane wave for the incoming and outgoing neutron, the following expression can be written for the matrix element appearing in eq.(3.1):

$$\langle \mathbf{k}_1\lambda_1|V|\mathbf{k}_0\lambda_0\rangle = \sum_j V_j(\mathbf{q})\langle\lambda_1|exp(i\mathbf{q}\cdot\mathbf{R}_j)|\lambda_0\rangle \tag{3.6}$$

with $V_j(\mathbf{q})$ being the Fourier Transform of $V_j(\mathbf{x}_j)$

$$V_j(\mathbf{q}) = \int V_j(\mathbf{x}_j) exp(i\mathbf{q}\cdot\mathbf{x}_j) d\mathbf{x}_j \tag{3.7}$$

and

$$V_j(\mathbf{x}_j) = \frac{2\pi\hbar^2}{m}\ b_j\ \delta(\mathbf{x}_j). \tag{3.8}$$

As a result

$$\left(\frac{d^2\sigma}{d\Omega dE_1}\right)_{\lambda_0\to\lambda_1} = \frac{k_1}{k_0}|\sum_j b_j \langle\lambda_1|exp(i\mathbf{q}\cdot\mathbf{R}_j)|\lambda_0\rangle|^2 \delta(E_{\lambda_0} - E_{\lambda_1} + E_0 - E_1). \tag{3.9}$$

V_j in eq.(3.8) is the so called *Fermi's pseudopotential*. The prefix "pseudo" refers to the fact that it does not correspond to the actual potential. A repulsive pseudopotential gives a positive scattering length but a positive scattering length does not necessarily imply a repulsive potential [26]. For the justification for the usefulness of the pseudopotential, see below. The δ-function in eq.(3.8) expresses the short range character of the nuclear potential within the static approximation. This equation relates the scattering process to a quantity b, called scattering length, being a measure for the amplitude of the wave function of the neutrons scattered on a fixed nucleus.

Since there is no proper theory of nuclear forces, there is no possibility to calculate or predict the values of b from other properties of the nucleus than from experimental ones. The above given scattering length is the so called *bound scattering length*.

If the nucleus of mass M is not fixed during the collision (i.e. when high energies and momenta are transferred during the scattering), then the scattering process must be treated within the center-of-mass system, i.e. the neutron mass m must be replaced by the reduced mass μ of the whole system and the so called *free scattering length* b_f becomes relevant. Since the potential (eq.(3.8)) is the same for a fixed and a free nucleus, it holds that

$$\frac{b_f}{\mu} = \frac{b}{m} \tag{3.10}$$

and therefore

$$b_f = \frac{M}{m+M}\ b. \tag{3.11}$$

The scattering length is related to the total scattering cross section σ_{tot} - which is of central importance for the present work - by [26]

$$\sigma_{tot} = 4\pi b^2. \tag{3.12}$$

When high values of energy are transferred during the scattering, as is the case in Neutron Compton scattering (NCS) applied in this work, the nuclei (e.g. protons, deuterons, etc.) are kicked out of their initial positions and therefore they are regarded as free (see section 3.2 for more details). In order to compare the measured scattering cross section densities with the tabulated ones, the conversion from the free to the bound scattering length (according to eq.(3.11)) is very essential for the present work.

The derivation of the scattering cross section is based on Fermi's Golden Rule [26]. For scattering processes, this is equivalent to the *Born Approximation* stating that if the perturbation on the incident wave due to scattering is small, then the wave function after the scattering process $|k_1\lambda_1\rangle$ can be replaced by the initial function of the total system [27]. Both Fermi's Golden Rule and the Born Approximation are based on first-order perturbation theory. The conditions for this theory to apply do not hold for the nuclear scattering of thermal neutrons because of high q values [26]. However, although the nucleon-nucleon interaction is very strong, it is sufficiently short-ranged that the scattering is a weak perturbation of the incident wave. Therefore, using Fermi's pseudopotential (eq.(3.8)) – which contains a δ-function of the nuclear position –, the scattering may be described in the first Born approximation. A further justification for the use of the Golden Rule in these circumstances is that, when combined with the Fermi pseudopotential, it gives the required result of s-wave (i.e. isotropic) scattering for a single fixed nucleus [26, 27].

Using the definition of the δ-function for the energies involved in the scattering process

$$\delta(E_{\lambda_0}-E_{\lambda_1}+E_0-E_1) = \frac{1}{2\pi\hbar}\int_{-\infty}^{+\infty} exp(i(E_{\lambda_0}-E_{\lambda_1})t/\hbar)exp(-i\omega t)dt, \quad (3.13)$$

using the eigenvalue equation for the system's state in the Heisenberg notation

$$exp(-i\hat{H}t/\hbar)|\lambda\rangle = exp(-iE_\lambda t/\hbar)|\lambda\rangle \quad (3.14)$$

and summing over the initial states $|\lambda_0\rangle$ and averaging over the final ones $|\lambda_1\rangle$, eq.(3.9) assumes the following form:

$$\frac{d^2\sigma}{d\Omega dE_1} = \frac{k_1}{k_0}\frac{1}{2\pi\hbar}\sum_{j,j'}^{N} b_j b_{j'}\int_{-\infty}^{+\infty}\langle exp(-i\mathbf{q}\cdot\mathbf{R}_{j'}(0))exp(i\mathbf{q}\cdot\mathbf{R}_j(t))\rangle exp(-i\omega t)dt \quad (3.15)$$

in which $\mathbf{R}_j(t)$ is the position operator of the j^{th} nucleus in the Heisenberg picture and

$$\langle ...\rangle = \sum W_n\langle n|...|n\rangle \quad (3.16)$$

is the appropriate combined quantal and thermodynamic average (over the classical probabilities W_n) related with the condensed matter system. The latter quantity is termed the *intermediate scattering function*

$$F_{jj'}(\mathbf{q},t) = \langle exp(-i\mathbf{q}\cdot\mathbf{R}_{j'}(0))exp(i\mathbf{q}\cdot\mathbf{R}_j(t))\rangle. \tag{3.17}$$

It is a density-density correlation function and is of central importance for the neutron scattering theory and its various applications in neutron scattering experiments.

It is worth noting here, that in the derivations shown above the Hamiltonian of the scattering system is assumed to be self adjoint and the states are assumed to be stationary. Therefore, this treatment neglects the presence of dynamic time dependent interactions. The unitarity of the evolution operator $U(t,t_0)$ arises from the presumption that the Hamiltonian is hermitian. The validity of the sum rules in turn arise from these assumptions [26]. In the presence of time dependent interactions, however, the evolution operator is no longer unitary. Consequently, it is justified to assume the Hamiltonian to be non-hermitian. The non-hermiticity of the Hamiltonian means that also the probability is not necessarily conserved [3]. This is well known from decaying states, also called Gamov states. Decoherence is a process which involves interactions and decaying (quantum entangled) states. Therefore, the derivations shown above are no longer valid for systems exhibiting decoherence.

3.2 Neutron Compton scattering

The neutron Compton scattering (NCS) technique [83, 84] (also called deep inelastic neutron scattering, DINS) uses "high energetic" (so-called epithermal) neutrons with kinetic energies up to some hundreds eV. Sufficiently intense fluxes of such neutrons are presently provided only by pulsed neutron spallation sources. The experiments the results of which are presented in this work have been performed with the VESUVIO spectrometer of the ISIS spallation neutron source (Rutherford Appleton Laboratory, U.K.). For instrument description see chapter 4.

Beside the Born Approximation which has been discussed in the previous section, the NCS relies on two other approximations, namely the *incoherent approximation* and the *impulse approximation*. Both approximations arise from the fact that high transfers of momentum and energy are involved in the scattering process.

3.2.1 Incoherent Approximation

When the momentum transfer

$$q \gg 2\pi/d, \tag{3.18}$$

where d is the nearest-neighbor distance, then interference effects due to scattering on different nuclei are averaged out. Therefore, eq.(3.17) reduces to those contributions excluding $j \neq j'$ thus giving the intermediate scattering function in the incoherent approximation

$$F_{jj}(\mathbf{q}, t) = \langle exp(-i\mathbf{q} \cdot \mathbf{R}_j(0)) exp(i\mathbf{q} \cdot \mathbf{R}_j(t)) \rangle. \tag{3.19}$$

Accordingly the partial differential cross section (eq.(3.15)) can be written as [85]

$$\frac{d^2\sigma}{d\Omega dE_1} = Nb^2 \frac{k_1}{k_0} \frac{1}{2\pi\hbar} \int_{-\infty}^{+\infty} \langle exp(-i\mathbf{q} \cdot \mathbf{R}_j(0)) exp(i\mathbf{q} \cdot \mathbf{R}_j(t)) \rangle exp(-i\omega t) dt \tag{3.20}$$

or more conveniently

$$\frac{d^2\sigma}{d\Omega dE_1} = Nb^2 \frac{k_1}{k_0} S_i(\mathbf{q}, \omega). \tag{3.21}$$

$S_i(\mathbf{q}, \omega)$ is termed *incoherent dynamic structure factor* and is the time Fourier Transform of the intermediate scattering function, eq.(3.17):

$$S_i(\mathbf{q}, \omega) = \frac{1}{2\pi\hbar} \int exp(-i\omega t) F(\mathbf{q}, t) dt. \tag{3.22}$$

It should be noted that $S_i(\mathbf{q}, \omega)$ is a part of $S(\mathbf{q}, \omega)$ [27] and because for high momentum transfers it holds that $S(\mathbf{q}, \omega) \approx S_i(\mathbf{q}, \omega)$, the scattering looks virtually identical to the scattering that would be observed if it were completely incoherent [27]. And therefore it is justified to use the total scattering cross section σ_{tot}; see eq.(3.12).

The incoherent approximation implies that each atom is regarded as scattering independently of the other $N-1$ atoms. However, this does not mean that the scattering atom is treated as non-interacting like in an ideal gas. Rather, the surrounding atoms influence through interatomic forces the time variation of $\mathbf{R}_j(t)$ and consequently also that of $F_{jj}(\mathbf{q}, t)$. This fact is included in the many body quantum state $|\lambda\rangle$ being implicit in the above equations.

3.2.2 Impulse Approximation

The impulse approximation, hereafter abbreviated by "IA", has been first introduced by Chew [86] for the collision of a fast nucleon with a deuteron. For neutrons the approximation consists in assuming the time τ, taken by a fast incident neutron to traverse over the neutron-nucleus interaction region, is short compared with the characteristic time period of the nucleus. The collision then can be regarded as an "impulse" during which the binding serving only to determine the momentum distribution of the nuclear wave function. This means that the neutron senses only how fast the nucleus is moving [85]. To express this short time behavior of the nucleus after the scattering, the Heisenberg operator $\mathbf{R}(t)$ is expanded in a Taylor series

$$\mathbf{R}(t) = \mathbf{R} + \left(\frac{\mathbf{p}}{M}\right) \cdot t + \left(\frac{\mathbf{f}}{2 \cdot M}\right) \cdot t^2 + ... \tag{3.23}$$

(M being the mass of the nucleus) and terms with time orders higher than unity are neglected. This means that the force $\mathbf{f}$ experienced by the nucleus after the scattering is of no importance and therefore, the particle will behave as if it were free. With the above expansion, the intermediate scattering function (3.19) becomes

$$F_{jj}(\mathbf{q}, t) = \langle exp(-i\mathbf{q} \cdot R_j(0)) exp(i\mathbf{q} \cdot \mathbf{R}_j(t) + \frac{it}{M}\mathbf{q} \cdot \mathbf{p}_j)\rangle. \tag{3.24}$$

If two operators $\mathbf{A}$ and $\mathbf{B}$ commute with $[\mathbf{A}, \mathbf{B}]$ then

$$exp(\mathbf{A}) \cdot exp(\mathbf{B}) = exp(\mathbf{A} + \mathbf{B}) \cdot exp\left(\frac{[\mathbf{A}, \mathbf{B}]}{2}\right). \tag{3.25}$$

Using this relation and because the commutator of the position and momentum is a c-number,

$$[\mathbf{R}, \mathbf{p}] = i\hbar, \tag{3.26}$$

the intermediate scattering function reduces to

$$F(\mathbf{q}, t) = \exp(i\omega_r t) \left\langle \mathcal{T} \exp\left(i\mathbf{q} \cdot \int_0^t \mathbf{p}(t')/M \, dt'\right)\right\rangle. \tag{3.27}$$

$\mathcal{T}$ is the time-ordering operator, $\hbar\omega_r = (\hbar q)^2/2m$ is the recoil energy of the nucleus, and $\mathbf{p}/M = d\mathbf{r}/dt = \mathbf{v}$ is its velocity operator [87]. For the limiting case that $q \longrightarrow \infty$, the expression in the brackets will give contributions only if $t \longrightarrow 0$. In that case $\mathbf{p}(t')$ becomes time independent and consequently

$$F(\mathbf{q}, t) \longrightarrow exp(i\omega_r t)\langle exp[it\mathbf{q} \cdot \mathbf{v}]\rangle \tag{3.28}$$

and therefore

$$S(\mathbf{q},\omega) = \frac{1}{2\pi\hbar}\int exp(-i(\omega+\omega_r)t)\langle exp[it\mathbf{q}\cdot\mathbf{v}]\rangle)dt. \tag{3.29}$$

This equation is equivalent to

$$S(\mathbf{q},\omega) = \int n(\mathbf{p})\,\delta(\omega-\omega_r-\mathbf{q}\cdot\mathbf{p}/M)\,d\mathbf{p}. \tag{3.30}$$

$n(\mathbf{p})$ is the momentum distribution of the scattering nucleus. Equation (3.30) is of central importance in most NCS experiments, since it relates the scattering cross-section directly to the momentum distribution. Furthermore, $n(\mathbf{p})$ takes into account that, if the scattering nucleus has a momentum distribution, the δ-function centered at ω_r will be Doppler broadened. It should be mentioned here that within the IA, the interatomic forces are neglected only in the final state. Departures from the IA and their corrections will be described later (section 3.2.4).

In an isotropic system, $S(\mathbf{q},\omega)$ can be translated into a function which depends only on one parameter by introducing a scaling parameter y_M [88, 89] by

$$y_M = \mathbf{p}\cdot\hat{\mathbf{q}} = \frac{\mathbf{M}}{\mathbf{q}}\left(\omega-\omega_{\mathbf{r}}\right). \tag{3.31}$$

y_M is the component of atomic momentum along the direction of $\mathbf{q}$ and $\hat{\mathbf{q}} = \mathbf{q}/|\mathbf{q}|$ is the unit vector along the direction of $\mathbf{q}$. By taking the z axis to be the direction of the scattering vector $\mathbf{q}$ it then follows [87]

$$S(q,\omega) = \frac{M}{q}\int \delta(y-p_z)n(\mathbf{p})d\mathbf{p} = \frac{M}{q}J(y_M,\hat{\mathbf{q}}). \tag{3.32}$$

$J(y_M,\hat{\mathbf{q}})$ is the directional Compton profile and is proportional to the probability that an atom has a momentum component along the direction of $\hat{\mathbf{q}}$.

The definition of y_M implies that $S(q,\omega)$ is a Doppler broadened single peak being symmetrically centered at $y_M = 0$, or, equivalently, at the recoil energy ω_r. One sees from eq.(3.32) that $S(q,\omega)$ is inverse proportional to q at a fixed y_M. In an isotropic system the direction of $\mathbf{p}$ is immaterial and the momentum distribution reduces to the Compton profile $J(y_M)$ which is the probability that an atom has a momentum component y along an arbitrary direction in space.

The mean kinetic energy $\langle E_{kin}\rangle$ in isotropic samples is related to $J(y)$ by [87]:

$$\langle E_{kin}\rangle = \frac{3}{2M}\int_{-\infty}^{+\infty} y^2 J(y)dy. \tag{3.33}$$

If the atom is (at least approximately) harmonically bound, the momentum distribution assumes the Gaussian form

$$n(p) = \frac{1}{\sqrt{2\pi\sigma_p^2}} \exp\left(-\frac{p^2}{2\sigma_p^2}\right) \tag{3.34}$$

which is centered at the recoil energy ω_r; σ_p is the standard deviation of the momentum distribution. When different atomic masses M_i are present in the sample, the scattered intensity consists of different peaks centered at different recoil energies $\omega_{r,i}$ and the peak widths are determined by the momentum distributions $n_i(p)$ for each corresponding atomic mass. The associated mean kinetic energy $\langle E_{kin} \rangle$ is related to the width of the momentum distribution [90] by

$$\langle E_{kin} \rangle = \frac{3\sigma_p^2}{2M}. \tag{3.35}$$

3.2.3 Validity of the impulse approximation

Strictly speaking, the impulse approximation is valid only for momentum transfers $q \longrightarrow \infty$. In a real experiment, however, only finite momentum transfers are accessible. Therefore, the question arises, when the impulse approximation starts to break down and its implications to fail. Relaxing the condition $q \longrightarrow \infty$, it becomes evident from eq.(3.27) that the integration time becomes relevant in so far as it can be interpreted as to be the time of interaction of the neutron with the system [87]. By introducing a quantity τ such that

$$q v_0 \tau = 1, \tag{3.36}$$

where τ is the relevant interaction time between the neutron and the nucleus, Sears [87] suggests the requirement for the impulse approximation to be

$$f_0 \tau \ll M v_0 \tag{3.37}$$

or equivalently

$$q \gg \frac{f_0}{M v_0^2}, \tag{3.38}$$

where f_0 is the root mean square force the surrounding atoms exert on the scattered atom and v_0 is the root mean square velocity of the atom. The product of this force and the duration of interaction, i.e. $f_0\tau$, is the additional impulse the scattering atom receives from its environment during the scattering process. This condition is in line with the neglect of the force in eq.(3.23). In other words the work done by the force f_0 is negligible as

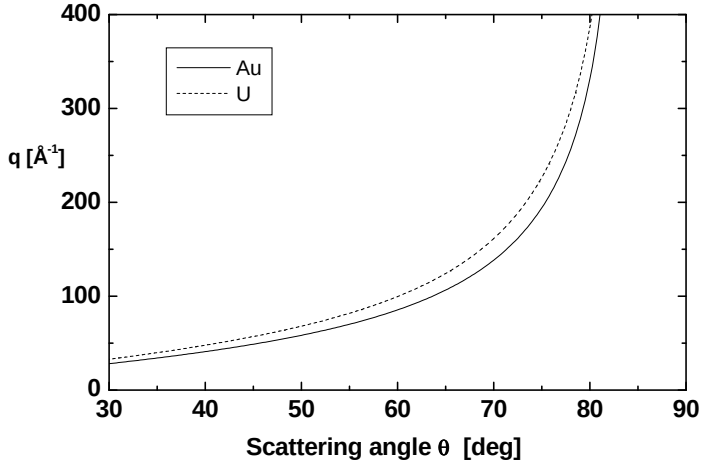

Figure 3.2: Momentum transfer q dependence on the scattering angle θ for scattering on protons using Au (full line) and U (dashed line) foils as energy analyzers.

compared with the root mean square kinetic energy associated with v_0 of the nucleus.

A different criterion for the validity of the impulse approximation at low temperatures has been given by Mayers [91]

$$q \gg p_i, \tag{3.39}$$

in which p_i is the root mean square atomic momentum in the initial state. Although low temperatures are of minor significance in this work, the criterion gives at least a lower limit for the validity of the impulse approximation, because as temperature increases p_i increases as well. In addition, this criterion agrees with criteria obtained also by other authors using different approaches [87, 92]. In particular, the criterion of Platzman and Tzoar [93]

$$q \gg \sqrt{2ME_B}, \tag{3.40}$$

is worth mentioning here, where E_B is the binding energy of the struck nucleus. The binding energy range of the proton in water or in a covalent bond is between [94]

$$4eV < E_B(H) < 5eV, \tag{3.41}$$

which gives in terms of momentum transfer

$$7\mathring{A}^{-1} < \sqrt{2ME_B(H)} < 8\mathring{A}^{-1}. \tag{3.42}$$

By inspection of Figs. 3.2 and 3.3, it is evident that the criterion of Platzman and Tzoar for the validity of the IA is fulfilled for protons.

Nevertheless, in order to be as comprehensive as possible, the inclusion of the forces exerted by the surrounding atoms on the scattered atom is given in the following section. Since this treatment refers to the state of the atom

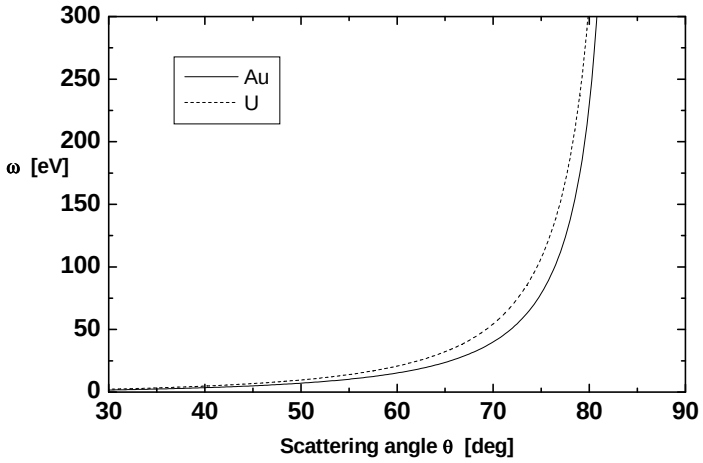

Figure 3.3: Energy transfer ω dependence on the scattering angle θ for scattering on protons using Au (full line) and U (dashed line) foils as energy analyzers.

after the scattering has occurred, it is termed *Final States Effects*. However, Mayers [91] showed that when the quantum nature of the system becomes relevant for the energy distribution, e.g. for the case of very low temperatures, also *Initial States Effects* will lead to deviations from the impulse approximation.

Initial state effects will not be discussed here since they become relevant at zero temperatures when the scattering system is quantum dominated and possesses the definite ground state energy and not an energy distribution (given by the momentum distribution) as is the case for higher temperatures [91].

3.2.4 Final States Effects

The impulse approximation is strictly valid only in the case for the transferred momentum approaches infinity. However, in a real experiment the momentum transfer is always finite. As a consequence, the measured dynamic structure factor shows deviations in shape and position: e.g. the high energy wing is overestimated and the low energy one is underestimated, resulting in an asymmetry. In addition, the center is slightly lower than the recoil energy ω_r and the width appear to be smaller than in the impulse approximation limit [87]. Therefore, careful corrections to the departure from the impulse approximation must be taken into account.

As was shown in eq.(3.23) the force $\mathbf{f}$ experienced by the nucleus after the scattering is of no importance if the impulse approximation is valid. If the force experienced by the scattering atom through interaction with the surrounding atoms is significant for the impulse approximation to be valid, certain corrections must be introduced. The magnitude and the form of the departures from the impulse approximation has been treated using different

approaches [95, 96]. In a real experiment, departures from the impulse approximation lead to a shift of the center of the peak to lower momentum transfers and introduce asymmetries in the shape of $J(y_M)$. The standard procedure is to symmetrize $J(y_M)$ about $y = 0$. This appears to be a natural approach since any antisymmetric components in the data is not physical because harmonically bound atoms are expected to move in positive and negative directions with equal proportions. It has been shown by Fielding et al. [97] that the method proposed by Sears [87], i.e., accounting for final states effects by expanding $J(y)$ into symmetric and anti-symmetric components in increasing powers of $1/q$, provides a simple and powerful procedure for correcting the data if necessary.

To be more concrete, the Sears expansion for the neutron Compton profile reads

$$J(y) = J_{IA}(y) - A_1 \frac{d^3 J_{IA}(y)}{dy^3} + A_2 \frac{d^4 J_{IA}(y)}{dy^4} - ... \tag{3.43}$$

in which

$$A_1 = \frac{M\langle \nabla^2 V \rangle}{36\hbar^2 q} \tag{3.44}$$

and

$$A_2 = \frac{M^2\langle f^2 \rangle}{72\hbar^4 q^2}. \tag{3.45}$$

$J_{IA}(y)$ is the neutron Compton profile for the case of the IA to be exactly valid. $\langle \nabla^2 V \rangle$ is the mean Laplacian of the interatomic potential with respect to the position of the scattering atom and $\mathbf{f}$ is the mean interatomic force on the struck nucleus. It can be seen that this expansion approaches the exact IA with increasing momentum transfer. The VESUVIO data analysis routines used for this work include these corrections. As will be shown later (section 6.3) the inclusion of FSE gives almost identical results as concerns the peak areas. Evans et. al have shown that at the energy and momentum transfers attained on VESUVIO is accurately described by the IA to within $\sim$5% in hydrogeneous samples [90].

3.2.5 Scattering time

Since the present work deals with the dynamics of the investigated systems, it is very important to consider the time scale of interaction between the probe particles (i.e. neutrons here) and the (probably) quantum entangled particles constituting the condensed matter system under consideration. In particular, according to previous work [41], it is the matching of this interaction time, hereafter termed as *scattering time* τ_s, with the characteristic time scale of

the destruction of the Quantum Entanglement, i.e. *decoherence time* τ_{dec}, which might explain the anomalous decrease of the scattering cross section density of the protons.

According to Sears [87], this interaction time is defined by (cf. eq.(3.36))

$$q \cdot v_0 \tau_s = 1. \tag{3.46}$$

As already discussed in sections 3.2.2 and 3.2.3, although without using the same terminology, this interaction time plays an important role for the validity of the IA. It might be tempting to relate τ_s to the time taken for a neutron wave packet to pass the vicinity of the nucleus. However, this means that the coherence of the neutron beam would play a role for the validity of the IA, which is largely erroneous as Watson has shown [85]. Rather, the scattering time τ_s is the characteristic decay time of the correlation function $F(\mathbf{q}, t)$ to zero, as eq.(3.27) shows. Therefore, assuming the forces on the nucleus to be finite and for the case that $S(q, \omega)$ possesses a simple structure and is not determined by several frequency scales, an estimate of the scattering time is according to Watson [85]

$$\tau_s \simeq \frac{M}{q(\theta)\langle p_q^2 \rangle^{1/2}}. \tag{3.47}$$

$\langle p_q^2 \rangle^{1/2}$ is the width of the momentum distribution and $q(\theta)$ the angle dependent momentum transfer. This equation results from the fact that within the IA the width of $S(q, \omega)$ is proportional to the width of the projection of the momentum distribution on the scattering vector $\mathbf{q}$. A similar expression can be found in ref. [92]. If $S(q, \omega)$ is highly structured, then $F(q, t)$ depends on more than one time scale and τ_s is determined by the longest one [85].

Introducing the angular dependence of q explicitly, it is possible to write, for scattering on protons ($M = m$),

$$\tau_s(\theta) = \frac{1}{tg(\theta)} \sqrt{\frac{m}{2E_1 \langle p_q^2 \rangle}}. \tag{3.48}$$

With a typical value of the proton momentum spread, $\langle p_q^2 \rangle^{1/2} \approx 4.5$ Å^{-1} (which can be derived from the VESUVIO-spectra or from the mean kinetic energy; see eq.(3.35)), and the range of angles used here, the data for H-scattering correspond to a time range

$$\tau_s \approx (0.2 - 1.2) \times 10^{-15} s. \tag{3.49}$$

Particular attention should be spent on the fact that τ_s exhibits a dependence on the momentum transfer q. This dependence means that different

time scales are scanned when the scattering is measured at different momentum transfers q. This is achieved not only by positioning detectors at different scattering angles, but also by involving different resonance absorption energies E_1 using different analyzer foils (gold and uranium) available on the VESUVIO instrument (see chapter 4). This fact becomes relevant in the context of the measurements done on water using these two analyzer foils (see section 7.1.1). Furthermore, because of the dependence of the momentum transfer on the scattering angle θ (see eq.(3.4)), different interaction time scales may become relevant and could reveal differences which becomes evident in the case of the metallic hydrides studied in this work (see section 7.3). For illustration see Fig. 3.4. There it is shown the τ_s dependence on the scattering angle θ for different foils (gold: Au, uranium: U, and rhodium: Rh) according to eq.(3.47) for scattering on protons with momentum spread of 4.5 Å^{-1}. It can be seen that (not too largely) differing time scales are involved using Au and U foils. But it is easily seen that the scattering time using Rh is longer than those using Au or U. This is due to the smaller resonance neutron absorption energy E_R of Rh (E_R(Rh)=1.3 eV) as compared to those of Au (E_R(Au)=4.9 eV) and U (E_R(U)=6.7 eV).

Furthermore, and most importantly for the present work, the scattering time is of the order of one *femtosecond* and less. This is the magnitude of the characteristic time of the electronic rearrangements accompanying the formation or breaking of a typical chemical bond in a molecule. Accordingly, the results of the present work are expected to be highly relevant for the investigation of the dynamics and mechanisms of chemical reactions.

In order to pinpoint the uniqueness of the VESUVIO instrument in accessing extremely short time windows with neutrons, let us compare the neutron Compton scattering time $\tau_{s,NCS}$ at VESUVIO with those of other neutron scattering techniques, as far as comparison is possible.

Let us consider the interaction time of the neutron with the scattering medium in the neutron interferometry (NI) technique. This technique involves elastic and coherent scattering. For a neutron that traverses a slab of material and that interacts with the assembly of nuclei creating an effective optical potential $V_{opt}(x)$ given by

$$V_{opt}(x) = \frac{2\pi\hbar^2}{m} b_c N, \tag{3.50}$$

being dependent only on position x, the phase shift depends only on the action of the kinetic momentum [98], i.e.

$$\Delta\Phi_{V(x)} = \frac{1}{\hbar}\int \Delta p_{kinetic} \cdot ds \tag{3.51}$$

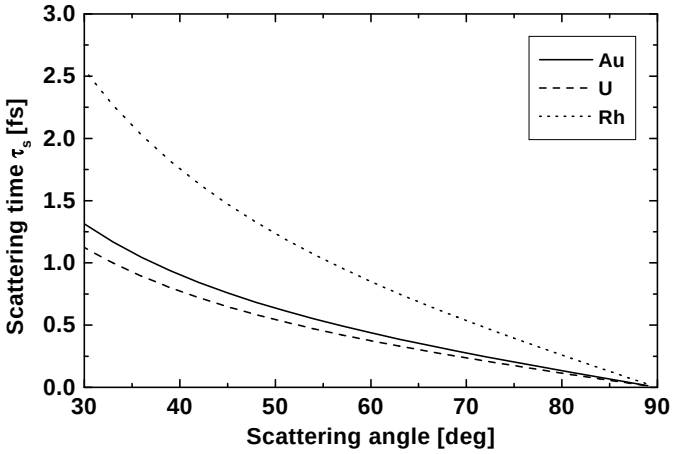

Figure 3.4: Scattering time τ_s dependence on the scattering angle for Au, U, and Rh (Rhodium) foils according to eq.(3.47) for scattering on protons. It is easily seen that the scattering time using Rhodium is longer than those using Au or U. This is due to the smaller resonance neutron absorption energy E_R of Rh (E_R(Rh)=1.3 eV) as compared to those of Au (E_R(Au)=4.9 eV) and U (E_R(U)=6.7 eV)

where $\Delta p_{kinetic}$ is the change of kinetic momentum of the neutron in the potential and the integration over s expresses the classical trajectory of the neutron through the sample. The time the neutron with momentum $p = \hbar k = h/\lambda$ needs to traverse the potential (barrier) is [99]

$$\tau_{NI} = \frac{md}{\hbar k}. \tag{3.52}$$

Using a typical neutron de Broglie wavelength of 2.7 Å used for neutron interferometry experiments and a sample thickness of ca. 1 mm, the resulting traversal time of the neutron through the sample amounts to

$$\tau_{NI} \approx 10^{-6} s. \tag{3.53}$$

Evidently this time window is many orders of magnitude larger than that of the NCS method being in the sub-femto second range (cf. e.g. eq.(3.49)).

As another neutron scattering technique the neutron spin echo (SE) should be mentioned which is a method that exploits the spin of the neutron and its Larmor precession about the axis of a uniform magnetic field. This technique is an inelastic one, the energy transfer of which is in the range

of neV. This method with which the intermediate scattering function of e.g. glasses can be determined involves a scattering time scale of [100].

$$\tau_{SE} \approx 10^{-12} s. \tag{3.54}$$

which is also three orders of magnitude larger than the relevant time scales of the scattering processes involved in the present work (cf. eq.(3.49)).

3.2.6 Coherence length

Whenever quantum interference effects are considered or assumed to be measured, the question of the relevant coherence length and coherence time arises. The question of the relevant coherence length in neutron scattering is not unambiguous.

The relevance of the neutron coherence length in connection with the NCS experiments has been pointed out first by Karlsson and Lovesey [56]. There it is claimed that the neutron coherence length – being set by the energy width of the energy analyzer used – plays a key role for the anomalous decrease of the H scattering cross section.

Given the neutron deBroglie wavelength by

$$\lambda_{dB} = \frac{h}{p} = \frac{h}{\sqrt{2mE_R}} \tag{3.55}$$

and using

$$\frac{d\lambda_{dB}}{dE_R} = -\frac{h}{2\sqrt{2m}} E_R^{-3/2} \tag{3.56}$$

yields

$$\Delta\lambda = \frac{1}{2} 9.04 \cdot E_R^{-3/2} |\Delta E_R|. \tag{3.57}$$

If one uses

$$l_{coh} = \frac{\lambda^2}{2\Delta\lambda} \tag{3.58}$$

as the definition of the neutron coherence length, $l_{coh} \approx 2.5$Å when using the gold foil analyzer with $E_R \approx 4.9eV$ and $\Delta E_R \approx 0.26meV$.

It should be mentioned that the validity of the theoretical model outlined in ref. [56] is strongly dependent on the validity of the definition of the neutron coherence length given above. There are a number of difficulties connected with this interpretation. First, Karlsson and Lovesey were motivated by a recent publication of Pitaevskii and Stringari [101] where the condition for measuring coherence properties of two spatially separated Bose Einstein

condensates is given by the fact that the experimental uncertainty Δq of the momentum transfer must be smaller than $\hbar/d$, where d is the spatial separation of the Bose Einstein condensate, i.e.,

$$\Delta q < \frac{1}{d} \tag{3.59}$$

which is in line with [102]. This means that the inverse of the resolution in momentum space must be larger than the H,H distance. This condition might be fulfilled in the case of a metal hydride like e.g. $NbH_{0.78}$ where the distance of two hydrogen atoms is of the order of

$$d_{HH} \approx 2\mathring{A} \quad or \quad \frac{1}{d_{HH}} \approx 0.5\mathring{A}^{-1}. \tag{3.60}$$

Consequently, this model could in principle explain any interference effect occurring in such a system. However, it can be proven experimentally that this model can not explain all intensity anomalies. Since according to the assertion, the coherence length is fixed by the energy width of the analyzer, one could use a sample in which the hydrogen atoms are too far apart to be covered by the neutron coherence length. Indeed, such an experiment has been conducted on VESUVIO using C_6HD_5 (see section 7.2.2). There, it has been found that no matter how far the hydrogen atoms are from each other (e.g. 6.6 Å in C_6HD_5), the scattering cross section is anomalously reduced to the same extent as for example in a C_6H_6/C_6D_6 mixture of the same D mole fraction.

Chapter 4

The Electron-Volt-Spectrometer VESUVIO at ISIS (Rutherford Appleton Laboratory)

4.1 The ISIS spallation source

The ISIS spallation neutron source (see Fig. 4.1) is the world's most powerful one. H^--ions are produced in an ion source and are linearly accelerated to ca. 70 MeV. As injected into a synchrotron of 25 m diameter, the electrons are removed from the H^--ions using an aluminum foil of ca. 0.3 μm. The circulating protons are accelerated to 800 MeV and bunched together to pulses of 100 ns duration and 230 ns separation. Then they are kicked out of the synchrotron by a kicking magnet and are guided to the target station. The neutrons are then produced by bombarding a heavy metal (tantalum or uranium) target with the high energetic protons. The frequency of this procedure is 50 Hz. For an 800 MeV proton beam about 15 neutrons are produced by each proton hitting the uranium target. After production, the neutrons are slowed down by moderators containing hydrogen (e.g. water or methane) being situated around the target, whereas the moderator temperature determines the desired velocity (i.e. wavelength) distribution of the neutrons.

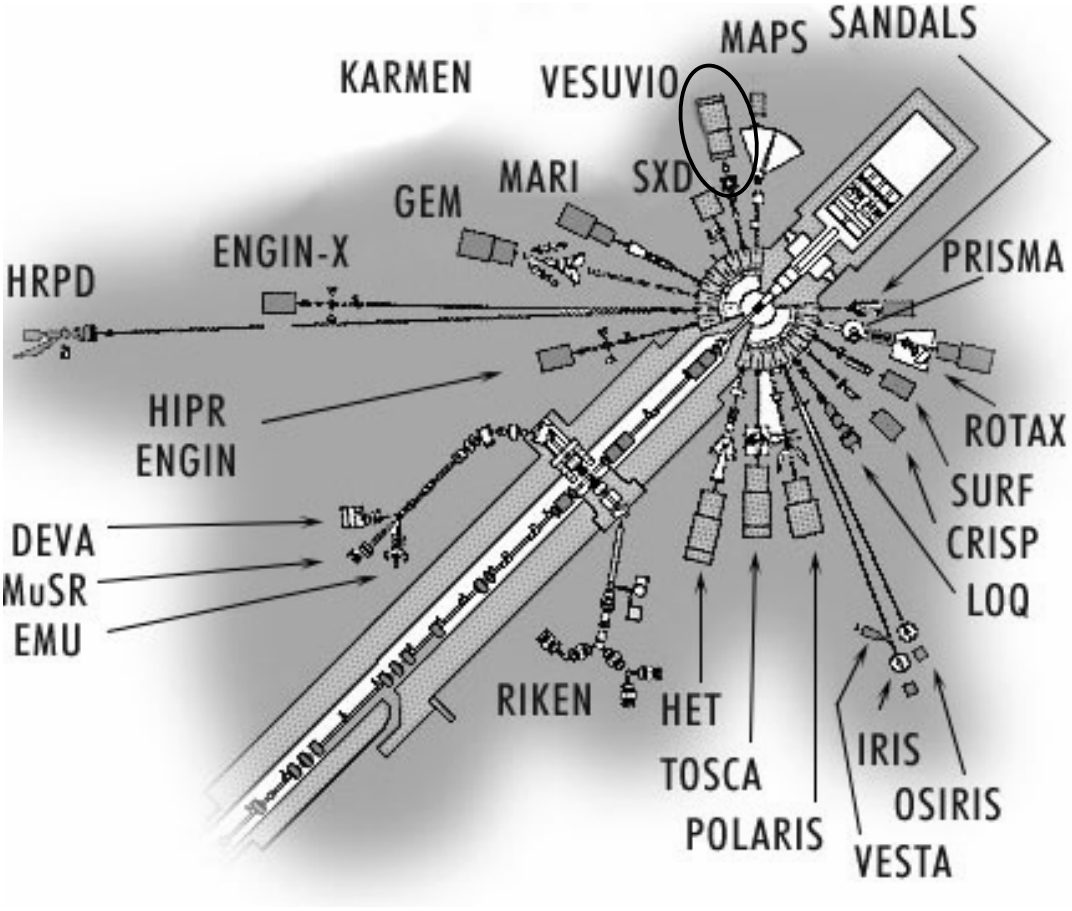

Figure 4.1: Shown is a schematic view of the instrument hall of the ISIS neutron spallation source. The instruments are grouped around the target station. The VESUVIO instrument used for the present work is highlighted with an ellipse.

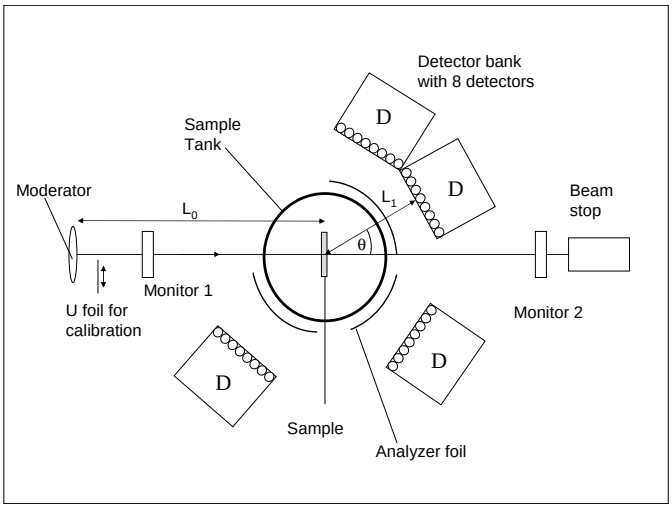

Figure 4.2: VESUVIO instrument setup: The polychromatic neutrons leave the spallation target, are slowed down by the moderator, pass the incident flight path length L_0, are scattered by the sample under an angle θ, pass the final flight path L_1 and reach one of the detectors D. The analyzer energy foils (optionally uranium or gold) are cycled in and out of the scattered neutron beam. See text for more details.

4.2 The VESUVIO instrument setup

The VESUVIO instrument (Fig. 4.2) was originally designed to directly measure atomic momentum distributions $n(\mathbf{p})$ and ground state kinetic energies by taking full advantage of the high flux of high energy neutrons produced by the ISIS target. $n(\mathbf{p})$, which is a fundamental single atom property of condensed matter systems, is related to the nuclear wave function by Fourrier transform and therefore to the spatial localization of a nucleus [103].

The time-of-flight (TOF) spectra of VESUVIO are recorded with respect to the time the neutron needs to travel from the moderator to the sample, to be scattered there and to travel from the sample to the detector (see Fig. 4.2). This time of flight is given by

$$t = \frac{L_0}{v_0} + \frac{L_1}{v_1} + t_0, \tag{4.1}$$

where L_0 is the distance from the moderator to the sample and L_1 is the distance from the sample to the detector being situated at angle θ with respect to the axis of the incident beam. v_0 and v_1 are the neutron velocities before and after the scattering process, respectively. t_0 is a time constant

that determines which channel in the time of flight spectrum corresponds to (infinitely fast) neutrons with zero time of flight. This is determined by electronic delay times in the detector-discriminator-electronics-computer chain. For the determination of the numerical values of these parameters, see section 4.2.1.

The VESUVIO instrument is a so-called inverted geometry spectrometer [83, 84]. In this experimental technique, the sample is exposed to a polychromatic neutron beam of circular cross section with an umbra of $R_u = 3$ cm and a penumbra of $R_p = 5$ cm diameter (for beam profile, see Fig. 4.3) and the energy of the scattered neutrons is analyzed. A foil situated between sample and detector strongly absorbs neutrons over a narrow range of energies, centered at the nuclear neutron absorption resonance specific to the material the foil consists of. In order to get TOF spectra allowing to analyze intensities corresponding to the different scattering nuclei, two measurements are taken: one with the foil between the sample and detector (Fig. 4.4a full line) and one with removed foil (Fig. 4.4a dashed line).

The difference between these two measurements is determined by the probability that the filter absorbs a neutron. This is

$$A(E_1) = 1 - \exp[-Nd\sigma(E_1)] \tag{4.2}$$

where N is the number of filter atoms/cm^3, the filter thickness is d and the filter total cross section is $\sigma(E_1)$. The effective detection probability $D(E_1)$ is equal to the product of the filter absorption with the detector efficiency $\eta(E_1)$

$$D(E_1) = A(E_1)\eta(E_1). \tag{4.3}$$

The difference between the foil in and foil out spectrum gives the final TOF spectrum, cf. Fig. 4.4. The line shape of a measured recoil peak is the convolution of the momentum distribution function of the nucleus $n(p)$ with the instrument resolution function (see section 4.2.1 and chapter 6). In most experiments of this work a gold foil analyzer which has a Lorentzian shaped resonance absorption centered at 4908 meV and a half width at half maximum (HWHM) of 130 meV has been used.

Another option available at the VESUVIO instrument is to use a uranium absorption resonance centered at 6771 meV with a HWHM of 63 meV, which is Gaussian shaped. This option is often used in such experiments, in which the primary goal is to determine precisely the shape of the recoil peak, rather than its integral intensity, as is the case in this work. However, the U resonant absorbance is much weaker than that of Au, which necessitates considerably longer measuring times. Furthermore, U has side absorptions (see Fig. 4.7)

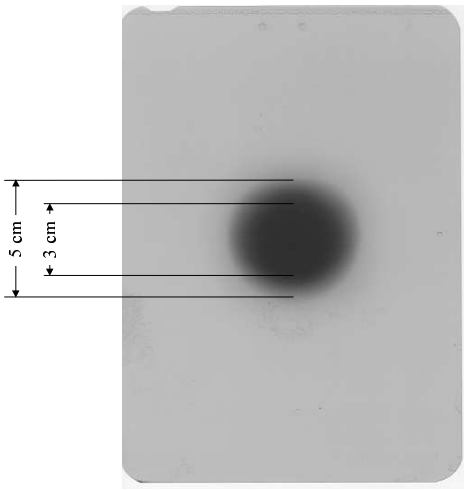

Figure 4.3: Beam profile at the VESUVIO instrument: The sample is exposed to a polychromatic neutron beam of circular cross section with an umbra of $R_u = 3$ cm and a penumbra of $R_p = 5$ cm diameter.

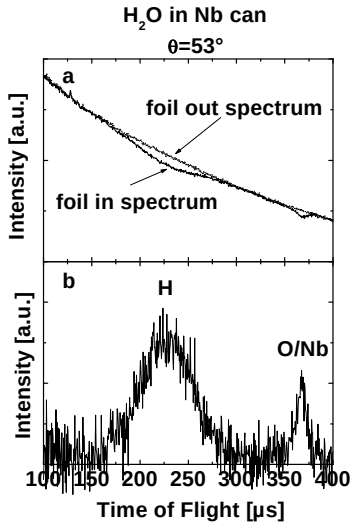

Figure 4.4: a. Foil in (thick line)/foil out (thin line) spectra of pure H_2O in a niobium can as measured at a detector angle of $\theta = 53°$. The dips in the foil in spectrum are due to the absorption of neutrons by the analyzer foil. b. Difference of the foil in/foil out spectra. The higher the mass of the scatterer, the larger is the time of flight position of the corresponding peak. For angle dependence of the time of flight position of the peaks, see Fig. 4.5.

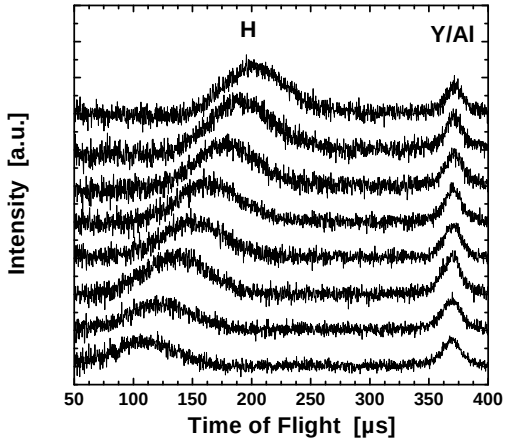

Figure 4.5: Angle dependence of the H (M_H=1.0079) peak position in the time of flight spectrum. Detector angles are in degrees 59 (spectrum at the top), 62, 64, 67, 69, 71, 74, and 76 (spectrum at the bottom) . Spectra are vertically shifted for the sake of visibility. Note that the combined Y/Al peak position do not move to smaller time of flights with increasing detector angle because of the high involved masses (M_{Al}=26.98; M_Y=88.91).

which limits the range of accessible angles. For possible differences in results using different analyzer foils, see sections 3.2.5 and 7.1.1.

It should be mentioned here that the use of analyzer foils consisting of different kinds of nuclei having different resonance absorption energies implies that neutrons of different incident energies interact with the scattering nuclei. This and because the energy transfer is directly connected with the momentum transfer means that the energy transfers involved using different analyzer foils results in involving different time scales for the scattering process.

The time at which the recoil peak of a specific nucleus appears in the TOF spectrum depends on the ratio of the velocity $v_1 = k_1/m$ of the scattered neutrons to that of the incident neutrons (i.e. $v_0 = k_0/m$). This ratio for the peak center is given by

$$\alpha(\theta) = \frac{v_1}{v_0} = \frac{k_1}{k_0} = \frac{\cos\theta + \sqrt{(M/m)^2 - \sin^2\theta}}{M/m + 1} \tag{4.4}$$

which, together with eq.(4.1), gives then the TOF of the peak position corresponding to each scattering nucleus of a specific mass M for a detector at angle θ. Therefore, the TOF spectra exhibit two features. First, the higher is the mass of the scattering nucleus the larger is the time its corresponding

peak position appears in the TOF spectrum (cf. Fig. 4.5). Second, for a nucleus of specific mass, increasing the scattering angle corresponds to a shift of the recoil peak to shorter times (cf. Fig. 4.5). Since high transfers of energy and momentum are involved in NCS, the recoil peaks of light particles (e.g. H) are well separated from those of heavier nuclei (e.g. C, Nb, Y etc.) in the TOF spectrum for a wide range of scattering angles (cf. Fig. 4.5).

The scattered neutrons were collected by ^{6}Li doped glass detectors. In these detectors the neutrons produce alpha and ^{3}He particles when hitting the ^{6}Li nuclei. The particles excite Ce-ions (also doped into the glass bars of 25 x 200 mm dimension each). The 380 nm photons from the Ce-decay are picked up by photomultiplier tubes producing pulses of about 100 ns duration.

The events from different detectors in each bank are collected in buffers and fed into one of the two available PPFM units (which one to chose can be selected externally, so as to minimize the load on each of them for the specific scattering angle ranges used). The information is then sent further for histogram formation.

The width in t due to the uncertainty in for example E_1, is calculated as

$$\Delta t_{ME_1} = \frac{\partial t_M}{\partial E_1} \Delta E_1 \tag{4.5}$$

with similar expressions for the other resolution components in L_0,L_1 and θ. All resolution components other than the energy resolution are assumed to have a Gaussian peak shape in t and their widths are therefore added in quadrature

$$\Delta t_{MI}^2 = \left(\frac{\partial t_M}{\partial L_0} \Delta L_0\right)^2 + \left(\frac{\partial t_M}{\partial L_1} \Delta L_1\right)^2 + \left(\frac{\partial t_M}{\partial \theta} \Delta \theta\right)^2 . \tag{4.6}$$

The resolution function for these components is represented as a Gaussian in t, with standard deviation Δt_{MI}.

4.2.1 Instrument calibration

The time of flight t along which the spectra are recorded is determined by the five quantities t_0, L_0, v_0, L_1, and v_1 given in eq.(4.1). The distance L_0 between the moderator and the sample is known from physical measurement and is $L_0 = 11.055$ m. The remaining parameters together with the angle θ_i of each detector and the final energy E_1 of the neutrons absorbed by the analyzer foil as well as their uncertainties and in particular the energy resolution σ_{E_R} of the analyzer foil have to be determined via calibration measurements.

The calibration of the VESUVIO instrument consists in exposing a flat lead (Pb) sample to the neutron beam and in performing two measurements that are called *uranium foil calibration* and *Pb calibration* (For details, see below). Lead is used for calibration because it has a narrow intrinsic width of the atomic momentum distribution. Therefore the measured signal will be dominated by the instrument resolution. Furthermore, its relatively low Debye temperature of $T_D = 88$ K [104] implies that to a good approximation, its motion can be treated within the classical limit so that its kinetic energy is given by $3/2 \times k_B T$, in which k_B is the Boltzmann constant and T the absolute temperature. Therefore, the momentum distribution width of Pb can be calculated straightforwardly according to eq.(3.35). For a Pb example spectrum in y space, see Fig. 4.6.

The calibration procedure exploits the opportunities offered by VESUVIO for measuring inelastic as well as diffraction spectra (for the determination of the detector angles, see below).

In the *Pb calibration* measurement the incident neutron beam hits the Pb sample with the analyzer foils cycling in and out of sample-to-detectors axes.

In the *U calibration* measurement the incident neutron beam passes a thin U foil (see the instrument setup in Fig. 4.2) before hitting the Pb sample and the analyzer foils remain out of the sample-to-detectors axes.

It is the interplay of both measurements which gives the final calibration of the instrument parameters L_0, L_1, E_1, θ, and t_0 and their resolutions necessary for the data analysis procedure.

4.2.1.1 Calibration of final flight path lengths and detector angles

Uranium absorbs neutrons at the following four energies in meV [105]: 6671, 20872, 36680, and 66020. These energies determine the initial velocities v_0 of the neutrons hitting the Pb sample. When the incident neutron beam passes the thin U foil then a spectrum as shown in Fig. 4.7 is obtained and each peak corresponds to one incident energy E_0 or v_0 and one time of flight. The time of flight positions of the resonance dips are determined by fitting a Gaussian to the ratio of the incident foil-in/incident foil-out data. Examples are shown in Figs. 4.8-4.10. The ratio of the neutron velocities v_0 and v_1 (with $v_0 > v_1$) before and after being scattered off a nucleus of mass M into a certain angle θ is given by eq.(4.4). Together with eq.(4.1) one obtains

$$t = \frac{1}{v_0}(L_0 + L_1/\alpha(\theta)) + t_0 \tag{4.7}$$

which is a linear equation with respect to $1/v_0$ so that $L_0 + L_1/\alpha(\theta)$ is then given by the gradient and t_0 is given by the ordinate-intercept; see Fig. 4.11.

From the diffraction spectra of the coherently and elastically scattered neutrons by the Pb nuclei and by knowing the d spacing parameters of the Pb lattice, it is possible to iteratively determine the angles θ_i of the detectors. This is done by using the de Broglie relation for the wavelength λ and the velocity of matter waves:

$$\lambda = \frac{h}{mv}. \tag{4.8}$$

Bragg peaks will appear in the spectrum of a detector at angle θ if Bragg's law

$$2d\sin(\theta/2) = n\lambda \tag{4.9}$$

is satisfied; n being the diffraction order. Since Bragg scattering is elastic, i.e. $v_0 = v_1 = v$, eq.(4.1) can be written as

$$v = \frac{L_0 + L_1}{t - t_0}. \tag{4.10}$$

The relationship between the measured time of flight at which the Bragg peaks appear in the diffraction spectrum (Fig. 4.12) is obtained by using eqs.(4.8) and (4.10), thus giving

$$2d\sin(\theta/2) = \frac{nh(t - t_0)}{m(L_0 + L_1)}. \tag{4.11}$$

Both L_1 and θ appearing in this equation are unknown. The following iterative procedure is then applied: First an arbitrary value is given for the angle θ for which $\alpha(\theta)$ is calculated according to eq.(4.4) for the case of scattering on Pb. By knowing the gradient of eq.(4.7) a first value of L_1 can be calculated. Then, a more accurate angle θ can be calculated using eq.(4.11). Repeating this procedure gives then the accurate values for L_1 and θ. Then the instrument parameter (IP) file containing the detector numbers, angles θ, primary and final flight paths L_0 and L_1 and the time delay t_0 can be created.

4.2.1.2 Calibration of final neutron energy and of the instrument resolution

Each measured peak in the time of flight is broadened by a variety of parameters which together give the instrument resolution. In order to extract from the measured spectra the accurate intrinsic neutron Compton profile $J(y)$ of the scattering nucleus (see eq.(3.32)), the measured signal has to be

deconvoluted from the instrument resolution function $R(y)$. The instrument resolution function is given by the distributions of the values of (i) the incident flight path length L_0 due to the finite depth of the moderator, (ii) the final flight path length L_1, (iii) the detector angle θ, and (iv) the final neutron energy E_1 due to the finite energy width of the resonance absorption of the analyzer foil as well as (v) the time delay t_0 due to inaccuracies in measuring the time of flight. Thus $R(y)$ is given by

$$R(y) = R_{L_0}(y) \otimes R_{L_1}(y) \otimes R_\theta(y) \otimes R_{E_1}(y) \otimes R_t(y). \tag{4.12}$$

The distributions for the angular, initial and final flight path lengths and time components of the resolution are given by Gaussians and are therefore represented by their standard deviations σ_{L_0}, σ_{L_1}, σ_θ, and σ_t, respectively, and their squares can be added:

$$\sigma_G{}^2 = \sigma_{t_0}{}^2 + \sigma_{L_0}{}^2 + \sigma_{L_1}{}^2 + \sigma_\theta{}^2. \tag{4.13}$$

The flight paths and time resolutions σ_{L_0}, σ_{L_1}, and σ_{t_0} are determined by measuring (i) the transmission of a thin uranium foil in the incident beam (see Fig. 4.2) and (ii) the scattering from the Pb sample. The angular resolution σ_θ is calculated using a Monte Carlo simulation taking into account the finite sizes of the moderator, detector and sample.

The energy resolution is dependent on the intrinsic shape of the resonance absorption of the analyzer foil used, which is approximated using a Lorentzian for gold (Au)

$$P(E) = \frac{\Delta E}{\pi} \frac{1}{(E - \langle E \rangle)^2 + \Delta E^2} \tag{4.14}$$

and using Gaussian for uranium (U)

$$P(E) = \frac{1}{\sqrt{2\pi\Delta E^2}} exp(\frac{-(E - \langle E \rangle)^2}{2\Delta E^2}). \tag{4.15}$$

where ΔE denotes the HWHM of the Lorentzian or the standard deviation of the Gaussian distribution, respectively. In order to find out the resolution of the used analyzer foil, the Pb scattering data are converted from time of flight into momentum space y_M (see eq.(3.31) and Fig. 4.6). In the case of Au foil analyzer, the Pb recoil peak is fitted with a Voigt function, yielding a Lorentzian width due to the energy resolution and a Gaussian width due to all the other contributions, i.e. θ, L_0, L_1 and t_0.

The required resonance energy and its width are obtained from the foil thickness and tabulated nuclear resonance parameters [106].

For the case of the U foil the Pb y-space data are fitted with a Gaussian using the IP file (see above) along with the resolutions σ_{t_0}, σ_{L_0}, σ_{L_1}, and σ_θ.

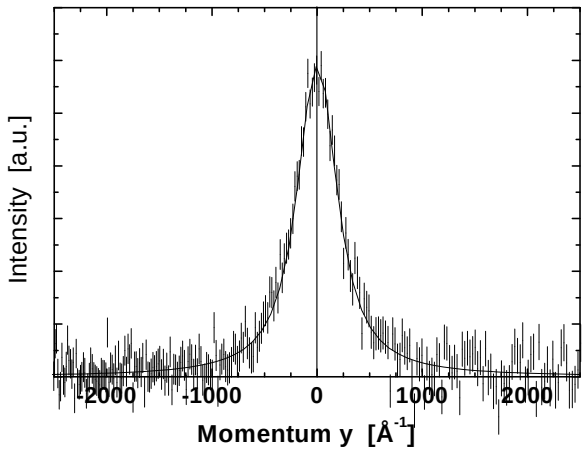

Figure 4.6: Pb recoil peak in atomic momentum y space at 39 deg (see eq.(3.31)) and the corresponding fit to the peak.

The momentum distribution of Pb is well described by a Debye model (see above). Its width in momentum space is 35.5 Å^{-1}. The center of the peak in y-space is dependent on the resonance energy and mass of the scatterer (being fixed at $M(Pb) = 207$). The calibrated resonance energy E_R can be derived from the shift of the fitted position of the peak from $y = 0$ and σ_{E_R} from the width of the recoil peak. Then the total resolution is given by:

$$\sigma_{total}(U)^2 = {\sigma_G}^2 + {\sigma_U}^2. \tag{4.16}$$

Some values for resolutions in momentum space for H and D are given in Figs. 4.13 and 4.14.

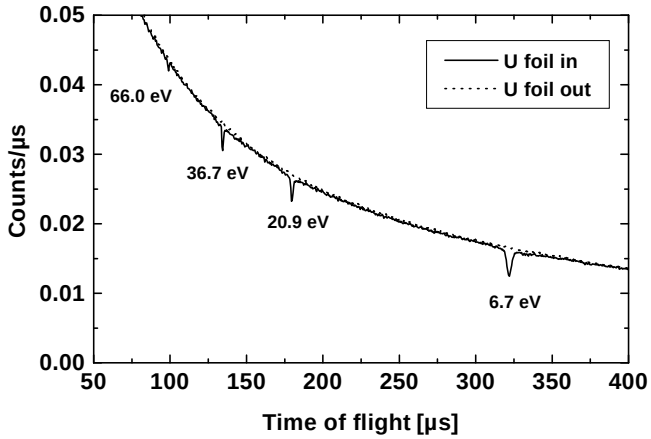

Figure 4.7: Pb spectra measured with U foil in (full line) and foil out (dotted line) of the incident neutron beam. Dips are due to neutron absorption by the U foil. The incident neutron velocities are determined from the known resonance energies.

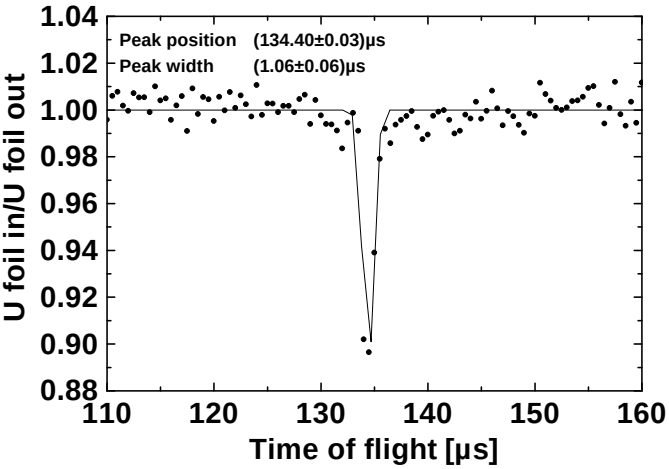

Figure 4.8: Ratio of the incident beam U foil in/foil out spectra for the absorption at 36.7 eV resonance. The position of the peak in time of flight is determined from a Gaussian fit to the data.

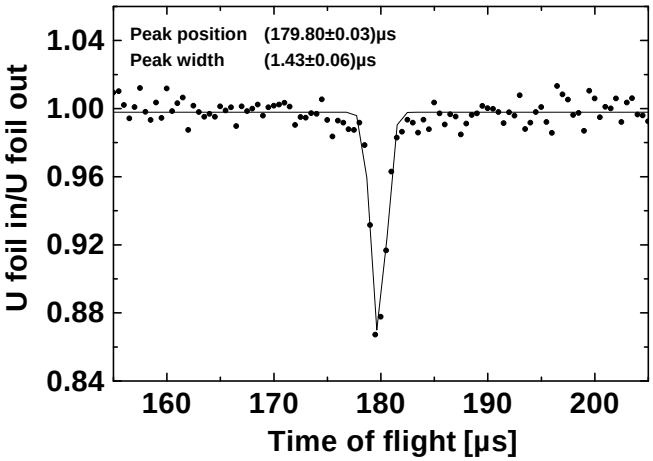

Figure 4.9: Ratio of the incident beam U foil in/foil out spectra for the absorption at 22.9 eV resonance. The position of the peak in time of flight is determined from a Gaussian fit to the data.

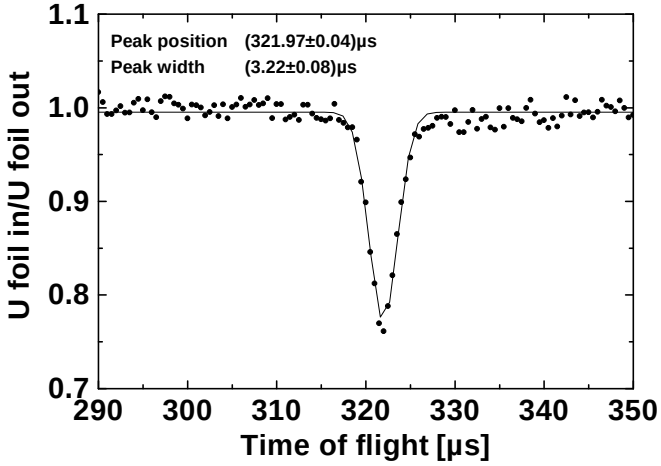

Figure 4.10: Ratio of the incident beam U foil in/foil out spectra for the absorption at 6.7 eV resonance. The position of the peak in time of flight is determined from a Gaussian fit to the data.

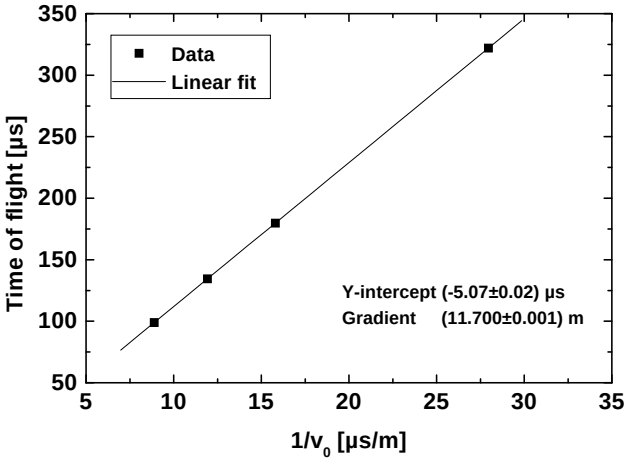

Figure 4.11: Time of flight vs. $1/v_0$ which has been determined from the fits given in Figs. 4.8-4.10 for the determination of the gradient and intercept of eq.(4.7).

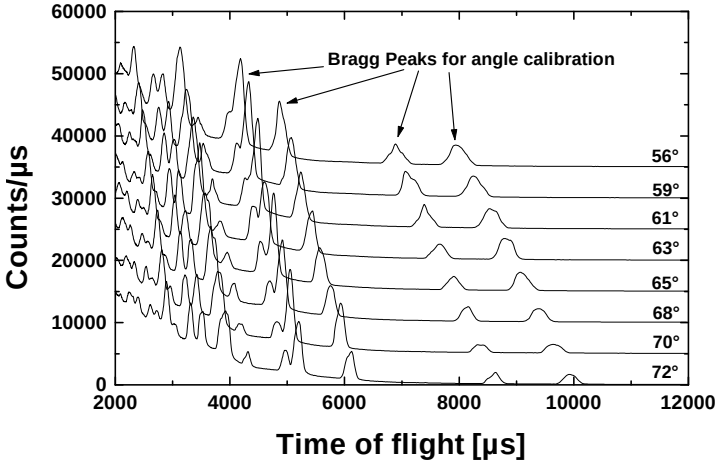

Figure 4.12: Diffraction spectra of Pb as measured at different angles. The angles θ of the detectors are determined from the peak positions in time of flight by knowing the d spacing parameters of the Pb lattice and using Bragg's diffraction law, eq.(4.9).

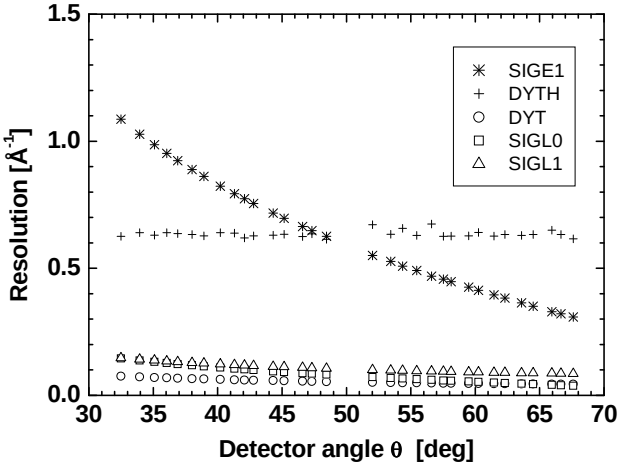

Figure 4.13: Dependence of the resolution components in momentum space on scattering angle for scattering on H and using the Au foil analyzer: final energy (stars), angle (crosses), time (circles), initial flight path (squares), and final flight path (triangles). One sees that the energy resolution becomes better as the scattering angle increases.

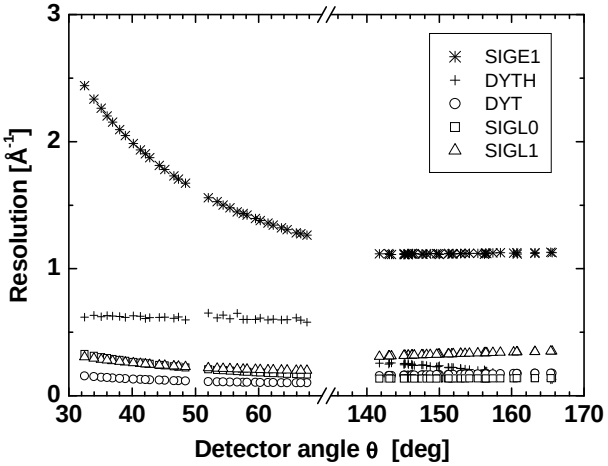

Figure 4.14: Dependence of the resolution components in momentum space on scattering angle for scattering on D and using the Au foil analyzer: final energy (stars), angle (crosses), time (circles), initial flight path (squares), and final flight path (triangles). One sees that the energy resolution becomes better as the scattering angle increases. The axis break between $\theta = 70$ deg and $\theta = 135$ deg is due to the detector gap in this angular range.

Chapter 5

Measurements: Instrument setup, sample environment, sample preparation

5.1 Setup and data accumulation

The detectors were put between 30° and 80°. Below 30° the H and D peaks are unresolved and no reliable area values are obtained. Detector angles higher than 85° provide spectra in which the H peak exits the time of flight spectrum (see Fig. 4.5). Most of the experiments were run with the Au foil analyzer for better counting statistics. The U foil analyzer has been also used for a small number of experiments (see below). Some detectors were put in the backscattering region (i.e. $\theta > 90°$) in order to achieve separation of the recoil peaks arising from heavy nuclei, namely C/Nb, O/Nb, etc. Due to space limitations in the VESUVIO instrument block house, the sample-detector distances could not be chosen to exceed ca. $0.60m$, which sometimes was too small, thus leading to saturation in the data acquisition electronics due to the large number of collected neutrons. In order to reduce background scattering, a vacuum in the sample tank including the beam tubes has been maintained by pumps being in standard use at VESUVIO.

Due to the available proton flux of ca. 180-190 μA at ISIS, each measurement was run for ca. 8-10 hours in order to achieve useful counting statistics. The accumulation time was increased accordingly when using the U foil analyzer because the absorption cross section of U is by a factor of ca. 10 smaller than that of Au.

5.2 Sample environment

- Cans

  Several cans providing different geometries and sample thicknesses were used for the experiments with the liquids (water, benzene, etc.). The water mixtures were measured with the following cans:

  - flat aluminum
  - flat vanadium
  - annular aluminum
  - annular niobium.

  Whereas the flat aluminum and vanadium cans are in standard use at ISIS, the annular aluminum and niobium cells were produced especially for the experiments presented in this thesis. As far as the standard Al cans have been used, the peak separation of the oxygen (of the water molecule) or carbon signal (of the benzene molecule) from that one of the can even at the highest accessible angles (see Fig. 5.1 upper part) was not satisfactory. Therefore, it was not possible to relate the H signal to that of O or C. However using a can made of material of a much heavier nucleus – e.g. Nb (M_{Nb}=93) –, improves the peak separation considerably (see Fig. 5.1 lower part).

  The first H_2O/D_2O measurements used in this work has been done using the vanadium (V) cans. Later measurements have been also done using flat Al, annular Al, and annular Nb can. The benzene samples were measured with the annular Nb can.

  As a result, the geometry of the can does not play a role for the effects found in this thesis (see section 8.1).

  The polymer foils and niobium hydride measurements were carried out without a can. The palladium hydrides were put in an Al cell (max. working pressure 2.8 bar) for in situ hydrogenation.

- Temperature

  Most experiments have been performed at room temperature. Some of the H_2O/D_2O mixtures and the metal hydrides NbH_xD_y and PdH_xD_y and also LiH have been measured at lower temperatures. Whereas an orange cryostat has been used for the H_2O/D_2O mixtures, PdH and LiH, a closed cycle one has been involved in the measurements on NbH.

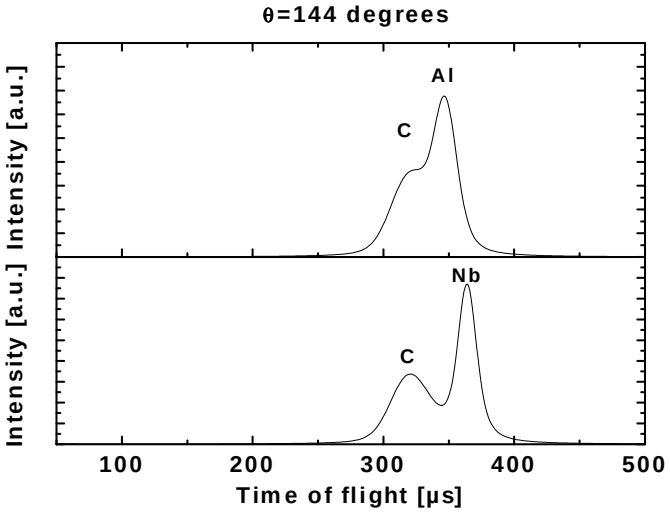

Figure 5.1: Simulated time of flight spectra for the possible separation of the Al or Nb scattering signal due to the can from that one of carbon C for a scattering angle of 144°.

5.3 Sample preparation

5.3.1 H_2O/D_2O, C_6H_6/C_6D_6 mixtures

The sample preparation procedure was equal for both liquids. The liquid H_2O/D_2O mixtures were prepared using purified water (of Millipore quality with an electric resistance of ca. 18 MΩ) of the ISIS chemistry lab and purchased D_2O (D content >99.9 %). The mole fractions of H_2O and D_2O in the mixtures were adjusted by weight with an accuracy of ±0.1 mg. After measurement, the densities of the mixtures were measured with an accuracy of 0.3 % in order to check the D mole fractions. All samples were prepared and measured at ambient conditions (room temperature, normal pressure). The same procedure has been applied for the H_6-benzene/D_6-benzene mixtures.

5.3.2 H_2O/D_2O/Urea and H_2O/D_2O/Amphiphile (2-iso-C_4E_1)

The urea molecule (or carbonylamide; H_2N-CO-NH_2) which has a relative mass of $M_{urea} = 60.04$ g/mol consists of a carbon atom doubly bonded to an oxygen atom and singly bonded to two -NH_2 groups (see Fig. 5.2.a). This organic compound which is very good solvable in water was chosen because it represents a very simple molecule of biochemical relevance. More important

A. B.

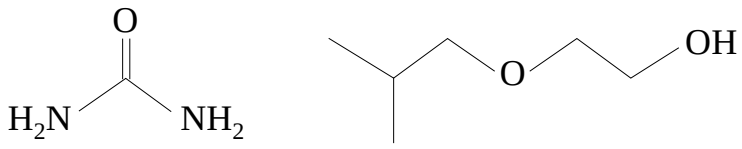

Figure 5.2: Structural formula of A. Urea (H_2NCONH_2) and B. 2-iso-butoxyethanol (2-iso-C_4E_1).

is the fact that aqueous solutions of urea contain hydrogen bonds involving nitrogen atoms. Thus, a suitable system is provided in order to investigate the contribution of the -N-H$\cdots$O- bond to the quantum entanglement effect previously detected in H_2O/D_2O mixtures [31]. The samples were prepared by dissolving urea powder in D_2O and H_2O/D_2O mixtures adjusting the same number density of urea molecules of 8 mol/l for all solutions. The initial H/D ratios of the stock H_2O/D_2O mixtures were chosen to give final D mole fractions $x_D = 0.8$, 0.70, 0.60, 0.50, and 0.40, where $x_D + x_H = 1$. Of course the H's originate from H_2O as well as from urea. All samples were prepared and measured at ambient conditions. For these experiments, the flat V cans has been used, because the annular Nb can were not available yet.

2-iso-C_4E_1, the structure of which is given in Fig. 5.2.b, is a very important short-chain nonionic amphiphilic molecule with chemical structure and physical properties being between those of alcohols and those of real surface active compounds. Amphiphiles possess a hydrophobic chain and a hydrophilic head. 2-iso-C_4E_1 is often used as a model compound for the investigation of interface structures of binary liquid mixtures. It exhibits a miscibility gap when mixed with water having a critical solution temperature of 26°C and a critical composition of $x = 0.052$ [107]. At temperatures below this temperature the system consists of a clear micelle solution. This molecule has been chosen because it forms a homogeneous solution at room temperature and at the concentration used in this experiment (see below) and because it allows to be dissolved in water (or D_2O) over a relatively wide dilution range [107], thus facilitating the NCS data accumulation and data analysis. Furthermore, this molecule contains many aliphatic C-H bonds (in contrast to the work on solid polystyrene which contains also aromatic C-H bonds; see below). The 2-isobutoxyethanol/D_2O solution was prepared by weighing 1.0235±0.0001 g of 2-iso-C_4E_1 and adding to it 7.7602±0.0001 g of D_2O (99.9%; purchased from Euriso-Top), thus giving a solution with molar composition 2-iso-C_4E_1:D_2O=0.0223:1. After the neutron scattering measurement, the composition has been confirmed independently by density

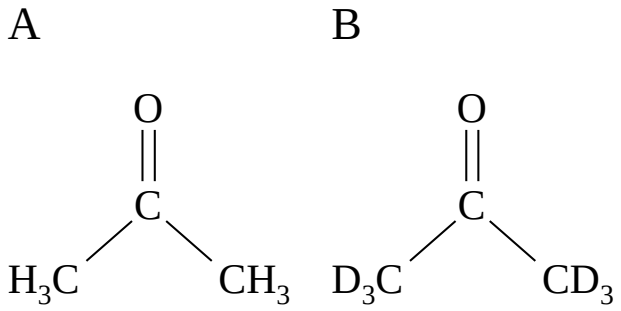

Figure 5.3: Structural formula of Acetone. A. fully protonated and B. fully deuterated.

measurements with an accuracy of 0.1%. Hence, the error of the mixture composition is negligibly small compared to the error of neutron counting statistics.

The liquid sample was put in an annular Nb-can which has been provided by the ISIS facility. In contrast to the usually used aluminum or vanadium cans, this special can provides the feature that, due to the high mass of the niobium nuclei, a separation of the combined carbon/oxygen recoil peak (due to 2-iso-C_4E_1 and D_2O) from that one of the can is possible. Thus it is possible to relate the H recoil peak intensity A_H to the combined C/O recoil peak intensity $(A_C + A_O)$.

5.3.3 H_6-acetone/D_6-acetone Mixtures

Since only a small amount of pure D_6-acetone was available, the mixtures had to be prepared by subsequently diluting a H_6-acetone/D_6-acetone mixture having a high D concentration by adding H_6-acetone. First, the mixture with D mole fraction x_D=0.8096 has been measured. Then the liquid was removed from the Nb can and weighted. The mass of the liquid determines then the required amount of H_6-acetone which has to be added in order to get the mixture with the next desired D mole fraction. The required amount has been calculated as follows:
The D mole fraction x_D of the existing mixture is given by:

$$x_D = \frac{n_D}{n_H + n_D}, \tag{5.1}$$

where n_H and n_D are the particle numbers (in mole) of H_6-acetone and D_6-acetone, respectively. The desired D mole fraction x'_D of the next mixture which has to be prepared by adding a certain amount n'_H of H_6-acetone is:

$$x'_D = \frac{n_D}{n_H + n_D + n'_H}, \tag{5.2}$$

which gives for n'_H

$$n'_H = \frac{n_D}{x'_D} - (n_H + n_D) \tag{5.3}$$

or, with M being the molecular weight and m_H and m_D being the masses of H_6-acetone and D_6-acetone, respectively, existent in the mixture

$$n'_H = \frac{m'_H}{M_H} = \frac{m_D}{M_H x'_D} - (\frac{m_H}{M_H} + \frac{m_D}{M_D}). \tag{5.4}$$

Now, the mass of the existing mixture after the measurement is

$$m_{mix} = m_H + m_D = n_H M_H + n_D M_D \tag{5.5}$$

or

$$\frac{m_{mix}}{n_H + n_D} = x_H M_H + x_D M_D. \tag{5.6}$$

Rearrangement gives

$$n_H + n_D = \frac{m_{mix}}{x_H M_H + x_D M_D}. \tag{5.7}$$

Using the mass density of the mixture ρ_{mix} as follows:

$$\rho_{mix} = x_H \rho_H + x_D \rho_D = x_H \rho_H + \frac{n_D}{n_H + n_D} \rho_D \tag{5.8}$$

gives

$$n_D = \frac{(\rho_{mix} - x_H \rho_H)(n_H + n_D)}{\rho_D}. \tag{5.9}$$

Using eqs.(5.7) and (5.9) in eq.(5.3) gives then

$$n'_H = \frac{1}{x'_D} \frac{(\rho_{mix} - x_H \rho_H) m_{mix}}{\rho_D (x_H M_H + x_D M_D)} - \frac{m_{mix}}{x_H M_H + x_D M_D}. \tag{5.10}$$

Since $n'_H = \frac{m'_H}{M_H}$, the required mass m'_H of H_6-acetone which has to be added to the existing mixture of D mole fraction x_D in order to give the desired D mole fraction x'_D is then finally given by

$$m'_H = \frac{m_{mix} M_H}{x_H M_H + x_D M_D} \left(\frac{(\rho_{mix} - x_H \rho_H)}{x'_D \rho_D} - 1 \right). \tag{5.11}$$

Accordingly, the subsequent D mole fraction of the new mixture is

$$x'_D = \left((\frac{m'_H (x_H M_H + x_D M_D)}{m_{mix} M_H} + 1) \frac{\rho_D}{\rho_{mix} - x_H \rho_H} \right)^{-1}. \tag{5.12}$$

These samples have been measured using the annular Nb can at $T = 298$ K. The three mixtures were of the following compositions: H:D=0.75:0.25; 0.45:0.55; 0.19:0.81.

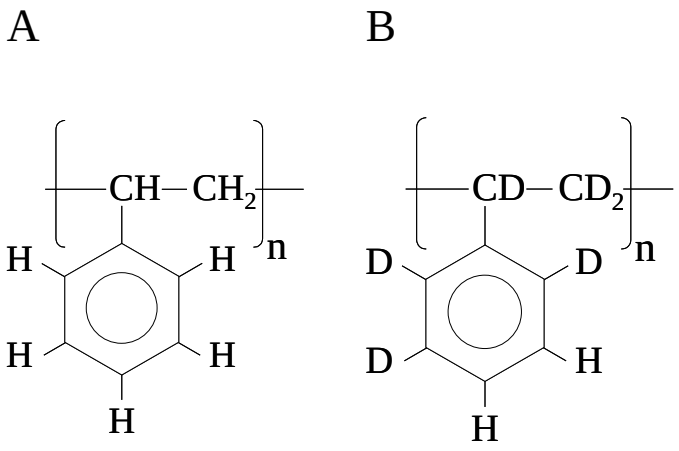

Figure 5.4: Structural formula of fully protonated polystyrene (A) and an example of a partially ring deuterated polystyrene (B).

5.3.4 Polymers

5.3.4.1 H-Polystyrene

For the preparation of the H-Polystyrene (Fig. 5.4.A) the following procedure has been applied. First, the liquid styrene monomer ($CH_3CH_2C_6H_5$) has been freed from the stabilizer by distillation under vacuum. Then, the polymerization has been started by adding less than 1 mol % AIBN (α,α'-Azoisobutyronitril) and was left at a temperature of 328 K in nitrogen atmosphere for 24 hours. The solid polymer has been dissolved in tetrahydrofurane (THF), precipitated in ethanol, filtered and then the same procedure has been repeated again. Then it was dried at 313 K over P_2O_5 until mass constancy was achieved.

5.3.4.2 Ring substitution

These samples (see Fig. 5.4.B) have been obtained by protonation of fully deuterated polystyrene (PS) through catalytic isotope exchange in the presence of ethylaluminium dichloride and traces of water as co-catalyst following the procedure described in Ref. [108]. This one step procedure is highly selective for aromatic hydrogen atoms and nearly free from steric effects.

A 10 wt.% solution of D-polystyrene in liquid H_6-benzene has been mixed with a 50% solution of ethylaluminium dichloride in hexane and μl quantities of liquid H_2O have been added. The solution was stirred slowly at room temperature. For stopping the protonation reaction, an excess of water was added in order to destroy the catalyst. The extent of protonation is dependent on the time elapsed from the start of the reaction to the addition of the excess water. After precipitating the partially deuterated polystyrene in methanol, freeing it from residuals of the catalyst with methanolic HCl and slowly evaporating the solvent in vacuum, an H-NMR spectrum had been recorded. The protonation extent was then determined from the areas of the

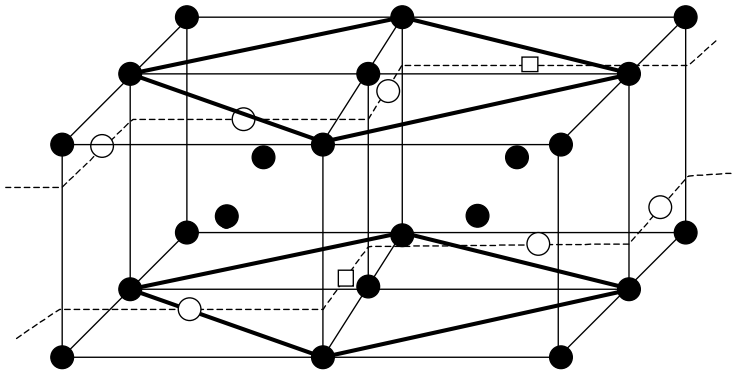

Figure 5.5: Tetragonally distorted b.c.c. lattice of β-phase NbH_x. The H sites form chains connecting tetrahedral positions in the Nb cube faces. Full circles denote the Nb host lattice, whereas the open circles denote H or D atoms and open squares indicate the remaining vacancies.

proton signal. The following protonations have been achieved: (i) 99.5 %; (ii) 87.0%; and (iii) 32.6 % and measured at VESUVIO. The foils were of circular shape with 40 mm diameter and ca. 0.2 mm thickness.

As these polymers are flat foils which are mechanically stable and chemically inert, no sample container is needed and they can be measured hanging freely e.g. on an Al frame.

5.3.5 Metal Hydrogen systems

5.3.5.1 Niobium hydrides

The Nb hydrides have a strong and well-characterized coupling between hydrogens and the host metal lattice [28]. Therefore, they were chosen as a test case for further investigation of the possibility of cross section anomalies of the protons/deuterons. The Nb hydride foils were produced at the Department of Physics of the Royal Institute of Technology in Stockhom/Sweden.

Most of the experiments on niobium hydrides were made with the hydrides in the β-phase, which is stable in NbH_x (or NbD_x) for x-values approximately between 0.73 and 1.00 and in the temperature range $200-370$ K [109]. In the β-phase, the b.c.c. Nb-lattice is slightly tetragonally distorted. The hydrogen occupies tetrahedral positions in the Nb cube faces and the energetically most favored H-sites form chains connecting such tetrahedral sites, as illustrated in Fig. 5.5, with empty tetrahedral sites in the layers in between being filled only at higher x. For temperatures below 200 K, at the x-values studied here,

the H- (or D-) sublattice orders such that the "strings" mentioned above are occupied by proton (or deuteron) pairs with regularly spaced vacancies in between, but the lattice remains tetragonally distorted, as in the β-phase.

In the tetrahedral positions, protons or deuterons are situated in potential wells whose properties have been studied by inelastic neutron scattering. For NbH_x in the β-phase, Verdan et al. [110] obtained for the difference between the zero point vibrational level (i.e., the ground state) and the first excited state an energy of 114 meV. The corresponding value for NbD, as measured by Conrad et al. [111] and Stump et al. [112], is $\Delta E^{vib} \approx 70$ meV. Assuming approximate harmonicity of the vibration and the relations $E_0^{vib} = (1/2)\hbar\omega$, $E_1^{vib} = (3/2)\hbar\omega$, one obtains a position of 57 meV for the zero-point level in NbH (and correspondingly, ca. 35 meV for NbD). From these values, the momentum distribution widths are estimated (using eq.(3.35); see also [90]) assuming the population of the excited vibrational states to be rather small at room temperature and below because the energy difference between the ground and the excited state is in both cases of the order of 100 meV. The standard deviations of the momenta thus determined were found to be $\sigma_p(H) = 4.5$ Å^{-1} and $\sigma_p(D) = 5.2$ Å^{-1}. These values agree well with those determined experimentally in this work: i.e., $\sigma_p^{exp}(H) = 4.33$ Å^{-1} and $\sigma_p^{exp}(D) = 5.0$ Å^{-1}.

When kept in a normal atmosphere, hydrogenated foils of Nb are covered by a thin natural oxide layer which serves as an efficient barrier for hydrogen up to temperatures of at least 450 K. The hydrogenated Nb foils, which had a thickness of 0.5 mm and an area of 30×50 mm could therefore be mounted, freely hanging in an Al-frame for measurements at room temperature. For the lower temperatures the Nb-foils were mounted in a thin-walled closed-cycle cryostat. In both arrangements, the scattering from surrounding material was kept at a minimum. NbH_xD_y hydrides with $x + y \approx 0.85$ ($x = 0.78$, $y = 0$; $x = 0.61, y = 0.28$; $x = 0.39$, $y = 0.46$; $x = 0.16$, $y = 0.70$; $x = 0.03$, $y = 0.80$) were prepared in a specialized hydrogenation setup [113] by first heating the Nb-foils in vacuum at 1000°C and then exposing them to pure H_2 , or D_2 gas at a pressure of $2 - 2.5$ bar and a temperature of 340°C for 1.5 hours. They were then used directly for the neutron scattering experiments.

For the pure $NbH_{0.85}$ and $NbD_{0.85}$ samples, the H and D concentrations were uniquely determined by weighing. But the mixed hydrides required an outgassing procedure using a calibrated mass spectrometer for determining the isotope ratios n_H/n_D with an accuracy of $\pm$ 2%. The total concentration n_H+n_D was kept approximately constant at ≈ 0.85. The mean distance of the hydrogens in Nb hydride $NbH_{0.85}$ is about 2.5 Å.

Because of the chemical as well as mechanical stability of the Nb hy-

dride foils, the ratios σ_H/σ_{Nb} and σ_D/σ_{Nb} can be determined directly from the measured spectra without extracting the scattering signal of any sample container. The foils were mounted on a thin Al-frame connected to a closed cycle cryostat for low temperature measurements. This geometry minimizes the scattering from the Al-frame and all the supporting arrangements. The whole arrangement was covered by an Al cylinder in order to protect the sample from heating by the heat radiation of the surrounding equipment.

5.3.5.2 Palladium hydrides

PdH_x possesses a β-phase structure at the concentrations used for this work, i.e. x=0.54 . The question of local clustering of H-atoms within the α-phase has been discussed by Cox et al. [114] who considered the stability of pairs of H-groups within the Pd lattice. In this phase the protons (or deuterons) occupy interstitial sites of octahedral symmetry. For the Pd-D system a partial ordering, with filling only of sites in alternating planes, (similar to that described for the chains of the Nb hydrides), has been observed by neutron diffraction [115] (see Fig. 5.6), and it is probable that a similar arrangement is valid also for the Pd-H system at the H concentrations studies here.

In the octahedral sites $E_1^{vib} - E_0^{vib} = 68(2)$ meV for PdH [116] (and 48(4) meV for PdD), which corresponds to $E_0^{vib} \approx 30$ meV for the zero-point vibration of H (and ≈ 20 meV for PdD). The values of σ_p were determined as $\sigma_p(H) = 3.4$ Å^{-1} and $\sigma_p(D) = 4.1$ Å^{-1}. The experimentally determined ones are $\sigma_p^{exp}(H) = 3.2$ Å^{-1} for the proton and $\sigma_p^{exp}(D) = 3.9$ Å^{-1} for the deuteron.

Work with Pd-hydrides requires hydrogenation "in situ" since the metal surface does not develop a protecting oxide layer as the Nb-hydrides. The Pd-metal sample used here was a disc of 60 mm diameter and of 0.5 mm thickness. It was placed in an Al-container with wall thickness 0.5 mm which was connected to a hydrogen gas rig. The whole arrangement was placed on the cold finger of a liquid He cryostat. The amount of hydrogen absorbed after an initial connection to a H_2 (or D_2) reservoir could be determined only from the decrease of pressure in the calibrated volume. From the absorption enthalpy curves for the Pd-H system it is expected that the H concentration should stabilize at $PdH_{x\approx0.60}$ where the pressure-composition diagram has a sharp kink upwards. This is expected to happen for pressures below the initial pressure used here. However, the pressure decrease actually measured corresponded to somewhat lower values, $PdH_{x\approx0.53}$ (the values calculated from the pressure change might therefore be affected by uncertainties in pressure and volume calibration).

Samples of the following H/D compositions have been produced in situ

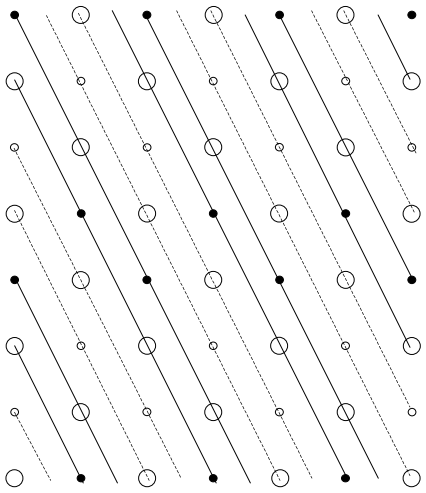

Figure 5.6: Top view of the $PdH_{0.5}$ f.c.c. lattice. Open large circles represent the Pd atoms. Interstitial H atoms (small full circles) are situated in the [420] planes alternating with pairs of empty H sites (open small circles)

and measured: $PdH_0D_{0.3}$, $PdH_{0.1}D_{0.3}$, $PdH_{0.2}D_{0.3}$, $PdH_{0.23}D_{0.3}$, and $PdH_{0.54}D_0$.

5.3.5.3 Yttrium hydrides

The investigations are extended to metal hydrides of higher H (and D) concentrations. The structures and physical properties of yttrium hydrides are well studied [117–119]. Yttrium dihydride, also called β-YH_2, possesses a CaF_2 structure [118] in which the hydrogen atoms fully occupy the interstitial tetrahedral sublattice created by the face centered-cubic lattice of the metal atoms. The corresponding hydrogen atom density is ≈ 57 atoms/nm^3 with near-neighbor H-H distances of 2.6 Å. Yttrium trihydride, also called γ-YH_3, possesses a hexagonal close packed metal lattice in which two-thirds of the H atoms are located in distorted tetrahedral sites while one-third are arranged in trigonal-type sites in the vicinity of the metal basal planes of an hcp Y sublattice. In this case, the corresponding hydrogen atom density is ≈ 78 atoms/nm^3 with smaller near-neighbor H-H distances in the range of $2.1 - 2.6$ Å.

According to the determined vibrational frequencies of the hydrogen in YH_2, YD_2, YH_3, and YD_3 [120, 121], the ground state vibrational energy E_0^{vib} and thus the standard deviation of the momentum distribution can be calculated. In the table below the values are given and compared to the experimentally determined ones. Whereas the hydrogens in the dihydrides are

equivalent, the hydrogens in the trihydrides involve three different frequencies, thus implying three different momentum distribution widths. Since the yttrium hydrides were polycrystalline, the hydrogen (H as well as D) momentum distribution determined experimentally with NCS is governed by the widest momentum distribution present in the sample.

In the table the vibrational frequencies ν, vibrational energies E_{vib}, momentum distribution widths σ_p calculated according to eq.(3.35) and the experimentally determined widths of momentum distributions σ_p^{exp} are given.

	ν [cm^{-1}]	E_0^{vib} [meV]	σ_p [Å^{-1}]	σ_p^{exp} [Å^{-1}]
YH_2	1030	64	3.2	3.9
YD_2	984	61	4.4	4.8
YH_3	1295 920 640	161 114 79	3.6 3.0 2.5	3.7
YD_3	916 651 453	114 81 56	4.3 3.6 3.0	4.7

The Yttrium hydrides with the following compositions: (i) $Y(H_{1-x}D_x)_2$ (x=0 and 1) and (ii) $Y(H_{1-x}D_x)_3$ (x=0, 0.2 and 1) were prepared at NIST, Gaithersburg, USA, by quantitatively controlled reaction of high-purity Y (99.99 atomic %) with H_2 and D_2 gases.

The yttrium hydride powders were put in square shaped Al pouches and placed in flat Al cans that were properly sealed to protect the hydride from air.

5.3.5.4 Lithium hydride

Hydrogen forms stable stoichiometric hydrides by reaction with all of the alkali metals: Li, Na, K, Rb, Cs [122] of which LiH has been chosen for investigation in this work. The reason for choosing LiH is that the Li recoil peak can be easily resolved from the Al can one. In the previously mentioned hydrides (NbH, etc.) the H occupies interstitial lattice sites where the H atoms can hop between the different cites. In contrast to those hydrides, LiH is an ionic hydride with the H – charged negatively – being rigidly bonded to the positively charged Li ions. X-ray studies [123] have shown that LiH crystallize with the rock-salt structure at room temperature. The structure and dynamics of LiH (and LiD) have been extensively studied [124].

The used LiH powder which has been purchased from Sigma Aldrich has been loaded in an Al pouch and placed in a standard Al can sealed with indium wire. A dry box has been used for sample loading in order to protect

the powder from degradation due to moisture. The measurements have been done at temperature $T = 20$ K and $T = 300$ K.

These measurements have been motivated by the fact that the electronic environment surrounding the H nuclei may be responsible both for the creation and destruction of quantum entanglement. Therefore, if the anomalous NCS effect considered in the present work arises from protonic quantum entanglement, then the change of the influence of the environment on the protons, e.g. by involving different electronic structures or changing the temperature, should influence the scattering behavior.

Chapter 6

Data analysis

6.1 General

We first consider a system of N identical atoms, scattering neutrons into a detector subtending a solid angle $d\Omega$, at scattering angle θ. It follows from the definition [27] of the partial differential scattering cross section $d^2\sigma/d\Omega dE$, that the number of neutrons with incident energies in the range E_0 to $E_0 + dE_0$, detected with final energies between E_1 and $E_1 + dE_1$ is

$$C_D(E_0, E_1)dE_0dE_1 = I(E_0)D(E_1)\frac{d^2\sigma(E_0, E_1, \theta)}{d\Omega dE_1}d\Omega dE_0dE_1 \tag{6.1}$$

where $I(E_0)dE_0$ is the number of incident neutrons/unit area with energies between E_0 and $E_0 + dE_0$ and $D(E_1)$ is the probability that a neutron of energy E_1 is detected.

The incident neutrons have energies in excess of 1 eV so that their intensity spectrum $I(E_0)$ is that of epithermal neutrons being slowed down by the moderator (see Fig. 4.2). The spectrum has the form [125]:

$$I(E_0) \propto E^{-\gamma} \tag{6.2}$$

with γ =0.9. For the determination of $I(E_0)$, see section 8.4.

It follows from standard theory [27] that for isotropic scattering,

$$\frac{d^2\sigma(E_0, E_1, \theta)}{d\Omega dE_1} = |b|^2 \sqrt{\frac{E_1}{E_0}} S(q, \omega) \tag{6.3}$$

where b is the nuclear scattering length, the energy transfer in the measurements is

$$\omega = m\left(v_0^2 - v_1^2\right)/2 \tag{6.4}$$

and the momentum transfer

$$q = m\left(v_1^2 + v_0^2 - 2v_0v_1\cos\theta\right)^{1/2}. \tag{6.5}$$

The velocity of the scattered neutron is

$$v_1 = \sqrt{2E_1/m} \tag{6.6}$$

with a similar expression for the velocity v_0 of the incident neutron, where m is the neutron mass. The neutron time of flight t is thus

$$t = \frac{L_0}{v_0} + \frac{L_1}{v_1} \tag{6.7}$$

where L_0 is the incident flight path and L_1 is the final flight path (Fig. 4.2). Equations (6.6) and (6.7) can be used to define E_0 in terms of E_1 and t

$$E_0(E_1, t) = \frac{m}{2}\left(\frac{L_0v_1}{v_1t - L_1}\right)^2. \tag{6.8}$$

The total number of neutrons detected in a time channel between t and $t+dt$ can be expressed as

$$C(t)dt = \left[\int C_D[E_0(t, E_1), E_1]\frac{dE_0(t, E_1)}{dt}dE_1\right]dt. \tag{6.9}$$

An alternative and equally valid approach, used by Blostein et al [126], is to calculate $C(t)$ by expressing E_1 as a function of t and E_0 and integrating over E_0. However, it is convenient to use eq.(6.9) for an *inverse geometry* instrument such as VESUVIO where the energy of the scattered neutron is analyzed. It follows from eqs. (6.6) and (6.8) that

$$\frac{dE_0}{dt} = \left(-\frac{2^{3/2}}{L_0m^{1/2}}\right)E_0^{3/2}. \tag{6.10}$$

For an ideal inverse geometry instrument, in which L_0, L_1, θ are precisely known and only neutrons of a precisely defined energy E_R are detected, i.e.

$$D(E_1) = D(E_R)\delta(E_1 - E_R) \tag{6.11}$$

it follows from eqs. (6.1) and (6.9) – (6.11) that

$$C(t) = 2\left(\frac{2}{m}\right)^{1/2}\frac{E_0^{3/2}}{L_0}I(E_0)D(E_R)N\frac{d^2\sigma}{d\Omega dE_1}d\Omega \tag{6.12}$$

where $E_0(E_R, t)$ is defined via eq.(6.8). Equation (6.12) is the standard expression for the count rate in an inverse geometry time of flight spectrometer [82].

Within the *Impulse Approximation* (see section 3.2.2), if atoms of different mass M are present in the sample, it follows from eq.(6.12) that the count rate is

$$C(t) = 2\left(\frac{2}{m}\right)^{1/2} \frac{E_0^{3/2}}{L_0} I(E_0) D(E_R) \sum_M N_M \frac{d^2\sigma_M}{d\Omega dE_1} d\Omega \tag{6.13}$$

where N_M is the number of atoms of mass M and $d^2\sigma_M/d\Omega dE_1$ is the partial differential cross section for mass M. The IA effectively treats the scattering as single atom *billiard ball* scattering with conservation of momentum and kinetic energy of the neutron + target atom. The dynamic structure factor for atoms of mass M is thus [27]

$$S_M(\mathbf{q}, \omega) = \int n_M(\mathbf{p}) \delta\left(\omega + \frac{p^2}{2M} - \frac{(\mathbf{p}+\mathbf{q})^2}{2M}\right) d\mathbf{p} \tag{6.14}$$

where $n_M(\mathbf{p})$ is the atomic momentum distribution for mass M. It is important to understand that the total scattering cross section given by the IA is the *free atom* value, which is not the same as the cross section in the neutron–nucleus center of mass frame. If

$$n_M(\mathbf{p}) = \delta(\mathbf{p}) \tag{6.15}$$

it follows from eqs. (6.14) and (6.3) that

$$\frac{d^2\sigma_M}{d\Omega dE_1} = b_M^2 \sqrt{\frac{E_1}{E_0}} \delta\left(\omega - \frac{q^2}{2M}\right) \tag{6.16}$$

where b_M is the *bound* scattering length for atoms of mass M. Integrating eq. (6.16) over the solid angle $d\Omega$ and final energies E_1 gives [27] the *free atom* cross section.

$$\int \frac{d^2\sigma_M}{d\Omega dE_1} d\Omega dE_1 = \frac{4\pi b_M^2}{(1+\frac{m}{M})^2} = \frac{\sigma_M}{(1+\frac{m}{M})^2} \tag{6.17}$$

where σ_M is the standard tabulated *bound* total scattering cross section for mass M.

It follows from eq. (6.14) that

$$S_M(\mathbf{q}, \omega) = \frac{M}{q} J_M(y_M) \tag{6.18}$$

where

$$y_M = \frac{M}{q}\left(\omega - \frac{q^2}{2M}\right) \tag{6.19}$$

and

$$J_M(y_M) = \int n_M(\mathbf{p})\delta(y_M - \mathbf{p}\cdot\mathbf{q}/q)d\mathbf{p}. \tag{6.20}$$

The *neutron Compton profile* $J_M(y_M)$ is the probability distribution of the momentum component of mass M along the direction of $\mathbf{q}$ and is analogous to the *Compton profile*, measured in Compton scattering of photons from electrons.

It follows from eqs. (6.18) and (6.3) that,

$$\frac{d^2\sigma_M}{d\Omega dE_1} = b_M^2\sqrt{\frac{E_1}{E_0}}\frac{M}{q}J_M(y_M). \tag{6.21}$$

Combining eqs. (6.13) and (6.21) we get

$$C(t) = \frac{E_0 I(E_0)}{q}\sum_M A_M M J_M(y_M) \tag{6.22}$$

where

$$A_M = \frac{2}{L_0}D(E_R)\sqrt{\frac{2E_R}{m}}\Delta\Omega N_M b_M^2 \tag{6.23}$$

is proportional to the scattering intensity from mass M.

In the derivation of eq. (6.22) it is assumed that the *instrument parameters* L_0, L_1, θ and E_1 are known exactly. In reality these quantities can be determined only according to some probability distribution $P(L_0, L_1, \theta, E_1)$, which determines the instrument resolution. The measured count rate $C_m(t)$ is an average over the possible values of these parameters, weighted by their probability of occurrence

$$C_m(t) = \int C(t)P(L_0, L_1, \theta, E_1)dL_0 dL_1 d\theta dE_1. \tag{6.24}$$

Thus the exact incorporation of the instrument resolution function would entail the evaluation of this four dimensional integral for each data point, in addition to the convolution in t, required to incorporate the uncertainty in the measurement of time of flight. To reduce data processing times, the approximation is made in the data analysis that the resolution can be incorporated as a single convolution in t space, with a different resolution function $R_M(y)$ for each mass. Thus eq. (6.22) is modified to

$$C_m(t) = \left[\frac{E_0 I(E_0)}{q}\right]\sum_M A_M M J_M(y_M)\otimes R_M(y). \tag{6.25}$$

The approximation of replacing the exact expression, eq. (6.24) by eq. (6.25) is referred to as the *convolution approximation* (CA). The instrument resolution function $R_M(y_M)$ is Gaussian for the U foil analyzer and a Voigt function for the Au foil analyzer (see chapter 4).

A second approximation of the data analysis is that $J_M(y_M)$ is assumed to have a normalized Gaussian form

$$J_M(y_M) = \frac{1}{\sqrt{2\pi\sigma_p^2}} \exp\left(\frac{-y_M^2}{2\sigma_p^2}\right). \tag{6.26}$$

The data analysis consists of fitting eqs. (6.25) and (6.26) to the data with two fitting parameters for each atomic mass, A_M and σ_p. A_M determines the integrated peak intensity corresponding to a mass M and σ_p determines the peak width. It follows from eq. (6.23) that

$$\frac{A_M}{A_{M'}} = \frac{N_M b_M^2}{N_{M'} b_{M'}^2} = \frac{N_M \sigma_M}{N_{M'} \sigma_{M'}} \tag{6.27}$$

where σ_M is the *bound* cross section for mass M and σ'_M that for mass M'. Thus, if the sample composition (and hence N_M/N'_M) is known, the ratios of cross sections for atoms of different masses can be determined from the ratio of the fitted parameters A_M and A'_M. Since the conventionally expected values of σ_M and σ'_M are given in standard tables, the validity of the basic eq.(6.27) is directly subject to experimental test. According to the QE effect under consideration in this work (see chapter 1), it is expected that this equation is violated for protons in various chemical systems.

It should be noted again that the data analysis procedure incorporates the well known "transformation" from the "free atom" to the "bound atom" cross section which is particularly relevant for light nuclei, like H. This is necessary in order to facilitate the comparison between experimental NCS results and conventional expectation, because, by convention, the bound atom cross sections (and scattering lengths) are those which are tabulated [26, 27]. Also final states effects (as described already in section 3.2.4) are included in the data analysis used in this work.

6.2 Determination of peak widths

In the data analysis, only the amplitude of the Gaussian is a free fitting parameter to a measured TOF spectrum, i.e., the width of the fitting function is kept constant. In each investigated system, e.g. liquid H_2O/D_2O, solid H/D-polystyrene, liquid C_6H_6/C_6D_6, NbH_xD_y, etc., the peaks widths of H

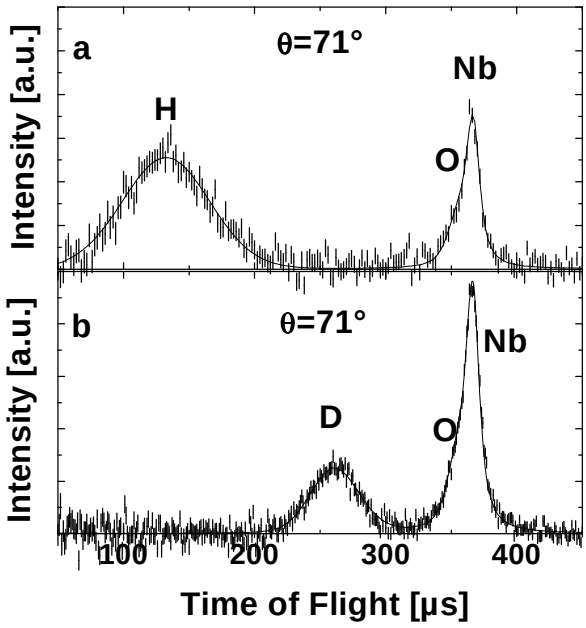

Figure 6.1: Measured time of flight spectra of a.) pure H_2O and b.) pure D_2O at an angle of $\theta = 71$ deg.

and D are determined by separate measurements of the isotopically pure compounds, i.e. pure H_2O, pure D_2O, pure D-polystyrene, pure C_6H_6, NbH_x, NbD_y etc., where there is no overlap of the H and the D peak; for an example of a time of flight spectrum, see Fig. 6.1 or Fig. 6.2 for the same Tof spectrum transformed to the momentum space y. For examples of fitted H and D peak widths, respectively, see Fig. 6.3.

It is a crucial advantage of the NCS technique that the H- and D-peaks are well resolved. This is due to the high energies of the incoming neutrons, and the related high energy and momentum transfers. For small scattering angles θ, however, the recoil peaks of C and O of the liquid mixtures, and that of the can (e.g. Nb), do overlap, see Fig. 6.4.a. Unfortunately, it turned out that the can subtraction procedure available at the VESUVIO instrument did not work properly to access the peak areas of the nuclei of intermediate mass (e.g. that of oxygen or carbon). In order to explore whether the peak might be resolved at higher accessible momentum and energy transfers, time of flight spectra simulations using the programs available at the VESUVIO instrument have been done. One example for a carbon peak has been already

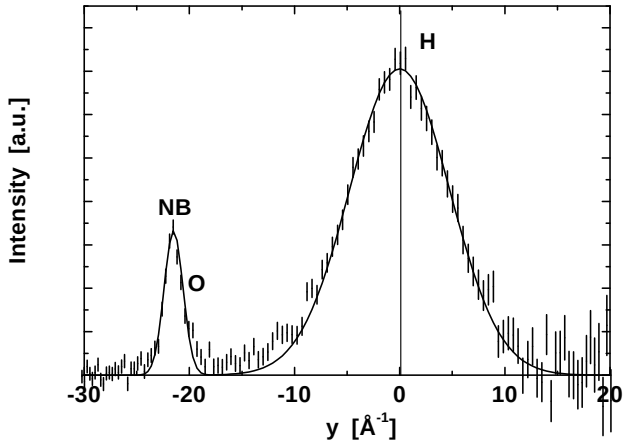

Figure 6.2: y-transformed time of flight spectrum of pure H_2O. Standard deviation of the proton momentum distribution is 4.7 Å^{-1}.

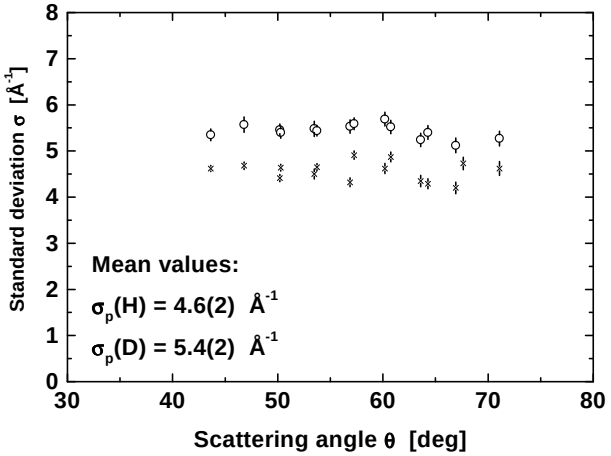

Figure 6.3: Fitted peak widths of H (crosses) and D (circles) in pure H_2O and pure D_2O, respectively. The fitted widths are evenly distributed over the scattering angles.

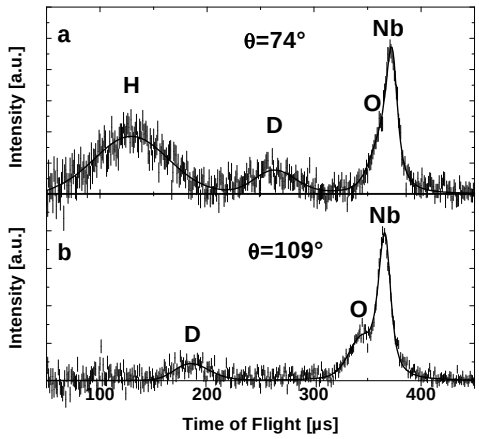

Figure 6.4: Spectra of a H_2O/D_2O mixture measured in a) forward ($\theta = 74$ deg) and b) backward ($\theta = 109$ deg) scattering. It can be seen that in the forward scattering no peak separation of O and Nb can be achieved. but in the backscattering direction the peaks of O and Nb are sufficiently separated to extract the O contribution.

shown in Fig. 5.1 (lower part). It can be seen that the C peak is well resolved from that of the Nb peak. Therefore, some detectors can be positioned in the "backward" scattering regime ($\theta > 90°$), where the momentum transfers are sufficiently larger than in the "forward" direction ($\theta < 90°$). Also in the case of H_2O/D_2O mixture the separation of the O peak from the Nb-peak is well visible in the backscattering regime; see Fig. 6.4.b (A separation of the C and O peaks, e.g. in the case of 2-iso-butoxyethanol or acetone, is not possible).

In order to extract the area of the intermediate heavy nuclei (i.e. C and/or O) from the area due to the sample can, the following procedure has been followed. First, spectra of an empty can (e.g. Nb) were recorded and the peak width σ_p in momentum space has been fitted; see Fig 6.5. Then this peak width is used for the analysis of the backscattering spectra of an O containing sample (e.g. pure H_2O) in order to find out the width in momentum space of the O peak. For an example for the resulting fitted width of the O peak, see Fig. 6.6. It can be seen very clearly, that there is no dependence of the width on angle, which means that the partial (and angle dependent) overlap of the O peak with the Nb one does not influence the analysis. Having thus determined the peak widths (of H, D, O, Nb, etc.), they are then used as fixed input parameters for fitting the areas of peaks

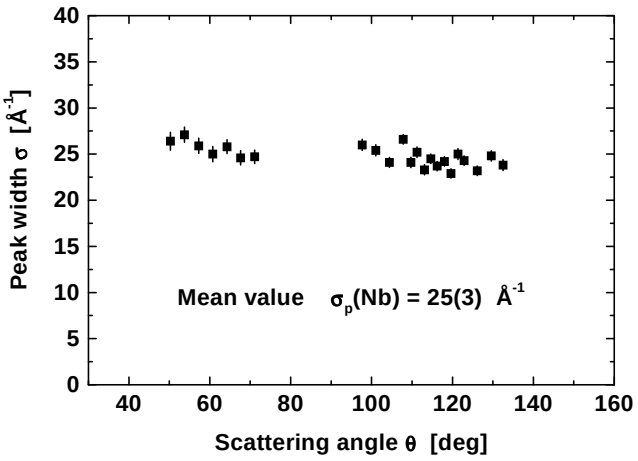

Figure 6.5: Fitted peak width of the empty Nb can to use it as fixed input parameter for later analysis.

of the corresponding samples assuming e.g. that the H peak width in H_2O remains unchanged when mixing D_2O to H_2O.

6.3 Determination of peak areas

The procedure for analyzing the data of a H_2O/D_2O mixture with H:D=1:1 is described in the following. First, the ratio of the peak areas $(A_{Nb}/A_O)_b$ is determined from the backscattering detectors. By knowing the joint peak areas of O and Nb from the forward scattering, namely $(A_{Nb} + A_O)_f$, the O peak area of the forward scattering can be extracted as:

$$A_O = \frac{(A_{Nb} + A_O)_f}{1 + (\frac{A_{Nb}}{A_O})_b}. \tag{6.28}$$

Having determined the intensity of the O recoil peak, the validity of the conventional theoretical expectation, eq.(6.27), can be tested using

$$R_{exp}(H) = A_H/A_O \; or \; R_{exp}(D) = A_D/A_O \tag{6.29}$$

where R_{exp} denotes the experimentally determined ratio as to be distinguished from the conventionally expected (or tabulated) one, R_{conv}. The conventionally expected value of this ratio is,

$$R_{conv}(H) = N_H\sigma_H/N_O\sigma_O \; or \; R_{conv}(D) = N_D\sigma_D/N_O\sigma_O \tag{6.30}$$

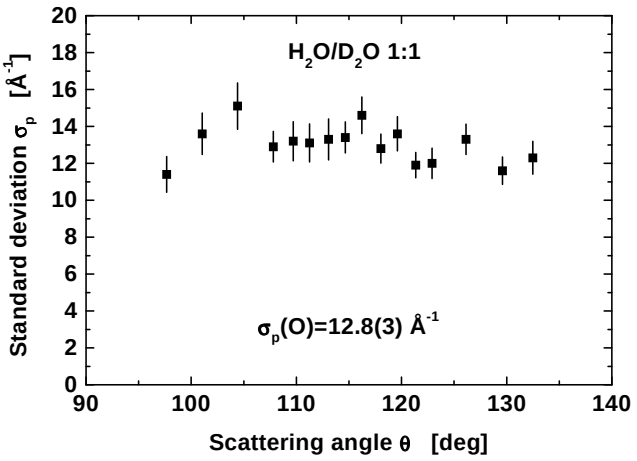

Figure 6.6: Fitted peak width of oxygen of liquid H_2O/D_2O (1:1) mixture to use it as fixed input parameter for later analysis. Although there is an angle dependent overlap of the O peak with the Nb one of the can (see Fig. 6.4.b), the fitted peak widths are evenly distributed over the scattering angles.

since the atom densities N_H, N_D and N_O, are precisely known through sample preparation and chemical formulae.

For the case of 2-iso-C_4E_1 in D_2O only the joint areas of O and C can be determined and this ratio reads $R_{exp}(H) = A_H/(A_O + A_C)$ where A_O refers to 2-iso-C_4E_1 and D_2O as well, since both molecules contain oxygen (see section 7.2.4).

In the context of NCS, the impulse approximation (IA) and the correction of it, the so-called final-state effects (FSE), are valid, cf. [85, 103, 127]. FSE may lead to slight distortions of the Gaussians used in the fits. It may be noted that these effects are important for the precise determination of the shape of a recoil peak and the corresponding momentum distribution of the nucleus in order to calculate the mean kinetic energy, but they do not affect appreciably the integral scattering intensity of a peak and thus the total cross section of the scatterer. Nevertheless, FSE using the Sears expansion (see eq.(3.43)) have been taken into account in the data analysis procedure of the present work. In order to learn to which extent the FSE may affect the values of the determined areas, data were analyzed including FSE corrections (as is in standard use at VESUVIO) and without using them. The results are depicted in Fig. 6.8 for the ratio σ_H/σ_O. It can be seen that FSE leave the results unaltered.

In addition, the data analysis procedure accounts for the factor v_1/v_0 (or

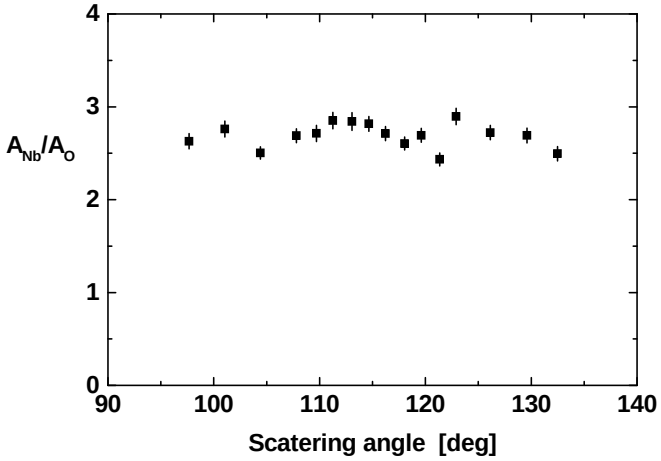

Figure 6.7: Angular distribution of the area ratio of Nb and O determined from the backscattering spectra.

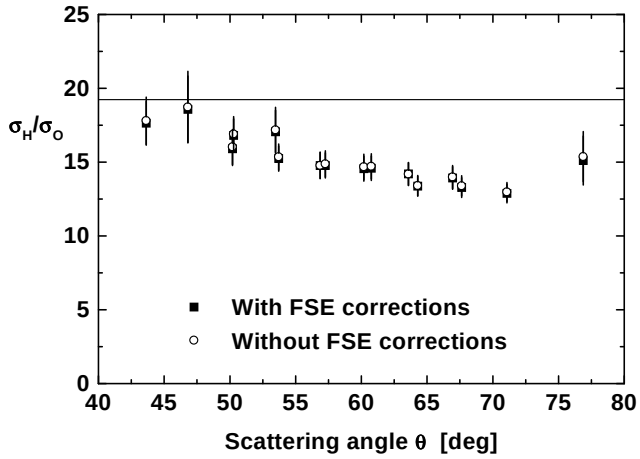

Figure 6.8: σ_H/σ_O ratio of H_2O/D_2O with x_D =0.5 determined a) without using the final states corrections (open circles) and b) after application of final states corrections (full squares). As can be seen, final states effects have negligible effect of the σ_H/σ_O ratio.

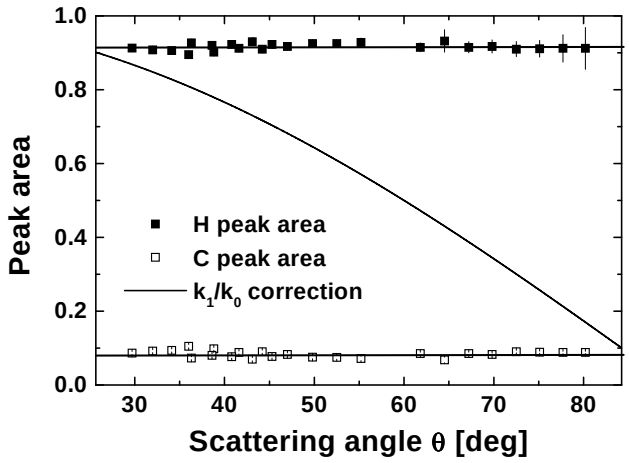

Figure 6.9: Fitted areas of H and C in polystyrene as a function of scattering angle. The constancy of the areas with respect to the scattering angle is evident and shows the accurate account for the intrinsic angle dependence of the scattering intensity; see e.g. eq.(6.21). Shown is also the factor k_1/k_0 (full line) for H which is included in the data analysis and which exhibits a strong dependence on the scattering angle.

equivalently k_1/k_0) appearing in the basic eq.(6.21); see Fig. 6.9. According to the applied angle corrections, no angle dependence of the scattering intensity is expected. Therefore, any angle dependent area should have its reason in genuine physics being beyond the conventional derivations. Fig. 6.9 shows an example of the k_1/k_0 correction factor for scattering on protons. It can bee seen that this factor is strongly dependent on the scattering angle. If this factor would not be included in the data analysis procedure, then all determined areas would also exhibit a strong dependence on scattering angle. However, as an example, the areas of C and H of polystyrene is depicted as full and open squares, respectively, exhibiting a strong constancy with respect to the angle and thus also to the k_1/k_0 ratio.

Chapter 7

Experimental results

In this chapter the results of the experiments conducted during this work will be presented. The results of the OH bonds, e.g. in water, urea/water (which also involves N-H bonds) and water with added electrolyte, are presented first and then followed by the work done on C-H bonds including organic materials like benzene, polymers, amphiphiles and acetone. This is followed by the presentation of the experimental results of the hydrides of niobium, palladium, yttrium, and lithium, respectively. Every section starts with the presentation of example time of flight spectra. The intensities are always given in arbitrary units (abbreviated by a.u.). Then intensity ratios of H to another heavy nucleus (e.g. D, O, C, respectively) depending on the context are presented. This chapter concludes with a summary and discussion of all results.

Some comments are in order here about the conditions of the experiments the results of which are presented here. Since the first experiments on H_2O/D_2O mixtures in 1995 many developments have taken place from the instrumental point of view. Although the presentation will start with the original experiments on H_2O/D_2O mixtures at room temperature, it will not be done in the historical order. For example, at the beginning of this work the cans made of aluminum or vanadium, respectively, which are in standard use at the VESUVIO instrument were used. Thus only the determination of σ_H/σ_D was possible, because the scattering peaks of "heavier" nuclei, O or C, could not be satisfactorily resolved from the can material one. Later, when more experience has been acquired during this work, it was suggested to use a can made of niobium. The high mass of the Nb nucleus would make it possible to extract the scattering contributions of O or C, respectively, and to facilitate the determination of σ_H/σ_O or σ_H/σ_C, respectively.

The VESUVIO spectrometer has undergone several changes when it was developed to from the eVS machine during the last few years and also due

to its transition to EVERDI. In its intermediate status it did not provide optimum performance and thus the accessibility of some quantities was affected. For example, the replacement of the original cylindrical sample tank (see Fig. 4.2) by a cubic one with stainless steel support at the corners made it impossible to place detectors in the intermediate scattering angle range in forward scattering. In addition a bulky equipment in the backscattering direction has been installed which prevented from positioning detectors there. Consequently, there was an experimental period in which it was not possible to resolve O or C, respectively, from the Nb can material. For example, the measurements of the acetone samples were again restricted to the determination of σ_H/σ_D. Since the access to the VESUVIO instrument is limited by the allocation of beam time by the international selection committee, it was not possible to repeat all measurements in order to get the optimum information of the desired quantities.

On the other hand, the instrument development included the installation of 44 new detectors positioned in the backscattering direction. This made possible to put the original 32 detectors in the forward scattering direction. In addition, the data acquisition electronics has also been developed at ISIS which included deeper memory and which made it possible in many cases to use all those detectors without suffering from electronics saturation.

7.1 OH bonds

7.1.1 H_2O/D_2O mixtures at room temperature

Because of their fundamental importance and because of the novelty of the anomalous results, the measurements on H_2O/D_2O mixtures at room temperature have been repeated many times involving different experimental setups, e.g., by changing the analyzer foils and by using a special annular niobium can instead of the usual vanadium or aluminum ones.

The first experiments on H_2O/D_2O mixtures (see Fig. 7.1 for an example) were done using the Au foil analyzer having a Lorentzian shaped resonance absorption band centered at $E_1 = 4908 \pm 130$ meV. The results obtained with this foil are shown in Fig. 7.2 (open circles). A very strong dependence of the ratio $Q = \frac{\sigma_H}{\sigma_D}$ on the D mole fraction of the H_2O/D_2O mixture has been observed. Furthermore, all values are below the conventionally expected one being $\frac{\sigma_H}{\sigma_D} = 81.67/7.61 = 10.7$ [31].

Because this result was very astonishing, possible instrumental artifacts have been searched for. It is for example in principle conceivable that the Au foils slightly underestimate the Q value as some weight gets transferred from

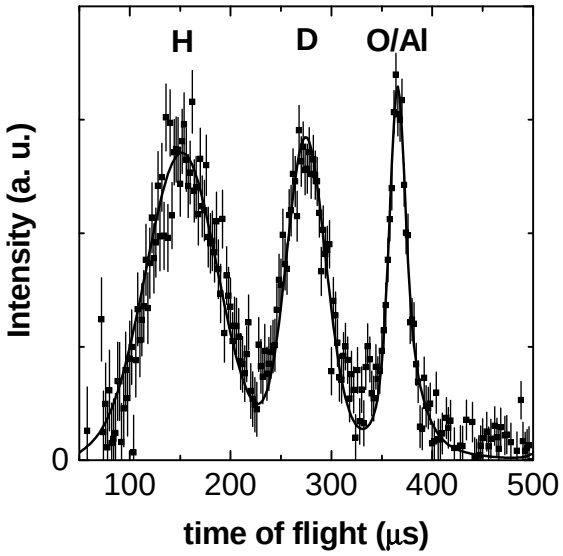

Figure 7.1: Shown is the time of flight spectrum of a H_2O/D_2O mixture with D mole fraction x_D=0.8 in an aluminum can at a scattering angle of 69° using the gold foil analyzer. The intensity is given in arbitrary units. Whereas the proton peak is well resolved from the deuteron one, the oxygen peak can not be resolved from the aluminum one.

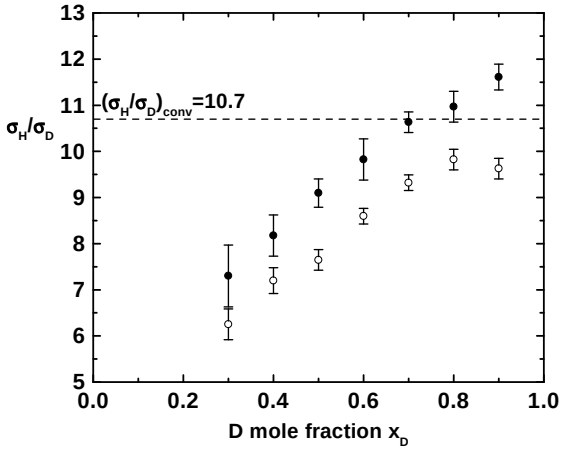

Figure 7.2: The ratio σ_H/σ_D as a function of the D mole fraction x_D in H_2O/D_2O mixtures at room temperature. Open circles indicate measurements done with the Au foil analyzer and full circles indicate the ones with the U foil analyzer. The horizontal dashed line at 10.7 represents the conventionally expected or tabulated value of σ_H/σ_D.

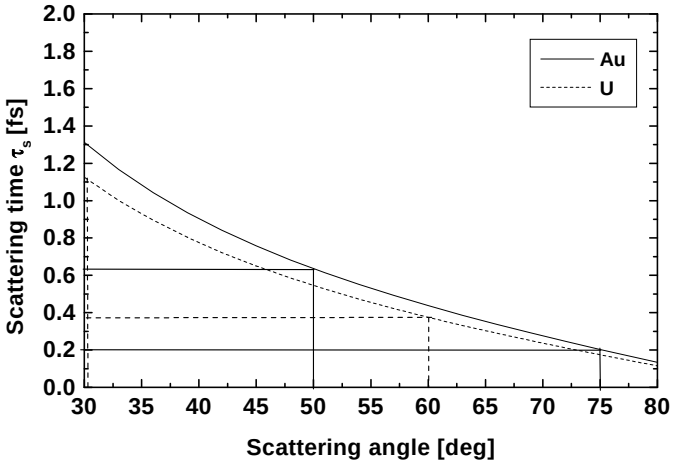

Figure 7.3: Dependence of the scattering time τ_s on scattering angle for scattering hydrogen (assumed momentum distribution width of 4.5 $\mathring{A}^{-1}$) if gold foil analyzer (full line) or uranium foil analyzer (dashed line) is used.

H to D because of the long tails of the Lorentzian Au resolution function. This effect should be negligible with U foils because of the narrow Gaussian shape of its resonance absorption band centered at $E_1 = 6771 \pm 63$ meV. Therefore, the measurements have been repeated using the U foil analyzer. The results are also depicted in Fig. 7.2 (full circles). As can be seen, while the dependence of Q on the D mole fraction of the mixtures is still significant, the Q values are indeed closer to the conventionally expected value. However, the experimentally determined differences between the U and Au values amount to ca. 25%. This is too high compared with the results of the Monte Carlo calculations predicting a difference of a few percent [34]. Therefore, there must be a different reason for this large difference between the Au and U results.

Meanwhile, in the same year the measurements have been done, Watson [85] has published a paper which let these large differences appear in a new light.

In contrast to the majority of the NCS experiments performed on VESUVIO for the investigation of peak shapes, in the present case the absolute value of the resonance energy does play an important role. For it follows from the kinematics conditions of the instrument that the change of final neutron energy leads to a change of the momentum transfer involved during the scattering process. Furthermore, according to Watson [85] different momentum transfers lead to different scattering times τ_s appearing as the rel-

evant interaction time between the neutron and the scattering nucleus within the impulse approximation (see section 3.2.5). This means that by changing the one analyzer foil by the other, different time windows are involved automatically and therefore the dynamics are looked at within different time scales. Therefore, it is not surprising that the data obtained using the gold foil analyzer give different results than using the uranium foil analyzer.

For illustration of these consideration, see Fig. 7.3. Here it is presented the dependence of the scattering time τ_s on the scattering angle for scattering on protons in water using Au (full line) and U (dashed line) analyzers. The horizontal and vertical straight lines indicate the angular range being accessible using the two different analyzer foils and the corresponding τ_s range. It can be seen that the angle range of U is limited to 60°. This is because for higher angles, the proton would overlap with side bands of the U absorption. Also the fact that the U foil data are closer to the conventionally expected value of 10.7 indicates the interdependence of the scattering time and the decoherence time. This is because – as is evident from Fig. 7.3 – the scattering on U involves on the average longer scattering time. I.e. the time window over which the entangled protons are looked at is longer than using the Au foil. Therefore, it is conceivable that during that time range, the phases of the entangled states are smeared out by averaging over a time range being too long for the decay dynamics (or decoherence). See also the very recent theoretical treatment [58].

Summarizing, the difference between the data obtained using Au and U might arise from the different time scales during which the protons in water are looked at. It is very important to note here that the "anomalous" effect is still evident and is not removed by the improved resolution of the U foil analyzer. That resolution effects do not play any role for the underlying effect is shown by the results of the extensive tests that have been undertaken in order to check these and other experimental data (see chapter 8).

In order to elucidate to what extent the scattering time plays a role for the found anomalies, more experiments with different analyzer foils are required. Related experiments using different foils, e.g. Rh, have been done. However, the foil-in/foil-out difference spectra obtained with Rh were not satisfactory to yield useful data. This is due to the fact that the thickness of the Rh foil used introduced an additional broadening in the energy resolution function. The use of a thinner foil will improve the energy resolution. Additionally, if the thick and the thin Rh foils are used in combination, thus exploiting the so called double difference technique recently implemented on VESUVIO (see section 8.3.3), a considerable improvement of the energy resolution of the instrument is achieved.

As long as the oxygen peak was not possible to be freed from the Al or V

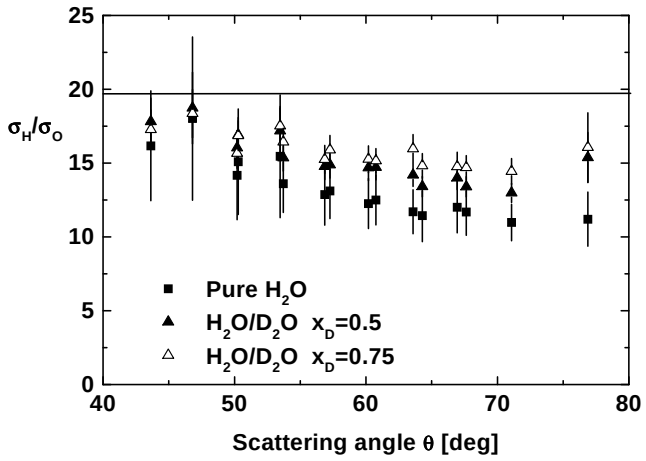

Figure 7.4: σ_H/σ_O ratio determined for H_2O/D_2O mixtures with D mole fractions x_D= 0; 0.5; and 0.75 vs. scattering angle. As can be seen this ratio decreases with decreasing x_D. The anomaly of σ_H/σ_O is the larger the smaller the amount of D is in the mixture. The horizontal line at 18.4 indicates the tabulated value for σ_H/σ_O.

can contributions, no information could be gained about the absolute changes of σ_H or σ_D with D mole fraction of the mixtures. Therefore, it was not possible to see whether σ_H or σ_D or probably both change when changing the D mole fraction of the sample. To overcome this problem and after learning more about the VESUVIO instrument, a new Nb can has been proposed and constructed in close collaboration with the ISIS staff. Nb has been chosen as a can material since it is heavy enough to be got separated from the oxygen peak in the tof spectra recorded at backscattering; see chapter 6. With this new experimental condition at hand, some of the experiments on H_2O/D_2O mixtures were repeated.

As can be seen from Fig. 7.4 σ_H/σ_O is considerably reduced compared with the tabulated value of 18.4 [27]. Furthermore, the reduction becomes larger with decreasing D mole fraction of the H_2O/D_2O mixture and is maximum for pure H_2O the time of flight spectra of which do not "suffer" from peak overlap of D with that of H. This observation is very important in the light of recent criticisms concerning the validity of the data analysis procedure followed at VESUVIO (see section 8) and concerning possible overlap effects of the H and D peak. In addition to these results, a slight scattering angle θ dependence of σ_H/σ_O is visible.

Fig. 7.5 shows σ_D/σ_O ratio ($(\sigma_D/\sigma_O)_{conv}$ = 7.61/4.23) in forward and

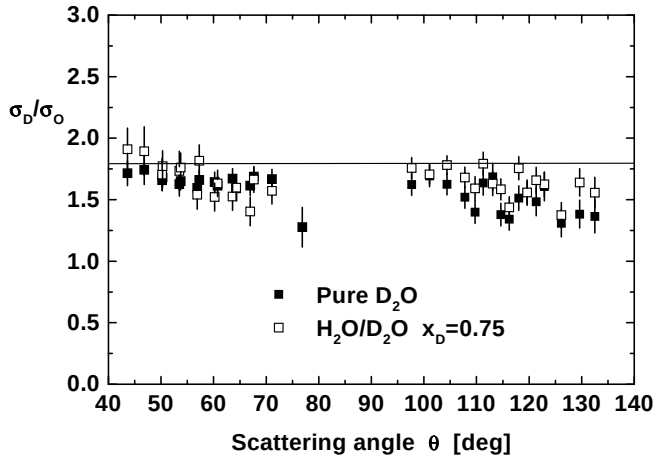

Figure 7.5: σ_D/σ_O ratio determined for H_2O/D_2O mixtures with D mole fractions x_D= 0 and 0.75 vs. scattering angle. The values are shown as determined from the forward and backward scattering spectra. As can be seen this ratio is independent of x_D in the forward scattering. The backscattering data show a systematic increase with increasing x_D. The horizontal line at 1.76 indicates the tabulated value for σ_D/σ_O.

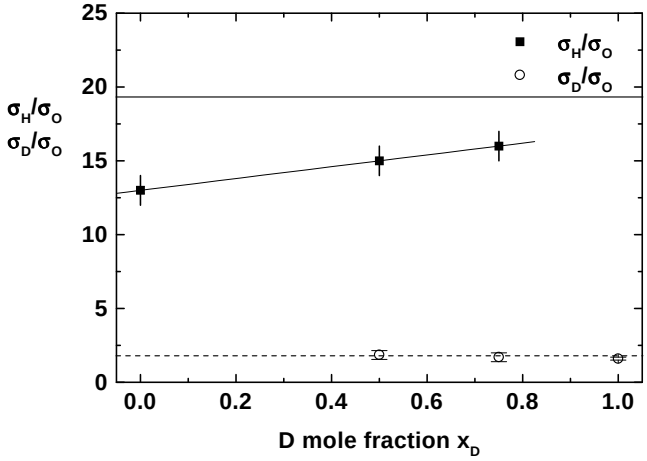

Figure 7.6: σ_H/σ_O and σ_D/σ_O ratios averaged over all scattering angles for H_2O/D_2O mixtures with D mole fractions x_D= 0; 0.5; 0.75; and 1 vs. x_D. While σ_D/σ_O is nearly independent of x_D, σ_H/σ_O is strongly dependent of x_D. Note, that the largest anomaly of σ_H/σ_O is observed where no overlap of H with D is present.

backward scattering of pure D_2O and of a H_2O/D_2O mixture with D mole fraction x_D=0.75. The results of the mixture with x_D=0.5 are omitted for the sake of visibility. One sees that the experimentally determined ratio is not much different from its tabulated value. However, there is a slight tendency towards lower values in the very high scattering angle region.

Fig. 7.6 shows σ_H/σ_O and σ_D/σ_O ratios, respectively, both averaged over the forward scattering angles. It can be clearly seen that the dependence of the σ_H/σ_D ratio shown in Fig. 7.2 on the D mole fraction of the mixture is mainly due to changes of the H scattering cross section rather than to changes of the D scattering cross section. The latter result is very important in the light of the criticism outlined above. This is because the "anomaly" is largest in pure H_2O, i.e., where there is no D peak overlapping with the H one. Additionally, since the peak intensity of D is much lower than that of H, the D signal should be much more affected by the tail of H than the H peak should be affected by the tail of the D peak, if overlap effects really play a role. In contrast, σ_D/σ_O is almost independent of the D mole fraction whereas σ_H/σ_O shows a strong dependence. All these results have been confirmed with a new experimental technique – called Double Difference – which involves a considerable improvement of the energy resolution function of the instrument (see section 8 for details).

7.1.2 Two selected H_2O/D_2O mixtures down to 4 K

These measurements have been performed when no Nb can was available yet. Therefore, the results are restricted to the determination of σ_H/σ_D only.

The low temperature investigations have been concentrated on two mixtures of H_2O/D_2O with D mole fractions $x_D = 0.5$ and $x_D = 0.7$. For both samples a wide temperature range has been scanned in order to explore to which extent the anomalies concerning σ_H/σ_D found in H_2O/D_2O mixtures at room temperature are affected by the nuclear motion. It has been expected that by decreasing the temperature, the decoherence effect would be diminished to a certain degree, so that the anomaly should become more pronounced.

However, surprisingly and very interestingly, although a large temperature range (between $T = 300$ K and $T = 4$ K) has been scanned, no significant difference has been detected as far as σ_H/σ_D is concerned for both mixtures. The results are shown in Fig. 7.7 for $x_D = 0.5$ and in Fig. 7.8 for $x_D = 0.7$ where the ratios σ_H/σ_D are depicted versus the scattering angle θ. Since no significant angle dependence is visible for the various temperatures, the ratio averaged over all detectors is calculated and presented in Fig. 7.9 for a better visibility.

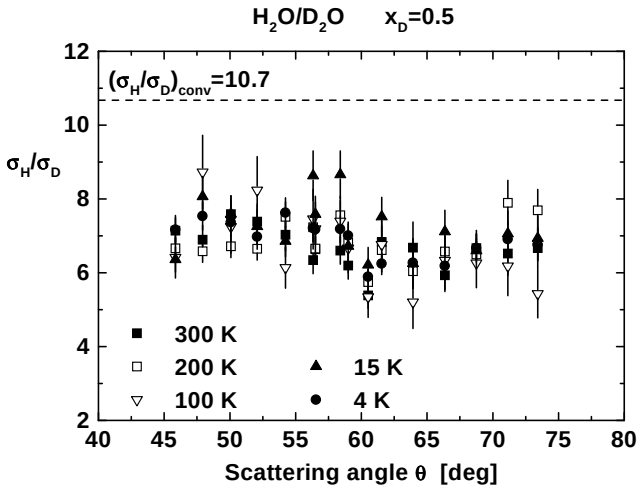

Figure 7.7: Scattering cross section ratio σ_H/σ_D of H and D of the H_2O/D_2O mixture with D mole fraction $x_D = 0.5$ at various temperatures vs. scattering angle. The conventionally expected ratio ($(\sigma_H/\sigma_D)_{conv} = 10.7$) is indicated by the horizontal dashed line. No significant angle or temperature dependence is observed.

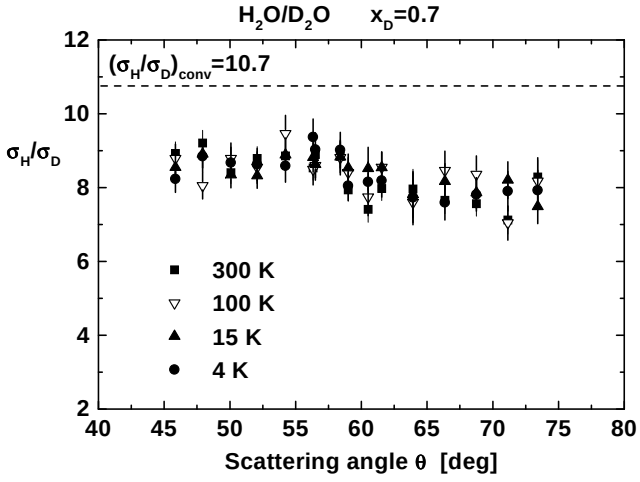

Figure 7.8: Scattering cross section ratio σ_H/σ_D of H and D of the H_2O/D_2O mixture with D mole fraction $x_D = 0.7$ at various temperatures vs. scattering angle. The conventionally expected ratio ($(\sigma_H/\sigma_D)_{conv} = 10.7$) is indicated by the horizontal dashed line. No significant angle or temperature dependence is observed.

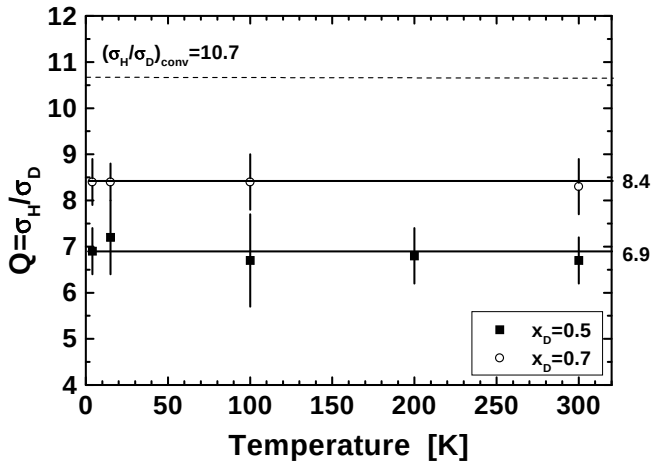

Figure 7.9: Scattering cross section ratio σ_H/σ_D of H and D vs. absolute temperature for the two H_2O/D_2O mixtures with D mole fractions $x_D = 0.5$ and $x_D = 0.7$, respectively. The conventionally expected ratio ($(\sigma_H/\sigma_D)_{conv} = 10.7$) is indicated by the horizontal dashed line. No significant temperature dependence is observed.

Although being a "null" result, i.e. σ_H/σ_D seems to be independent of temperature, it is presented here because later experiments on LiH showed in contrast a significant temperature dependence of σ_H (see section 7.3).

7.1.3 Urea/H_2O/D_2O

In this experiment urea has been dissolved in H_2O/D_2O mixtures (see section 5.3). The results of these measurements are depicted in Fig. 7.10 and compared with those obtained from H_2O/D_2O mixtures of previous measurements [31]. It can be seen, that σ_H/σ_D of these solutions does also exhibit strong dependence on the D mole fraction. The fact that not only OH- but also NH-bonds are involved does influence the ratio σ_H/σ_D. It should be noted that at the time these measurements have been performed, there was no Nb can available. Thus the analysis was restricted to the determination of the ratio σ_H/σ_D only, instead of e.g. $\sigma_H/(\sigma_O + \sigma_N + \sigma_C)$, which would have given more information about the changes of σ_H (due to the assumption that the nuclei C, N, and O do not exhibit quantum entanglement, due to their relatively high masses).

For low H concentrations the ratio σ_H/σ_D of the urea solution is similar to that of the H_2O/D_2O mixtures without dissolved urea. This is an indication

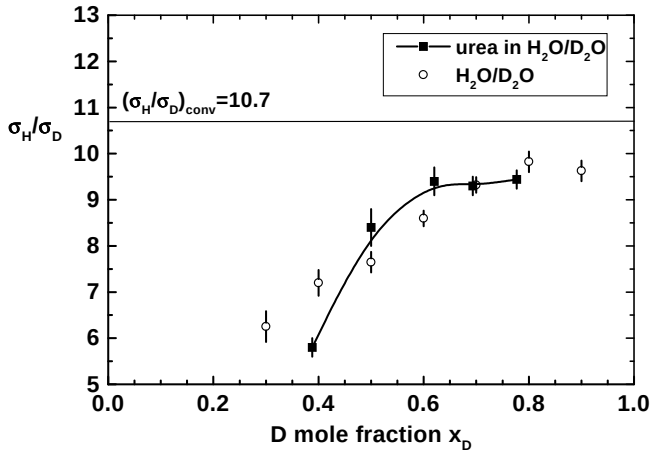

Figure 7.10: Dependence of the ratio σ_H/σ_D (full squares) on the D mole fraction x_D of the H_2O/D_2O-urea solution. For comparison, the data of H_2O/D_2O mixtures without dissolved urea are shown (open circles). The line connecting the urea data are guides to the eye.

that the effect of quantum entanglement in the urea solutions is of similar degree to that of the H_2O/D_2O mixtures without dissolved urea. For the high H concentration (i.e. $x_D < 0.5$) the effect of quantum entanglement becomes very dominant, thus giving a value of σ_H/σ_D significantly below that of the H_2O/D_2O mixture at the same H concentration. This result means that at low D concentration the effect of quantum entanglement of hydrogen bonds involving also nitrogen atoms is larger than that of hydrogen bonds involving only oxygen atoms. Since in nature, the biomolecules (DNA, enzymes, etc.) occur in their protonated and very rarely (less than 0.02%; i.e. the natural abundance of D) in the deuterated form, and due to the fact that these molecules contain large amounts of hydrogen bonds involving nitrogen atoms, the above results provide a very strong indication for the relevance of quantum entanglement in biological systems, too [35].

7.1.4 H_2O/D_2O with added electrolyte

In this experiment a 3 M solution of KCl in liquid H_2O/D_2O mixture with $x_D = 0.5$ at a temperature of $T = 100K$ has been measured. The NCS experiment on the KCl solution of liquid H_2O/D_2O mixture with x_D=0.5 is of course not representative. It was done when the proposed programme for using the beam time has been finished, so this experiment was to use the

remaining beam time.

This experiment was motivated by similar experiments which have been done using Raman light scattering. In the Raman light scattering experiments, it was found that the ratio of the scattering cross section of the intramolecular OH stretching mode σ_{OH} to that one of the intramolecular OD stretching mode σ_{OD}, i.e.

$$Q_R = \sigma_{R,OH}/\sigma_{R,OD} \tag{7.1}$$

increased significantly by adding NaCl with a concentration of c(NaCl)=3 mol/l [35]. The index R denotes the quantities related to the Raman experiment. Similar Raman scattering experiments using KCl of the same concentration gave the same result [128].

In contrast to the Raman experiment, which showed large differences, the NCS experiment did not exhibit any significant change of σ_H/σ_D. This ("null result") is insofar interesting as it pinpoints the difference of the fundamental forces being involved in the Raman (electromagnetic interactions) on the one hand and the neutron Compton scattering (strong interaction) on the other [35].

7.2 C-H bonds

7.2.1 C_6H_6/D_6H_6

Here the experimental results of pure C_6H_6, pure D_6H_6, and mixtures of them at room temperature are presented. The liquids were put in a special annular metallic can made of Nb (see section 5.2). Sample spectra in forward and backward scattering directions, respectively, are shown in Fig. 7.11. Also here the extraction of the C peak area has been done following the procedure given in section 6.

The ratio $R_{exp} = N_H\sigma_H/N_C\sigma_C$ for C_6H_6/C_6D_6 (0.500:0.500) normalized to the conventionally expected one R_{conv} vs. scattering angle θ is given in Fig. 7.12. For all samples investigated, the values of R_{exp} seem to exhibit only a slight dependence on the scattering angles and the associated scattering times in contrast to the metallic hydrides which will be shown later (section 7.3). Therefore, the average has been taken over all detectors. The results are given in Fig. 7.13 and reveal an "anomalous" decrease of R_{exp} of about 20% with respect to the conventional value of R_{conv}. It is also observed that the anomalous decrease is – within experimental errors – independent of the D mole fraction in the sample. Therefore, in contrast to the results of H_2O/D_2O

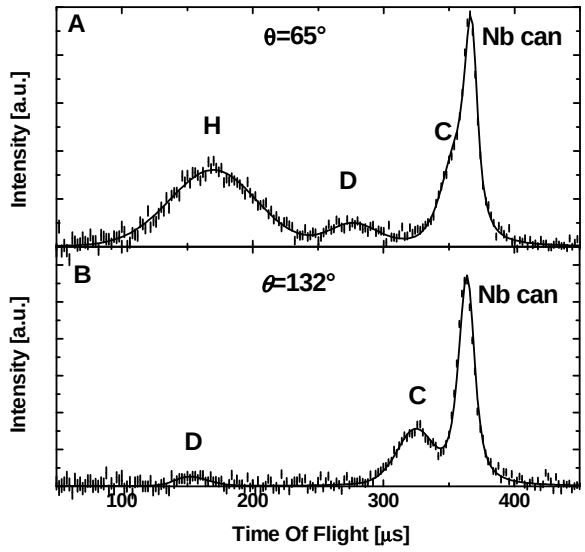

Figure 7.11: Spectrum of a C_6H_6/C_6D_6 mixture with D mole fraction x_D=0.5. While the C peak overlaps heavily with that of the Nb can one in the forward scattering direction (θ =65°), they are satisfactorily resolved in the backscattering direction (θ =132°).

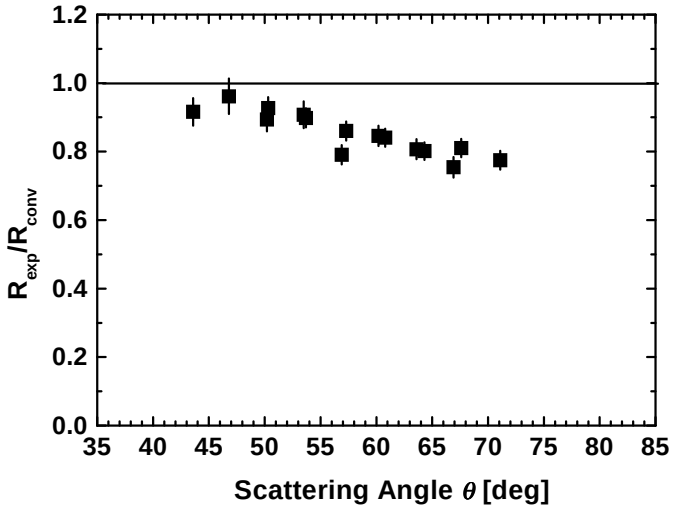

Figure 7.12: The ratio $R_{exp}(H,C)/R_{conv}(H,C)$ of the total neutron scattering cross-sections of H and C of a C_6H_6/C_6D_6 mixture with H:D=0.500:0.500 vs. scattering angle θ.

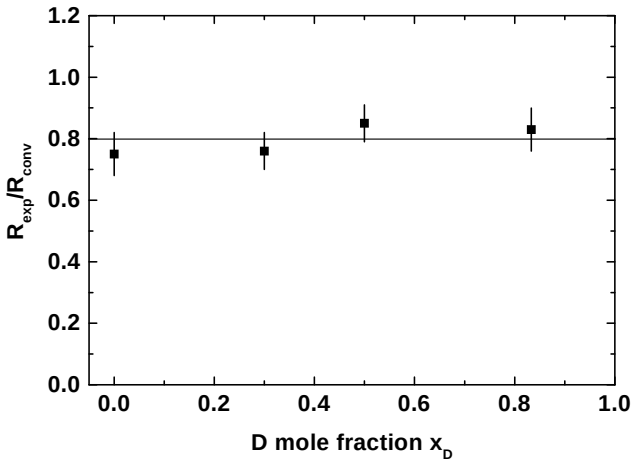

Figure 7.13: R_{exp}/R_{conv} of H for C_6H_6/C_6D_6 mixtures with x_D=0; 0.25; 0.5; and 0.75 vs. D mole fraction x_D. In contrast to the results of the H_2O/D_2O mixtures, C_6H_6/C_6D_6 mixtures seem to show no dependence on x_D.

mixtures, the considered effect appears to be mainly of intramolecular origin [42].

The D data for fully deuterated benzene are shown in Fig. 7.14. Again a slight but systematic shortfall of D scattering cross section is observed. Interestingly, the D cross section has a decreasing tendency at the very high scattering angle region. This is a phenomenon which is not observed in the mixture with D mole fraction of x_D=0.3 (see Fig. 7.15).

7.2.2 C_6D_5H

The results presented in the previous part strongly suggest that the anomaly is mainly of intramolecular origin. In order to find out whether the found anomalies are governed by entanglement between two or more protons or by entanglement between one proton with its electronic environment, the C_6D_5H molecule has been measured. This molecule, as the formula shows, contains only one carbon bonded with a proton, whereas all other carbon atoms are bonded with deuterons. In this molecule intramolecular entanglement of protons is definitely excluded because the proton is isolated. Furthermore, intermolecular entanglement is less conceivable because the protons in this system are on the average ca. 6.6 Å apart from each other. This distance is easily verified by simple calculations using the density ρ, the molar mass M of D_6-benzene and assuming the volume of the benzene molecule as a sphere.

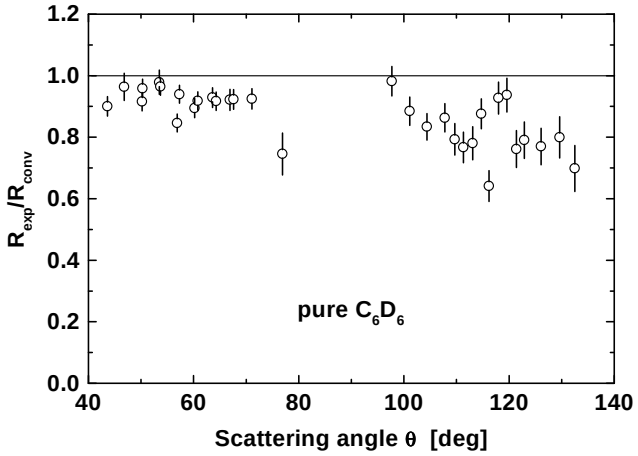

Figure 7.14: R_{exp}/R_{conv} of D for pure C_6D_6 vs. scattering angle. It can be seen that R_{exp}/R_{tab} approaches unity for small angles and decreases gradually as the scattering angle increases in the backscattering.

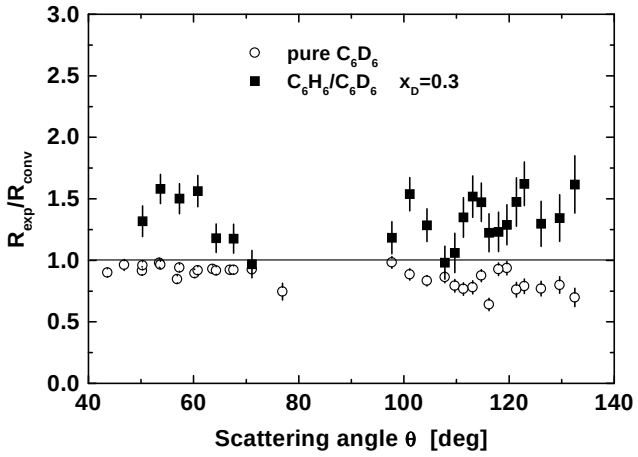

Figure 7.15: R_{exp}/R_{conv} of D for pure C_6D_6 (open circles) and C_6H_6/C_6D_6 with x_D=0.3 vs. scattering angle. It can be seen that whereas R_{exp}/R_{conv} of pure C_6D_6 is only slightly smaller than unity, R_{exp}/R_{conv} of the C_6H_6/C_6D_6 mixture is higher than unity by ca. 25%. It is very interesting that the increase of R_{exp}/R_{conv} with respect to unity is evenly distributed over the scattering angles in the forward and in the backward scattering illustrating that the increase in the forward scattering can not be caused by overlap with hydrogen because there is no hydrogen scattering contribution in the backscattering direction.

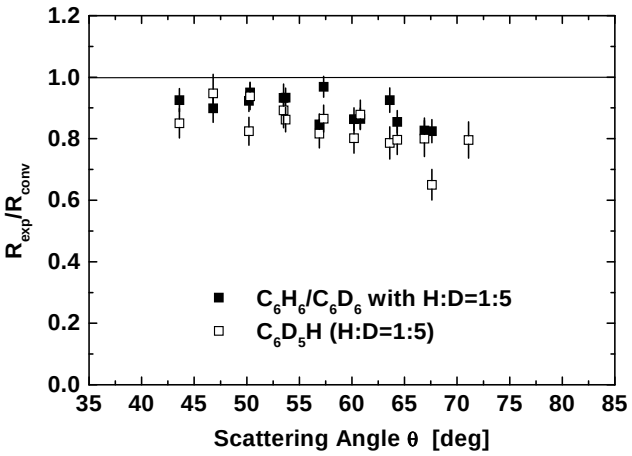

Figure 7.16: R_{exp}/R_{conv} of H for $C_6D_5H_1$ (open squares) and C_6H_6/C_6D_6 mixture with same D mole fraction of x_D=0.833 vs. scattering angle. It can be seen that there is essentially no difference between both data sets.

This result is confirmed by recent neutron diffraction measurements on liquid C_6D_6 at room temperature which gives for the center of mass correlation length of 6.3 Å [129]. Accordingly, this molecule provides an appropriate system to investigate whether the electronic environment is involved in the quantum entangled states.

The result is shown in Fig. 7.16 in comparison with a C_6H_6/C_6D_6 mixture with the same H:D ratio, i.e. H:D=0.167:0.833. As can be seen, there are no significant differences between these two different molecular systems. Both measurements exhibit an anomalous decrease of the R_{exp} of ca. 20% with respect to the conventionally expected value R_{conv}. Furthermore, a slight angle dependence is visible. This similarity of results indicate very clearly that it is the entanglement of the proton with the surrounding electrons and its decoherence which is responsible for the found anomalies in the benzene system.

It is also worth mentioning that – regarding the completely different H-H distances in the C_6H_6/C_6D_6 mixture on the one hand and in $C_6D_5H_1$ on the other – the concept of the neutron coherence length (see section 3.2.6) evidently is irrelevant, because otherwise there should be differences in the results of C_6H_6/C_6D_6 and $C_6D_5H_1$ because of the very different H-H distances.

For the results concerning the D signal, see Fig. 7.17. Also the D peak area of the C_6H_6/C_6D_6 mixture does not differ from that of the $C_6D_5H_1$

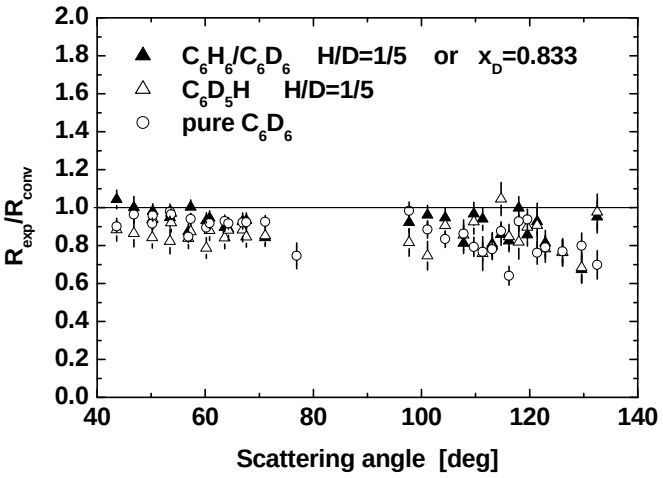

Figure 7.17: R_{exp}/R_{conv} of D for $C_6D_5H_1$ (open up triangles), C_6H_6/C_6D_6 mixture with same D mole fraction of x_D=0.833 (full up triangles), and for pure C_6D_6 vs. scattering angle.

molecule. R_{exp}/R_{conv} for D is systematically smaller than unity but the amount of the reduction is much smaller than for H. In addition, the data is too noisy to allow any further conclusion.

7.2.3 Polystyrene

An example of a measured TOF spectrum of fully protonated polystyrene is given in Fig. 7.18, for a given scattering angle θ =71°. Since the sample is solid (flat foil of thickness ca. 0.2 mm), no container is necessary. This greatly facilitates the data analysis. The procedure mentioned above, eq.(6.27), yields straightforwardly the measured ratio $R_{exp} = N_H\sigma_H/N_C\sigma_C$ of the cross-section densities of H and C for polystyrene. In Fig. 7.19 is presented the ratio R_{exp}/R_{conv}, where R_{conv} denotes the expected value of this ratio according to conventional theory. The atomic ratio H:C for polystyrene is 1:1. It then follows that $R_{conv} = 81.67/5.564 = 14.7$.

It can be clearly seen that the experimentally determined ratio R_{exp} is "anomalously" smaller, by ca. 20% on the average, than expected according to conventional theory. Furthermore, the measured values of R_{exp} at different scattering angles θ appear to exhibit no significant dependence on θ, and thus also on the related momentum transfer q and the associated scattering time τ_s; see eq.(3.47). The constancy of this quantity with respect to τ_s implies that the decoherence time of the considered QE effect is of the order of the time window realized in the present experimental NCS setup.

Since the polystyrene foils were arranged perpendicular to the incoming neutron beam, the objection could be raised that multiple scattering effects could affect the experimental results for high scattering angles thus giving rise to the found anomalous result. Therefore, the polystyrene foil has been tilted by 30° with respect to the direction of the incoming neutron beam and

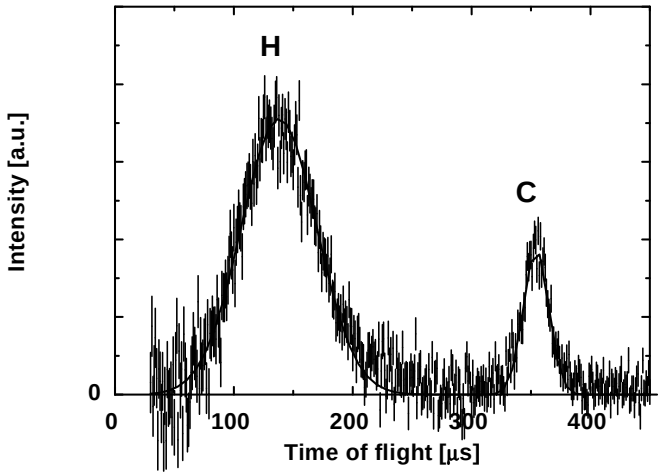

Figure 7.18: Measured time-of-flight spectrum of polystyrene for scattering angle of θ=71.4°. The full line represents the fit to the experimental data.

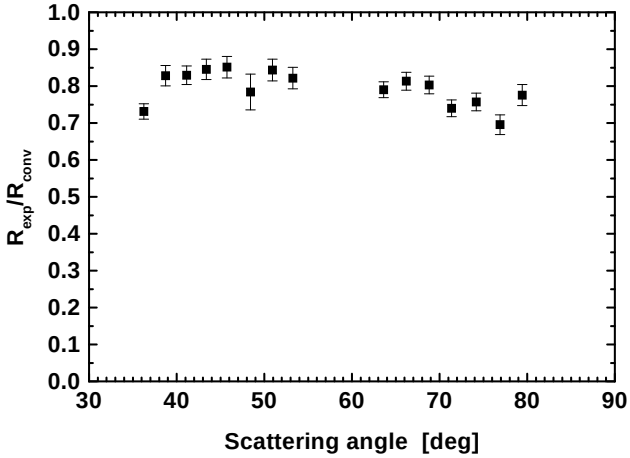

Figure 7.19: R_{exp}/R_{tab} vs scattering angle. The average of R_{exp} is ca. 20% anomalously smaller than its tabulated value. No significant scattering angle dependence of R_{exp} is visible within experimental error.

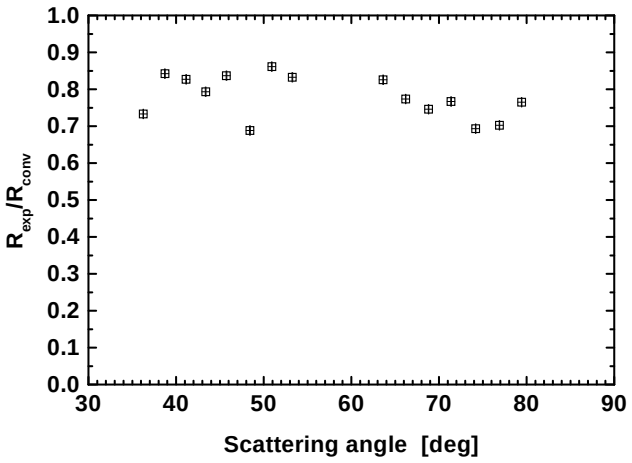

Figure 7.20: R_{exp}/R_{tab} vs scattering angle for a polystyrene foil tilted by 30° with respect to the incident beam. The average of R_{exp} is again ca. 20% anomalously smaller than its tabulated value and no significant scattering angle dependence of R_{exp} is visible within experimental error. No significant differences are visible between the not tilted (see Fig. 7.19) and the tilted sample.

a complete measurement has been done. This experiment gave essentially the same results for the ratio R_{exp} as has been obtained for the not tilted foil (see Fig. 7.20).

Summarizing the striking experimental results presented above, it may be concluded that the protonic QE effect under consideration does strongly affect the quantum dynamics of H-atoms of C-H bonds. Due to the smaller mass of H, the observed effect is attributed to hydrogen, rather than to the heavier C. In rather oversimplified terms, this new effect might be viewed to be caused by (a novel kind of) short-time destructive interference of adjacent H atoms [41].

Motivated by the earlier NCS measurements on H_2O/D_2O mixtures, the breaking of covalent C-H bonds of various partially deuterated samples of polystyrene has been also investigated in addition to those of the fully protonated polystyrene. The mixtures had the following H/D compositions:
(*ii*) $(–CD_2CDC_6H_{4.97}D_{0.03}–)_n$ with H:D=0.621:0.379 and
(*iii*) $(–CD_2CDC_6H_{4.35}D_{0.65}–)_n$ with H:D=0.544:0.456.

As an example, a measured TOF spectrum of one partially deuterated polystyrene (with H:D=0.544:0.456) is presented in Fig. 7.21. In this experiment 15 detectors were positioned in the scattering angle range between 36°

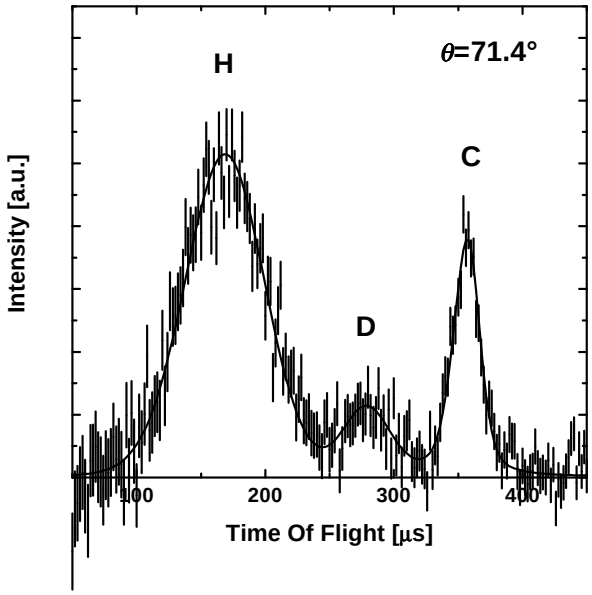

Figure 7.21: An example spectrum of one partially deuterated polystyrene (with H:D=0.544:0.456).

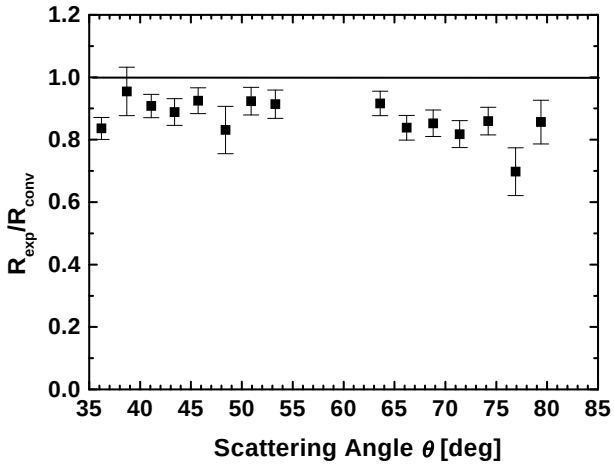

Figure 7.22: R_{exp}/R_{tab} vs scattering angle for partially deuterated polystyrene with H:D=0.544:0.456. The average of R_{exp} is ca. 18% anomalously smaller than its tabulated value and again no significant scattering angle dependence of R_{exp} is visible within experimental error.

and 79°. The result of this experiment is clearly visible in Fig. 7.22. Here, for a specific sample (with H:D=0.544:0.456), it is shown that $R_{exp}/R_{conv} = 0.87$. The results from all samples are summarized in the table below.

H:D	1:0	0.621:0.379	0.544:0.456
R	0.80±0.05	0.82±0.05	0.87±0.05

For all samples investigated, the ratios R_{exp}/R_{conv} appear to exhibit only a slight – i.e. within present experimental error – dependence on the scattering angle θ, and thus also on the momentum transfer q and the associated scattering time τ_s; see eq.(3.47) [42]. Further experiments with considerably longer accumulation times are required to make a clear assessment about a possible τ_s-dependence of the anomalous decrease of R_{exp}/R_{conv}.

7.2.4 Amphiphile (2-isobutoxyethanol)

A sample spectrum of this compound in a Nb can is shown in Fig. 7.23. As can be seen, the joint C/O peak is separated from the Nb peak only in the backscattering regime (Fig. 7.23.a). Again, the ratios $A_H/(A_C + A_O + A_{Nb})$ and $A_{Nb}/(A_C + A_O)$ are determined from the forward and the back scattering spectra, respectively. Then the ratio

$$R_{exp}(H) = A_H/(A_C + A_O) \tag{7.2}$$

is determined (see section 6.3). Note that A_O in the denominator of this ratio refers to 2-iso-C_4E_1 and D_2O as well, since both molecules contain oxygen. The conventionally expected value of this ratio is

$$R_{conv}(H) = N_H\sigma_H/(N_C\sigma_C + N_O\sigma_O) = 4.95 \tag{7.3}$$

since the atom densities N_H, N_C and N_O, are precisely known through sample preparation and chemical formulae.

Again a strong deviation of the experimentally determined quantity $R_{exp}(H)$ from the conventionally expected $R_{conv}(H)$, i.e.

$$R_{exp}(H) \approx 0.8 \cdot R_{conv}(H) \tag{7.4}$$

is found. This effect is clearly visible in Figure 7.24. Here is presented the ratio $R_{exp}(H)/R_{conv}(H)$. The considered effect is given by the "anomalous" decrease of $R_{exp}(H)$, which is about 20%. Note that all detectors (positioned in scattering angles between 36° and 79°) have provided the same result, within experimental error, thus indicating an independence of momentum

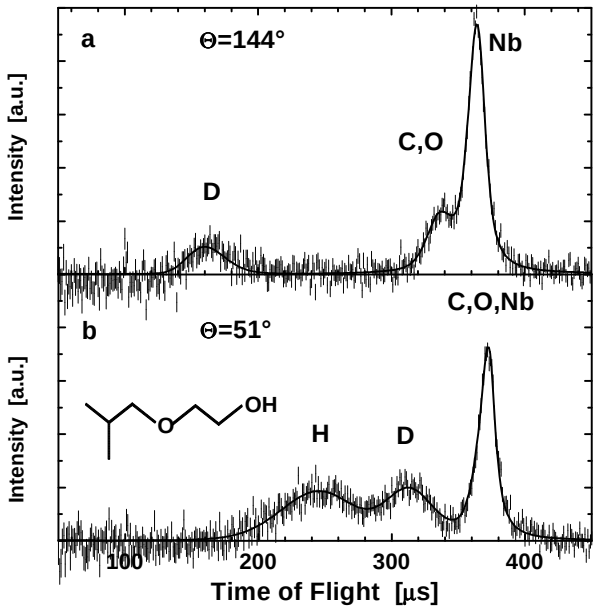

Figure 7.23: Example spectra of iso-C_4E_1 in D_2O as measured for scattering angles (a) θ=144° and (b) θ= 51°. The structure of iso-C_4E_1 is also shown. The full lines represent the fitted theoretical TOF spectra to the measured data. Note the separation of the joint C,O peak from the Nb can peak in spectrum (a), which is necessary for data analysis.

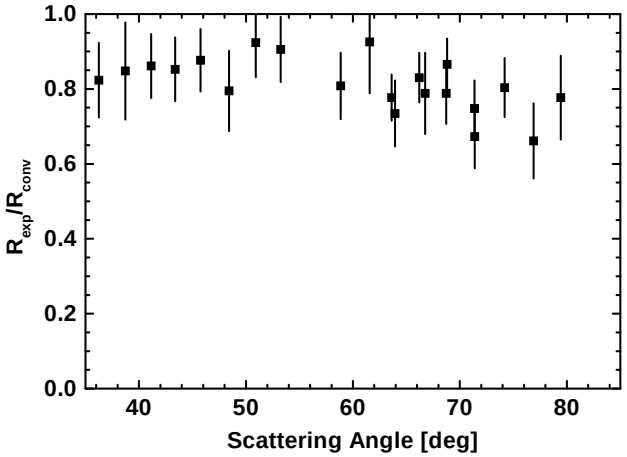

Figure 7.24: R_{exp}/R_{tab} vs scattering angle for iso-C_4E_1 in D_2O vs. scattering angle. The average of R_{exp} is "anomalously" smaller than the tabulated value ca. 20%. No significant angle dependence is visible.

transfer or, equivalently, of the scattering time τ_s characterizing the duration of the neutron-proton collision process (see eq.(3.47)).

The experimental result reveal that the observed "anomaly" appears to be just as great in the diluted 2-iso-C_4E_1 molecules as it was in bulk polystyrene (see the previous section). Therefore, it must be concluded that the considered effect is mainly of intramolecular origin [43].

7.2.5 H_6-acetone/D_6-acetone

Unfortunately, before this experiment was performed, the VESUVIO instrument has experienced a rearrangement including a bulky equipment in the back scattering as well as a cubic sample tank with stainless steel supports. This setup made it impossible to put detectors in the backscattering direction. Therefore, it was not possible to separate the peak of the Nb can from the combined one of C and O of acetone and thus prevented us from determining the ratio $\sigma_H/(\sigma_C + \sigma_O)$ and one was limited to the determination of the ratio σ_H/σ_D only.

The results of this experiment are shown as full squares in Fig. 7.25. As can be easily seen, the values of σ_H/σ_D (averaged over the detectors) are strongly decreased with respect to the tabulated value (= 81.7/7.6= 10.7) [27]. This decrease is strongly dependent on the D mole fraction x_D of the liquid H-acetone/D-acetone mixtures. Moreover, and more strikingly, all ratios σ_H/σ_D have been found to be significantly smaller than the σ_H/σ_D values of the H_2O/D_2O mixtures (open circles). The latter result implies that either a different number of protons are involved in the entangled states or different dynamics of the decoherence process is involved due to different electronic environments [44]. It should be stressed that mixing bosons (D) to fermions (H) could change both the magnitude of QE as well as its decoherence time [31].

The observed "anomalous" NCS effect in acetone does not depend significantly within present experimental errors on the scattering angle or, equivalently, on the scattering time τ_s, thus indicating that the dynamics of QE does not change significantly within the time window given by the experiment. This finding is in clear contrast to the very strong τ_s-dependence of the cross-section density of protons in niobium and palladium hydrides [36, 37] (see also 7.3), but is in line with the experiments on solid polystyrene [41](see also 7.2.3). This indicates that the electronic environments of the protons play a significant role in the sub-femtosecond dynamics of protons in condensed matter. These indications are strongly supported by later measurements on LiH (see section 7.3.4).

The result that σ_H/σ_D of the acetone mixtures is systematically and

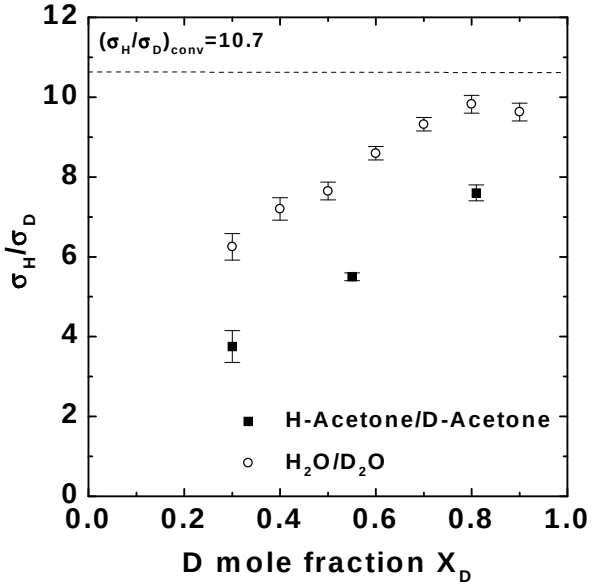

Figure 7.25: σ_H/σ_D ratios a) of the H-acetone/D-acetone mixtures (full squares) vs. D mole fraction x_D and for comparison b) of liquid H_2O/D_2O mixtures (open circles). As can be seen the acetone results are significantly more anomalous than the water ones.

significantly smaller than the corresponding one of the water mixtures has very important implications for the following reason: The objection might be raised that the effect – i.e. the strong "anomalous" decrease of σ_H/σ_D with respect to the tabulated value – detected in liquid H_2O/D_2O might be caused by some saturation effects due to the high hydrogen number density in water. However, it may be mentioned here that the hydrogen number density in acetone is ca. 30% smaller than in water. Therefore, the fact that the ratios σ_H/σ_D of liquid H-acetone/D-acetone are even smaller than their corresponding values of liquid H_2O/D_2O is a clear evidence that the effects detected both in liquid H_2O/D_2O and in liquid H-acetone/D-acetone are of real physical origin and do not arise from any saturation effects. Therefore, the combination of both experiments may be also viewed as a test for the influence of largely different proton number densities on the detected effect [44]. For further tests see section 8.

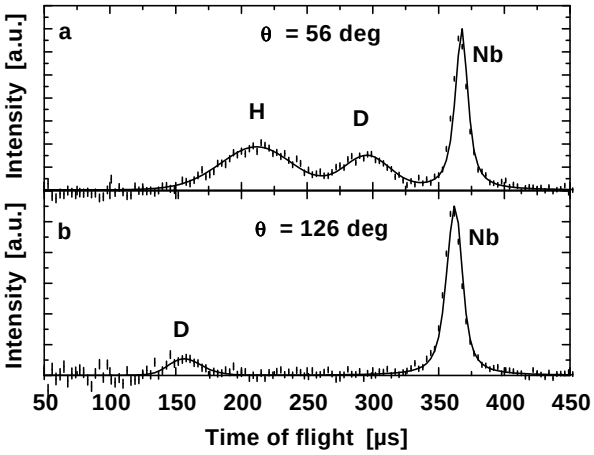

Figure 7.26: Measured time of flight spectra of $NbH_{0.16}D_{0.70}$ measured at a) $\theta = 65°$ and b) $\theta = 126°$ together with their corresponding fits.

7.3 Metal Hydrogen systems

7.3.1 Niobium hydrides

An example of a time of flight spectrum of a Nb-hydride containing protons as well as deuterons, $NbH_{0.16}D_{0.70}$, is given in Fig. 7.26 for the scattering angles $\theta = 56°$ and $\theta = 126°$.

Like the polystyrene samples, the metal hydrides allow to determine the degree of anomaly separately for H- and D-scattering because they were freely hanging in the evacuated sample tank without using a container (e.g. Al) the scattering peak of which would overlap with that of the heavy atom peak (due to e.g. Nb) of the sample.

As explained in chapter 6, according to conventional neutron scattering theory, the peak areas A_M are proportional to the number of nuclei of mass M present in the sample, multiplied by their cross-section σ_M. The measured ratios

$$A_H/A_{Nb} = x\sigma_H/\sigma_{Nb}; and \quad A_D/A_{Nb} = y\sigma_D/\sigma_{Nb} \tag{7.5}$$

provide values for σ_H/σ_{Nb} , etc., with an accuracy determined by the uncertainties in A_M, and x and y, respectively.

The $A_M/A_{M'}$ ratios calculated in the way described in chapter 6 are expected to be independent of scattering angle. This seems indeed to be the case for the pure deuteride $NbD_{0.80}$ as concerns the forward scattering direction; see Fig. 7.29. But a similar plot of the σ_H/σ_{Nb} of $NbH_{0.78}$ exhibits

striking deviations from this expectation (see Fig. 7.30). It shows a clearly decreasing trend with increasing scattering angle, reaching anomalies up to 40% for the highest scattering angles. It is also notable that the curve starts out with normal values of σ_H/σ_{Nb} at small angles around ca. 45° but has strong deviations already at scattering angles around 55-60°.

According to eq.(3.48) high scattering angles correspond to short scattering times τ_s. In order to learn about the dynamics of the proton within the accessible scattering time range of NCS, the data were analyzed in terms of scattering time by transforming the θ-dependence to a dependence on τ_s. The results for the $NbH_{0.78}$ sample are displayed in Fig. 7.31. It can be seen that H-nuclei in $NbH_{0.78}$ show an anomalous neutron cross section only for scattering times shorter than ca. $0.6\text{x}10^{-15}$ s. This is a clear indication for the proton to undergo a dynamical change during the involved time region of $0.1< t <1.0$ fs. This result is in line with the prediction (motivation) of Ref. [7] of improper interaction of the system – that is short time entangled particles – with the incoming (matter) field. This experiment shows that the entanglement of the protons survive at least for a time of ca. 0.5 fs and is completely decayed after ca. 1 fs.

Furthermore, it can be seen from Fig. 7.27 that σ_H/σ_{Nb} is independent of x_D in the short scattering time range. I.e. similar anomalies are exhibited for $NbH_{0.78}$, $NbH_{0.61}D_{0.29}$, and $NbH_{0.16}D_{0.73}$ in the time range $\tau_s \approx 0.2 - 0.5$ fs. However, whereas σ_H/σ_{Nb} of $NbH_{0.78}$ assumes the conventionally expected value for $\tau_s \approx 0.6 - 0.8$ fs, it remains anomalous in this time range for the other two samples. For the metallic hydrides containing both H and D, similar plots (cf. Fig. 7.27) of the effective H/Nb cross section [36] show a similar strong reduction at short times but with a slower increase approaching the conventional value.

As concerns σ_D/σ_{Nb}, it seems to be independent of x_D for small scattering angles, i.e. longer scattering times. The comparison of σ_D/σ_{Nb} at higher scattering angles, i.e. shorter scattering times, however, shows slightly higher values for $NbH_{0.15}D_{0.69}$ than for $NbHD_{0.81}$. The most interesting result is that for both samples, σ_D/σ_{Nb} at higher angles is smaller than at smaller angles. This result means that the decoherence process is already fully at action at the scattering times corresponding to the smaller angles and is still not fully effective at the shorter scattering times. This effect is much more pronounces in the yttrium hydride samples (see section 7.3.3).

It is interesting to observe that the reduction in H-cross section as observed in the hydrides is much larger than that of the D-cross section. This is in line with the interpretation that the reduction of σ_H/σ_D by ca. 30% in the water experiments (see section 7.1.1 and Ref. [31]) is mainly due to a reduced effective H-cross section, rather than a change of D-cross section as

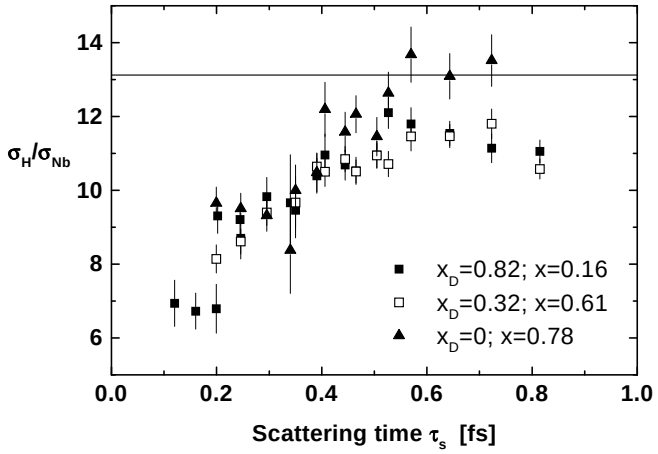

Figure 7.27: The cross section ratio σ_H/σ_{Nb} of three NbH_xD_y samples vs. scattering time τ_s at $T = 293$ K after transformation of the scattering angle θ to τ_s according to eq.(3.48). σ_H/σ_{Nb} is anomalously reduced up to 0.6 fs and assumes then the conventionally expected value (horizontal line at 13.2). Whereas the tabulated value is reached by the σ_H/σ_{Nb} value of the purely protonated sample (x_D=0; x=0.78) at $\tau_s \approx 0.6$ s, the σ_H/σ_{Nb} values of the other two samples do not reach it.

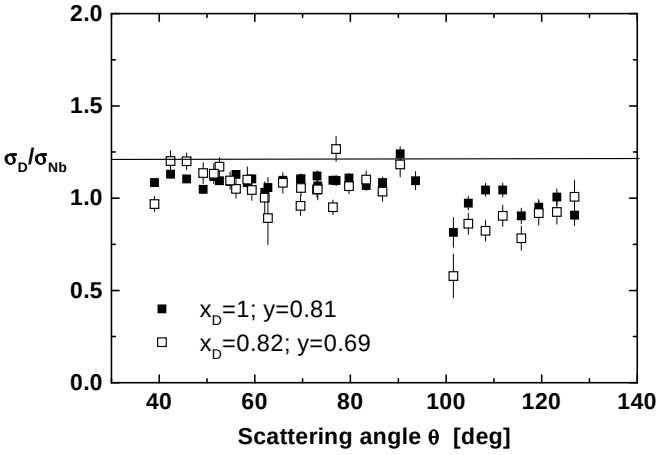

Figure 7.28: The cross section ratio σ_D/σ_{Nb} of two NbH_xD_y samples vs. scattering angle. No significant reduction of σ_D/σ_{Nb} with respect to the tabulated value (horizontal line at 1.22) is observed.

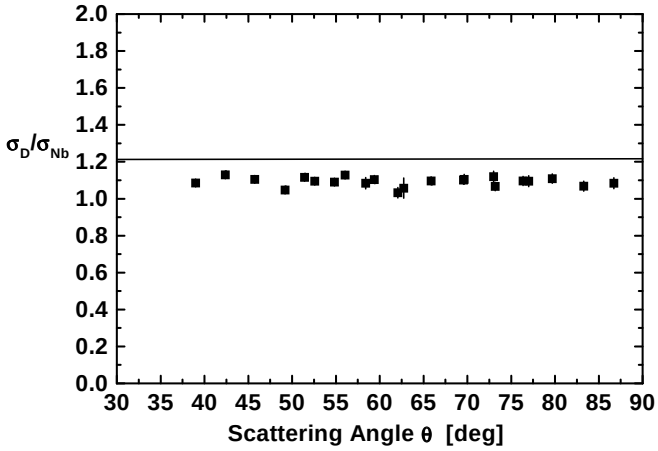

Figure 7.29: The cross section ratio σ_D/σ_{Nb} of $NbD_{0.80}$ vs. scattering angle θ. The horizontal line indicates the conventionally expected value $\sigma_D/\sigma_{Nb} = 7.63/6.25 = 1.22$. An angle independent small reduction of σ_D/σ_{Nb} with respect to this value is observed.

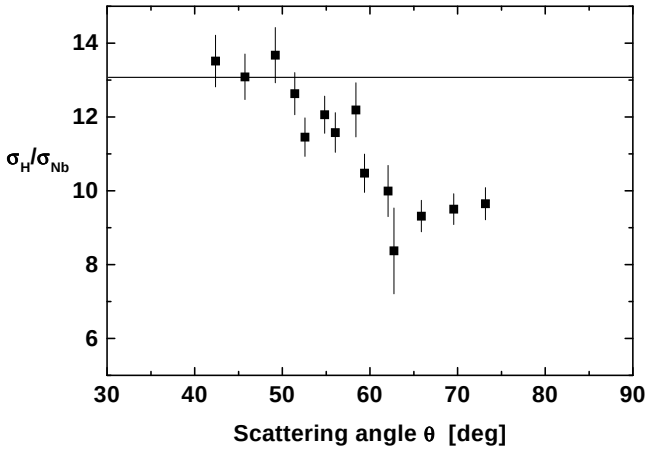

Figure 7.30: The cross section ratio σ_H/σ_{Nb} of $NbH_{0.78}$ vs. scattering angle θ. The horizontal line indicates the conventionally expected value $\sigma_H/\sigma_{Nb} = 81.67/6.25 = 13.1$. A strong angle dependent reduction of σ_H/σ_{Nb} with respect to this value is observed. The conventionally expected value is approached at $\theta \approx 50°$.

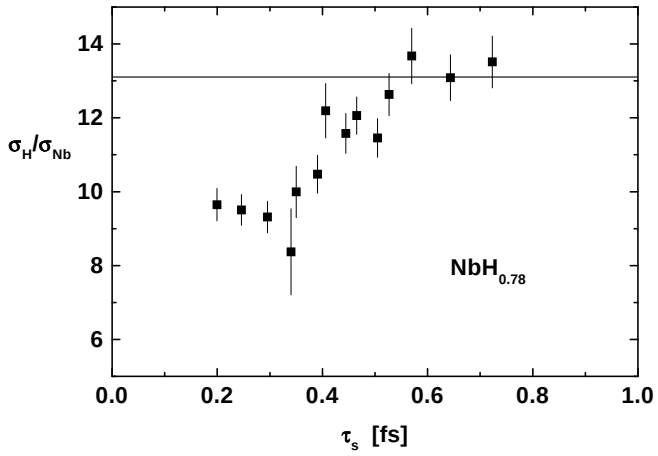

Figure 7.31: The cross section ratio σ_H/σ_{Nb} of $NbH_{0.78}$ vs. scattering time τ_s according to eq.(3.48). The horizontal line indicates the conventionally expected value $\sigma_H/\sigma_{Nb} = 81.67/6.25 = 13.1$. A strong angle dependent reduction of σ_H/σ_{Nb} with respect to this value is observed. The conventionally expected value is approached at $\tau_s \approx 0.6$ fs.

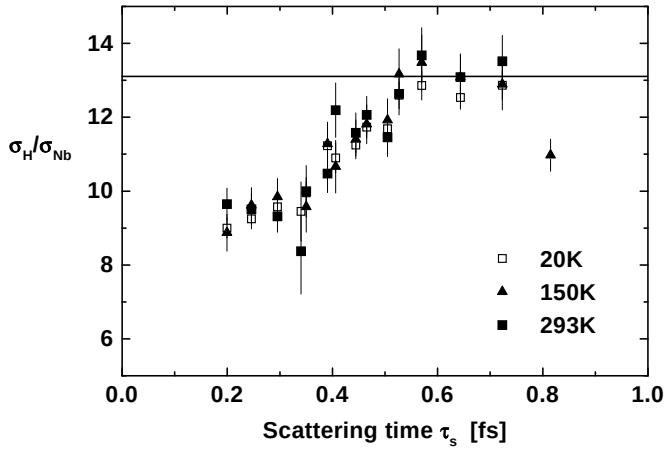

Figure 7.32: The cross section ratio σ_H/σ_{Nb} of $NbH_{0.78}$ vs. scattering time τ_s at $T = 20$ K (full squares), $T = 150$ K (full triangles), and $T = 293$ K (open squares) after transformation of the scattering angle θ to τ_s according to eq.(3.48). σ_H/σ_{Nb} is anomalously reduced up to 0.6 fs and assumes then the conventionally expected value (horizontal line at 13.2). No differences are observed between measurements at these largely differing temperatures.

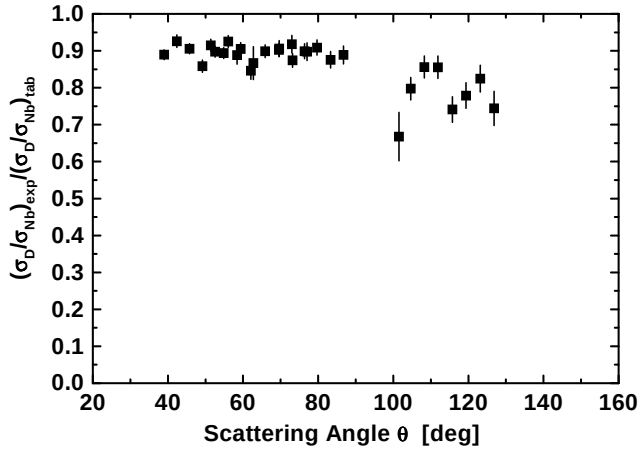

Figure 7.33: The cross section ratio $(\sigma_D/\sigma_{Nb})_{exp}$ normalized with the tabulated one $(\sigma_D/\sigma_{Nb})_{tab} = 7.63/6.25 = 1.22$ of $NbD_{0.80}$. A slight angle dependence can be seen if the forward results are compared with the backward ones; i.e. $\theta > 90°$.

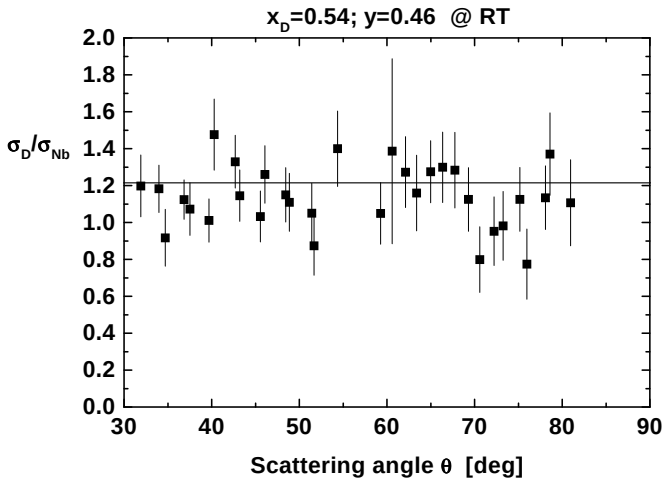

Figure 7.34: The cross section ratio σ_D/σ_{Nb} of $NbH_{0.39}D_{0.46}$ vs. scattering angle. No significant reduction of σ_D/σ_{Nb} with respect to the tabulated value (horizontal line at 1.22) is observed.

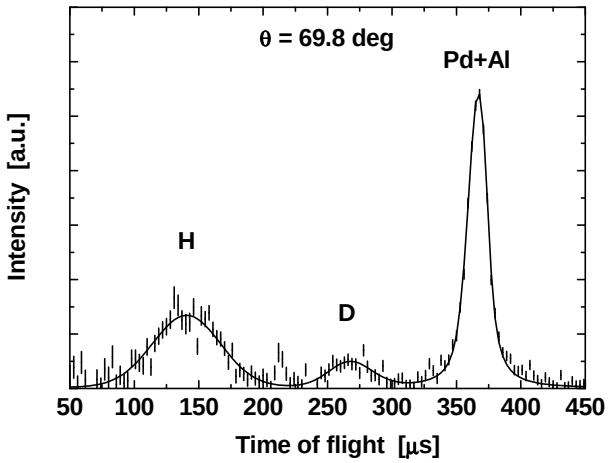

Figure 7.35: Example spectrum of $PdD_{0.3}H_{0.2}$ at 69.8° together with its corresponding fit.

has been shown in section 7.1.1; see also Ref. [130].

It was expected that measurements of the temperature dependence may help to elucidate the character of the present anomalies. Therefore, most samples were also run at various temperatures. The results are shown in Fig. 7.32. Within experimental error no significant temperature dependence was found for σ_H/σ_{Nb} in all mixtures. This result is similar to earlier low temperature experiments on H_2O/D_2O (see Ref. [131] and section 7.1.2) but is in contrast to later measurements on LiH (see section 7.3.4).

7.3.2 Palladium hydrides

An example spectrum of an H/D mixed palladium hydride is shown in Fig. 7.35. As mentioned in section 5.3.5.2, palladium disks were put in an Al can and the hydrides were produced in situ. Again, in the TOF-spectra recorded at backscattering (angles $\theta > 120°$) the peaks corresponding to Pd and Al could be partially resolved. In order to extract the Pd signal area from the joint Al/Pd peak due to their overlap, the procedure described in section 6.3 was followed.

One of the data sets is presented in Fig. 7.36 where A_H/A_{Pd} is given as function of detector angle θ. This curve has a characteristic plateau at low detector angles, falling off relatively abruptly for $\theta > 65°$ (i.e. at a considerably higher angles compared to the corresponding Nb-H curve, Fig. 7.30). When converted to a scattering time dependence, τ_s, this drop in scattering intensity turns out to correspond to the same $\tau_s \approx 0.6$ fs as in the Nb-H case. This is due to the fact that different momentum distribution widths of H are involved in the Nb and Pd systems, respectively.

The values derived for the effective cross section ratio σ_H/σ_{Pd} depend on the actual H-concentration. With the composition $PdH_{0.53}$ calculated from the pressure data the long-time saturation value of $\sigma_H/\sigma_{Pd} = A_H/(0.53A_{Pd})$

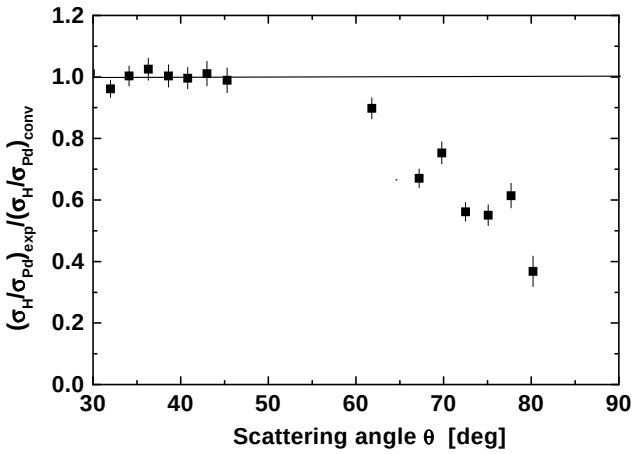

Figure 7.36: The cross section ratio σ_H/σ_{Pd} of $PdH_{0.54}$ vs. scattering angle θ. The horizontal line indicates the conventionally expected value $\sigma_H/\sigma_{Pd} = 81.67/5.1 = 16.0$. A strong angle dependent reduction of σ_H/σ_{Nb} with respect to this value is observed. The conventionally expected value is approached at $\theta \approx 60°$ which is different to the angle dependence of the niobium hydride being at $\theta \approx 50°$; see Fig. 7.30.

comes out about 15% higher than the tabulated cross section ratio 16.0. The saturation value of A_H/A_{Pd} corresponds actually more closely to the composition $PdH_{0.6}$ expected from the thermodynamic data. To avoid this uncertainty, the Pd-H data were instead normalized by dividing all points A_H/A_{Pd} by the saturation value for long times (i.e., the mean of data taken for $\theta < 50°$). These data are compared with the corresponding values from Fig. 7.32 for $NbH_{0.8}$ in Fig. 7.38.

The information from Fig. 7.38 is interesting. Large cross section anomalies exist for neutron scattering on protons in both materials; at the smallest τ_s the Pd-H anomalies are even somewhat larger than for Nb-H. The time within which the anomalies disappear is very similar, about 0.6 fs. Similar results are observed from the $PdD_{0.3}H_{0.2}$ data.

A few experiments were performed with deuterated Pd, because difficulties in sample preparation allowed only a limited set of data to be obtained. Fig. 7.39 shows the experimentally determined values of σ_D/σ_{Pd} for $PdD_{0.3}$ and $PdD_{0.3}H_{0.2}$. There is a tendency of σ_D/σ_{Pd} towards values higher than the tabulated one. But due to the large statistical error bars it is not possible to get a conclusive information.

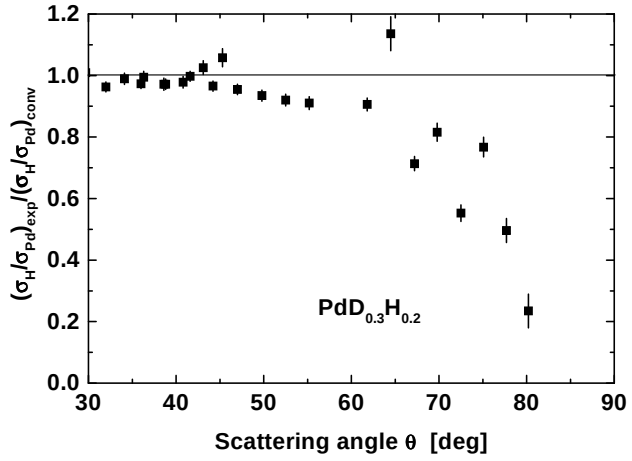

Figure 7.37: The cross section ratio σ_H/σ_{Pd} of $PdD_{0.3}H_{0.2}$ normalized to its conventionally expected value ($\sigma_H/\sigma_{Pd} = 81.7/5.1 = 16.0$) vs. scattering angle.

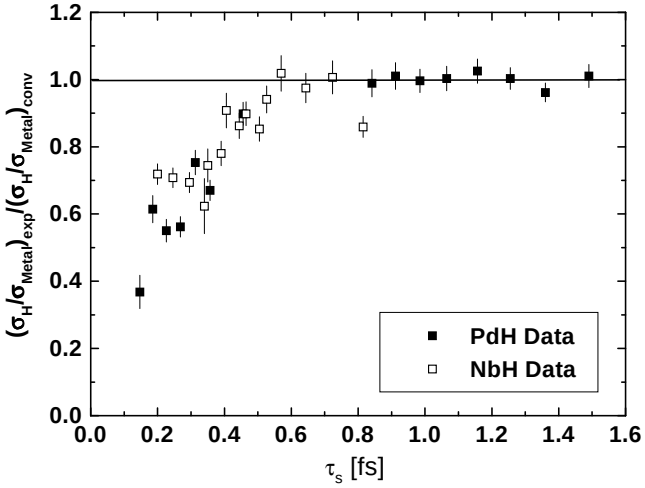

Figure 7.38: The cross section ratio σ_H/σ_{Pd} of $PdH_{0.54}$ and σ_H/σ_{Nb} of $NbH_{0.78}$ vs. scattering time τ_s after normalization with their corresponding conventional values for comparison ($\sigma_H/\sigma_{Nb} = 81.7/6.25 = 13.1$ and $\sigma_H/\sigma_{Pd} = 81.7/5.1 = 16.0$). Despite their different angle dependence behaviors (see Fig. 7.30 and Fig. 7.36), the same dependence on τ_s is observed.

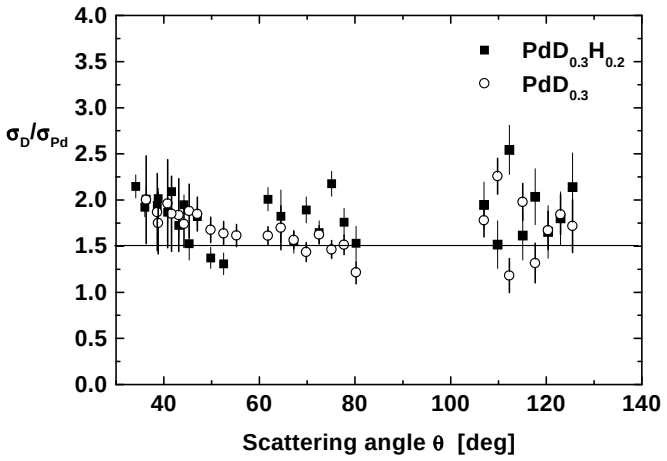

Figure 7.39: The cross section ratio σ_D/σ_{Pd} of $PdD_{0.3}$ and $PdD_{0.3}H_{0.2}$ vs. scattering angle. The conventional value of $\sigma_D/\sigma_{Pd} = 7.63/5.1 = 1.5$ is indicated by the horizontal full line.

7.3.3 Yttrium hydrides

Figs. 7.40 and 7.41 show examples of TOF spectra taken for YH_3 and YD_3 at $\theta = 71°$. The Y-signal can not be easily distinguished from that of the Al-container, since the Al-peak falls only slightly below the Y-peak in TOF spectra taken at forward scattering angles ($\theta < 90°$). However, these peaks can be reasonably well resolved in the spectra collected at back scattering ($\theta > 90°$). As described in section 6.3, the ratio A_Y/A_{Al} determined from the back scattering spectra (with $\theta > 90°$) was then used to extract the Y-fraction from the composite high mass peaks for spectra taken at $\theta < 90°$.

Fig. 7.42 shows, the experimentally determined ratios σ_H/σ_Y normalized to the tabulated value of 10.6 [27] versus scattering angle. The results reveal that the measured σ_H/σ_Y ratios are far below the tabulated value. There is also an angle dependence visible which starts at ca. 55-60°. Furthermore, in contrast to the results of the niobium hydrides, $(\sigma_H/\sigma_Y)_{exp}$ does not assume the tabulated value at low scattering angles. Although still within the statistical error, there is a small tendency towards larger "anomaly" for YH_3 as compared to YH_2 in the higher angle region.

Fig. 7.43 shows, the experimentally determined ratios σ_D/σ_Y normalized to the tabulated value of 0.99 [27]. The results show that the measured σ_D/σ_Y ratios are ca. 10% lower than the tabulated value at scattering angles <90° and become even smaller with increasing scattering angles thus reaching an anomaly of 35% at the maximally accessible scattering angle of ca. 145°.

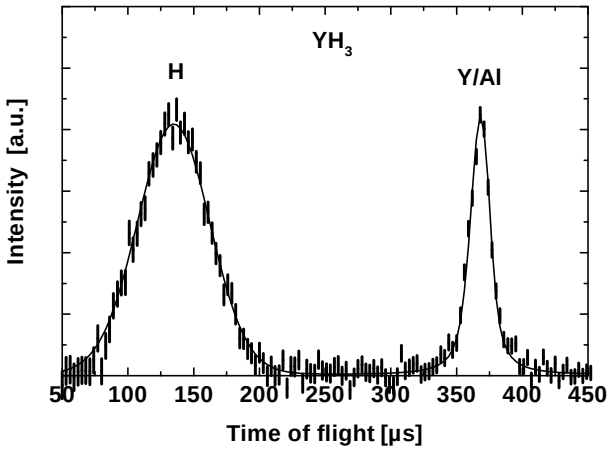

Figure 7.40: Time of flight spectrum of YH_3 at scattering angle $\theta = 71.4°$.

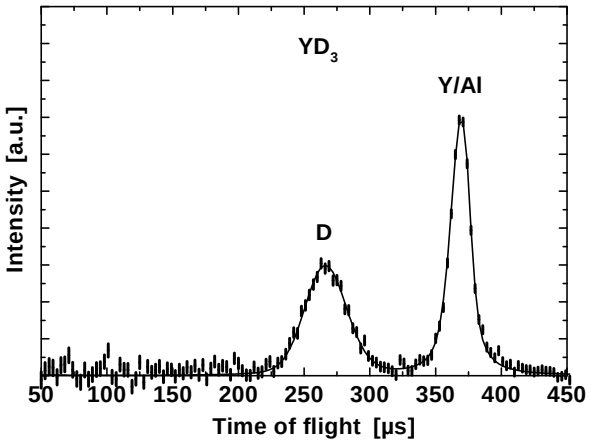

Figure 7.41: Time of flight spectrum of YD_3 at scattering angle $\theta = 71.4°$.

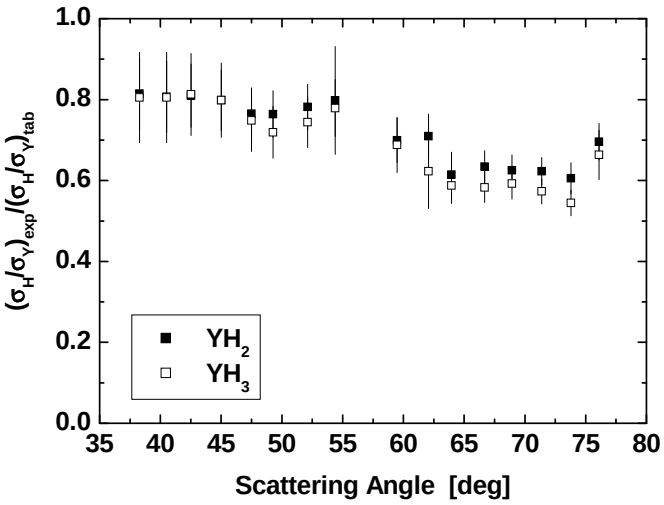

Figure 7.42: The cross section ratio $(\sigma_H/\sigma_Y)_{exp}$ normalized by the tabulated value $(\sigma_H/\sigma_Y)_{tab} = 81.67/7.70$ for YH_2 (full squares) and YH_3 (open squares).

There is no visible difference between the YD_2 and the YD_3 data.

Fig. 7.44 shows σ_D/σ_Y normalized to the tabulated value for YD_2, YD_3 and the mixed hydride $Y(H_{0.2}D_{0.8})_3$. Also here, it seems that the dynamics in the mixed hydride does not affect neither the amount nor the angle dependence of the D cross section anomaly.

Both hydrides, YH_3 and YH_2, exhibit the same anomalies. Furthermore, for YH_3 there is at the smaller scattering times a tendency towards lower σ_H/σ_Y values than for YH_2; cf. Fig. 7.45.

The data of YH_3 and YH_2 are additionally plotted as function of the scattering time τ_{sc} in Fig. 7.45 and can be compared with the result of the Nb-H data [36]. A very slight tendency towards the conventional value with decreasing hydrogen concentration is visible for low scattering times τ_{sc}. A general trend seems to be that the cross section reduction exhibits the same features (within present experimental error) for all yttrium hydride samples investigated.

It can be seen from Fig. 7.45 that $(\sigma_H/\sigma_Y)_{exp}$ approaches but does not assume the conventionally expected value at higher τ_s values. This is in contrast to the results obtained with the niobium hydrides.

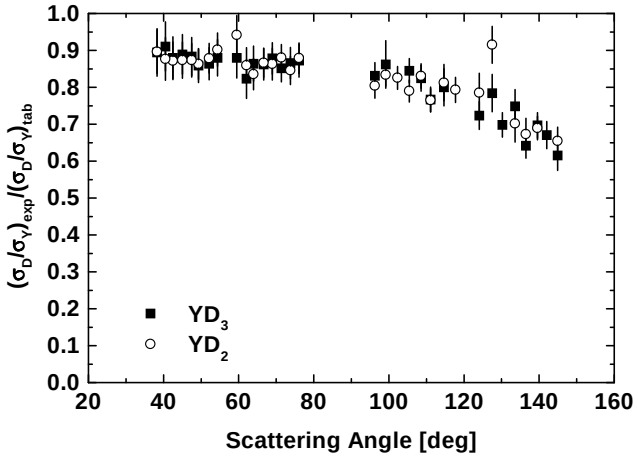

Figure 7.43: The cross section ratio $(\sigma_D/\sigma_Y)_{exp}$ normalized by the tabulated value $(\sigma_D/\sigma_Y)_{tab} = 7.63/7.70$ for YD_3 (full squares) and YD_2 (open circles).

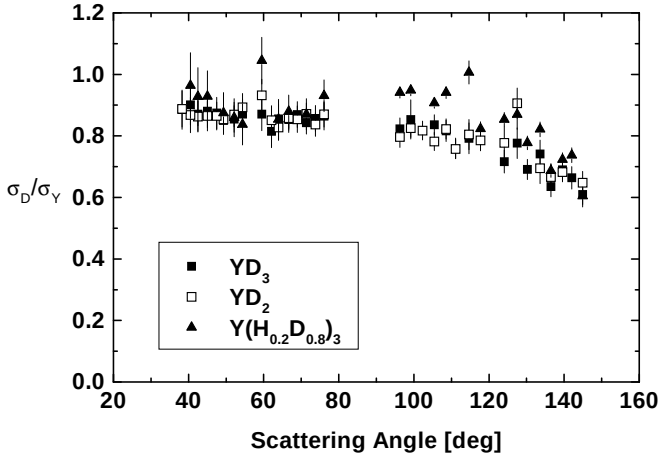

Figure 7.44: The cross section ratio $(\sigma_D/\sigma_Y)_{exp}$ normalized by the tabulated value $(\sigma_D/\sigma_Y)_{tab} = 7.63/7.70$ for YD_3 (full squares), YD_2 (open squares), and $Y(H_{0.2}D_{0.8})_3$.

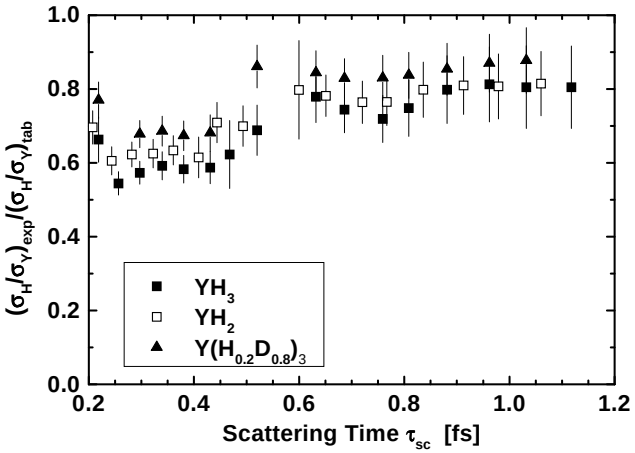

Figure 7.45: $(\sigma_H/\sigma_Y)_{exp}/(\sigma_H/\sigma_Y)_{tab}$ of YH_2, YH_3 and $Y(H_{0.2}D_{0.8})_3$ versus scattering time τ_s.

7.3.4 Lithium hydride

An example of a time-of-flight (TOF) spectrum at room temperature is shown in Fig. 7.46. The detectors covered the angular ranges $33° < \theta < 67°$ in forward scattering and $141° < \theta < 167°$ in backscattering directions.

The area ratio of A_{Al}/A_{Li} is determined from the backscattering spectra at e.g. $\theta = 144°$ (see Fig. 7.47) and is used to extract the Li area of the forward scattering spectra in order to relate the H area to the one of Li, thus giving σ_H/σ_{Li}. This procedure (see section 6.3) is followed for each temperature separately, so that any change of A_{Al}/A_{Li} due to possible change of sample geometry is accounted for properly.

The experimentally determined quantity $(\sigma_H/\sigma_{Li})_{exp}$ divided by the tabulated one $(\sigma_H/\sigma_{Li})_{tab} = 58.3$ [27] is shown in Fig. 7.48 [33]. As is easily seen, both value sets (at $T = 20$ K and $T = 300$ K) are significantly smaller than the tabulated one and are strongly angle dependent. This "anomaly" is much more pronounced than that of the previously measured $NbH_{0.78}$ and the LiH values do not assume $(\sigma_H/\sigma_{Li})_{tab}$ at low angles. The most important result, however, is that the LiH data shows significant differences at the two different temperatures being in clear contrast to the NbH, PdH or water data.

Due to technical problems, the room temperature measurement has been performed without a cryostat in the sample tank so that the objection might be raised that these differences in the results might be caused by the varying experimental conditions of the room temperature and the low temperature

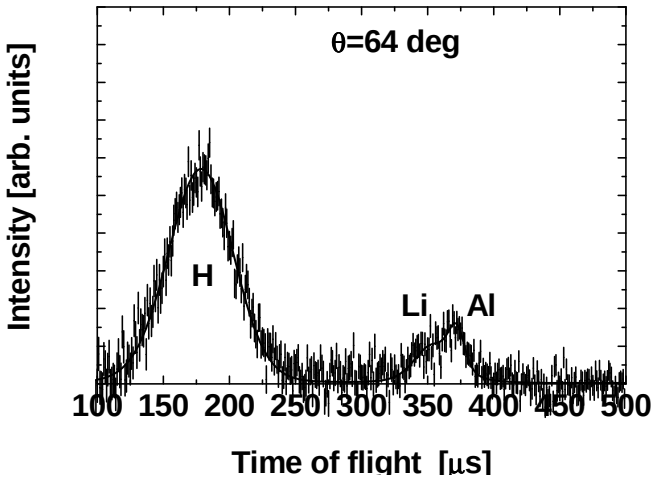

Figure 7.46: TOF spectrum of LiH at $T = 300$ K taken at scattering angle of $\theta = 64°$. The H recoil peak is well separated from the Li and Al recoil peaks, respectively (the latter is due to the sample container). The Li and Al recoil peaks are not very well resolved but in the backscattering direction (see Fig. 7.47) at $\theta = 141°$ they are. From the backscattering spectra the area ratio of Li/Al is determined and used to extract the Li area from the forward scattering spectra in order to relate the H area to the one of Li, thus giving σ_H/σ_{Li}. Similar spectra are obtained for the sample measured at $T = 20$ K.

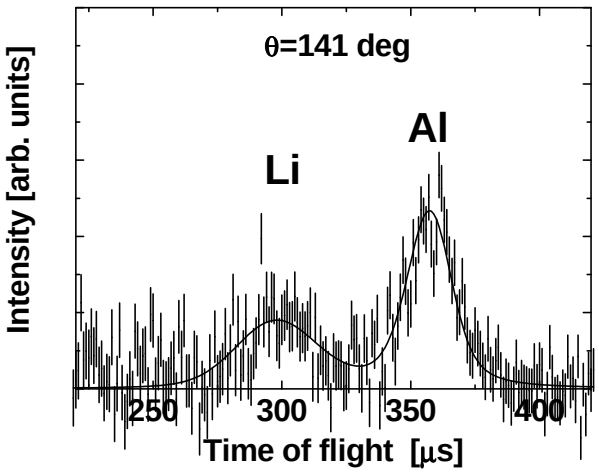

Figure 7.47: TOF spectrum of LiH at $T = 300$ K taken at scattering angle of $\theta = 141°$. The Li and Al recoil peaks are satisfactorily resolved. Similar spectra are obtained for the sample measured at $T = 20$ K.

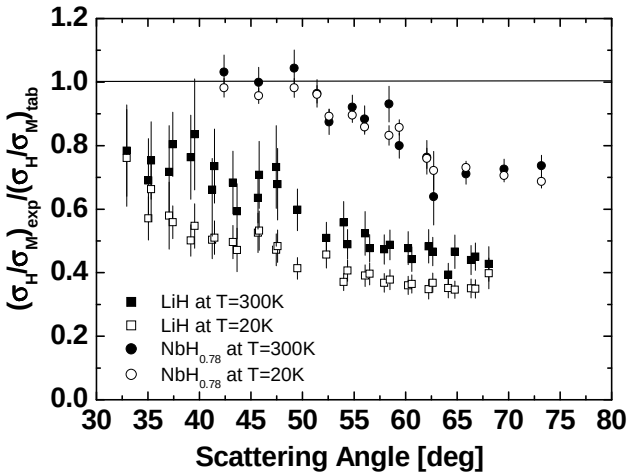

Figure 7.48: Experimentally determined ratios $(\sigma_H/\sigma_M)_{exp}$ (M representing Li or Nb, respectively) normalized by the tabulated ratio $(\sigma_H/\sigma_M)_{tab}$ vs. scattering angle θ. Full squares: LiH data at $T = 300$ K; open squares: LiH data at $T = 20$ K. Full circles: $NbH_{0.78}$ data at $T = 300$ K; open circles: NbH data at $T = 20$ K. The LiH data show larger anomalies than NbH. A significant difference upon temperature change is observed in the LiH case, while no such difference is observed in the $NbH_{0.78}$ case.

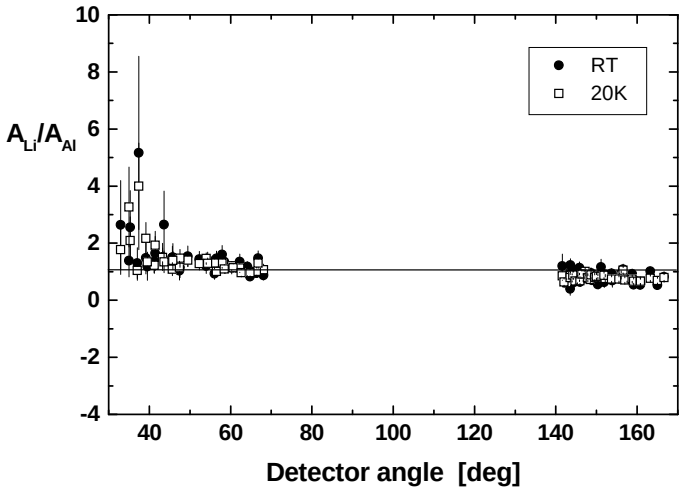

Figure 7.49: Ratio A_{Li}/A_{Al} of the peak areas of Li and Al, respectively, for T=300 K (full circles) and T=20 K (open squares) in forward and backward scattering directions as a function of detector angle. Its constancy illustrates that the change of $(\sigma_H/\sigma_{Li})_{exp}$ (see Fig. 7.48) is caused exclusively by changes in σ_H.

measurements, respectively. However, two arguments refute this doubt: *(i)* the Al contribution of the cryostat overlaps completely with the Al contribution of the can containing the sample. The overall Al contribution is determined from the backscattering spectra (see Fig. 7.47). And this procedure always ensures the proper account for all existing Al contributions; *(ii)* the scattering power of the cryostat is extremely low (1% and less). This can be seen from Fig. 7.49. There the angular distribution of the area ratio of Li and Al, i.e. A_{Li}/A_{Al}, is shown. It is clearly seen that the use of the cryostat (see open squares of Fig. 7.49) does not change the A_{Li}/A_{Al} ratio at all.

7.4 Summary

The experiments performed on VESUVIO and the related data analysis allow only to determine the product of the scattering cross section σ_X and the number density N_X, i.e., the scattering cross section density, of the nuclei in the sample. Therefore, although the plots in the previous sections show the comparison between the experimentally determined scattering cross sections and the tabulated one, it should not be confused with the fact that here actually the effective number of scattering nuclei is decreased. So, instead of

saying that the scattering cross section is reduced by a certain amount, one could say that the effective number of scattering nuclei is reduced.

Staying in terms of the scattering cross section, the results might be summarized as follows:

The experiments on liquid mixtures of H_2O/D_2O [31, 32] have shown that the ratio of the neutron scattering cross sections of H and D, i.e., σ_H/σ_D, was strongly decreased with respect to the tabulated value $(\sigma_H/\sigma_D)_{tab}$ =10.7. In addition, this decrease which amounts to ca. 40% of $(\sigma_H/\sigma_D)_{tab}$ at the lowest measured D mole fraction x_D is strongly dependent on x_D of the mixture but is rather independent of temperature [33]. These measurements were taken using a gold foil as energy analyzer with final energy of E_1=4.9 eV. Repeated measurements using a uranium foil analyzer with E_1=6.8 eV have shown a σ_H/σ_D which is still anomalous but higher than that obtained using the gold foil analyzer. Given by the kinematic conditions of the experiment, the different resonance energies of gold and uranium involve different scattering times on the protons. This difference might be the explanation for the different scattering behaviors of the protons in water.

Later experiments on pure H_2O, pure D_2O and mixtures of them showed that, under the assumption that the O atom behaves conventionally, the decrease of σ_H/σ_D is governed by a decrease of σ_H rather than an increase of σ_D and that this decrease is largest for pure H_2O. Some of the measurements of the H_2O/D_2O mixtures were repeated using a new experimental technique with a considerably improved energy resolution. These experiments [34] fully confirm the original results [31].

Measurements on solutions of urea ($CO(NH_3)_2$) dissolved in D_2O showed similar results as liquid H_2O/D_2O but higher anomalies for the lowest x_D [35].

Pure C_6H_6 and pure C_6D_6 and mixtures of them have been also measured. The experimentally determined σ_H/σ_C of these liquids is ca. 20% smaller than the tabulated one and is, in contrast to the results of the H_2O/D_2O mixtures, almost independent of the D mole fraction which indicates the intramolecular origin of the effect in benzene. Furthermore, σ_H/σ_C depends only slightly on the scattering angle, i.e., scattering time. In addition, the experimental results of C_6D_5H (having a H:D ratio of 1:5) turned out to be identical to those of a C_6H_6/C_6D_6 mixture with H:D=1:5. This result further indicates the intramolecular character of the effect. It also has far reaching consequences for a recent theoretical model [55, 56] claiming the explanation of the effect of anomalous neutron cross section of the protons. This model relies on the existence and relevance of the neutron coherence length. The neutron coherence length is larger than the H-H distance in C_6H_6 whereas is it smaller than the H-H distance in C_6D_5H. However, the anomalous effect is

the same for both samples. The D signal was too weak to give comprehensive information about σ_D in the benzene system. However, pure C_6D_6 showed a σ_D/σ_C which is slightly smaller than $(\sigma_D/\sigma_C)_{tab}$ in forward scattering and a further decrease in the backscattering direction.

The experiments on fully protonated polystyrene showed that the measured σ_H/σ_C is ca. 20% smaller than $(\sigma_H/\sigma_C)_{tab}$ and that this decrease is independent of scattering time [41]. Similar anomalies were also found in partially deuterated polystyrene and benzene [42]. In contrast to the strong dependence of σ_H/σ_O on the D mole fraction of the water mixture, σ_H/σ_C seem to be only slightly dependent on the D mole fraction of the H-polystyrene/D-polystyrene mixtures.

The same effect is observed in an amphiphilic molecule (2-iso-C_4E_1) dissolved in D_2O [43]. Similar to the results of polystyrene, the experimentally determined $\sigma_H/(\sigma_C+\sigma_O)$ here is ca. 20% smaller than $(\sigma_H/\sigma_C)_{tab}$. It should be noted that although H and D overlap is present in this system, the effect is as large as in the fully protonated polystyrene which does not contain D.

Similar experiments on liquid mixtures of H_6-acetone and D_6-acetone showed the same D mole dependence as was found in the H_2O/D_2O system but with a significantly larger anomaly [44].

The hydrides of niobium, palladium and yttrium show also a proton cross section anomaly. However, here this anomaly is strongly dependent on the scattering angle and according to Compton scattering theory also on the scattering time [32, 36–39]. Whereas at low scattering angles – which corresponds to long scattering times – σ_H/σ_{metal} approaches its conventionally expected value, it is strongly decreased (about 40%) at higher scattering angles (i.e., shorter scattering times). Similar to the results of the H_2O/D_2O mixtures, no temperature dependence has been found for these hydrides [36–38, 40]. In the case of the yttrium hydrides, the measured σ_H/σ_Y does not assume the tabulated value $(\sigma_H/\sigma_Y)_{tab}$. The dependence of σ_H/σ_{Nb} on the D mole fraction in the mixed H/D niobium hydride is visible only in the low scattering angle region.

No significant angle dependence has been found for the deuterated metallic hydrides at forward (low) scattering angles. However, a significant decrease of σ_D/σ_{metal} in the backscattering direction is observed. This effect is most pronounced for YD_2 and YD_3, very small for the hydrides of niobium and almost invisible for those of palladium. No differences are observed in the data of YD_2 and YD_3. I.e., the dependence on angle of σ_D/σ_Y is independent of the D concentration in the host. Similar to σ_H/σ_{metal}, the experimentally determined values of σ_D/σ_{metal} are rather independent of the D mole fraction in the sample.

In contrast to the above mentioned results of water and the metallic hy-

drides, the experimental data of LiH showed for the first time a temperature dependence of the proton scattering cross section density decrease. Concretely, the anomalous decrease was larger at 20 K than at 300 K [33].

In summary, it has been found that the protonic scattering cross section σ_H is strongly reduced in these systems, whereas σ_D shows only small anomalies. The metal hydrides showed a strong angle, or equivalently, scattering time dependence of the anomalies. Temperature dependence has been found only in the ionic hydride LiH.

Chapter 8

Independent experimental tests

Since the experimental results found in this work contradict conventional expectations, their reliability must be checked against all possible artifacts possibly occurring in the chain from neutron production to data reduction and analysis. For example, detector efficiency, detector saturation, dead time effects and/or data overload due to the very high scattering cross section of the protons might lead to missing counts which would be interpreted as a shortfall of the measured scattering intensity. The shortfall of the scattering intensity of the protons in general could be also caused by severe multiple scattering effects which might be more pronounced particularly in the high scattering angle regime.

Very recently, the accuracy of the description of the energy distribution of the incident neutron beam (see eq. (6.2)) has been doubted by Cowley [132]. Also he attributed the angle dependence of, e.g., the niobium hydride data (see section 7.3.1) to the flawed conversion of the spectra from time of flight to q space [132].

Another important issue is the peak overlap of, for example, H and D which may lead to an intensity transfer from the H peak to the D one. For example, very recently, Blostein et al. [126] criticized the expression of the experimentally observed spectral intensity as a convolution (see eq.(6.25)) and concluded that this data analysis procedure leads among others to incorrect values of peak areas in the case of two (or more) overlapping recoil peaks, in particular those of H and D according to the misrepresentation of the "right tail" of the peaks.

This chapter is dedicated to the presentation of all the tests which have been done in order to check the doubts and criticisms outlined above. These tests consist either in performing additional experiments by changing specific experimental conditions (see below) or by putting the doubts and criticisms to experimental tests, i.e., by comparing different experimental results with

the implications and consequences of the criticisms.

8.1 Multiple scattering effects

Multiple neutron scattering effects on the detected intensity of scattering particles is a well known problem particularly for strongly scattering particles like hydrogen. One may object that the D mole fraction dependence of σ_H/σ_D in the H_2O/D_2O mixtures, i.e. that σ_H/σ_D approaches the tabulated value of 10.7 with increasing x_D (see section 7.1.1), might be due to the fact that multiple scattering effects become accordingly smaller. In the following this possibility is considered.

The results of a series of measurements on H_2O/D_2O mixtures with x_D=0.5 with a variety of sample geometries and scattering intensities varying by a factor ∼5 are summarized in table 8.1. These measurements have given the same ratio σ_H/σ_D within error [34]. The fact that the results are independent of the sample size is a very strong evidence that sample attenuation effects and multiple scattering play no significant role in the observed anomalies.

In addition Monte Carlo (MC) simulations of the deep inelastic neutron scattering have been done on H_2O/D_2O mixtures following the procedure described in [133]. A simulation was done for the thickest sample used in the H_2O/D_2O experiments (0.5 mm) and the ratio σ_H/σ_D, obtained from fitting data, with and without a correction for multiple scattering. The MC simulations showed that multiple scattering effects are indeed negligible [34].

Measurements of NbH [36] and Formvar [45] samples of thicknesses varying by a factor two showed no difference to the cross section ratios. Similar to the water data the metal hydride data have been subject to additional MC simulations. The samples used for these simulations were thin slabs of thickness $D \leq 0.5$ mm, placed either perpendicular or with a tilt angle with respect to the incoming beam. It was found that, with the relatively thin foils used in the metal hydride measurements, the multiple scattering intensity was always negligibly small in comparison to that for single scattering. This is also the case for the highest angle θ =72.5° where the neutron path length in the sample is relatively large [38].

In conclusion, multiple scattering effects can not account for the large anomalies found in the various condensed matter systems, like water, metal and carbo hydrides.

Table 8.1 Given is the ratio σ_H/σ_D of the scattering cross section of H and D, respectively, of H_2O/D_2O mixtures with H:D=1:1 measured at different experimental periods using the gold foil analyzer. Note the various can materials used as well as the largely differing sample thicknesses and scattering powers (SP). The scattering power was determined by comparing the sample scattering at 60°, with that from a 1mm thick lead sample. The "anomalous" decrease of σ_H/σ_D with respect to its conventionally expected value (=10.7) is independent of the geometry of the sample. The results indicate that multiple scattering effects are irrelevant here.

Period	*Can Material*	*Geometry*	*Thickness*	*SP*	σ_H/σ_D
March 1995	Al	Flat	0.5 mm	6.5 %	8.0 ± 0.5
July 1995	V	Flat	0.2 mm	3.3 %	7.6 ± 0.2
May 1997	Al	Flat	0.5 mm	15 %	7.4 ± 0.2
Aug 1997	V	Flat	0.2 mm	7.5 %	7.8 ± 0.5
June 1998	Al	Annular	0.5 mm	12 %	7.5 ± 0.5
June 1998	Nb	Annular	0.5 mm	12 %	7.0 ± 0.4
July 2003	Nb	Annular	0.5 mm	8.4 %	8.2 ± 0.1

8.2 Saturation effects

The possibility of saturation in the detection system of VESUVIO is a well known problem which occurs if the scattering cross section density of the sample is high [134]. But it should be stressed that this saturation does not take place in the detectors, but rather in the data acquisition electronics (DAE) system. A method to overcome the saturation (in those cases in which it exists) is to connect pair wise a high counting rate detector bank (forward scattering direction) and a low counting rate detector bank (back scattering direction) with the same data acquisition device and to give the high rate detector bank the higher acquisition priority. If saturation persists, it is also possible to disconnect a detector bank in order to reduce the load of data to be collected by the DAE. Using these procedures, it is always possible to make sure that "saturation" does not affect the results.

Since the first observation (1995) of the considered "anomalous" effect on H_2O/D_2O mixtures using VESUVIO, the measurements were repeated many times using many different liquid cans with various sample thicknesses and shapes (see table 8.1). In these tests, the amount of liquid sample was varied significantly, thus changing also the scattering power, the component due to multiple scattering, and the saturation probability of the DAE. However, the detected anomalous shortfall of σ_H/σ_D [31] has been always reproduced very

well.

In addition, measurements on liquid mixtures of H_6-acetone/D_6-acetone (see section 7.2.5) further rule out saturation effects to be responsible for the effect. Although the hydrogen number density in acetone is ca. 30% smaller than in water, the measured σ_H/σ_D ratios of the acetone samples are even significantly smaller than the corresponding values of H_2O/D_2O, i.e., the anomaly is larger.

In recent experiments on liquid hydrogen [135, 136], the sample-detectors distances has been increased from ca. 0.5 m to ca. 1.0 m in order to reduce the scattering intensity by a factor of four, thus significantly reducing possible saturation effects. Moreover, the first experiment on H-polystyrene [42] has been repeated using another polystyrene foil and the very recently modified configuration of VESUVIO, in which (among other changes) the sample-detectors distances are about 70 cm, instead of ca. 50 cm realized in the previous experiment [41]. All these changes let the previously obtained results completely unchanged.

8.3 Energy resolution and convolution formalism

Since the first experiments on water in 1995 it was objected that the effect of the shortfall of the cross section ratio σ_H/σ_D might be due to the overlap of the strong H peak with that of the weaker D one in the time of flight spectra. This overlap is mainly due to the limited energy resolution of the gold analyzer foil used thus far. In addition, Blostein et al. [126] presented recently a theoretical investigation concerning the convolution method used to analyze the VESUVIO data.

In summary, both the energy resolution as well as its theoretical description (i.e. its approximation) are subject to critics. In this section various experiments will be presented which will show that these doubts and criticisms are unjustified. The experimental tests will comprise various methods for energy resolution improvements as well as sample modifications. All these tests will show that overlap effects are irrelevant here.

8.3.1 Energy resolution: Experiments with U foil analyzer

The first experiments on H_2O/D_2O mixtures (1995) were done with a gold foil analyzer which is known to have a Wigner shaped energy resolution

function being approximated with a Lorentzian function. As is well known, the Lorenztian possesses long tails. Therefore, the scattering contributions of H and D nuclei might overlap considerably in the long tail regions. As a consequence, the anomalous reduction of the cross section ratio of H and D might be caused by some intensity shift from the H signal to the D one, leading to an underestimation of the H intensity and an overestimation one for the D intensity.

To rule out this possibility, the experiments were repeated using a uranium (U) foil analyzer. This foil provides a twofold improvement of the energy resolution: (1) the half width at half maximum is ca. half of that of gold; (2) the energy resolution function of U is Gaussian in nature and thus does not posses the long tails. Consequently, the peak overlap of H and D, for example, in H_2O/D_2O mixtures is considerably reduced. Thus, if the effects found with the gold foil analyzer were caused by the long tails, they should vanish as the energy resolution function improves significantly. However, as shown in Fig. 7.2, the effect is still present and possesses the same x_D dependence [31]. Interestingly, according to the calculations of Blostein et al. [126] the anomaly should be larger using the U foil. This result, however, is rather counterintuitive since U has a better energy resolution and should yield smaller anomaly according to their argument.

8.3.2 Convolution formalism

Ignoring the results of the improved energy resolution using the U foil analyzer [31], Blostein et al. [126] examined critically the data analysis procedure of the TOF spectra obtained with the VESUVIO instrument and criticized the expression of the experimentally observed spectral intensity $c(t)\Delta t$ at "time channel t" as a convolution. Instead, Blostein et al. proposed a qualitatively different procedure based on the complete absorption cross section of the used absorption foil (usually Au or U) and conclude that the usually employed data analysis procedure based on the "convolution formalism", eq.(6.25), fails in the inferred peak positions in the TOF spectra and the momentum distribution widths of the peaks. Furthermore, every peak in the TOF spectra is erroneously represented and leads to incorrect values of peak areas in the case of two (or more) overlapping recoil peaks, in particular those of H and D. To check this possibility additional experiments have been performed.

At that time when the original paper on H_2O/D_2O mixtures has been published [31] it was not possible to extract the oxygen peak from the joint peak of oxygen and the can one. However, the use of Nb as can material and putting some detectors at high angles in the backscattering direction

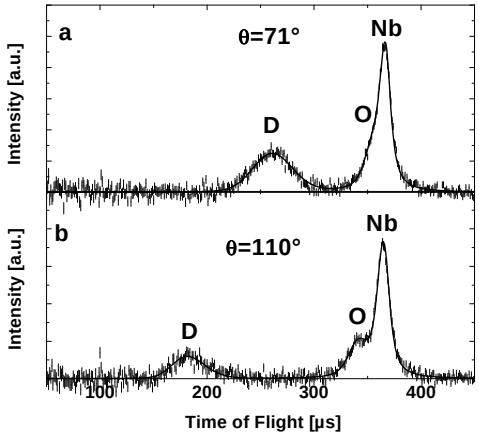

Figure 8.1: Example spectra of liquid D_2O in a Nb can (a) in forward scattering and (b) in backscattering. Whereas the O peak is not resolved form the Nb one in forward scattering, it is in backscattering direction.

made a separation of the O signal and the Nb one possible. With this peak separation it was possible to relate, e.g., the H or D signal, respectively, to the O one.

The check of the claims of Blostein et. al consists in the comparison of σ_D/σ_O determined from H_2O/D_2O mixtures with x_D=0.5 with that one of a pure D_2O sample. Whereas the former exhibits an overlap of the H and D peaks there is no such overlap in the latter – due to the missing H peak. Compare Figs. 6.4 and 8.1.

The experimental results which are depicted in Fig. 8.2 [130] show very clearly that σ_D/σ_O have the same value regardless whether a hydrogen peak exists or not. These experimental results reveal that the objections of Blostein et al. concerning the peak areas are of no relevance for the QE effect in this work.

It is important to stress that the D peak is much more sensitive to overlaps with the H peak, because D scatters less than H by a factor of ca. 3. Therefore, an intensity shift from H to D would imply that the D signal is much more changed than the H one, due to the fact that the H intensity is much larger than the D one. However, the experimentally determined σ_H/σ_O and σ_D/σ_O do not show this implication.

A further evidence for the irrelevance of the peak overlap between the H and D signal in the time of flight spectra as measured on VESUVIO is evident from the measurements on the metal hydrides. As can be seen from

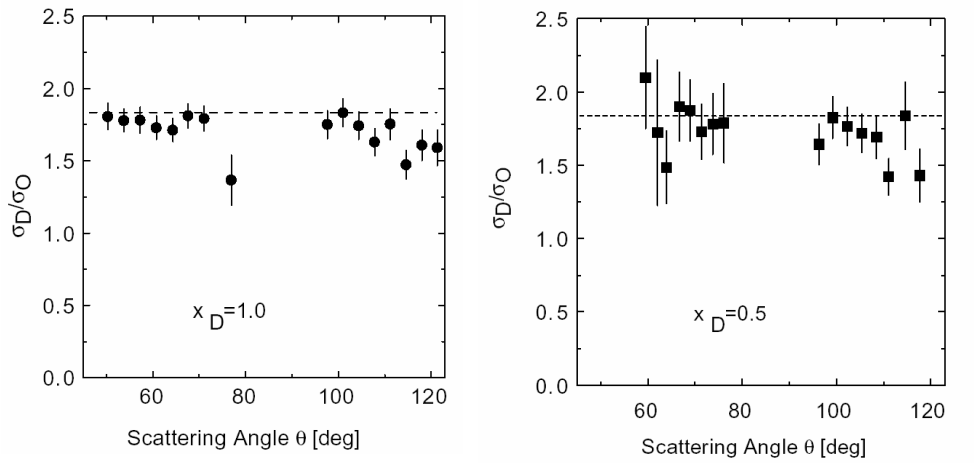

Figure 8.2: Here is shown the experimentally determined σ_D/σ_O ratio for pure D_2O (left frame) and for a H_2O/D_2O mixture with x_D=0.5 (right frame). It can be clearly seen that pure D_2O shows the same σ_D/σ_O ratio as the mixture does. Both values agree within experimental error with the tabulated value of $(\sigma_D/\sigma_O)_{tab}$=1.8. This means that overlapping effects do not play any role for the found effect and that the decrease of σ_H/σ_D is solely due to a decrease of σ_H.

the constancy of σ_D/σ_{Nb} (see for instance Fig. 7.34) in connection with the strong angle dependence of σ_H/σ_{Nb} (see Fig. 7.30), the peak intensities seem to be completely independent of each other. Moreover, if there is any overlap influence, then σ_H/σ_{Nb} should approach the conventional value at the high angles and not at the low ones.

An additional evidence that overlap effects are not the cause for the found anomalies is provided by the fact that the found anomaly for σ_H/σ_O is largest in pure H_2O (see Fig. 7.4). This means the largest anomaly is found for the case where the H signal does not interfere with D.

8.3.3 Double difference method

In recent years the VESUVIO instrument has been subject to a significant improvement concerning the energy resolution function. This improvement consists in employing the so called double difference method being described in the following. In this method three measurements are taken, with no filter, a filter of thickness d_1 and absorption $A_1(E_1)$ and a filter of thickness d_2 and absorption $A_2(E_1)$. The "double difference" of the three measurements is

$$R_{DD}(E_1) = A_1(E_1) - \frac{d_1}{d_2} A_2(E_1). \tag{8.1}$$

The DD technique relies upon the fact that when $\sigma(E)$ is small,

$$A_1(E_1) = 1 - \exp[-N d_1 \sigma(E_1)] \sim N d_1 \sigma(E_1) \tag{8.2}$$

with a similar expression for $A_2(E_1)$. Thus when $\sigma(E)$ is small $R_{DD}(E) = 0$ and the wings of the function $A_1(E_1)$ in single difference (SD) are removed, whatever their functional form. This is illustrated in Fig. 8.3 where the calculated energy resolution functions $R_{SD}(E_1)$ and $R_{DD}(E_1)$ for an Au analyzer is shown.

Blostein et al. reported a neutron transmission (NT) experiment on liquid H_2O/D_2O mixtures [137]. They inferred the ratio of the neutron total scattering cross section of H and D, σ_H/σ_D, and found a good agreement with the tabulated value of 81.67/7.63=10.7. They conclude that the anomalous effect of σ_H/σ_D reductions [31] are an artifact of the data analysis employed at VESUVIO. In the following it will be shown that these claims are unjustified. The validity of the DINS data analysis on VESUVIO are confirmed by additional experimental results.

The objection of Blostein et al. [126] which led them to perform the NT experiment [137] is that, the incorporation of the energy resolution function R_E (being the dominating part of the instrument resolution function

on VESUVIO) as a convolution in time of flight is a crude approximation. In their opinion, this approximation leads to serious errors due to the long tails of the absorption resonance of Au being used as energy analyzer [126]. Concretely, the H peak area would be underestimated due to its overlap with the D or other heavy atom peak thus causing the anomalies.

Now, the *working hypothesis* for the following test is:

if the data analysis does not account properly for R_E, then a significant improvement of the experimental R_E should give different results for σ_H/σ_D when applying the same data analysis.

Such an improvement of R_E is provided by the so called Double Difference (DD) technique [106, 138]. as illustrated in Fig. 8.3 and is given by the following:

(1) For significant $E - E_0$, R_E^{DD} (dashed line) is more than one order of magnitude smaller than R_E^{SD} (full line);

(2) The width of R_E^{DD} is significantly smaller than that of R_E^{SD}.

Consequently, these features imply that overlapping effects are considerably reduced in the case of DD.

Measurements on a liquid 50:50 H_2O/D_2O mixture using SD and DD showed that in direct contrast to the *working hypothesis* the same σ_H/σ_D ratios are obtained:

- $Q_{SD} = 6.9(2)$ using SD and
- $Q_{DD} = 6.9(6)$ using DD.

The results clearly show that (1) σ_H/σ_D is ca. 35% smaller than theoretically expected (10.7) being in line with the previous results (see 7.1.1) [31] and (2) more importantly in the present context that this effect is independent of the used technique. The larger error for the DD value is due to the fact that performing a double difference, the counting statistics is reduced accordingly.

Summarizing, although the DD technique introduces a significant improvement to the energy resolution function, the ratio σ_H/σ_D is here the same as that obtained from the SD technique employing the same data analysis. This result demonstrates that the data analysis procedure always accounts properly for the resolution function. Otherwise different results should be obtained when using SD or DD. Therefore, the *working hypothesis* must be rejected and as a consequence the conclusion of Blostein et. al [137] that the validity of the DINS data analysis procedure performed on VESUVIO is limited is incorrect.

In addition, recent Monte Carlo calculations involving the exact energy resolution function showed that the convolution approximation has no effect

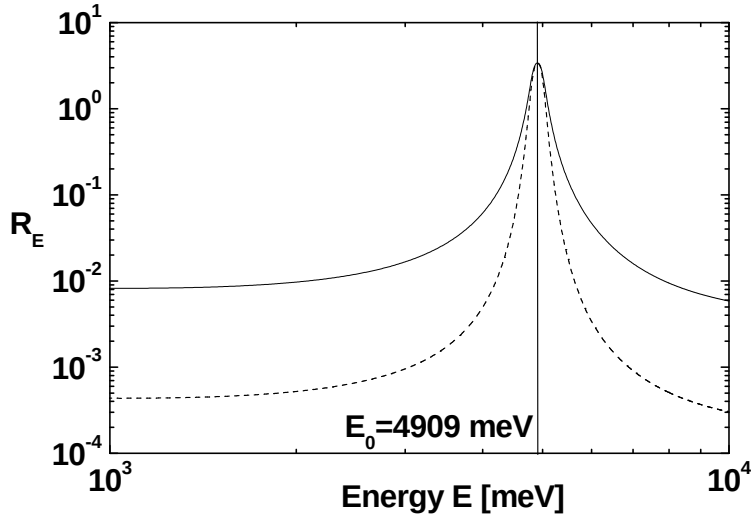

Figure 8.3: Energy resolution R_E of the gold foil at resonance energy E_0 =4909 meV using SD (full line) and DD (dashed line). R_E^{DD} is more than one order of magnitude smaller for significant $E - E_0$ than R_E^{SD} is. The shapes have been confirmed by measurements on a lead sample.

on σ_H/σ_D [34]. It is also very important to stress that, very recently, similar anomalous effects have been observed applying electron Compton scattering (ECS) from protons [45]. The energy resolution function of ECS [45] does not contain any long tails.

8.4 Determination of the incident energy spectrum $I(E_0)$

It has been stressed [126, 132, 137, 139] that an accurate determination of the incident neutron intensity $I(E_0)$ is essential for the determination of cross section ratios on VESUVIO. $I(E_0)$ was measured using the VESUVIO incident beam monitor 1 (see Fig. 4.2). The incident energy of the neutrons is related to their time of flight measured in the monitor via

$$E_0(t) = \frac{1}{2} m \left(L/t\right)^2 . \tag{8.3}$$

The incident beam intensity is related to the measured monitor counts $C_m(t)dt$ via

$$I(E_0)dE_0 = \frac{C_m(t)}{\eta_m(E_0)} \frac{dt}{dE_0} dE_0 \tag{8.4}$$

where $\eta_m(E_0)$ is the monitor efficiency at energy E_0. An example of a measurement of $I(E_0)$, determined from eq.(8.4), is shown in Fig. 8.4, together with a fit to the function

$$I(E_0) \propto E^{-\gamma} \tag{8.5}$$

with γ as adjustable parameter.

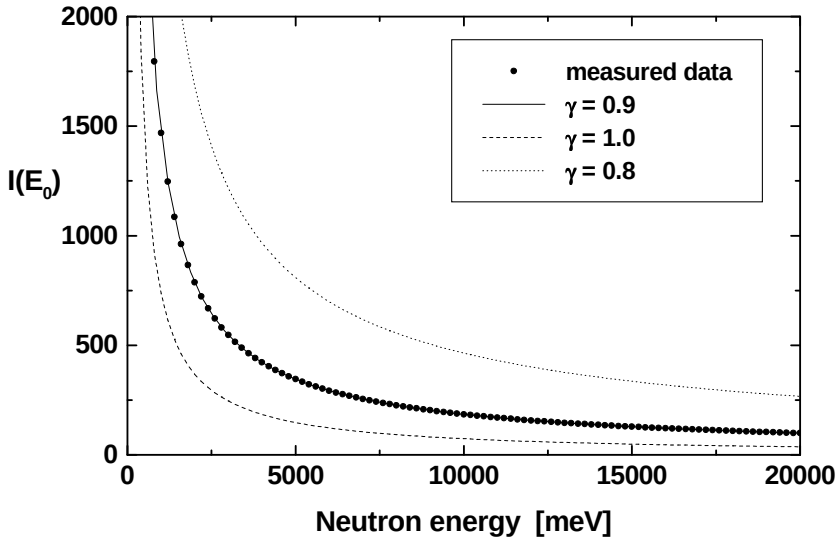

Figure 8.4: Full circles: The measured incident neutron spectrum after correction for the monitor efficiency. Solid line: The fit to the measured data using eq.(8.5). The fit yields γ=0.9. The dashed and dotted lines represent eq.(6.2) with γ=1.0 and γ=0.8.

The fit gave $\gamma = 0.90$ with statistical errors at the $\sim 10^{-5}$ level, in agreement with Monte Carlo calculations of the moderator performance [125], which predict that $\gamma = 0.9$. A large number of such data sets, collected over the past 10 years, all give consistent values $\gamma = 0.90 \pm 0.01$ [34].

As a further test on the accuracy of the measurement of $I(E_0)$, a second procedure was used to determine γ. A Uranium filter was cycled in the incident beam (see Fig. 4.2) and the difference between the counts with the foil in and foil out was calculated. An example of such a difference measurement is shown in Fig. 8.5.

The difference foil out - foil in is given by

$$\Delta(t)dt = I(E_0)\frac{dE_0}{dt}dt\eta_m(E_0)A(E_0) \tag{8.6}$$

where $A(E_0)$ is the filter absorption, defined in eq.(4.2). It follows from eq.(8.6) that the sum of counts in time of flight, over the area of a single resonance peak, centered at E_R, is

$$\int_{t_1}^{t_2} \Delta(t)dt = \int I(E_0)\eta_m(E_0)A(E_0)dE_0 \approx I(E_R)\eta_m(E_R)\alpha_R \tag{8.7}$$

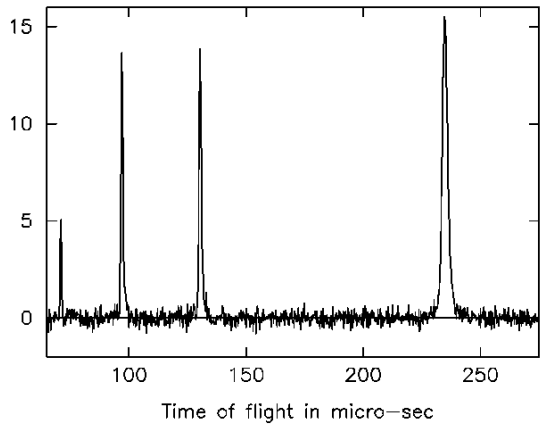

Figure 8.5: Difference between monitor spectra obtained with a Uranium foil in the incident beam and with no foil in the beam (see Fig. (4.2)). The four peaks correspond to resonances at 6.7, 22, 37 and 66 eV.

where t_1 and t_2 are chosen to include only a single resonance peak and

$$\alpha_R = \int A(E_0)dE_0 \tag{8.8}$$

is the total absorption corresponding to the resonance peak chosen. $I(E_0)$ and $\eta(E_0)$ can be taken outside the integral in eq.(8.7) due to the narrowness of the peaks. The absorption factor α_R was also calculated from eq.(4.2) and eq.(8.8) for uranium resonances at 6.7 eV, 21 eV, 37 eV and 66 eV, using tabulated resonance parameters for uranium [105]. The quantity Nd was determined by weighing the filter, which has uniform thickness over a 10 by 10 cm area. The detector efficiency $\eta_m(E_R)$ can also be calculated and for the 0.5 mm thick glass beads used in standard ISIS monitors is $\propto 1/\sqrt{E_R}$ to $\sim$1%. Using calculated values of α_R and $\eta_m(E_R)$, $I(E_R)$ was calculated from α_R for each of the four resonance peaks. These values of $I(E_R)$ were then fitted to the function $I(E_0)$ defined in eq.(6.2), to obtain γ. The advantage of this measurement over the direct determination of γ from the full monitor spectra, is that γ is determined only by the neutrons absorbed by the foil. Thus for example, any delayed neutron background, has little effect on γ values obtained in this way. The results obtained are shown in column 1 of table 8.2. For comparison, values of γ obtained by direct fitting of the spectra as in Fig. 8.4 are also given. There is a small systematic difference in γ values obtained by the two different methods, but as will be shown in the

Table 8.2 Shown are the γ values obtained from U foil transmission measurements and from direct measurements of the incident neutron beam.

U foil transmission	*Direct measurement*
0.93	0.89
0.90	0.89
0.94	0.89
0.90	0.89
0.96	0.90
0.93±0.01	0.89±0.02

following section, this difference is much too small to explain the anomalies observed.

8.4.1 Effects of errors in $I(E_0)$

The measurements described in section 7.1 were of the ratio of the H and D cross sections, σ_H/σ_D, in mixtures of D_2O and H_2O as a function of D_2O concentration x_D. In order to test how sensitive these measurements are to the accuracy with which γ is known, complete data sets were simulated by DINSMS, as described in [133], using perfect resolution. Incident intensities of the form in eq. (6.2), with $\gamma = 0.8$, $\gamma = 0.9$ and $\gamma = 1.0$ were input to three different simulations. These three simulations were then fitted using the standard data analysis routines, which assume $\gamma = 0.9$. Values of σ_H/σ_D were calculated from the fitted parameters, as an average over the angular range 50-75°, following exactly the same procedure used for real data. Figure 8.6 shows values of σ_H/σ_D as a function of x_D, obtained using the three different values of γ input to the simulation (see above). Also shown are the measured data. With an input value to DINSMS of γ=0.9, the fitted parameters were identical within statistical error to the values input to the simulation. As γ increases above this value, the values of σ_H/σ_D obtained from the fit decrease, but it is clear from Fig. 8.6 that γ would have to be $\sim$1.1 to account for the large anomalies observed in the data. Similar comments apply to anomalies observed in other systems. This is well outside the errors in the measurement of γ given in table 8.2.

It was pointed [132] out that there is a large Jacobian factor

$$J = 1 - \frac{m}{M}(1 - \frac{k_1}{k_0}cos\theta) \tag{8.9}$$

involved in any conversion between a VESUVIO time of flight scan in q, ω space and a constant q scan. It was suggested that any errors in the incor-

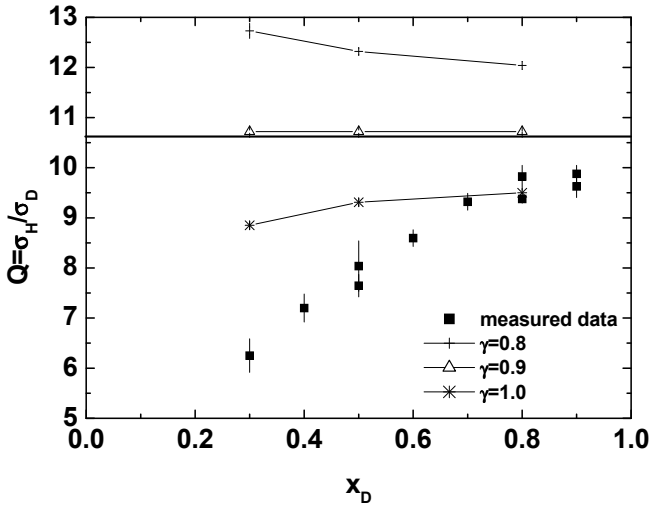

Figure 8.6: The crosses were obtained from fits to simulations for H_2O/D_2O mixtures with γ=0.8, the up triangles were for γ=0.9 and the stars for γ=1.0. The full squares show the results from VESUVIO data collected using an Au filter.

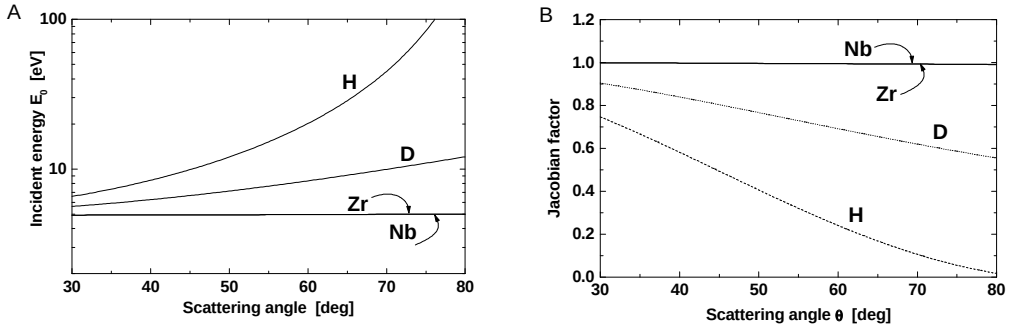

Figure 8.7: A) Dependence of the involved incident energy on the scattering angle for different masses: H (M =1), D (M =2), Zr (M =91), and Nb (M =93). The same incident energy is involved for Zr and Nb. B) Dependence of the involved Jacobians (see eq.(8.9)) for H, D, Zr, and Nb. The same Jacobian factor is involved for both, Zr and Nb.

poration of this factor could seriously affect the peak areas obtained from the fitting. However, the only Jacobian, dE_0/dt, involved in the fitting expression is well known [82]. Furthermore, neglecting resolution effects, if the IA is valid, eq.(6.25) is an *exact* expression for the count rate as a function of t and is true for any point in q, ω space accessed by the spectrometer. Thus the exact line of the scan in q, ω space is immaterial, since in principle every scan will give the same values for the fitting parameters, whether it is at constant q or constant θ. For example fitting DINSMS simulations with perfect resolution to eq.(6.25) recovers the cross section ratios input to the simulation to within a statistical error $\sim$1%, at any scattering angle as can be seen in the $\gamma = 0.9$ simulation shown in Fig. 8.6.

It should also be noted that any errors in either the assumed Jacobian dE_0/dt, or $I(E_0)$, would produce a consistent angular dependence in the cross section ratios of H to heavier atoms in *all* samples, which is not observed. The ratio σ_H/σ_D obtained from measurements on H_2O/D_2O mixtures is essentially independent of angle as can be seen from Figures 7.7 and 7.8.

To further investigate the possibility of incorrect Jacobians, measurements on ZrH_2 are compared with those of $NbH_{0.8}$. It is very important to note that the masses of Nb and Zr are almost identical, i.e. M_{Nb} =93 and M_{Zr} =91 a.u. This leads to the fact that the same energy transfer is involved for scattering on Zr and Nb, respectively. For this reason and because the final energy E_1 is fixed by the resonance energy of the analyzer foil, the same incident neutron energies E_0 are involved for scattering on Zr and Nb (see

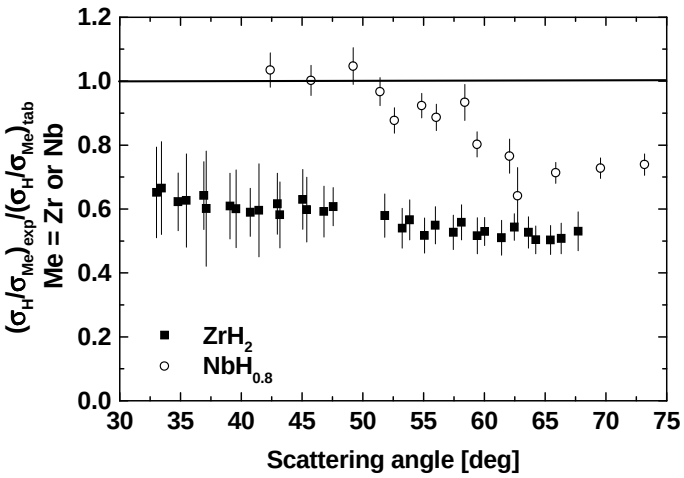

Figure 8.8: The experimental ratios $(\sigma_H/\sigma_{Nb})_{exp}$ (open circles) and $(\sigma_H/\sigma_{Zr})_{exp}$ (full squares) of the scattering cross section of H to that of Nb and Zr of $NbH_{0.8}$ and ZrH_2, respectively, each one normalized to its tabulated value (i.e. $(\sigma_H/\sigma_{Nb})_{tab}$ and $(\sigma_H/\sigma_{Zr})_{tab}$ as a function of scattering angle θ). Whereas, the $NbH_{0.8}$ shows strong angle dependence, the ZrH_2 data are very flat although the same Jacobian (see Fig. 8.7) and the same incident neutron intensities are involved for both $NbH_{0.8}$ and ZrH_2.

Fig. 8.7.A). Consequently, the same correction of incident neutron spectrum is involved in the data analysis. In addition, again due to the similarity of the masses of Zr and Nb, the same Jacobians are involved for the scattering on those nuclei (see Fig. 8.7.B). Now, if the intensity distribution $I(E_0)$ of the incident neutrons and the involved Jacobians are not correctly incorporated into the data analysis on VESUVIO - which is claimed to be the case thus leading to the angle dependence in the case of, for example, $NbH_{0.8}$ [36] - then the same angle dependence should be observed also for the ZrH_2 data.

However, in contrast to Ref. [132], the experimental results (see Fig. 8.8) show that $NbH_{0.8}$ (open circles) and ZrH_2 (full squares) exhibit completely different results:

1. While the largest anomaly found in $NbH_{0.8}$ is about 30%, an intensity deficit of ca. 45% is observed for ZrH_2;

2. More importantly, in contrast to the $NbH_{0.8}$ results, ZrH_2 does not show a significant angle dependence.

Summarizing, neither the angle dependence nor the magnitude of the anomaly of $NbH_{0.8}$ is reproduced by the results of ZrH_2 although the same data analysis procedure is applied. Thus no single γ value can explain anomalies observed in different samples.

It might be objected that while ZrH_2 necessitates the use of an Al can, NbH does not thus leading to the different experimental results. However, comparison of the ZrH_2 data with PdH necessitating an Al can (see section 7.3.2) shows that this objection is not valid because the PdH data show the same angle dependence as the NbH does.

8.5 Dead time effects

Dead time effects of the detectors and/or data acquisition electronics were also studied in detail. These effects would affect the experiments on metallic hydrides [36, 37] in which an angle dependent decrease of H intensity (i.e. at shorter time of flight – see Fig. 4.5) has been detected. If present, dead time effects should become more and more pronounced at high angles (i.e. short time of flight). Test experiments changing by purpose the dead time showed that the dead time effect did not play any role in those experiments. Another observation demonstrating that dead time effects do not play any role is that significant angle dependence of the "anomalous" decrease of the H scattering cross section occurred in the special cases of niobium hydride, palladium hydride, and yttrium hydride, but not in liquid water, benzene, or polystyrene

although the same setup have been used and although the polystyrene foils had similar scattering power as the metallic-hydrides samples.

8.6 Tilted samples

Since the polystyrene foils [41] as well as the Nb-H foils [36] were arranged perpendicular to the incoming beam, the objection could be raised that certain artifacts (e.g., multiple scattering or "shadowing" effects) could lead to a decrease of the H area of the TOF spectra at high angles. However, additional measurements with samples tilted by ca. 20° gave the same "anomalous" results. Compare Fig. 7.20 with Fig. 7.19.

8.7 Detector efficiency

Since the distribution of neutron energies detected is fixed, the detector neutron counting efficiency is the same for all masses of scattering nuclei, and therefore is the same for all values of TOF. In addition, even if there would be a "smooth" time dependence of detector efficiency, then this would play no role for the following reason: The areas of the scattering signals used for the calculation of σ_H/σ_D, σ_H/σ_C, σ_H/σ_{Nb}, etc. are obtained by a difference technique, i.e. by subtraction of an analyzer foil-in spectrum from an associated analyzer foil-out one. Therefore, if there is a smooth time of flight dependence of detector efficiency, it will be expressed for both spectra (foil-in and foil-out) and therefore would cancel out by subtraction.

8.8 PS foil into Nb can

As a last possibility it has been considered whether the use of a can could lead to an anomalous effect in the scattering intensities at shorter time of flight values, i.e. of hydrogen and/or deuterium intensity in the liquids, e.g. H_2O/D_2O, H_6-Benzene/D_6-Benzene, H_6-acetone/D_6-acetone. Therefore, a polystyrene foil was put in the Nb can and a spectrum has been recorded the result of which compared with the run with freely hanging polystyrene foil. No differences were visible between the results of the two runs. It should be mentioned that the PS foil had to be rolled in order to fit in the Nb can. Therefore, this test measurement might be regarded as a test for the possible influence of qualitatively different geometries, i.e. flat vs. annular polystyrene geometry, on the anomalous effects found.

Chapter 9

Discussion

The subject of the present work is the experimental investigation of a qualitative theoretical prediction [7] about the existence of short lived quantum entangled states in condensed matter at room temperature. According to this theoretical work [7] the scattering behavior of particles participating in such states is different from what is expected from conventional scattering theory [26, 27]. The experimental results of the present work constitute a novel effect of condensed matter physics.

Due to the fact that the proton has a relatively long thermal de Broglie wavelength because of its low mass, it is particularly suitable for exhibiting quantum effects. It is the purpose of the present work to investigate physicochemical compounds involving hydrogen in different chemical environments in order to investigate the influence of bonding conditions, electronic environments and of its dynamics on the neutron scattering behavior. For this reason the following materials have been chosen for the experiments: H_2O and D_2O and mixtures of them, urea in H_2O/D_2O mixtures, C_6H_6 and C_6D_6 and mixtures of them, H_6-acetone/D_6-acetone mixtures, polystyrene, iso-C_4E_1/D_2O solutions, and metal hydrogen systems like NbH_xD_y, PdH_xD_y, YH_xD_y and LiH.

The involved condensed matter systems cover a wide range of different chemical bonds the hydrogen is involved in. For example, the hydrogen atom is covalently bonded with the oxygen atom in water with the bond being strongly polarized due to the high electronegativity difference between H (and equivalently D) and O. Due to the lone electron pairs of the oxygen atom, the hydrogen atoms are subject to rapid exchange between the water molecules. This means that if H_2O is mixed with D_2O, the majority of the H_2O molecules will exchange their H atoms with the D atoms of D_2O giving HDO as an additional species in the mixture. In contrast, in the case of the organic systems benzene, acetone, and polystyrene, there is no such hydrogen

exchange. Whereas the hydrogens change their positions in NbH_xD_y, Pd_xD_y, and Y_xD_y by hopping from one interstitial site to the other, they are rigidly bonded in the ionic hydride LiH. The various ways the hydrogen is bonded to the backbones of the condensed systems have various implications on the scattering behavior.

The experimental method used is neutron Compton scattering. This technique is highly inelastic (energy transfer the proton is $4< \hbar\omega <100$ eV) and it operates at the femto- and sub-femtosecond time range for scattering on protons.

The above mentioned qualitative theoretical prediction has been confirmed in the present work and further new features have been revealed. In short, it is found that the scattering cross section density of protons in these materials (water [31], metallic hydrides [36, 38] etc., organic materials [41–44], ionic metal hydrides [33], etc.) is significantly decreased with respect to the values known from the tabulated cross section, from sample preparation and chemical formulae. These striking experimental findings constitute the novelty of the present work. The deuterons showed only small anomalies. This already indicates that a quantum mechanical effect is detected here. This is because the mass of D is twice as big as that of H. Thus the thermal de Broglie wave length of D is smaller than that of H, so that D is less predestinated for exhibiting quantum properties due to its smaller spatial delocalization. The short time scale of the neutron Compton scattering process – being in the femto- and sub-femtosecond regime – suggest that the effect found here is dynamical in nature. The first direct evidence for the existence of short lived nuclear quantum entanglement in condensed matter using a neutron scattering technique is provided by the results on H_2O/D_2O mixtures [31]. The experiments on H_2O/D_2O mixtures have also indicated for the first time the relevance of the scattering time for the underlying effect. It was already mentioned in section 7.1.1 that the fact that the found anomalies for the H_2O/D_2O mixtures using the U foil analyzer are smaller than those using the Au foil analyzer arises from the different scattering times involved in these experiments. However, this significance has not been recognized in the original publication [31] in the extent it deserves.

The strong dependence of σ_H/σ_D on the D mole fraction x_D in water indicate that the effect is of intermolecular origin. However, the measurements on the benzene and the polystyrene systems, respectively, – which showed only small dependence on x_D – suggest that for the C-H bond the anomaly is rather of intramolecular origin. Also the results of the amphiphilic molecule iso-C_4E_1 in D_2O indicate the intramolecular character of the shortfall of scattering intensity. This is because the iso-C_4E_1 concentration in D_2O has been kept small in order to increase the distance between H's belonging to differ-

ent molecules – thus increasing possible intramolecular contributions to the QE of protons as compared with the intermolecular ones.

It is believed that the physical origin of this effect is mainly given by interactions of protons with electrons, rather than by the well-known "exchange correlations" between identical particles. Since the protons are spatially well localized in their C-H bonds and they do not exchange their sites, the QE between two neighboring protons should be of the type represented by eq.(2.3), rather than of the hydrogen-molecule type given by eq.(2.4). In other terms, the well-known "exchange correlations" between identical particles do not seem to play a dominant role in the present context. In this connection, the recent theoretical model [55, 56] of the NCS effect should be mentioned, which however proposed the exchange-correlations mechanism to be the sole source of this effect. The conclusion of the present work is that the electronic environment is involved in causing the various features of the anomalies. This conclusion is strongly supported by the experiments on C_6HD_5 and C_6H_6/C_6D_6 mixture with the same H/D composition, i.e., H:D=1:5, which both showed the same anomalies. This means also that the effect is independent of the H-H distance which is largely differing in the two systems. This result has also far reaching consequences for the above mentioned recent theoretical model [55, 56] which aims at the explanation of the anomalous effects for example in water and the metallic hydrides (see below).

In the light of the results of water on the one side and the benzene and the polymers on the other, it is concluded that these anomalies may be of intermolecular as well as of intramolecular origin. Taking the decoherence concept into account and bearing in mind that intermolecular and intramolecular interactions, respectively, induce different decoherence mechanisms and have different associated decoherence times, it is conceivable that while the anomaly in one material is governed by intermolecular interactions, it might be governed by intramolecular decoherence in a different one. Therefore, the results of acetone which contains C-H bonds and which showed a strong x_D dependence of the anomaly may also be caused both by intra- as well as intermolecular interactions.

While the anomalies in water and polystyrene are independent of the scattering angle and equivalently on the scattering time τ_s, in certain cases (for example for some metallic hydrides) this anomaly is strongly dependent on this quantity. This result is quite interesting because it further illustrates that the involvement of different chemical and electronic environments influence the scattering behavior of the protons. The scattering time τ_s can be regarded as the time window within which the dynamics of the nucleus is sampled. In the case of $NbH_{0.78}$, the anomalies are large at short scatter-

ing times ($<0.5\text{x}10^{-15}$s) and seem to vanish for long τ_s. If these anomalies are attributed to the existence of short-lived quantum entangled particles involving mainly the protons, this τ_s dependence may be interpreted such that at short times quantum interferences are revealed while at longer τ_s a time average is taken thus leading to the disappearance of the anomalies.

One might argue that the dependence of σ_H/σ_{Me} on the scattering angle is caused by the fact that the energy resolution for H falls below the angular resolution for scattering angles higher than ca. 50°. However, σ_D/σ_{Me} is also angle dependent for angles higher than ca. 100° although the energy resolution for D never falls below the angular one. See for example Figs. 4.13 and 4.14. Furthermore, the dissimilarity in the θ dependence and similarity in τ_s dependence of the data of niobium hydride and palladium hydride, respectively, demonstrate that the experimental results are not arising from H/D peak overlaps.

The observed anomalous NCS effect in benzene and polystyrene depends only weakly – within experimental errors – on the scattering angle or, equivalently, on the scattering time. This indicates that the dynamics of QE does not change very much within the time window given by the experiment. This finding is in clear contrast to the very strong τ_s-dependence of the cross-section density of protons in niobium and palladium hydrides. These comparisons indicate that the electronic environments of the protons play a highly significant role in the sub-femtosecond dynamics of protons in condensed matter, the clarification of which remains a challenge to modern theory.

Comparing the low- and high-temperature results for $NbH_{0.78}$ it is noted that the data in Fig. 7.32 for 20 K and 300 K practically coincide. This is an indication that the time for losing coherence (i.e., the decoherence time τ_{dec}) is not governed by thermal processes in the present type of materials, but probably *(i)* by characteristic response times of electron densities surrounding the scattering nuclei (see Refs. [42, 43]), and/or *(ii)* by the perturbations caused by the measuring process (i.e., the neutron-proton collision) itself. E.g., it is to be expected that in Compton scattering, which is a violent process, spatial quantum coherence between two protons (or deuterons) will be destroyed as soon as one of them starts to leave the equilibrium position, producing excitations in the metal hydride lattice and/or electronic excitations in the surrounding equilibrium electron density. With typical recoil energies, the first fs corresponds to motion over distances of $0.1 - 1$ Å. Phonons can be excited in the metal- as well as in the H-sublattices (and also in the D-sublattices, in the mixed hydrides). A dependence of the coherence loss on the composition of the hydrides (as visible from Fig. 7.27 for the NbH_xD_y-system) is therefore not unexpected, since the phonon densities of states are

different for NbH, NbD and the NbH_xD_y mixed hydrides. It is conceivable that the strong local perturbation associated with the recoil is more likely to excite the highest energy modes (which are those of the H-sublattice vibrations) than the less energetic ones. This is a hypothesis that may explain why the transition to "normal" cross sections is faster for $NbH_{0.78}$ than for the NbH_xD_y samples.

Within the framework of quantum theory, the environment is usually responsible both for the creation and destruction of QE. Therefore, if the anomalous NCS effect stated above arises from protonic QE, then a proper change of the influence of the environment on the protons (e.g. involving significantly different electronic structures or changing temperature) should have an impact on the scattering behavior. In contrast to the previously investigated hydrides where the H occupies interstitial lattice sites, LiH is an ionic hydride with the H charged negatively.

The LiH system is the only system investigated thus far that shows a change of anomaly upon temperature variation. This difference might be caused by the difference of the electronic structures in these two systems. Whereas the H atom can move between different sites in the niobium lattice, it is rigidly bonded in LiH implying different interactions of the H atom with its environment. If protonic QE exists in these systems and if QE is responsible for the anomalous neutron scattering cross section density of H in LiH, then the reason for the larger anomaly at lower temperature might arise from the fact that at 20 K the QE is not disturbed by the environment to the same extent as at 300 K due to the fact that the surrounding particles movement is slower. This interpretation in terms of QE is also supported by the fact that the anomalies found in the LiH system is larger than was found in the interstitial hydrides, like e.g. in NbH or PdH [36, 38].

Experiments on LaH_2 – which exhibits metallic properties – and LaH_3 – which is an isolator – showed significant differences of the cross section anomaly [50]. These experiments strongly indicate the relevance of the electronic environment for the decoherence process [33].

In some cases it was impossible to determine the changes of the scattering properties of H and D separately. This was due to the following reasons: First, the available sample containers (made of aluminum or vanadium) did not allow to separate the scattering contribution of the heavy nucleus of the sample – for example, the oxygen contribution of water – from that of the sample container. Secondly, the intermediate development of the VESUVIO instrument the experiments were performed on, restricted the accessible dynamical range preventing again a separation of the scattering contributions of the sample and container, respectively. There is no permanent access to this instrument and therefore some of the experiments could not be repeated

with optimum experimental conditions.

The considered NCS effect is attributed to QE effects between protons and adjacent particles (e.g. electrons) – rather than to QE between heavier nuclei or between nuclei of different kind. Moreover, the theoretical considerations of chapter 2 reveal that entanglement between protonic and deuteronic – and perhaps more interestingly between nuclear and electronic – degrees of freedom is also feasible. In this connection, it should be borne in mind that the scattering time τ_s of NCS – being determined by the experimental setup and the molecular properties – is similar to the characteristic time of the electronic rearrangements accompanying the formation and/or breaking of a typical CH bond, which lies in the sub-femtosecond time scale. This seems to support the relevance of QE between protonic and electronic degrees of freedom, in the physical context of the NCS effect.

The experimental observations of the present work strongly contradict standard theoretical treatments of neutron scattering. Interestingly, the NCS experiments on the liquid H_2O/D_2O mixtures [31] showed a similar D mole dependence of the scattering anomalies of the proton as was found in previous Raman light scattering experiments [30]. The NCS experimental results were thoroughly scrutinized. Additional test experiments have been performed to check the reproducibility of the data and to account for recent objections related to the data analysis procedure. These test experiments fully confirm the found anomalous scattering cross section density of the protons in the investigated materials [34].

In view of the experiments of liquid water, the objection may be raised, that the apparent decrease of the ratio $Q = \sigma_H/\sigma_D$ may be caused by an intensity transfer from the H to the D signal due to their overlapping in the TOF spectra [126, 137, 139]. However – besides the additional experiments performed using the U foil analyzer having a much narrower resolution than the previously used gold one – the fact that the metallic hydrides have shown an angle dependence supports the conclusion that the decrease of scattering cross section of the protons does not arise from the transfer of intensity to the signal of D because of partial overlapping. This is because the decrease of the H cross section becomes larger with higher angle, i.e., where the H and D peaks become more separated [140]. In addition, in a recent paper [130] it has been shown that the D signal remains unaltered in the H_2O/D_2O mixture with x_D=0.5 which means that the anomaly of $Q = \sigma_H/\sigma_D$ can not be explained as due to an intensity transfer from the H signal to the D one. Furthermore and equally important, the test experiments of chapter 8 utilizing among others the Double Difference technique with the significantly improved energy resolution showed no differences to the data obtained using the Single Difference technique [34]. Also the well known energy dependent

detector efficiency might be a possible cause of the scattering anomalies found in this work. However, it is a big advantage of the inverted geometry spectrometers VESUVIO that in the "foil-in/foil-out" difference spectrum the neutrons contributing to a scattering intensity have the same final energy over the whole TOF regime [83, 84]. Therefore, the possible energy dependence of the detector efficiency becomes irrelevant in the present physical context. Particular care was also taken to avoid overload of the data acquisition electronics, which could lead to counting losses at certain angles. Dead time losses were kept below a few percent, even at highest counting rates used. The performance of the whole data acquisition system was also checked repeatedly by interchanging buffers and electronic units between the different detector banks. All these changes left the anomalies unaltered. One may also object that the strong angle dependence of these observations might be due to artifacts of the scattered neutrons at large scattering angles. This is conceivable, since the samples were put perpendicular to the incoming neutron beam, so that the count rates at higher scattering angles might be more affected than those at lower angles. However, measurements done on liquid hydrogen [42, 136] which showed also an angle dependence were repeated after rotating the flat Al can by ca. 20°. It was found that the angle dependence remained unchanged [136]. Furthermore, considerably increasing the sample detector distance from ca. 60 cm to 100 cm, a conceivable influence of possible dead-time effects of the detectors for short times on the intensity of the H-signal has clearly been ruled out [136]. Very recently, neutron transmission (NT) experiment of Blostein et al. [137] showed no anomalies of the total scattering cross section of the protons and deuterons in liquid H_2O/D_2O mixtures. This experiment lead the authors to conclude that the analysis of the VESUVIO data performed thus far is flawed. However, while the discrepancy of this experimental result and the NCS ones remains unresolved yet, it has been shown that the data analysis procedure followed on VESUVIO is indeed correct [34]. Altogether, multiple scattering and saturation effects due to the sample geometry, effects due to the possible errors in describing correctly the incident neutron beam intensity and the related Jacobian, as well as peak overlap effects due to the limited energy resolution of the instrument have been ruled out as possible reasons for the found anomalies.

Having discussed the reliability of the experimental data we turn now to some fundamental question of the underlying novel effect.

Recently, Ioffe et al. [141] reported about the measurement of the coherent scattering length density (Nb) of liquid H_2O/D_2O mixtures at room temperature using a high precision technique of neutron interferometry (NI). The data analysis showed in essence, that there is no deviation of the mea-

sured Nb values from those conventionally calculated on the basis of simple random mixing of two liquids. Since this finding is fully consistent with conventional theory, it was claimed that these results are not consistent with the predicted deviations due to quantum entanglement between protons and deuterons as was found in, for example, water [31]. Consequently, the impression arose that the NI results of Ref. [141] can be interpreted as being in conflict with the NCS results and with the theoretical investigations concerning short lived quantum entanglement. However, such a conflict does not exist as is explained in the following. As a matter of fact, the relevant physical conditions of the inelastic and incoherent NCS method (see chapter 3) differ significantly from those of the (elastic and coherent) NI technique [142]. It is essential to note that the characteristic time window (or scattering time) $\tau_{s,NCS}$ of NCS lies in the sub-femtosecond time range; see Fig. 7.3 and eq.(3.49), whereas the characteristic time window τ_{NI} of the NI technique (which here may be called traversal time [99]) is many orders of magnitude larger than $\tau_{s,NCS}$. For illustration, the following simple example is given The neutrons used in [141] have a de Broglie wavelength of ca. 2.7 Å, thus having a velocity of ca. 1500 m/s. The used cans were ca. 0.2 and 3 mm thick [141], which implies that the traversal times [99] of the neutrons through the samples are of the order of microseconds. The NI method (representing elastic coherent scattering in the forward direction) determines the average value of Nb of the total sample, and therefore it should be characterized by the time window $\tau_{NI} = 10^{-6}s$. In other words $\tau_{NI} \geq 10^{9}\tau_{s,NCS}$. In simple terms, the "slow" NI technique is by no means able to detect the short-time entanglement being revealed with the "fast" NCS technique [51]. Thus, it can be concluded that the NI experiment as performed by Ioffe et al. [141] neither falsified nor verified the existence of short-time quantum entanglement for the simple reason, that the NI technique operates at a considerably longer time window than the NCS technique [51]. Rather, the result of the NI experiment strongly supports the short-time nature of the NCS results found in this work and their relation to QE dynamics.

The anomalous effects found in this work rely on the impulse approximation and on the fact that the scattering nuclei (H, D, etc.) are harmonically bound and therefore possess Gaussian distributed ground state momenta. Therefore, the objection might be raised that the harmonic approximation can not be applied for liquids because diffusive motions are present there. As has been discussed by Egelstaff [143] and Egelstaff and Schofield [144], the shape of $S(q,\omega)$ changes with momentum transfer from pure Lorentzian for small q to Lorentzian at the center with Gaussian wings for large q and finally to pure Gaussian at the limiting case of infinite q. Therefore, the anomalies found might be due to an overestimation of the D signal when us-

ing the harmonic approximation due to the overlap of the H signal with the D one. These objections are clearly refuted by the experimental fact given earlier in this work; see Figs. 7.9 and 7.32. The results of the H_2O/D_2O and the metallic hydride measurements at low temperatures are within experimental error identical to those at room temperature although the diffusive motion is significantly different at those different temperatures. In addition the measurements on the fully protonated polystyrene (see Fig. 7.19), where no proton diffusion takes place, showed also anomalies. In this system there is no (D) peak which could overlap with that one of the H to give rise to an artificial reduction of the H scattering signal. Furthermore, the characteristic time of diffusion is ca. 10^{-12}s [145] whereas the scattering time for protons in the neutron Compton regime is of the order of $\tau_s \approx 10^{-15}$s and less (see eq.(3.49) and Fig. 3.4). Finally, recent measurements on pure H_2O and H_2O/D_2O mixtures in an Nb can allowed to determine the ratio of the H signal to that one of the O atom. These measurements revealed that the anomalous reduction of H peak area was maximum for pure H_2O, again the spectrum of which does also not possess any overlap of the H peak with any other one.

In addition, it has been argued that it is essential that the energy resolution is better than the energy splitting of two entangled spin configurations if quantum entanglement features are to be revealed [132]. As the energy resolution of the VESUVIO spectrometer is about 0.1 eV, i.e., much larger than any quantum splitting of the energy levels in solids, it was claimed that this spectrometer cannot reveal any effects of quantum entanglement. However, this statement is not always correct: E.g., as is well known, thermal neutrons scattered from, or transmitted through, liquid H_2 are able to distinguish between ortho- and para-H_2, because of the strongly different total cross sections (cf. e.g. Ref. [26]) independently of any resolution requirements.

Before we turn to the possible theoretical explanation of the underlying effect, let us mention that the shortfall of the scattering intensity of the protons found in this work has been very recently confirmed using a completely different experimental method, namely with the electron proton Compton scattering [45, 46]. NCS and ECS experiments were done on formvar and polyethylene. The experimental result for both compounds and for both experimental methods was an anomalous decrease of the scattered intensity of ca. 20%. It is quite remarkable that the anomaly is the same although the underlying interactions of the probe (being a neutron in NCS and an electron in ECS) are completely different, namely being strong interactions in the case of NCS and electromagnetic in the case of ECS [45, 46]. In addition, it is interesting to note that the experimental conditions of NCS and ECS are also

completely different. While the incident beam of NCS is polychromatic, it is monochromatic in the case of ECS. The energy resolution of ECS is orders of magnitude better than that of NCS and its shape is strongly Gaussian in contrast to the mostly Lorentzian one of the gold foil analyzer on VESUVIO.

Considerable effort has been spent by several groups in order to give the experimentally found striking shortfall of the proton cross section a theoretical interpretation. All these theories have in common that quantum effects are responsible for the observed effect. While the theoretical model put forward by Chatzidimitriou-Dreismann [58] takes the decoherence into account from the first steps of the derivations, the theory of Karlsson and Lovesey [55, 56] starts from a static model and imposes decoherence afterwards to explain the angle dependence of the metal hydride results. This approach has been utilized by Karlsson [146] in order to model the original experimental results of the H_2O/D_2O mixtures [31]. However, while the latter theoretical model quantifies the anomaly, the former is rather qualitative (due to the complexity which decoherence involves). While both theories are based on the existence of quantum entangled protons in the material, Gidopoulos [60] and Reiter and Platzman [61] suggested different theoretical models having in common the basic assumption of the breakdown of the Born-Oppenheimer approximation, i.e., they assume that in addition to the recoil of the proton during the scattering process, electronic states are excited as well.

The model of Chatzidimitriou-Dreismann (hereafter referred to as CD) [58] considers the scattering system as an open quantum system and utilizes accordingly a special solution ($\rho_S(t, \mathbf{x}, \mathbf{x}') \approx \rho_S(0, \mathbf{x}, \mathbf{x}')e^{-\Lambda(\mathbf{x}-\mathbf{x}')^2 t}$, see eq.(2.32)) of the Lindblad type equation of motion ($\hat{L}\rho_S = -i[H, \rho_S] - \Lambda[\mathbf{x}, [\mathbf{x}, \rho_S(t)]]$, see eq. (2.31)) that describes the non-unitary time evolution of the open system. Specifically, the matrix elements inducing the transitions from the initial states to the final ones averaged over the duration of the scattering (i.e., the scattering time τ_s) contain the exponential factors $\exp(-\Lambda|\xi - \xi'|^2 t)$. $\{|\xi\rangle\}$ is the set of state vectors in the preferred representation selected by the quantum dynamics of the system [58]. The exponential factors are the key quantities leading to the reduction of the scattering intensity, as observed in the NCS experiments. The same arguments are valid for the interpretation of the electron-proton Compton scattering results described above [45, 48, 49]. It has been objected [147] that the solution $\rho_S(t, \mathbf{x}, \mathbf{x}')$ is valid for "macroscopic" objects only. While this is true as concerns the original work of Joos and Zeh [76], it turned out that this approach can also be successfully used for various physical applications, for example, for the quantum Brownian motion in the high temperature limit, for decoherence through spontaneous and thermally induced transitions of internal degrees of freedom, and for decoherence by scattering of an incoming particle

flux [4].

Since decoherence is not governed by one dynamical process, it is of course conceivable that the dynamics of coherence loss is not governed by only one decoherence time but could in principle follow many decay laws [9]. If one would have an explicit expression for the decoherence rate Λ, it would be possible to model the scattering anomalies. Actually, one should be more precise and consider many decoherence rates Λ_j instead of just one. This is due to the many different ways the quantum entangled objects may interact with their environments. Having this in mind, this model seems to be potentially suitable to explain why the anomalies appear to be of intramolecular origin in some cases, while appearing to be of intermolecular origin in others. An important consequence of the theoretical model of CD [58] is that the conventional and widely used theoretical concept of electronic Born-Oppenheimer (BO) energy surfaces breaks down. This is because the BO surfaces are determined by considering the nuclei as classical mass points fixed at various spatial configurations, which allows then to solve the associated electronic Schrödinger equation. However, the theoretical result of Ref. [58] demonstrates that the protons cannot be described as classical mass points in the sub-femtosecond time scale. Reiter and Platzman [61] and Gidopoulos [60] have taken independently the break down of the BO scheme as a starting point for the development of their theoretical models to explain the anomalous shortfall of scattering intensity of the protons (see below).

The model of CD leaves the scattering length b (or equivalently the scattering cross section σ) untouched, whereas attributing the shortfall of intensity to a depletion of the transition matrix elements of the scattering process due to the decoherence process being assumed to exist in the system. In contrast, the model put forward by Karlsson and Lovesey (hereafter referred to as KL) attempts to explain the anomalies by the calculation of the scattering cross section for an entangled pair of indistinguishable particles. The starting point of this model is a pure initial state for two protons being labelled by α and β and their spins by I_α and I_β, i.e., $|\nu\rangle = \frac{1}{\sqrt{2}}\{\phi_1(R_\alpha)\phi_2(R_\beta)+\zeta\phi_1(R_\beta)\phi_2(R_\alpha)\}\sum_{mn}(I_\alpha m I_\beta n|JM)|I_\alpha m\rangle|I_\beta n\rangle$. The first part of this state represents the spatial wavefunction while the second one is the spinor of the system. The final state is assumed to be $|\nu'\rangle = \frac{1}{\sqrt{2\Omega}}\{\exp(ip'\cdot R_\alpha)\psi(R_\beta) + \zeta'\exp(ip'\cdot R_\beta)\psi(R_\alpha)\}\chi^{J'}_{M'}(\alpha,\beta)$. I.e., the energy of the neutron has been transferred to one particle of the pair while the other one is "frozen". The scattering particle is represented by a plane wave $\exp(ip'\cdot R_{\alpha,\beta})$ and the "frozen" one by $|\psi\rangle$. The neutron nuclear potential for the two particles is $V = b_\alpha\exp(ik\cdot R_\alpha) + b_\beta\exp(ik\cdot R_\beta)$. As a result, the cross section for Compton scattering differs from that one of independent particles by a fac-

tor $f = \sigma_{inc}\{|T_1|^2 + |T_2|^2\}/4\sigma$ which gives the shortfall of the cross section per particle. Here σ_{inc} is the incoherent and σ the total single-atom cross sections. T_1 and T_2 are given by $T_{1,2} = \int \psi^*(\overrightarrow{R})\phi_{1,2}(\overrightarrow{R})d\overrightarrow{R}$. This means that there is a non-vanishing overlap between the initial and the final spatial wave functions of the unperturbed particle before and after the scattering process. KL interpret this result as the incoherent addition of intensity for each center which is in line with the incoherent nature of the Compton scattering. The shortfall f of the cross section is constant for it does not contain any quantity varying with the parameters of, for example, the scattering kinematics or dynamics of the system. Therefore, an experimentally determined change of the shortfall of intensity has to be accounted for by introducing additional parameters and mechanisms. E.g., in order to account for the scattering time dependence of the shortfall of the scattering intensity of the protons in the hydrides of niobium and palladium, respectively, (see section 7.3) decoherence due to the coupling of the protons to the environment is additionally introduced qualitatively. The basic assumption of this model [55, 56] is actually that the quantum particles do not overlap or interact directly so that the correlations are purely due to quantum entanglement of spatial and spin degrees of freedom. This kind of entanglement is known as *exchange correlations*. In other words, this model is valid only for systems exhibiting exchange correlations. The question is now, why the neutron with a typical de Broglie wavelength of λ_{dB} =0.1 Å should be able to sample two protons separated by ≈2 Å. Addressing this question, KL [55, 56] refer to a recent work of Pitaevskii and Stringari where the cross section for the Compton scattering of laser light by two identical Bose-Einstein condensates separated by a potential sufficiently high to prevent overlap between both systems is calculated [101]. Pitaevskii and Stringari showed that the momentum distribution displays the coherence between the two condensates if the condition is fulfilled that the experimental uncertainty in the momentum transferred by the photons is smaller than $\hbar/d$ with d being the spatial separation of the Bose-Einstein condensates [101]. Based on this argument it has been suggested by KL that the neutron coherence length $l_c = \lambda^2/2\Delta\lambda$ plays an essential role for the interpretation of the neutron scattering intensity shortfall [56]. l_c is calculated from the energy resolution of the Au foil energy analyzer used in the experiments (see section 3.2.6) to be $l_c = 2.5$ Å. Thus, their argument is that although the neutron wavelength is smaller than the typical proton-proton distances ($d \approx 2$ Å in the metallic hydrides), there is still a longitudinal coherence so that more than one scattering center contributes to the scattering process. In their original work [55] KL developed their theoretical model for the case that $J' \neq J$, i.e., by choosing the spin final state to be orthogonal to the initial one. In a later publication [56], this condition

has been relaxed. However, as Cowley [132] and Colognesi [147] pointed out, this additional requirement is not needed because $\langle final|initial\rangle \rightarrow 0$ without invoking any orthogonality in the spin space. Furthermore, inspection of the equations for f and $T_{1,2}$ (see above) reveals that the shortfall of intensity is not governed by the properties of the scattering particle but by those of the particle which remains "frozen" at its position. Furthermore, it was pointed out that the anomalies expressed by the quantity f are caused by the use of an unjustifiably restricted set of final states [147].

In addition to the above mentioned theoretical models of CD and KL, respectively, there is another class of models having in common the starting point of the breakdown of the Born-Oppenheimer scheme. Due to the very short time scale of the neutron Compton scattering process, the proton wave packet after the collision has a large energy spread ΔE which allows it to access excited electronic states [60, 61]. According to Gidopoulos [60], if this non-adiabatic excitation concerns only one excited level, then the dynamic structure factor $S(q,\omega)$ (see chapter 3) is split into two parts $S(q,\omega) = |\alpha_q|^2 S_1(q,\omega) + |\beta_q|^2 S_2(q,\omega)$, where $S_{1,2}(q,\omega)$ are scattering functions centered at $\hbar^2 q^2/(2M) - \Delta E^2/\overline{E}$ and $\hbar^2 q^2/(2M) + \overline{E} + \Delta E^2/\overline{E}$, respectively, where $\overline{E}$ is the mean energy separation of the electronic levels. α is the amplitude for the electrons to remain in their ground states and β the one for their excitation during the scattering process. Thus, according to this theoretical model [60] there exists a redistribution of intensity at energies higher than the nuclear recoil energy and a slight shift of the main neutron intensity peak to lower energies. It is the loss of intensity in the main part of the dynamic structure factor which represents the explanation of the loss of scattering intensity of the protons. It should be noted that this model fulfills the first moment sum rule of neutron scattering theory [26, 27] since $|\alpha_q|^2 + |\beta_q|^2 = 1$. This theoretical approach has been motivated by a previous theoretical treatment of the anomalous effect [41] where it was pointed out that for very short times, the time-scale separation between the electronic and protonic motions is not well defined and hence the concept of electronic BO surfaces is not applicable. The above model [60] has been successfully used to model the dependence of the experimentally determined intensity shortfall of the protons on the scattering angle or equivalently on the momentum transfer of the hydrides of niobium and palladium [37]. However, it should be pointed out that the probability of electronic excitation by the nucleus is very small so that just the fact that the nuclear kinetic energy is much higher than the gap of the electronic levels is not sufficient to cause significant non-adiabatic electronic excitations. Rather, also the non-adiabatic couplings between the electronic levels, the matrix elements of which are difficult to calculate, have to be taken into account [60]. Although this theoretical model sounds reasonable,

the following example shows that it does not reflect the experimental reality. The shift of $S_1(q,\omega)$ is very small and should not be visible in the spectra. But the appearance of the additional contribution $S_2(q,\omega)$ should be visible in the measured spectra should it explain an intensity shortfall of 30% if its position in the energy transfer space is visible. However, a typical energy transfer spectrum of a hydrogen containing material (see Fig. 9.1) shows no signature of an additional contribution. On the other hand, as stated in the beginning, the splitting of $S(q,\omega)$ into just two contributions is related to the situation that – for the sake of the simplification of the underlying problem – only one excited electronic level has been considered in the theoretical treatment. Therefore, if excitation into more than one electronic level is considered, then $S(q,\omega)$ will split into the main peak consisting again of $S_1(q,\omega)$ and many additional parts $S_i(q,\omega)|_{i>1}$ depending on the number of involved electronic levels. This might be the reason why there is no visible indication for the predicted additional high energy contribution in the measured spectra. This means that the additional contributions are absorbed by the actual recoil peak. However, if this would be the case, then all contributions $S_i(q,\omega)|_{i>1}$ would be more or less covered by $S_1(q,\omega)$ which should add to the normal (tabulated) value of scattering cross section and not give rise to an anomalous shortfall of intensity. Turning back to the original situation in which only one electronic level is excited, another argument against this model becomes apparent. The shift of $S_2(q,\omega)$ with respect to ω_r is determined by the energy gap to the electronic level and is of the order of several eV [60]. However, as is shown on Fig. 9.1, the recoil peak of the proton covers a wide range of energy transfers probably containing all contributions related to the electronic excitations predicted by the theoretical model of Gidopoulos [60].

Another theoretical model has been proposed by Reiter and Platzman and is based on the breakdown of the BO scheme in the final state of the scattering process containing a rapidly moving proton with kinetic energy being sufficiently high to mix the electronic states of the system [61]. The kinetic energy of the proton is treated as a perturbation acting on the full Hamiltonian of the system thus distorting the electronic wavefunctions. As a result, the excited states have significant overlap with the ground state and there is a non-vanishing amplitude for the scattered neutron to transfer parts of its energy to the electronic system. The normalization of the electronic ground state in the presence of the fast proton leads to a reduction of the intensity by an amount of $\Delta I = \sum_n |(\hbar^2\overrightarrow{q}/M)\cdot\alpha_{0,n}|^2$, where $\alpha_{0,n} = \langle\alpha_0|(\delta H_0/\delta\overrightarrow{R_1})/(E'_n - E'_0)^2|\alpha_n\rangle$ is the perturbing action of the recoiling particle on the electronic states [61]. As can be seen, the intensity shortfall would be dependent on q^2. However, this feature is not observed

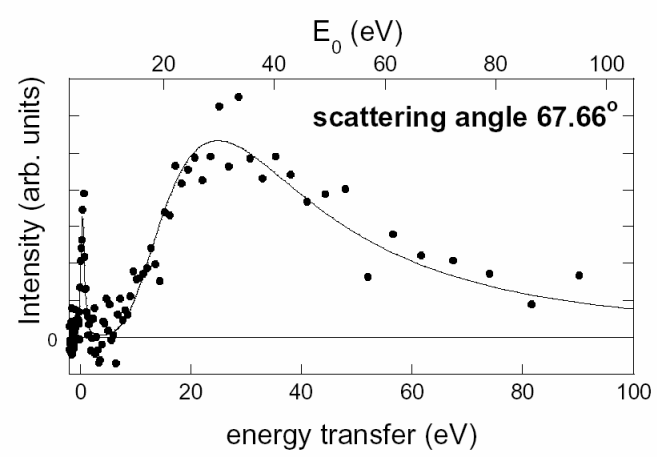

Figure 9.1: Shown a typical spectrum of a hydrogen containing material versus energy transfer. As one can see the recoil peak of the proton centered at ca. 30 eV covers a wide range of energy transfers.

in all experiments. Some of the experimental results, for example, in the hydrides of niobium and palladium, are indeed strongly dependent on q but most of them are not (see chapter 7). To overcome this problem the derivations have been extended beyond the lowest order perturbation theory using a mode coupling approximation to include the decay of the excited states. The result of this approach is an intensity shortfall which is now independent of q. The authors of this model [61] argue that the experiments are done in an intermediate q range where a mixture of a q^2 dependence and a q independence of the shortfall is observed.

It was stressed [132] that the existing theories [55, 56, 58] explaining H decrease in experiments with VESUVIO should be incorrect because they are inconsistent with the first moment sum rule (FMSR) for $S(q, \omega)$ [26, 27]. However, there are different theoretical models [60, 61] which are indeed consistent with the FMSR. Additionally, as pointed out in Ref. [58], the scattering systems under consideration ought to be described as open quantum systems. Consequently they always exhibit decoherence and thus a non-unitary time evolution. But, the derivations of the sum rules are based on unitary quantum dynamics which do describe closed systems only (see text books, e.g., Ref. [26]). Therefore, it is expected that the conventional neutron scattering theory has to be extended into the context of open quantum systems in order to account for the anomalies found here.

For example, footing on the basic principles of scattering theory and including decoherence dynamics explicitly, it is possible by means of the theoretical model of CD to explain qualitatively the anomalous shortfall of the

intensity of neutrons scattered from protons assumed to be quantum entangled on a short time scale. Another advantage of this approach is its applicability regardless whether the particles are subject to exchange correlations or not [58].

The theoretical models described above have been partly tested experimentally. For example, the irrelevance of exchange correlations for the underlying effect is most represented by the fact that very recent experiments on H_2/D_2 as well as on the HD molecule have shown equal anomalies in the σ_H/σ_D ratios. It is obvious that whereas the H_2 molecule exhibits exchange correlations, there is no such correlations in the HD molecule [148]. In addition, the irrelevance of the coherence length for the underlying effect is obvious from the comparison of the data of the liquid C_6H_6/C_6D_6 mixture with H:D=1:5 with those of liquid C_6HD_5 obviously having the same H/D particle number ratio. The experimental data of those systems show no difference although the H-H distance in C_6HD_5 (ca. 6 Å) is significantly larger than that in the liquid C_6H_6/C_6D_6 mixture (ca. 1 Å) (see section 7.2.2).

In conclusion, the suggested theoretical models outlined above obviously can not be reconciled. Some of them seem to be rather inconceivable or are inconsistent with some experimental findings. In the model of CD as well as in those of Gidopoulos on the one hand and Reiter and Platzman on the other, the spin degrees of freedom do not play an explicit role, while they are essential for the model of KL.

As can be seen from the preceding discussion of the theoretical models, standard neutron scattering theory is not able to account for the striking experimental findings. This is basically just due to the fact that it relies on several assumptions being not generally valid in a condensed matter system observed over a very short time range. For example the assumption of the stationarity of the involved states has obviously to be dropped because of the interaction the particles are subject to in condensed systems. Furthermore, the states of the constituents of the condensed system evolve according to a non-unitary dynamics again due to the complicated interaction present between the particles and their environments. Now the moment sum rules for the dynamic structure factor [26] results from the normalization of the stationary states involved in the conventional theoretical derivations. However, if the states are not stationary, normalization is not trivial [5]. Consequently, usual sum rules are not necessarily applicable in the short time scale of the present experiments.

Now, why is the novel effect found in this work important for chemistry?

According to the present-day knowledge, chemical bonds are theoretically treated by solving the electronic Schrödinger equation, using the well

known Born-Oppenheimer (BO) scheme [64] and obtaining the wave functions which describe the distribution of electrons in molecules. Furthermore, one describes a chemical reaction as the "movement" of nuclei considered as classical mass points or as quantum mechanical wave packets on electronic BO energy surfaces; cf. [62, 63]. Both treatments, however, have a common feature: the number of particles as well as the particle-field coupling constant (σ in NCS) cannot change. More precisely, (i) in classical mechanics, particles never "disappear"; (ii) according to "standard" quantum mechanics (as presented in widely used textbooks, like e.g. refs. [64] and [73]), in which the fundamental phenomenon of decoherence is discarded, the time evolution of the wave function of the particles is always unitary, thus conserving the normalization of the wave function and, equivalently, the number of particles.

With respect to chemistry, the following observation may be of considerable importance. The scattering time τ_s of the NCS experiments in this work is of the order of magnitude of the characteristic time of the electronic rearrangements accompanying the formation and/or breaking of a typical bond in a molecule. In other words, within the sub-femtosecond time window of this NCS process there is no well defined separation of time scales of electronic and protonic motions – the latter being subject to the neutron-proton collision process. (It should be reminded, however, that such a well defined time scale separation represents a necessary condition for the validity of the BO approximation; [64]) Furthermore, in the setup of the present NCS experiment, the energy transfer from a neutron to a proton exceeds 5 eV for scattering angles larger than ca. 45°. Due to the experimental fact that within this time range and during the breaking of the bond the proton shows anomalous scattering behavior being attributed to dynamical quantum entanglement, it is conceivable that these short lived quantum states are also important for chemical and biological processes. Therefore, the results presented in this work reveal a thus far unknown microdynamical property of an elementary chemical reaction, *viz.*, in our case, the dissociation of a chemical bond.

Since electrons and nuclei are strongly coupled due to the Coulombic interactions, protonic QE might also affect the rates of, and electron transfer in, various chemical and biochemical reactions involving H atoms. Indeed, this seems to be the case. Very recent electrochemical experiments explored the reaction rates of water molecule splitting and/or hydrogen evolution from liquid H_2O, D_2O and H_2O/D_2O mixtures at room temperature, measured as a function of the H/D composition. (In the frame of these investigations, a possible spin dependence of the protonic/deuteronic entanglement and its decoherence was assumed as working hypothesis.) The results revealed that these reaction rates strongly deviate from the H/D dependence predicted by

standard electrochemical theory [65].

Due to the high transfers of energy and momentum, respectively, the time scale of the neutron scattering process is in the range of $10^{-16} - 10^{-15}$s, i.e., in the femto- and sub-femtosecond regime. This time range coincides with that one for the rearrangement of electronic charges, for example, during chemical reactions.

It is also important to note that the experimental results found in this work are strongly supported by other experimental results obtained using different techniques. The most important on is the above mentioned electron-proton Compton scattering experiment [45, 46]. This experiment, which has attracted a lot of interest by the international scientific community [48, 49], has confirmed the striking findings of the present work with a completely independent experimental method. Additionally, neutron reflectivity experiments at the interface of Si and liquid H_2O-D_2O mixtures revealed an increase of the scattering length density of the H_2O/D_2O mixtures with respect to the values derived from tabulated scattering lengths and densities of H, D and O and the knowledge of the composition of the system [66]. It should be borne in mind that the neutron reflectivity technique is elastic and coherent and thus completely different than the neutron Compton scattering (NCS) technique which is highly inelastic and incoherent. The results of neutron reflectivity support the results of NCS as the increase of the scattering length density is equivalent to a decrease of the effective number density of the protons. This is due to the fact that the proton possesses a negative coherent scattering length [26].

Chapter 10

Conclusion

The present work deals with the occurrence of a striking effect concerning a shortfall of the intensity of neutrons scattered from protons in various chemical compounds. This effect is attributed to the existence of short lived dynamical quantum entanglement of protons in condensed matter. This effect of anomalous shortfall of the neutron scattering cross section density of protons occurs in various hydrogen containing condensed matter systems and its features depend on the electronic structures the hydrogen atoms are imbedded in in the different materials. The anomalies are of intramolecular as well as of intermolecular origin. It depends on the particular system whether the former or the latter is predominating. For some of the metallic hydrides the decoherence mechanism just sets in within the time window of the experiment and leads for longer scattering times to the disappearance of the anomaly, i.e., recovering the normal scattering cross section density.

The experimental findings strongly contradict every conventional theoretical treatment of the scattering process. In the standard theoretical treatment of neutron scattering it is always assumed that the studied system obeys the condition of stationarity. However, the experimental results suggest that this assumption has to be dropped in the time scale of the experiment being in the femtoseconds range and less.

The high transfers of energy which lead to bond breaking as well as the short time window of the experiment suggest the breakdown of Born-Oppenheimer-approximation which is widely applied in chemistry. Since the underlying striking short time quantum effect is observed for protons in various physico-chemical systems employing different chemical hydrogen bonds, it is strongly believed to be of fundamental importance for chemical and biological processes. It is also believed that this effect has far reaching consequences for the understanding of chemical reaction rates in condensed matter. This is due to the fact that it occurs in condensed matter within a time scale

which is comparable to the rearrangement of electronic densities during bond breaking and formation. It is anticipated that the present results are also important for moderator techniques which use hydrogen containing materials to slow down high energy neutrons. The present work triggered considerable efforts to find a theoretical interpretation the discussion of which is still going on.

The impact the experimental results presented in this work have achieved can be seen, for example, from the scientific activity of the theory group of the ISIS Facility at the Rutherford Appleton Laboratory [55, 56, 60, 149] and others [58, 61, 146]. Furthermore, since this effect has attracted a wide interest amongst theoreticians and experimentalists alike, a first "International Workshop on the Anomalous Cross Section" has been organized on this subject by ISIS [150, 151].

In conclusion, after consolidating the experimental results by independent measurements, it can be safely said that the present work represents a new field of physics and chemistry which concerns the detection of effects occurring in the femto- and attosecond time regime.

Acknowledgement

- It is a great pleasure to express my deepest gratitude to Prof. Aris Chatzidimitriou-Dreismann under whose supervision the present work has been done and from whom I have benefitted a lot to view the world of physics and chemistry beyond the horizon of ordinary text books.
- Prof. Gernot Renger is gratefully acknowledged for reviewing this work and for his great interest in this subject.
- Many thanks to Dr. Jerry Mayers – my teacher in neutron Compton scattering.
- Many thanks to Prof. Lubitz for his substantial support in getting the formalities done for a two years grant according to NaFöG.
- Pleasant and fruitful discussions with Prof. E. B. Karlsson, Prof. G. Reiter, Dr. D. Colognesi, Dr. N. Gidopoulos are greatfully acknowledged.
- Special thanks to the ISIS staff who provided excellent technical support.
- I would like to thank Prof. H. Sillescu and Prof. J. Springer for providing the polystyrene foils, Dr. T. Udovic for providing the yttrium hydride samples, and Prof. E. B. Karlsson and his group for the niobium hydride samples.
- Many thanks to my friend Tilman Rassy for his patient support in Latex, as well as to Marco Sielaff and Martin Kowall for their support in many software problems.
- Many thanks to Dr. Maciej Krzystyniak for many discussions and for reading parts of the manuscript.
- Many thanks to the Stranski Laboratory at the Institut für Chemie at the Technical University of Berlin for hosting me and for the generous financial support for many chemicals.
- Thanks to all my friends who always stood by me despite the lack of time I had during the becoming of this work.
- I would like to thank my family for their patience and understanding and for the provided necessary emotional backing.

- Last but not least: Nadja, at the end you have been the drive for everything! Thank you very much for having remained entangled with me and for keeping mutual coherence despite the long separating distance.

Bibliography

[1] K. Blum, *Density Matrix Theory and Applications* (Plenum Press, New York, 1981).

[2] L. D. Landau, E. M. Lifschitz, *Statistical Physics*, 3. ed. (Pergamon, Oxford, 1980).

[3] C. Cohen-Tannoudji, B. Diu, F. Laloë, *Quantum Mechanics Vol. 1* (Wiley-Interscience, Paris, 1977).

[4] H.-P. Breuer and F. Petruccione, *The Theory of Open Quantum Systems* (Oxford University Press, Oxford, 2002).

[5] L. D. Landau, E. M. Lifschitz, *Quantum Mechanics*, 3. ed. (Pergamon, Oxford, 1980).

[6] E. B. Davies, *Quantum Theory of Open Systems* (Academic Press, London, 1976).

[7] C. A. Chatzidimitriou-Dreismann, Adv. Chem. Phys. **80**, 201 (1991).

[8] D. Bouwmeester, A. Ekert, and A. Zeilinger (eds.), *The Physics of Quantum Information* (Springer, Berlin, 2000).

[9] J. R. Anglin, J. P. Paz, W. H. Zurek, Phys. Rev. A **55**, 4041 (1997).

[10] D. Giulini, E. Joos, C. Kiefer, J. Kupsch, I.-O. Stamatescu, and H. D. Zeh (eds.), *Decoherence and the Appearance of a Classical World in Quantum Theory* (Springer, Berlin, 1996).

[11] I. Prigogine, *From Being to Becoming* (Freeman, San Fransisco, 1980).

[12] W. H. Zurek, Rev. Mod. Phys. **75**, 715 (2003).

[13] M. B. Mensky, *Quantum Measurements and Decoherence* (Kluwer, Dorderecht, 2000).

[14] A. Stern, Y. Aharonov, and Y. Imry, Phys. Rev. A **41**, 3436 (1990).

[15] M. Tegmark, Phys. Rev. E **61**, 4149 (2000).

[16] W. H. Zurek, Physics Today **44**, 36 (Oct. 1991).

[17] S. Haroche, Physics Today **51**, 36 (Jul. 1998).

[18] R. Omnès, *The Interpretation of Quantum Mechanics* (Princeton Univ. Press, Princeton, 1994).

[19] A. Einstein, B. Podolsky, and N. Rosen, Phys. Rev. **47**, 777 (1935).

[20] J. S. Bell, Physics **1**, 195 (1964).

[21] B. d'Espagnat, *Conceptual Foundations of Quantum Mechanics*, 2. ed. (Addison-Wesley, Redwood City, 1989).

[22] A. Peres, *Quantum Theory, Concepts and Methods* (Kluwer, Dorderecht, 1995).

[23] D. M. Greenberger, M. A. Horne, and A. Zeilinger, Physics Today **46**, 22 (Aug. 1993).

[24] M. A. Nielsen, L. Chuang, *Quantum Computation and Quantum Information* (Cambridge Univ. Press, Cambridge, 2000).

[25] P. Berman, *Atom Interferometry* (Academic Press, San Diego, 1997).

[26] G. L. Squires, *Introduction to the Theory of Thermal Neutron Scattering* (Dover Publications, Mineola, 1996).

[27] S. W. Lovesey, *Theory of Neutron Scattering from Condensed Matter* (Clarendon, Oxford, 1984).

[28] G. Alefeld and J. Völkl (eds.), *Hydrogen in Metals I, II, Topics in Applied Physics, Vols. 28/29* (Springer, Berlin, 1978).

[29] Y. Fukai (eds.), *Hydrogen in metals* (Springer, Berlin, 1993).

[30] C. A. Chatzidimitriou-Dreismann, U. K. Krieger, A. Möller, M.Stern, Phys. Rev. Lett **75**, 3008 (1995).

[31] C. A. Chatzidimitriou-Dreismann, T. Abdul-Redah, R. M. F. Streffer, and J. Mayers, Phys. Rev. Lett. **79**, 2839 (1997).

[32] C. A. Chatzidimitriou-Dreismann,T. Abdul Redah, R. M. F. Streffer, and E. B. Karlsson, ISIS 2000 - The Rutherford Appleton Laboratory, ISIS Facility Annual Report **1**, 58 (2000).

[33] T. Abdul-Redah and C. A. Chatzidimitriou-Dreismann, Physica B **350**, e1035 (2004).

[34] J. Mayers and T. Abdul-Redah, J. Phys.: Cond. Matter **16**, 4811 (2004).

[35] C. A. Chatzidimitriou-Dreismann, T. Abdul Redah, and R. M. F. Streffer, Ber. Bunsenges. Phys. Chem. **3**, 544 (1998).

[36] E. B. Karlsson, C. A. Chatzidimitriou-Dreismann, T. Abdul Redah, R. M. F. Streffer, B. Hjörvarsson, J. Öhrmalm, and J. Mayers, Europhys. Lett. **46**, 617 (1999).

[37] T. Abdul Redah, R. M. F. Streffer, C. A. Chatzidimitriou-Dreismann, B. Hjörvarsson, E. B. Karlsson, and J. Mayers, Physica B **276-278**, 824 (2000).

[38] E. B. Karlsson, T. Abdul Redah, R. M. F. Streffer, B. Hjörvarsson, J. Mayers and C. A. Chatzidimitriou-Dreismann, Phys. Rev. B **67**, 184108 (2003).

[39] E. B. Karlsson, T. Abdul-Redah, T.J. Udovic, B. Hjörvarsson, C.A. Chatzidimitriou-Dreismann, Appl. Phys. A **74**, S1203 (2002).

[40] T. Abdul-Redah, C. A. Chatzidimitriou-Dreismann, E. B. Karlsson, Neutron News **15**, 14 (2004).

[41] C. A. Chatzidimitriou-Dreismann, T. Abdul Redah, and J. Sperling, J. Chem. Phys. **113**, 2784 (2000).

[42] C. A. Chatzidimitriou-Dreismann, T. Abdul Redah, R. M. F. Streffer and J. Mayers, J. Chem. Phys. **116**, 1511 (2002).

[43] C. A. Chatzidimitriou-Dreismann, T. Abdul Redah, and B. Kolaric, J. Am. Chem. Soc. **123**, 11945 (2001).

[44] T. Abdul Redah and C. A. Chatzidimitriou-Dreismann, Appl. Phys. A **74**, S1379 (2002).

[45] C. A. Chatzidimitriou-Dreismann, M. Vos, C. Kleiner, and T. Abdul-Redah, Phys. Rev. Lett. **91**, 057403 (2003).

[46] M. Vos, C. A. Chatzidimitriou-Dreismann, T. Abdul Redah, J. Mayers, Nucl. Instr. Meth. B **227**, 233 (2004).

[47] M. Vos, Phys. Rev. A **65**, 012703 (2002).

[48] Physics Update, Physics Today **September**, 9 (2003).

[49] Scientific American **October**, 34 (2003).

[50] T. Abdul-Redah, P. A. Georgiev, D. K. Ross, M. Krzystyniak, C. A. Chatzidimitriou-Dreismann, J. Alloys and Comp. , accepted (2005).

[51] C. A. Chatzidmitriou-Dreismann, T. Abdul-Redah, R. M. F. Streffer, and B. Hessmo, Phys. Rev. Lett. **84**, 2036 (2000).

[52] S. Ikeda and F. Fillaux, Phys. Rev. B **59**, 4134 (1999).

[53] F. Fillaux, Physica D **113**, 172 (1998).

[54] F. Fillaux, A. Cousson and D. A. Keen, Phys. Rev. B **67**, 054301 (2003).

[55] E. B. Karlsson and S. W. Lovesey, Phys. Rev. A **61**, 62714 (2000).

[56] E. B. Karlsson and S. W. Lovesey, Physica Scripta **65**, 112 (2002).

[57] E. B. Karlsson, Phys. Rev. Lett. **90**, 95301 (2003).

[58] C. A. Chatzidimitriou-Dreismann, J. Alloys and Comp. **356-357**, 244 (2003).

[59] L. van Hove, Phys. Rev. **95**, 249 (1954).

[60] N. I. Gidopoulos, Phys. Rev. B **71**, 054106 (2005).

[61] G. F. Reiter and P. M. Platzman , Phys. Rev. B **71**, 054107 (2005).

[62] A. H. Zewail, *Femtochemistry: Ultrafast Dynamics of the Chemical Bond* (World Scientific, Singapore, 1994).

[63] J. Manz and L. Wöste (eds.), *Femtosecond Chemistry* (VCH Verlagsgesellschaft, Weinheim, 1995).

[64] A. Bohm, *Quantum Mechanics: Foundations and Applications* (Springer, New York, 1993).

[65] J. Sperling, H. Tributsch, R. M. F. Streffer, T. Abdul-Redah, and C. A. Chatzidmitriou-Dreismann, J. Electroanal. Chem. **477**, 62 (1999).

[66] R. M. F. Streffer, T. Abdul Redah, J. Bowers, I.A. McLure, R. Steitz, F. Mezei, and C. A. Chatzidimitriou-Dreismann, Physica B **266**, 198 (1999).

[67] R. Penrose, *The Emperor's New Mind* (Penguin, New York, 1991).

[68] E. B. Karlsson, E. Brändas, Physica Scripta **T76**, 1 (1998).

[69] O. Carnal and J. Mlynek, Phys. Rev. Lett. **66**, 2689 (1991).

[70] D. W. Keith, C. R. Ekstrom, Q. A. Turchette, and D. E. Pritchard, Phys. Rev. Lett. **21**, 2693 (1991).

[71] M. S. Chapman, C. R. Ekstrom, T. D. Hammond, R. A. Rubenstein, J. Schmiedmayer, S. Wehinger, and D. E. Pritchard, Phys. Rev. Lett. **74**, 4783 (1995).

[72] L. Hackermüller, S. Uttenthaler, K. Hornberger, E. Reiger, B. Brezger, A. Zeilinger and M. Arndt, Phys. Rev. Lett. **91**, 090408 (2003).

[73] J. J. Sakurai, *Modern Quantum Mechanics* (Addison-Wesley, Reading, 1995).

[74] A. Müller, H. Zbinden, N. Gisin, Europhys. Lett. **33**, 334 (1996).

[75] A. Zeilinger, Scientific American **282**, 32 (2000).

[76] E. Joos and H. D. Zeh, Z. Phys. B **59**, 223 (1985).

[77] S. Nakajima, Progr. Theor. Phys. **20**, 948 (1958).

[78] R. Zwanzig, J. Chem. Phys. **33**, 1338 (1960).

[79] F. Shibata, Y. Takahashi, and N. Hashimoto, J. Stat. Phys. **17**, 171 (1977).

[80] S. Chaturvedi and F. Shibata, Z. Phys. **B35**, 297 (1979).

[81] F. Shibata and T. Armitsu, J. Phys. Soc. Jap. **49**, 891 (1980).

[82] C. G. Windsor, *Pulsed Neutron Scattering* (Taylor and Fracis, London, 1981).

[83] J. Mayers, T. M. Burke, and R. J. Newport, J. Phys.: Condens. Matter **6**, 641 (1994).

[84] R. M. Brugger, A. D. Taylor, C. E. Olsen, J. A. Goldstone, and A. K. Soper, Nucl. Instr. and Meth. **221**, 393 (1984).

[85] G. I. Watson, J. Phys.: Condens. Matter **8**, 5955 (1996).

[86] G. F. Chew, Phys. Rev. **80**, 196 (1950).

[87] V. F. Sears, Phys. Rev. B **30**, 44 (1984).

[88] G. B. West, Phys. Rep. C **18**, 263 (1975).

[89] S. Stringari, Phys. Rev. B **35**, 2038 (1987).

[90] A. C. Evans, D. N. Timms, J. Mayers, and S. M. Bennington, Phys. Rev. B **53**, 3023 (1996).

[91] J. Mayers, Phys. Rev. B **41**, 41 (1990).

[92] G. Reiter, R. N. Silver, Phys. Rev. Lett **54**, 1047 (1985).

[93] P. Platzman and N. Tzoar, *Compton Scattering* (McGraw Hill, New York, 1977), Chap. 2, p. 28.

[94] R. Von Brill and A. Tippe, Acta Crystallogr. **23**, 343 (1967).

[95] R. N. Silver, Phys. Rev. B **39**, 4022 (1989).

[96] H. R. Glyde, Phys. Rev. B **50**, 6726 (1994).

[97] A. L. Fielding, D. N. Timms, A. C. Evans, and J. Mayers, J. Phys.: Condens. Matter **8**, 7205 (1996).

[98] H. Rauch and S. A. Werner, *Neutron Interferometry: Lessons in Quantum Mechanics* (Clarendon Press, Oxford, 2000).

[99] M. Büttiker, Phys. Rev. B **27**, 6178 (1983).

[100] F. Mezei, A. P. Murani, J. Magn. Magn. Mater **14**, 211 (1979).

[101] L. Pitaevskii and S. Stringari, Phys. Rev. Lett. **83**, 4237 (1999).

[102] F. Mezei, *Neutron scattering and collective dynamics in liquids and glass In Liquides, Cristallisation et Transition Vitreuse. Les Houches, Session LI* (North-Holland, Amsterdam, 1991).

[103] J. Mayers, Phys. Rev. Lett. **71**, 1553 (1993).

[104] N. W. Ashcroft and N. D. Mermin, *Solid State Phyiscs* (Saunders College, Philadelphia, 1976).

[105] S. F. Mughabghab, *Neutron Cross-sections* (Academic Press, Orlando, Florida, 1984).

[106] P. A. Seeger, A. D. Taylor, and R. M. Brugger, Nucl. Instr. and Meth. A **240**, 98 (1985).

[107] G. Perron, F. Quirion, D. Lambert, J. Ledoux, L. Ghaicha, R. Bennes, M. Privat, and J.E. Desnoyers, J. Sol. Chem. **22**, 107 (1993).

[108] J. L. Garnett, Tetrahedron Lett. **41**, 4075 (1973).

[109] U. Kölber and J.-M. Welter, J. Less. Common Met. **84**, 225 (1982).

[110] G. Verdan, R. Rubin and W. Kley, J. Phys. Chem. Solids **31**, 2361 (1970).

[111] H. Conrad, G. Bauer, G. Alefeld, T. Springer and W. Schmatz, Z. Phys. **266**, 239 (1974).

[112] N. Stump, G. Alefeld, and D. Tochetti, Sol. State. Comm. **19**, 805 (1976).

[113] S. Olafsson, Comprehensive Summaries of Uppsala Dissertations, Faculty of Science and Technology **135**, 37 (1995).

[114] S. F. J. Cox, D. K. Ross, D. Witchell, O. Hartmann, R. Hempelmann, D. Richter, and A. M. Stoneham, Hyperfine Interactions **31**, 105 (1986).

[115] O. Blaschko, P. Fratzl, and R. Klemencic, Phys. Rev. B **24**, 277 (1981).

[116] W. Drexel, A. Murani, T. Tocchetti, and W. Kley, J. Chem. Phys. Solids **37**, 1135 (1976).

[117] T. J. Udovic, Q. Huang, J. J. Rush, J. Phys. Chem. Solids **57**, 423 (1996).

[118] D. Khatamian, W. A. Kamitakahara, R. G. Barnes, D. T. Peterson, Phys. Rev. B **21**, 2622 (1980).

[119] T. J. Udovic, J. J. Rush, and Andersson, Phys. Rev. B **50**, 15739 (1994).

[120] H. E. Flotow, D.W. Osborne, and K. Otto, J. Chem. Phys. **36**, 866 (1962).

[121] H. E. Flotow, D.W. Osborne, K. Otto, and B. M. Abraham, J. Chem. Phys. **38**, 2620 (1963).

[122] W. M. Müller, J. P. Blackledge, G. G. Libowitz, *Metal Hydrides* (Academic Press, New York, 1968).

[123] E. Zintl and A. Harder, Z. Phys. Chem. B **14**, 265 (1931).

[124] A. K. M. A. Islam, Phys. Stat. Sol. B **180**, 9 (1993).

[125] A. D. Taylor, *SNS Moderator Performance Predictions* (Rutherford Appleton Laboratory Report, RAL-84-120, 1984).

[126] J. J. Blostein, J. Dawidowski, and J. R. Granada, Physica B **304**, 357 (2001).

[127] C. Andreani, D. Colognesi, A. Filabozzi, E. Pace, and M. Zoppi, J. Phys.: Condens. Matter **10**, 7091 (1998).

[128] T. Abdul-Redah, Master thesis, Technical Univ. Berlin, Germany, 1996.

[129] M. I. Cabao, Y. D. Danten, M. Besnard, Y. Guissani, and B. Guillot, J. Phys. Chem **101**, 6977 (1997).

[130] C. A. Chatzidimitriou-Dreismann, T. Abdul-Redah, and J. Mayers, Physica B **315**, 281 (2002).

[131] T. Abdul Redah and C. A. Chatzidimitriou-Dreismann, ISIS Annual Report **2**, RB8021 (1998).

[132] R. A. Cowley, J. Phys.: Cond. Matter **15**, 4143 (2003).

[133] J. Mayers, A. L. Fielding, and R. Senesi, Nucl. Instr. and Meth. A **481**, 454 (2002).

[134] J. Mayers and A. C. Evans, *Measurement of Atomic Momentum Distribution Functions by Neutron Compton Scattering; Progress on the eVS Spectrometer during 1990* (Rutherford Appleton Laboratory Report, RAL-91-048, 1991).

[135] T. Abdul Redah and C. A. Chatzidimitriou-Dreismann, ISIS Annual Report **2**, RB12117 (2001).

[136] C. A. Chatzidimitriou-Dreismann and T. Abdul-Redah, Physica B **350**, 239 (2004).

[137] J. J. Blostein, J. Dawidowski, S. A. Ibanez, and J. R. Granada, Phys. Rev. Lett. **90**, 105302 (2003).

[138] C. Andreani, D. Colognesi, E. Degiorgi, A. Filabozzi, M. Nardone, E. Pace, A. Pietropaolo and R. Senesi, Nucl. Instr. Methods A **497**, 535 (2003).

[139] J. J. Blostein, J. Dawidowski, and J. R. Granada, Physica B **334**, 257 (2003).

[140] T. Abdul-Redah, C. A. Chatzidimitriou-Dreismann, J. Alloys and Comp. **356-357**, 249 (2003).

[141] A. Ioffe, M. Arif, D. L. Jacobson, and F. Mezei, Phys. Rev. Lett. **82**, 2322 (1999).

[142] V. F. Sears, *Neutron Optics* (Oxford University Press, Oxford, 1989).

[143] P. A. Egelstaff, Adv. Phys. **11**, 203 (1962).

[144] P. A. Egelstaff and P. Schofield, Nucl. Sci. Engin. **12**, 260 (1962).

[145] T. Springer, *Quasielestic Neutron Scattering for the Investigation of Diffusive Motions in Solids and Liquids*, Vol. 64 of *Springer Tracts in Modern Physics* (Springer Verlag, Berlin, 1972), .

[146] E. B. Karlsson, Phys. Rev. Lett. **90**, 95301 (2003).

[147] D. Colognesi, Physica B **344**, 73 (2003).

[148] C. A. Chatzidimitriou-Dreismann and T. Abdul Redah , ISIS Annual Report **2**, RB12755 (2003).

[149] N. I. Gidopoulos, ISIS 2005 - The Rutherford Appleton Laboratory, ISIS Facility Annual Report , (2005).

[150] T. Abdul-Redah (ed.), *Anomalous Cross Section Workshop* (Rutherford Appleton Laboratory, To be published, 2005).

[151] T. Abdul-Redah and J. Tomkinson, Neutron News **16**, 5 (2005).

Publications

Published results of this work

1. C. A. Chatzidimitriou-Dreismann, **T. Abdul Redah**, R. M. F. Streffer, J. Mayers: Anomalous Deep Inelastic Neutron Scattering from Liquid H_2O-D_2O: Evidence of Nuclear Quantum Entanglement, *Phys. Rev. Lett.* **79** (1997) 2839.

2. **T. Abdul-Redah**, C. A. Chatzidimitriou-Dreismann, E. B. Karlsson: Neutron Compton scattering unveils short-lived quantum entanglement of hydrogen in condensed matter, *Neutron News* **15** (2004) 14.

3. E. B. Karlsson, C. A. Chatzidimitriou-Dreismann, **T. Abdul Redah**, R. M. F. Streffer, B. Hjörvarsson, J. Öhrmalm, J. Mayers: Anomalous neutron Compton Scattering in Nb hydride: Indications of proton correlations, *Europhys. Lett.* **46** (1999) 617.

4. C. A. Chatzidimitriou-Dreismann, **T. Abdul-Redah**, J. Sperling: Sub-femtosecond dynamics and dissociation of C-H bonds in the condensed phase: Effects of entangled protonic states, *J. Chem. Phys.* **113** (2000) 2784.

5. C.A. Chatzidimitriou-Dreismann, **T. Abdul-Redah**, B. Kolaric: Entanglement of Protons in Organic Molecules: An Attosecond Neutron Scattering Study of C-H Bond Breaking, *JACS* **123** (2001) 11945.

6. C.A. Chatzidimitriou-Dreismann, **T. Abdul-Redah**, R. M. F. Streffer, J. Mayers: Sub-femtosecond dynamics and dissociation of C-H bonds in solid polystyrene and liquid benzene, *J. Chem. Phys.* **116** (2002) 1511.

7. E. B. Karlsson, **T. Abdul Redah**, R. M. F. Streffer, B. Hjörvarsson, J. Mayers, C. A. Chatzidimitriou-Dreismann: Anomalous neutron Compton scattering cross sections in niobium and palladium hydrides, *Phys. Rev. B* **67** (2003) 184108.

8. C.A. Chatzidimitriou-Dreismann, **T. Abdul-Redah**, J. Mayers: Experimental test of a theoretical analysis of deep inelastic neutron scattering experiments for H and D nuclei, *Physica B* **315** (2002) 281.

9. C. A. Chatzidimitriou-Dreismann, **T. Abdul Redah**: Short lived quantum entanglement of protons and dissociation of C-H bonds in condensed matter - A new effect, *Foundations of Quantum Mechanics in the Light of New Technologies - ISQM - Tokyo '01, Y.A. Ono and K. Fujikawa (Eds.)*, World Scientific 2002, p 299.

10. E. B. Karlsson, **T. Abdul Redah**, T. Udovic, B. Hjörvarsson, C. A. Chatzidimitriou-Dreismann: Short-lived proton entanglement in Ytrrium hydrides, *Foundations of Quantum Mechanics in the Light of New Technologies - ISQM - Tokyo '01, Y.A. Ono and K. Fujikawa (Eds.)*, World Scientific 2002, p 295.

11. C. A. Chatzidmitriou-Dreismann, **T. Abdul-Redah**, R. M. F. Streffer, B. Hessmo: Comment on "Precision Neutron Interferometrc Search for Evidence of Nuclear Quantum Entanglement in Liquid H_2O-D_2O Mixtures", *Phys. Rev. Lett.* **84** (2000) 2036.

12. C. A. Chatzidimitriou-Dreismann, **T. Abdul-Redah**, R. M. F. Streffer, E. B. Karlsson: Neutron scattering reveals short-lived quantum entanglement of protons in condensed matter, *Science Highlight in ISIS Annual Report* (Oct. 2000) 58.

13. C. A. Chatzidimitriou-Dreismann, **T. Abdul Redah**, R. M. F. Streffer: Quantum Dynamical Entanglement of Protons in Liquid Water: New Raman Light Scattering and Inelastic Neutron Scattering Experiment, *Ber. Bunsenges. Phys. Chem.* **3** (1998) 544.

14. C. A. Chatzidimitriou-Dreismann, **T. Abdul Redah**, J. Sperling: Short lived "Schrdinger's cat" states of protons in metal-hydrogen systems: A new effect, *J. Alloys and Compounds* **330-332** (2002) 414.

15. C. A. Chatzidmitriou-Dreismann, **T. Abdul-Redah**, R. M. F. Streffer: Quantum Dynamical correlation of protons in water at T=298K: New Raman light scattering and neutron Compton scattering experiments, *Quantum Coherence and Decoherence - ISQM - Tokyo '98, Y.A. Ono and K. Fujikawa (Eds.)* 1999, Elsevier Science B.V. p. 327.

16. E. B. Karlsson, C. A. Chatzidimitriou-Dreismann, **T. Abdul Redah**, R. M. F. Streffer, B. Hjörvarsson, J. Öhrmalm, J. Mayers: Evidence

for anomalous correlations of protons in a metallic hydride, *Quantum Coherence and Decoherence - ISQM - Tokyo '98, Y.A. Ono and K. Fujikawa (Eds.)* 1999, Elsevier Science B.V. p. 331.

17. **T. Abdul-Redah**, R. M. F. Streffer, C. A. Chatzidimitriou-Dreismann, B. Hjörvarsson, E. B. Karlsson, J. Mayers: Anomalous neutron Compton scattering in metallic hydrides: new experiments, *Physica B* **276-278** (2000) 824.

18. C. A. Chatzidimitriou-Dreismann, **T. Abdul Redah**: Neutron Scattering from Short Lived Quantum Entangled Protons in Condensed Matter at T=293 K: A New Scattering Effect, *Molecular Physics Reports* **31** (2001) 34.

19. C. A. Chatzidimitriou-Dreismann, B. Kolaric, **T. Abdul Redah**: C-H bond breaking in the attosecond timescale: A new effect, *Proceedings of the 6th International Conference on Fundamental and Applied Aspects of Physical Chemistry* (2002) Vol 1, p. 49.

20. **T. Abdul Redah**, C. A. Chatzidimitriou-Dreismann: Decoherence of entangled protons and attosecond dynamics of C-H bond breaking, *Appl. Phys. A* **74**, (2002) S1379-S1381.

21. E. B. Karlsson, **T. Abdul Redah**, T. J. Udovic, B. Hjörvarsson, C. A. Chatzidimitriou-Dreismann: Short-lived proton entanglement in yttrium hydrides, *Appl. Phys. A* **74** (2002) S1203-S1205.

22. **T. Abdul-Redah**, C. A. Chatzidimitriou-Dreismann: Anomalous neutron scattering in metallic hydrides and the validity of the convolution formalism, *J. Alloys and Compounds*, **356-357C** (2003) 249.

23. **T. Abdul-Redah** and C. A. Chatzidimitrou-Dreismann, Protonic Quantum Entanglement, Decoherence, And Anomalous Scattering Of Protons, *Proceedings of the "4th international Conference on Hydrogen Treatment of Materials - HTM2004"*, (2004) 369.

24. **T. Abdul-Redah**, C. A. Chatzidimitriou-Dreismann: Anomalous neutron scattering and coupling of protons to the environment at different temperatures, *Physica B* **350 S1** (2004) E1035.

Publications related to this work

25. C. A. Chatzidimitriou-Dreismann, M. Vos, C. Kleiner, **T. Abdul Redah**: Comparison of electron and neutron Compton scattering from entangled protons, *Phys. Rev. Lett.* **91** (2003) 057403.

26. R. Senesi, D. Colognesi, A. Pietropaolo, **T. Abdul-Redah**: Deep inelastic neutron scattering from orthorhombic ordered HCl: short-time proton dynamics and anomalous neutron cross-sections, *Physical Review B* **72** (2005) 054119.

27. C. A. Chatzidimitriou-Dreismann, **T. Abdul-Redah**, M. Krzystyniak: Anomalous neutron Compton scattering from molecular hydrogen, *Phys. Rev. B* **72** (2005) 054123.

28. C. A. Chatzidmitriou-Dreismann, **T. Abdul-Redah**, B. Kolaric, I. Juranic: Reply to Comment on "Evidence of Quantum Correlation Effects of Protons and Deuterons in Raman Spectra of Liquid H_2O-D_2O" of H. Torii, *Phys. Rev. Lett.* **84** (2000) 5237.

29. C. A. Chatzidmitriou-Dreismann, **T. Abdul-Redah**: Reply to Comment on "Evidence of Quantum Correlation Effects of Protons and Deuterons in Raman Spectra of Liquid H_2O-D_2O" of M Grimsditch, *Phys. Rev. Lett.* **82** (1999) 4368.

30. J. Mayers, **T. Abdul-Redah**: Measurement of Anomalous Neutron Inelastic Cross-sections at eV energy Transfers, *J. Physics C: Condensed Matter* **16** (2004) 4811.

31. G. F. Reiter, J. C. Li, J. Mayers, **T. Abdul-Redah**, P. Platzman: The proton momentum distribution in water and ice, *Brazilian Journal of Physics* **34** (2004) 142.

32. M. Vos, C. A. Chatzidimitriou-Dreismann, **T. Abdul Redah**, J. Mayers: Neutron and electron scattering from polymer films at high momentum transfer, *Nucl. Instr. Meth. B* 227 (2005) 233.

33. R. M. F. Streffer, **T. Abdul Redah**, J. Bowers, I. A. McLure, R. Steitz, F. Mezei, C. A. Chatzidimitriou-Dreismann: Anomalous neutron reflectivity of H_2O-D_2O mixtures at the silicon/liquid interface, *Physica B* **266** (1999) 198.

34. **T. Abdul-Redah**, C. Daub, R. M. F. Streffer, C. A. Chatzidimitriou-Dreismann: Anomalous neutron reflectivity at the Quartz/H_2O-D_2O interface, *Physica B* **291** (2000) 314.

35. J. Sperling, H. Tributsch, R. M. F. Streffer, **T. Abdul-Redah**, C. A. Chatzidmitriou-Dreismann: Anomalous H/D isotopic effect in the kinetics of polarographic hydrogen evolution, *J. Electroanal. Chem.* **477** (1999) 62.

36. J. Sperling, **T. Abdul-Redah**, R. M. F. Streffer, C. A. Chatzidmitriou-Dreismann, H. Tributsch: Electrolytic Water Splitting: Indications for the Existence of Protonic Quantum Interferences, *Phys. Chem. Chem. Phys.* **3** (2001) 301.

37. C. Halcoussis, **T. Abdul-Redah**, H. Naumann, G. Monaco and C. A. Chatzidimitriou-Dreismann: First Observation of Molecular Vibrational Excitation of Water with Inelastic X-Ray Scattering, *ESRF Newsletter* **33** (2000) 17.

38. C. A. Chatzidimitriou-Dreismann, **T. Abdul-Redah**: Attosecond entanglement of protons in molecular hydrogen: neutron Compton scattering results, *Physica B* **350** (2004) 239.

39. J. Mayers, **T. Abdul-Redah**: Anomalous neutron inelastic cross sections at ev Energy transfers, in *Decoherence, Entanglement and Information Protection in Complex Quantum Systems*, V. M. Akulin, A. Sarfati, G. Kurizki and S. Pellegrin (Eds), Kluwer Academic Publisher, Boston/Dordrecht/London, 2005.

40. **T. Abdul-Redah**, M. Krzystyniak, C. A. Chatzidimitriou-Dreismann: Quantum entanglement and decoherence due to coupling of protons to electronic environment, in *Decoherence, Entanglement and Information Protection in Complex Quantum Systems*, V. M. Akulin, A. Sarfati, G. Kurizki and S. Pellegrin (Eds), Kluwer Academic Publisher, Boston/Dordrecht/London, 2005.

41. C. A. Chatzidimitriou-Dreismann, **T. Abdul-Redah**, M. Krzystyniak, M. Vos: Attosecond effects in scattering of neutrons and electrons from protons. Entanglement and decoherence in C-H and O-H bond breaking, in *Decoherence, Entanglement and Information Protection in Complex Quantum Systems*, V. M. Akulin, A. Sarfati, G. Kurizki and S. Pellegrin (Eds), Kluwer Academic Publisher, Boston/Dordrecht/London, 2005.

42. Hendrik Naumann, **T. Abdul-Redah**, C. A. Chatzidimitriou-Dreismann: Probing quantum entanglement with inelastic x-ray scattering: Preliminary experimental results, in *Decoherence, Entanglement and Information Protection in Complex Quantum Systems*, V. M. Akulin, A. Sarfati, G. Kurizki and S. Pellegrin (Eds), Kluwer Academic Publisher, Boston/Dordrecht/London, 2005.

Publications not related to this work

43. D. Colognesi, A. J. Ramirez-Cuesta, M. Zoppi, R. Senesi and **T. Abdul-Redah**: Extraction of the density of phonon states in LiH and NaH, *Physica B* **350 S1** (2004) E983.

44. J. Mayers, J. Tomkinson, **T. Abdul-Redah**, W.G. Stirling, C. Andreani, R. Senesi, M. Nardone, D. Colognesi, E. Degiorgi: VESUVIO - the double difference inverse geometry spectrometer at ISIS, *Physica B* **350 S1** (2004) E659.

45. **T. Abdul-Redah**, C. Andreani, A. D'Angelo, G. Gorini, S. Imberti, J. Mayers, R. J. Newport, A. Pietropaolo, N. J. Rhodes, E. M. Schooneveld, R. Senesi, M. Tardocchi, J. Tomkinson: Recent developments of the e.Verdi Project at ISIS, *Physica B* **350 S1** (2004) E837.

46. G. F. Reiter, J. C. Li, J. Mayers, **T. Abdul-Redah**, P. Platzman: The proton momentum distribution in water and ice, *Brazilian Journal of Physics* **34** (2004) 142.

47. **T. Abdul-Redah**, "Nernst, Walther Herman (1864-1941)." In Macmillan Encyclopedia of Energy, ed. John Zumerchik, New York: Macmillan Reference USA (2001) p. 840-842.

Accepted papers

48. **T. Abdul-Redah**, M. Krzystyniak, C. A. Chatzidimitriou-Dreismann: Neutron Compton scattering from water studied with the Double-Difference technique, *Physical Review B* (2005).

49. **T. Abdul-Redah**, P. A. Georgiev, D. K. Ross, M. Krzystyniak, C. A. Chatzidimitriou-Dreismann: Short Lived Protonic Quantum Entanglement And Coupling To The Electronic Environment In $\mathbf{LaH_2}$ And $\mathbf{LaH_3}$, *J. Alloys and Comp.* (2005).

50. **T. Abdul-Redah**, M. Krzystyniak, J. Mayers, C. A. Chatzidimitriou-Dreismann: Anomalous Neutron Compton Scattering Cross Section In Zirconium Hydride, *J. Alloys and Comp.* (2005).

51. **T. Abdul-Redah**, C. A. Chatzidimitriou-Dreismann: Irreversible hydrogen quantum dynamics and anomalous scattering behaviour in liquids and solids, *International Journal of Hydrogen Energy* (2005).